

DEVELOPMENT OF SPECIMEN GEOMETRIES FOR MODE I FRACTURE  
TOUGHNESS TESTING WITH DISC TYPE ROCK SPECIMENS

A THESIS SUBMITTED TO  
THE GRADUATE SCHOOL OF NATURAL AND APPLIED SCIENCES  
OF  
MIDDLE EAST TECHNICAL UNIVERSITY

BY

ÇİĞDEM ALKILIÇGİL

IN PARTIAL FULFILLMENT OF THE REQUIREMENTS  
FOR  
THE DEGREE OF DOCTOR OF PHILOSOPHY  
IN  
MINING ENGINEERING

JUNE 2010

Approval of the thesis:

**DEVELOPMENT OF SPECIMEN GEOMETRIES FOR MODE I  
FRACTURE TOUGHNESS TESTING WITH DISC TYPE ROCK  
SPECIMENS**

submitted by **ÇİĞDEM ALKILIÇGİL** in partial fulfillment of the requirements  
for the degree of **Doctor of Philosophy in Mining Engineering Department,**  
**Middle East Technical University** by,

Prof. Dr. Canan Özgen  
Dean, Graduate School of **Natural and Applied Sciences**

\_\_\_\_\_

Prof. Dr. Ali İhsan Arol  
Head of Department, **Mining Engineering**

\_\_\_\_\_

Assoc. Prof. Dr. Levent Tutluoğlu  
Supervisor, **Mining Engineering Dept., METU**

\_\_\_\_\_

**Examining Committee Members:**

Prof. Dr. Naci Bölükbaşı  
Mining Engineering Dept., METU

\_\_\_\_\_

Assoc. Prof. Dr. Levent Tutluoğlu  
Mining Engineering Dept., METU

\_\_\_\_\_

Prof. Dr. Reşat Ulusay  
Geological Engineering Dept., Hacettepe University

\_\_\_\_\_

Prof. Dr. Celal Karpuz  
Mining Engineering Dept., METU

\_\_\_\_\_

Assoc. Prof. Dr. H. Aydın Bilgin  
Mining Engineering Dept., METU

\_\_\_\_\_

**Date:**

\_\_\_\_\_

**I hereby declare that all information in this document has been obtained and presented in accordance with academic rules and ethical conduct. I also declare that, as required by these rules and conduct, I have fully cited and referenced all material and results that are not original to this work.**

Name, Last name: iğdem Alkılıçgil

Signature :

## ABSTRACT

### DEVELOPMENT OF SPECIMEN GEOMETRIES FOR MODE I FRACTURE TOUGHNESS TESTING WITH DISC TYPE ROCK SPECIMENS

Alkılıçgil, Çiğdem

Ph.D., Department of Mining Engineering

Supervisor: Assoc. Prof. Dr. Levent Tutluoğlu

June 2010, 172 pages

Flattened Brazilian disc and modified ring test methods are attractive methods being simpler compared to the other mode I fracture toughness testing methods on rock cores. The aim of this study is to improve these simple methods to yield fracture toughness values that are close to the ones determined by the suggested methods. ABAQUS finite element program was used to determine stress intensity factors of models with various dimensions. Comparing fracture toughness to the results obtained by semicircular bending method tests (0.94 MPa $\sqrt{m}$  for andesite and 0.56 MPa $\sqrt{m}$  for marble) and the cracked chevron notched Brazilian disc method tests (1.45 MPa $\sqrt{m}$  for andesite and 1.08 MPa $\sqrt{m}$  for marble), proper geometrical parameters were investigated by changing diameter, central-hole diameter, and loading angle of Ankara andesite and Afyon marble specimens. Semicircular bending method results were lower than the cracked chevron notched Brazilian disc method results. With flattened Brazilian disc method, the closest results (1.45 MPa $\sqrt{m}$  for andesite and 1.12 MPa $\sqrt{m}$  for marble) to the suggested method was obtained by 54 mm diameter discs with loading angles between 32.5° and 38.0° and with thicknesses between 19 mm and 34 mm. With modified ring test on andesite, the closest results to the suggested method was obtained by 75 mm diameter discs with 8 mm central-hole diameter and 25° loading angle (1.47 MPa $\sqrt{m}$  for andesite and 1.07 MPa $\sqrt{m}$  for marble), and with 14 mm central-hole diameter and 16° loading angle (1.50 MPa $\sqrt{m}$  for andesite and 1.05 MPa $\sqrt{m}$  for marble).

Keywords: Fracture Mechanics, Finite Element Analysis, Stress Intensity Factor,  
Rock Fracture Toughness Testing, Specimen Geometries

## ÖZ

### DİSK TİPİ KAYA ÖRNEKLERİNDE MOD I ÇATLAK TOKLUĞU DENEYİ İÇİN ÖRNEK GEOMETRİLERİNİN GELİŞTİRİLMESİ

Alkılıçgil, Çiğdem

Doktora, Maden Mühendisliği Bölümü

Tez Yöneticisi: Doç. Dr. Levent Tutluoğlu

Haziran 2010, 172 sayfa

Düzleştirilmiş Brazilyan disk yöntemi ve uyarlanmış halka deneyi kaya karotlarında uygulanan diğer mod-I çatlak tokluğu deneyleriyle karşılaştırıldıklarında daha kolay yöntemler olduklarından cazip yöntemlerdir. Bu çalışmanın amacı, bu basit yöntemlerin geliştirilmesi ve bunların kullanılarak, önerilen yöntemlerle elde edilen çatlak tokluğu değerlerine yakın değerlerin elde edilmesidir. Çeşitli ebatlara sahip modellerin gerilme şiddeti faktörleri ABAQUS sonlu eleman programı kullanılarak belirlenmiştir. Deneysel analizlerde, çatlak tokluğu değerleri yarı dairesel eğilme yöntemi sonuçları (andezit için 0,94 MPa√m ve mermer için 0,56 MPa√m) ve V-tipi çentikli Brazilyan disk yöntemi sonuçlarıyla (andezit için 1,45 MPa√m ve mermer için 1,08 MPa√m) karşılaştırılıp uygun geometrik parametreler; Ankara andeziti ve Afyon mermeri örneklerinin örnek çapları, delik çapları ve yükleme açıları değiştirilerek incelenmiştir. Yarı dairesel eğilme yöntemi sonuçları, V-tipi çentikli Brazilyan disk yöntemi sonuçlarından düşüktür. Düzleştirilmiş Brazilyan disk yöntemi ile önerilen yöntemle en yakın sonuçlar 54 mm çapındaki diskler ile 32,5° ile 38,0° yükleme açıları ve 19 mm ile 34 mm kalınlık aralığındaki örneklerde (andezit için 1,45 MPa√m ve mermer için 1,12 MPa√m) elde edilmiştir. Uyarlanmış halka deneyi ile önerilen yöntemle en yakın sonuçlar 75 mm çapındaki disklerde 8 mm merkezi delik çapı ile 25° yükleme açısı olan ve 14 mm merkezi delik çapı ile 16° yükleme açısı olan örneklerde (andezit için 1,47 MPa√m ve mermer için 1,07 MPa√m) elde edilmiştir.

Anahtar Kelimeler: Kırılma Mekaniđi, Sonlu Eleman Analizi, Gerilme Őiddeti Faktörü, Kaya Çatlak Tokluğu Deneyi, Örnek Geometrileri

To My Family



## **ACKNOWLEDGEMENTS**

I would like to express my deepest gratitude to my supervisor, Assoc. Prof. Dr. Levent Tutluođlu, for his guidance, helpful comments and advice throughout the present thesis.

I want to thank to the examining committee the members, Prof. Dr. Reřat Ulusay, Prof. Dr. Celal Karpuz, Prof. Dr. Naci Blkbařı and Assoc. Prof. Dr. Aydın Bilgin for their valuable comments and suggestions.

I wish to express my appreciation to Tahsin Iřıksal and Hakan Uysal for their help with the experiments.

I would like to show my gratitude to my best friends Firdes Yenilmez and Esra Burcu zdemir. They are always with me, in my best and worst times.

I thank my fianc, Serhat Keleř, and his family for their support. Serhat was there for me whenever I need help.

Finally, I want to express my deepest appreciation to my family for their patience, care and support. They made it possible for me to achieve goals in my life.

## TABLE OF CONTENTS

ABSTRACT .....	iv
ÖZ .....	vi
ACKNOWLEDGEMENTS .....	ix
TABLE OF CONTENTS .....	x
LIST OF TABLES .....	xiv
LIST OF FIGURES.....	xvi
LIST OF SYMBOLS AND ABBREVIATIONS.....	xxii
CHAPTERS	
1. INTRODUCTION.....	1
1.1 General .....	1
1.2 Statement of the Problem and the Thesis Objective.....	1
1.3 Methodology .....	2
1.4 Sign Convention .....	3
1.5 Outline of the Thesis .....	3
2. ROCK FRACTURE MECHANICS .....	5
2.1 History of Fracture Mechanics for Brittle Materials.....	5
2.2 Stress Intensity Factor .....	6
2.3 Fracture Toughness .....	7
2.4 Linear Elastic Fracture Mechanics .....	7
2.5 Fracture Modes.....	7
2.6 Crack Tip Stress Component for Mode I .....	8
2.7 Crack Tip Displacement Components for Mode I .....	9
3. SOME APPLICATION AREAS OF ROCK FRACTURE MECHANICS.....	10
3.1 Hydraulic Fracturing .....	10
3.2 Rock Blasting .....	11
3.3 Rock Cutting.....	12
3.4 Underground Coal Mine Dust Control.....	12
3.5 Underground Opening Design.....	13

3.6 Comminution in Mineral Processing.....	13
4. MODE I FRACTURE TOUGHNESS TESTS .....	14
USED IN ROCK CORES .....	14
4.1 Tests Applied with Tensile Load .....	14
4.1.1 Short Rod Method .....	14
4.2 Tests Applied with Compressive Load .....	18
4.2.1 Cracked Straight Through Brazilian Disc Method.....	18
4.2.2 Diametral Compression Test .....	20
4.2.3 Cracked Chevron Notched Brazilian Disc Method .....	22
4.2.4 Modified Ring Test.....	25
4.2.5 Brazilian Disc Specimen .....	27
4.2.6 Flattened Brazilian Disc Method.....	28
4.3 Tests Under Bending Load .....	30
4.3.1 Straight Notched Semi-circular Bending Method .....	30
4.3.2 Chevron Notched Semi-circular Bending Method.....	32
4.3.3 Chevron Bend Test .....	33
4.3.4 Straight Edge Cracked Round Bar Bending Method .....	35
4.4 Comparison Between Mode I Fracture Toughness Values .....	37
4.5 Comparison of Mode I Fracture Tests on Disc Type Specimens .....	40
5. NUMERICAL MODELLING WITH ABAQUS PROGRAM.....	45
5.1 ABAQUS Program .....	45
5.2 Verification Examples .....	47
5.2.1 Central Crack in Infinite Plate.....	47
5.2.2 Infinite Plate with a Hole and Symmetric Double through Cracks ...	48
6. NUMERICAL MODELING OF FLATTENED BRAZILIAN DISC .....	51
6.1 Parameters Affecting Stress Analyses.....	51
6.1.1 Boundary Conditions.....	52
6.1.2 Effect of Specimen Thickness .....	59
6.1.3 Effect of Specimen Diameter .....	63
6.1.4 Effect of Mesh Intensity .....	65
6.1.5 Effect of Friction Coefficient .....	68
6.1.6 Effect of Loading Angle .....	71
6.2 Crack Initiation Location According to Stress Analyses .....	72

6.3 Stress Intensity Factor Analyses .....	76
6.3.1 Contour Integral Region.....	78
6.3.2 Mesh Intensity in the Contour Integral Region .....	79
6.3.3 Maximum Stress Intensity Factor Computations .....	81
7. NUMERICAL ANALYSES OF MODIFIED RING TEST .....	85
7.1 Parameters Affecting Stress Analyses.....	85
7.1.1 Boundary Conditions.....	85
7.1.2 Effect of Specimen Thickness .....	86
7.1.3 Effect of Mesh Intensity .....	89
7.1.4 Effect of Friction Coefficient .....	93
7.1.5 Effect of Specimen Diameter .....	93
7.1.6 Effect of Central-hole Diameter .....	96
7.1.7 Effect of Loading Angle.....	98
7.2 Stress Intensity Factor Analyses .....	101
7.2.1 Maximum Stress Intensity Factor Computations .....	102
8. FRACTURE TOUGHNESS TESTS .....	105
8.1 Relevant Mechanical Properties of Andesite and Marble .....	105
8.2 Mode I Fracture Toughness Tests with SCB and the Suggested CCNBD Methods.....	108
8.2.1 Tests with SCB Method .....	108
8.2.2 Specimen Geometries for SCB Method Tests.....	111
8.2.3 Fracture Toughness Evaluation for SCB Method Tests.....	112
8.2.4 Tests with CCNBD Method .....	114
8.2.5 Specimen Geometries for CCNBD Method Tests .....	118
8.2.6 Fracture Toughness Evaluation for CCNBD Method Tests.....	120
8.3 FBD Method Tests for Mode I Fracture Toughness Determination .....	122
8.3.1 Specimen Geometries for FBD Method Tests .....	124
8.3.2 Fracture Toughness Evaluation for FBD Method Tests.....	125
8.4 MR Tests for Mode I Fracture Toughness Determination .....	127
8.4.1 Specimen Geometries for MR Tests .....	130
8.4.2 Fracture Toughness Evaluation for MR Tests.....	132
9. RESULTS AND DISCUSSION .....	136
9.1 FBD Method Results.....	136

9.1.1 Effects of Specimen Diameter and Loading Angle on Mode I Fracture Toughness for FBD Tests .....	137
9.1.2 Effect of Thickness on Mode I Fracture Toughness for FBD Tests	140
9.1.3 Effect of Loading Rate on Mode I Fracture Toughness for FBD Tests .....	141
9.1.4 Fracture Toughness Results for Andesite and Marble with Proposed Geometrical Parameters for FBD Tests .....	142
9.2 MR Test Results .....	144
9.2.1 Effects of Specimen Diameter, Central-Hole Diameter and Loading Angle on Mode I Fracture Toughness for MR Tests .....	145
9.2.2 Fracture Toughness Results for Andesite and Marble with Proposed Geometrical Parameters for MR Tests .....	153
10. CONCLUSIONS AND RECOMMENDATIONS.....	155
REFERENCES.....	159
APPENDICES	
A. CALCULATION OF MAXIMUM STRESS INTENSITY FACTOR.....	166
B. PETROGRAPHIC ANALYSES OF ROCKS.....	169
C. PROPER SPECIMEN GEOMETRIES FOR FRACTURE TOUGHNESS TESTING.....	170
VITA.....	171

## LIST OF TABLES

### TABLES

Table 4. 1 SR Specimen dimensions (Ouchterlony, 1988) .....	15
Table 4. 2 Fracture toughness values of some rock types determined by using SR method.....	17
Table 4. 3 Fracture toughness values of some rocks analyzed by using SNBD method.....	20
Table 4. 4 Fracture toughness values of some rocks determined by using DC test .	22
Table 4. 5 Fracture toughness values of some rocks by using CCNBD Method.....	24
Table 4. 6 Dimensional restrictions for CCNBD Method.....	24
Table 4. 7 Fracture toughness values of some rocks determined by using MR test	26
Table 4. 8 Fracture toughness values of some rocks determined by using Brazilian Test.....	28
Table 4. 9 Fracture toughness values of some rocks determined by using Flattened Brazilian Disc Method .....	30
Table 4. 10 Fracture toughness values of some rocks analyzed by using SCB method.....	32
Table 4. 11 Fracture toughness values of some rocks determined by using CNSCB Method .....	33
Table 4. 12 CB Specimen dimensions (Ouchterlony, 1988).....	34
Table 4. 13 Fracture toughness values of some rocks determined by using CB Method .....	35
Table 4. 14 Fracture toughness values of some rocks obtained by using SECRBB method.....	37
Table 4. 15 Fracture toughness values of some rocks.....	37
Table 4. 16 (continued) Fracture toughness values of some rocks .....	38
Table 4. 17 (continued) Fracture toughness values of some rocks .....	39
Table 4. 18 Comparison between fracture tests .....	43

Table 5. 1 Normalized stress intensity factor values for different geometries (Wang, 1996).....	50
Table 8. 1 UCS data and results of andesite rock.....	106
Table 8. 2 UCS data and results of marble rock.....	106
Table 8. 3 Brazilian test data and results of the andesite rock .....	107
Table 8. 4 Brazilian test data and results of the marble rock .....	107
Table 8. 5 Dimensions of the andesite SCB specimens .....	111
Table 8. 6 Dimensions of the marble SCB specimens .....	112
Table 8. 7 Dimensionless stress intensity factors, failure loads and fracture toughness values of andesite specimens.....	113
Table 8. 8 Dimensionless stress intensity factors, failure loads and fracture toughness values of andesite specimens.....	114
Table 8. 9 Dimensions of the andesite CCNBD specimens .....	120
Table 8. 10 Dimensions of the marble CCNBD specimens .....	120
Table 8. 11 Values of $u$ and $v$ (Fowell, 1995).....	121
Table 8. 12 $u$ , $v$ , $Y_{min}^*$ , $F_{max}$ and $K_{Ic}$ values of andesite specimens .....	121
Table 8. 13 $u$ , $v$ , $Y_{min}^*$ , $F_{max}$ and $K_{Ic}$ values of marble specimens .....	122
Table 8. 14 Dimensions of the andesite FBD specimens .....	125
Table 8. 15 $\Phi_{max}$ , $F_{min}$ , and $K_{Ic}$ values of FBD andesite specimens .....	127
Table 8. 16 Dimensions of the andesite MR specimens (dimensions in mm, loading angle in $^{\circ}$ ) .....	131
Table 8. 17 $\Phi_{max}$ , $F_{min}$ (kN), and $K_{Ic}$ (MPa $\sqrt{m}$ ) values of MR andesite specimens.....	134
Table 8. 18 (continued) $\Phi_{max}$ , $F_{min}$ (kN), and $K_{Ic}$ (MPa $\sqrt{m}$ ) values of MR andesite specimens .....	135
Table 9. 1 Average fracture toughness values of FBD andesite specimens for various diameters and loading angle ranges.....	137
Table 9. 2 $K_{Icavg}$ of andesite rock according to $2\alpha$ 's for various specimen dimensions .....	152
Table A. 1 Stress intensity factor values according to crack lengths .....	166
Table A. 2 MATLAB code to determine Mode I maximum stress intensity factor value .....	167
Table C. 1 Proper specimen geometries for fracture toughness testing with FBD and MR methods .....	170

## LIST OF FIGURES

### FIGURES

Figure 2. 1 Alan Arnold Griffith .....	5
Figure 2. 2 Fracture modes (Key to Metals Database, 2010).....	7
Figure 2. 3 Location of local stresses near a crack tip (Key to Metals Database, 2010).....	9
Figure 3. 1 Hydraulic fracturing method (Boss International, 2009).....	11
Figure 3. 2 An indenter and a drag bit, respectively .....	12
Figure 4. 1 SR Specimen dimensions and loading conditions (Modified from DiJon Inc., 2009) .....	15
Figure 4. 2 Correction factor definition based on Load-CMOD plot.....	16
Figure 4. 3 SNBD Specimen dimensions and loading conditions for mode I and mode II or mixed mode I-II, respectively .....	19
Figure 4. 4 Diametral Compression Test Specimen dimensions and loading conditions .....	21
Figure 4. 5 CCNBD Specimen dimensions and loading conditions .....	23
Figure 4. 6 Dimensional restrictions for CCNBD Method (Fowell, 1993).....	25
Figure 4. 7 Modified ring test specimen dimensions and loading configuration .....	25
Figure 4. 8 Brazilian disc specimen dimensions and loading condition .....	27
Figure 4. 9 FBD specimen dimensions and loading conditions .....	29
Figure 4. 10 SCB specimen dimensions and loading conditions .....	31
Figure 4. 11 CNSCB Specimen dimensions and loading conditions .....	32
Figure 4. 12 CB Specimen dimensions and loading conditions.....	34
Figure 4. 13 SECRBB Specimen dimensions and loading conditions.....	36
Figure 4. 14 A typical load-displacement curve (for $D=75\text{mm}$ , $d=8\text{ mm}$ , $2\alpha=35^\circ$ ) .....	133
Figure 4. 15 $K_I$ versus relative crack length (for $D=75\text{ mm}$ , $d=8\text{ mm}$ , $2\alpha=25^\circ$ ).....	133
Figure 5. 1 J-integral contour path surrounding a crack-tip .....	46
Figure 5. 2 Central crack in infinite plate model.....	47



Figure 5. 3 Infinite plate with hole model .....	49
Figure 6. 1 Geometry and boundary conditions of FBD Specimen .....	51
Figure 6. 2 Boundary conditions of Option 1.....	53
Figure 6. 3 (S11) and vertical (S22) stress distribution for Option 1 .....	53
Figure 6. 4 Horizontal (U1) and vertical (U2) displacement contours for Option 1	53
Figure 6. 5 Boundary conditions of Option 2.....	55
Figure 6. 6 Horizontal (S11) and vertical (S22) stress distribution for Option 2.....	55
Figure 6. 7 Horizontal (U1) and vertical (U2) displacement contours for Option 2	55
Figure 6. 8 Boundary conditions of Option 3.....	56
Figure 6. 9 Horizontal (S11) and vertical (S22) stress distribution for Option 3.....	57
Figure 6. 10 Horizontal (U1) and vertical (U2) displacement contours for Option 3 .....	57
Figure 6. 11 Boundary conditions of Option 4.....	58
Figure 6. 12 Horizontal (S11) and vertical (S22) stress distribution for Option 4...	58
Figure 6. 13 Horizontal (U1) and vertical (U2) displacement contours for Option 4 .....	58
Figure 6. 14 Specimen models in various thicknesses in 3D .....	59
Figure 6. 15 Path used in stress distribution graphs .....	60
Figure 6. 16 S11 and S22 versus $y_i/R$ graphs, respectively .....	61
Figure 6. 17 $S11*t$ and $S22*t$ versus $y_i/R$ graphs .....	62
Figure 6. 18 Specimen sketch in different radii .....	63
Figure 6. 19 Figure S11 versus $y_i/R$ and S22 versus $y_i/R$ graphs, respectively .....	64
Figure 6. 20 $S11*D$ and $S22*D$ versus $y/R$ graphs.....	65
Figure 6. 21 Number of elements along the central line for different mesh intensities .....	66
Figure 6. 22 Convergence in stresses with increasing mesh intensity along vertical center line .....	67
Figure 6. 23 Horizontal (U1) displacement contours for 70 elements and 200 elements respectively .....	68
Figure 6. 24 Vertical (U2) displacement contours for 70 elements and 200 elements respectively.....	68
Figure 6. 25 S11 and S22 stresses for models having $\mu=0.0$ and $\mu=50$ , respectively .....	69

Figure 6. 26 Stresses along the horizontal distance through the flattened end .....	69
Figure 6. 27 Horizontal (U1) displacement contours for having .....	70
Figure 6. 28 Vertical (U2) displacement contours for having friction coefficients of 0.0 and 50 respectively.....	70
Figure 6. 29 Stress intensity factor versus relative crack length for $\mu=0$ and $\mu=50$ . 71	
Figure 6. 30 Specimen sketch in different loading angles .....	71
Figure 6. 31 S11 versus y and S22 versus y graphs, respectively.....	72
Figure 6. 32 Normalized stress versus normalized vertical distance graphs.....	74
Figure 6. 33 Dimensionless principal stresses versus dimensionless vertical distance plot.....	75
Figure 6. 34 Dimensionless equivalent stress versus dimensionless vertical distance plot.....	76
Figure 6. 35 Contour integral region, crack tip and extension direction.....	77
Figure 6. 36 Stress intensity factor variation according to contour integral ring radius .....	78
Figure 6. 37 A typical cracked specimen geometry with mesh .....	79
Figure 6. 38 Crack tip elements and crack tip subtend angles .....	80
Figure 6. 39 Various mesh intensities at the contour integral region.....	80
Figure 6. 40 Stress intensity factor variation according to number of contours in contour integral region .....	81
Figure 6. 41 Dimensionless stress intensity factor versus relative crack length.....	82
Figure 6. 42 Maximum dimensionless stress intensity factor versus normalized vertical distance.....	84
Figure 7. 1 Geometry of MR Specimen .....	85
Figure 7. 2 Quarter model geometry considering symmetry along x and y axes.....	86
Figure 7. 3 Specimen models with various thicknesses in 3D.....	87
Figure 7. 4 S11 and S22 versus $y_i/R$ graphs, respectively.....	88
Figure 7. 5 S11*t and S22*t versus $y_i/R$ graphs .....	89
Figure 7. 6 Number of elements along the central line for different mesh intensities .....	90
Figure 7. 7 Convergence in stresses with increasing mesh intensity on vertical center line .....	91

Figure 7. 8 Horizontal (U1) displacement contours for 60 elements and 200 elements, respectively .....	92
Figure 7. 9 Vertical (U2) displacement contours for 60 elements and 200 elements, respectively.....	92
Figure 7. 10 Specimen sketch in different specimen radii .....	93
Figure 7. 11 S11 and S22 versus dimensionless vertical distance graphs, respectively.....	95
Figure 7. 12 S11*D and S22*D versus normalized distance graphs .....	96
Figure 7. 13 Specimen sketch in various central- hole radii .....	97
Figure 7. 14 S11 and S22 versus vertical distance graphs, respectively .....	98
Figure 7. 15 Various loading angles studied in analyses .....	99
Figure 7. 16 S11 and S22 versus vertical distance plots, respectively.....	100
Figure 7. 17 Mesh intensity in whole model and in contour integral region .....	101
Figure 7. 18 Stress intensity factor versus dimensionless crack length for various loading angles (for D = 75 mm and d = 15 mm).....	102
Figure 7. 19 $\Phi_{\max}$ versus relative crack length ( $a/R$ ) for various $d/D$ ratios .....	103
Figure 7. 20 3D graph and surface fitted for $\Phi_{\max}$ versus $\cos\alpha$ and $d/D$ .....	104
Figure 8. 1 UCS test specimen with circumferential extensometer before and after the test .....	106
Figure 8. 2 Brazilian disc specimen before and after the test .....	107
Figure 8. 3 Boring Machine (on the left) and polishing machine (on the right) ....	110
Figure 8. 4 Diametral line drawing with goniometer (on the left) and fixed disc on cutting machine with holding fixture (on the right) .....	110
Figure 8. 5 Cutting platform for half disc specimens (on the left).....	110
Figure 8. 6 Semi-circular bending specimens after cracking and fracturing .....	110
Figure 8. 7 Specimen coding; SCB: semi circular bending, .....	111
Figure 8. 8 Diametral line drawing with goniometer (on the left) and line perpendicular to diametral line drawing with goniometer and set-square (on the right).....	116
Figure 8. 9 A flat block with knife piece (on the left), horizontal plane measurement perpendicular to notch (on the center) and horizontal plane measurement parallel to notch (on the right).....	116

Figure 8. 10 Digital caliper adjustment (on the left) and plum-line and flat iron stick adjustment (on the right) .....	116
Figure 8. 11 Specimen placed exact location before cutting (on the left) and after cutting (on the right).....	116
Figure 8. 12 Plum-line and flat iron stick adjustment for the second notch (on the left), specimen placement (at the center) and prepared specimen (on the right)....	117
Figure 8. 13 Loaded specimen through diametral plane (on the left) and loading setup of CCNBD specimen with transducers (on the right).....	117
Figure 8. 14 CCNBD specimens after fracturing.....	117
Figure 8. 15 The CNBD specimen geometry with recommended test fixture (Fowell, 1995).....	118
Figure 8. 16 CCNBD specimen geometries in Fowell's graph.....	119
Figure 8. 17 Specimen coding; CCNBD: cracked chevron notched Brazilian disc, A: rock type (A for andesite and M for marble), 4: specimen number .....	119
Figure 8. 18 Flattening loading end with grinding machine .....	123
Figure 8. 19 Adjustment to get parallel loading ends .....	123
Figure 8. 20 FBD specimen under loading .....	123
Figure 8. 21 FBD specimens after fracturing.....	123
Figure 8. 22 Specimen coding; A: rock type (A for andesite), 75: specimen diameter, 00: central-hole diameter, 25: loading angle, 2: specimen number .....	124
Figure 8. 23 Lathe with drilling bit .....	129
Figure 8. 24 Drilled specimens .....	129
Figure 8. 25 MR specimen while loading .....	129
Figure 8. 26 MR specimens after fracturing .....	129
Figure 8. 27 Specimen coding; A: rock type (A for andesite), 54: specimen diameter, 08: central-hole diameter, 35: Loading Angle, 1: specimen number .....	130
Figure 9. 1 Average fracture toughness values of andesite for dimensionless vertical distance and various specimen diameters.....	138
Figure 9. 2 Variations of dimensionless mode I fracture toughness with dimensionless vertical distance for various diameters of FBD andesite rock cores .....	139
Figure 9. 3 Variations of dimensionless fracture toughness value with dimensionless thickness for the FBD andesite specimen .....	141

Figure 9. 4 Mode I fracture toughness versus loading rate for andesite FBD tests	142
Figure 9. 5 Variations of dimensionless fracture toughness value with loading angle in the andesite and marble FBD specimens .....	144
Figure 9. 6 Dimensionless fracture toughness value of andesite rock versus dimensionless vertical distance plot for various specimen diameter and central-hole diameter.....	145
Figure 9. 7 Dimensionless fracture toughness value of andesite rock versus dimensionless vertical distance plot with fitting equation .....	147
Figure 9. 8 $\Phi_c$ versus dimensionless vertical distance ( $D = 54$ mm) .....	148
Figure 9. 9 $\Phi_c$ versus dimensionless vertical distance ( $D = 75$ mm) .....	149
Figure 9. 10 $\Phi_c$ versus dimensionless vertical distance ( $D = 100$ mm).....	151
Figure 9. 11 Dimensionless fracture toughness value of andesite and marble rock types versus dimensionless vertical distance plot for proper specimen geometries in 75 mm diameter group .....	154
Figure A. 1 Stress Intensity Factor versus Crack Length plot .....	168
Figure B. 1 Thin sections of andesite .....	169

## LIST OF SYMBOLS AND ABBREVIATIONS

2D	: two dimensional
2S	: support span
3D	: three dimensional
$a$	: crack length (or notch length)
AND	: andesite
BAS	: basalt
BD	: Brazilian disc
CB	: chevron bend
CCNBD	: cracked chevron notched Brazilian disc
CNSCB	: chevron notched semi-circular bending
CSTBD	: cracked straight through Brazilian disc
$D$	: specimen diameter
$d$	: central-hole diameter
DC	: diametral compression
DIO	: diorite
DOL	: dolerite
DST	: dolostone
$E$	: elastic modulus
$F$	: applied load
FBD	: flattened Brazilian disc
$F_{\max}$	: maximum local load
$F_{\min}$	: minimum local load
$F_y$	: vertical load
$G$	: energy release rate
GRT	: granite
GRW	: greywacke
ISRM	: International Society for Rock Mechanics
$J$	: J integral

JST	: Johnstone
$K$	: stress intensity factor
$K_c$	: fracture toughness
$K_I$	: mode I stress intensity factor
$K_{Ic}$	: mode I fracture toughness
LEFM	: linear elastic fracture mechanics
LST	: limestone
MR	: modified ring
MRB	: marble
$r_i$	: central-hole radius
$R$	: specimen radius
SCB	: semi-circular bending
SCH	: schist
SECBD	: single edge crack Brazilian disk
SECRBB	: straight edge cracked round bar bending
SENRRB	: straight edge-notched round bar in bending
SNSCB	: straight notched semi-circular bending
SR	: short rod
SST	: sandstone
$t$	: specimen thickness
$w$	: specimen width
$y_i$	: vertical distance
$\Phi_c$	: dimensionless fracture toughness
$\Phi_{max}$	: dimensionless maximum stress intensity factor
$\alpha$	: half of the loading angle
$\beta$	: crack tip subtend angle
$\mu$	: friction coefficient
$\sigma$	: normal stress
$\sigma_1$	: maximum principal stress
$\sigma_3$	: minimum principal stress
$\tau$	: shear stress
$\nu$	: Poisson's ratio

# CHAPTER 1

## INTRODUCTION

### 1.1 General

Rock fracture mechanics is the science of describing how a crack initiates and propagates under applied loads in many engineering materials like ceramics, rocks, glasses and concretes. Rock fracture mechanics is generally applied in the field of earth sciences such as petroleum engineering, geological engineering, mining engineering and civil engineering.

Materials like ceramics, rocks, glasses and concretes behave as brittle and in brittle materials; the crack initiation is determined by using the linear elastic stress field around the crack tip. This application belongs to Linear Elastic Fracture Mechanics (LEFM) assumption. This assumption is valid, when plastic deformation around the crack is negligible.

### 1.2 Statement of the Problem and the Thesis Objective

Mode I fracture toughness determination is important in rock fracture mechanics to understand the behavior of crack in brittle materials. In order to assess fracture toughness values of brittle materials like rocks, International Society for Rock Mechanics (ISRM) suggests three methods which are short rod (SR) specimen (Ouchterlony, 1988), chevron bend (CB) specimen (Ouchterlony, 1988) and cracked chevron notched Brazilian disc (CCNBD) specimen (Shetty et al., 1985). However, performing these methods is really difficult. In addition to these methods, there are several methods introduced and developed to determine mode I fracture toughness value of rocks. Some of these methods have also some difficulties and limitations. The difficulties and limitations faced in performing all of these tests are covered in Chapter 4.



The aim of this study is to determine a simpler method which produces a mode I fracture toughness close to the suggested methods. In this study, to determine mode I fracture toughness of rocks flattened Brazilian disc method (FBD) and modified ring (MR) test were considered for their relative easiness in specimen preparation and testing. To confirm the validity of mode I fracture toughness values determined with these methods, the results were compared with those of semi-circular bending (SCB) method, which is one of the favorable methods in rock fracture testing, and results of CCNBD method which is one of the suggested methods by ISRM.

### **1.3 Methodology**

In experimental studies, during mode I fracture testing, pink colored Ankara andesite and white colored Afyon marble were used. Both rocks are used in construction of pavements, roadways, stairs etc. Therefore, it is important to determine mode I fracture toughness values of these rocks to have an idea on their behavior against crack initiation and propagation. Andesite is an igneous rock whereas marble is a metamorphic one. This variation helps us to examine the variation in mode I fracture toughness according to the rock type. Quarries of the andesite and the marble rocks are not so far from the laboratory where the experimental work was conducted therefore achieving these rock types is convenient.

In investigation of FBD and MR methods, firstly, mechanical properties of the rocks were determined. Then these values were used as input parameters in stress analyses. Stress analyses were performed by using ABAQUS finite element package program and the results gave an idea about location of crack initiation in the materials. Stress distributions in models were examined for various specimen geometries. Proper geometries for fracture tests were determined with numerical modeling. By considering proper geometry ranges, andesite and marble specimens were prepared and tested with the methods above. Specimen geometries were modeled with ABAQUS for stress intensity factor computations. After finding stress intensity factors and experimental load at the onset of stable crack propagation in Brazilian discs, fracture toughness values were evaluated.

In numerical modeling, effects of boundary conditions, elastic constants, thickness, diameter, central-hole diameter, mesh intensity, friction coefficient between specimen and loading platens, and loading angle of the specimen models were considered for stress analysis and stress intensity factor evaluation.

In fracture testing on andesite, various specimen geometries having different central-hole diameters, outer diameters, thicknesses, loading angles were investigated. Effect of loading rate variations on mode I fracture toughness for FBD method was studied.

The mode I fracture toughness values of andesite and marble determined from the FBD method and MR test with the proposed geometrical parameters were compared with the SCB and CCNBD methods and the results were discussed.

## **1.4 Sign Convention**

Although in rock mechanics, compressive stresses are accepted to be positive and tensile stresses are accepted to be negative, in LEFM and in ABAQUS finite element program. Compression is negative and tension is positive. LEFM and the program assumptions were applied in this work, i.e., compression is negative while tension is positive.

## **1.5 Outline of the Thesis**

This thesis is organized into ten (10) chapters and begins with a brief introduction to rock fracture mechanics, statement of the problem, thesis objective, and methodology in studies. Chapter 2 covers the history and the terminology of the fracture mechanics. Chapter 3 continues with application areas of rock fracture mechanics. Mode I fracture toughness tests used in rock cores are summarized according to the load application method, and their advantages, drawbacks and limitations are presented in Chapter 4. Explanation of ABAQUS program used in analyses and verification examples performed with ABAQUS are given in Chapter 5. Numerical analyses of FBD method and MR test are given in Chapter 6 and 7, respectively. In Chapter 8, experimental studies including uniaxial compressive strength test, Brazilian test, and fracture toughness tests with SCB, CCNBD, and

FBD and MR methods are presented in detail in terms of specimen preparation, loading setup and fracture toughness evaluation. Chapter 9 covers the results and discussions. In Chapter 10 conclusions drawn from this research study and the recommendations are presented.

## CHAPTER 2

### ROCK FRACTURE MECHANICS

#### 2.1 History of Fracture Mechanics for Brittle Materials

The earliest works considering fracture mechanics in brittle materials belonged to Griffith (1920) (Figure 2. 1). He was a British aeronautical engineer and while he was working at the Royal Aircraft Establishment in Farnborough, he investigated the fracture of glass sheets.



Figure 2. 1 Alan Arnold Griffith

The Griffith theory began from hypothesis that brittle materials include elliptical microcracks and high stress concentrations occur at these cracks' tips. He developed a relationship between crack length ( $a$ ), surface energy connected with traction-free crack surfaces ( $2\gamma$ ) and applied stress:  $\sigma^2=(2\gamma E)/(\pi a)$ . (Ceriolo and Tommaso, 1998)

Although Griffith's theory was so significant, there were some limitations on his theory. Griffith's theory predicted that compressive strength of a material is eight times greater than its tensile strength. However, this case cannot be always valid for some materials. Therefore, Irwin (1957), a professor of mechanical engineering at Lehigh University, provided the extension of Griffith's theory to an arbitrary crack

and proposed the criterion for a growth of this crack. According to the criterion, the strain energy release rate is the total energy absorbed during cracking per unit increase in crack length and per unit thickness. Moreover, Irwin explained that the stress field around the crack tip is evaluated by the stress intensity factor.

Applications of fracture mechanics to brittle materials like rocks follow with significant delay those to ductile materials like metals. The rock fracture problem takes up a well-known position regarding underground constructions such as mines, excavations, tunnels etc. to the point that in the early sixties the first application of Griffith's model to stone and concrete-like materials took place. Mc Clintock and Walsh (1962) established the friction between crack faces, whereas Kaplan (1961) focused on the possibility of applying linear elastic fracture mechanics to concrete. Early research about rocks was performed by Bieniawski and Hoek (1965), in South Africa, where mine failures were urgent problems to be solved (Ceriolo and Tommaso, 1998).

## 2.2 Stress Intensity Factor

The stress intensity factor,  $K$  (after Kies, a colleague of Irwin, 1952-1954), defines the magnitude of the local stresses around the crack tip. This factor depends on loading, crack size, crack shape, and geometric boundaries. Engineers mostly pay attention to the maximum stress near the crack tip and whether it surpasses the fracture toughness. If  $K$  exceeds the toughness, crack initiates and propagates.

Stress intensity factor is a stress-based measure and it is calculated mainly from the expression below:

$$K = \sigma \sqrt{\pi \times a} \times f\left(\frac{a}{w}\right) \quad (2.1)$$

where:

$\sigma$  : remote stress applied to component

$a$  : crack length

$f(a/w)$ : correction factor that depends on specimen and crack geometry

$w$  : specimen width

## 2.3 Fracture Toughness

Fracture toughness is termed as critical value of stress intensity factor and denoted as  $K_{Ic}$ . It shows the resistance of the materials to fracture. It is a material property, and generally, it depends on temperature, environment, loading rate, the composition of the material and its microstructure together with geometric effects.

## 2.4 Linear Elastic Fracture Mechanics

Linear Elastic Fracture Mechanics (LEFM) assumes that the material is isotropic and linear elastic. Isotropic and linear elastic mean that the material properties are independent of direction and these materials have only two independent elastic constants which are elastic modulus ( $E$ ) and Poisson's ratio ( $\nu$ ).

In LEFM assumption, the stress field near the crack tip is calculated by considering the theory of elasticity and this assumption is valid only when the inelastic deformation is smaller than the size of the crack.

## 2.5 Fracture Modes

Typically, cracks can initiate and propagate in three ways in a material. These are mode I, mode II and mode III (Figure 2. 2).

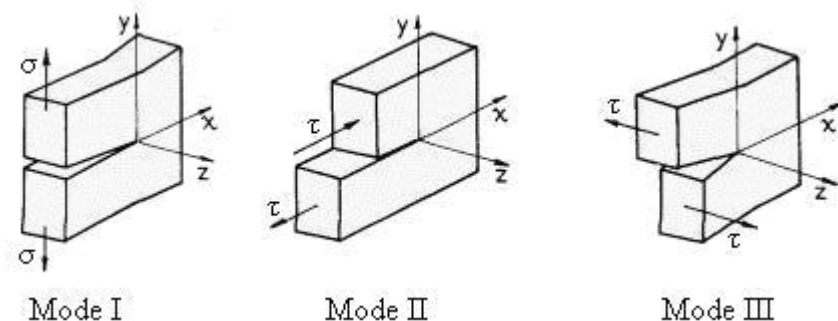


Figure 2. 2 Fracture modes (Key to Metals Database, 2010)

Mode I: In mode I, the crack faces separate in a direction normal to the plane of the crack. It is also called the tensile opening mode.

Mode II: the crack faces are mutually in the direction normal to the crack front in mode II and it is termed as in-plane sliding or shear mode,

Mode III: the tearing or out of plane mode is mode III. Namely, the crack faces are sheared parallel to the crack front in mode III.

These crack deformations can occur separately or in any combinations. Combinations of the modes are called as mixed mode.

In brittle materials, mode I is the essential failure mode since brittle materials are weak in tension.

## 2.6 Crack Tip Stress Component for Mode I

The crack tip stress components of a brittle material can be expressed for Mode I as follows (Figure 2. 3):

$$\sigma_{xx} = \frac{K_I}{\sqrt{2\pi r}} \cos\left(\frac{\theta}{2}\right) \left[1 - \sin\left(\frac{\theta}{2}\right) \sin\left(\frac{3\theta}{2}\right)\right] \quad (2. 2)$$

$$\sigma_{yy} = \frac{K_I}{\sqrt{2\pi r}} \cos\left(\frac{\theta}{2}\right) \left[1 + \sin\left(\frac{\theta}{2}\right) \sin\left(\frac{3\theta}{2}\right)\right] \quad (2. 3)$$

$$\sigma_{zz} = \begin{cases} 0 & \text{(Plane Stress)} \\ \nu(\sigma_{xx} + \sigma_{yy}) & \text{(Plane Strain)} \end{cases} \quad (2. 4)$$

$$\tau_{xy} = \frac{K_I}{\sqrt{2\pi r}} \cos\left(\frac{\theta}{2}\right) \sin\left(\frac{\theta}{2}\right) \cos\left(\frac{3\theta}{2}\right) \quad (2. 5)$$

$$\tau_{yz} = 0 \quad (2. 6)$$

$$\tau_{zx} = 0 \quad (2. 7)$$

where,

$K_I$  : Stress intensity factor in mode I

$\sigma$  : normal stresses

$\tau$  : shear stresses

$r$  : distance from crack tip

$\theta$  : angle from horizontal (x-direction)

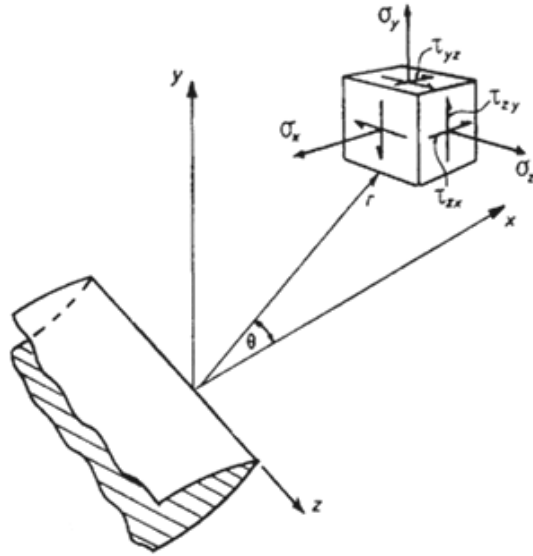


Figure 2. 3 Location of local stresses near a crack tip (Key to Metals Database, 2010)

## 2.7 Crack Tip Displacement Components for Mode I

The crack tip displacement components of a brittle material can be expressed for mode I as follows:

$$u_x = \frac{K_I}{2\mu} \sqrt{\frac{r}{2\pi}} \cos\left(\frac{\theta}{2}\right) \left[ \kappa - 1 + 2 \sin^2\left(\frac{\theta}{2}\right) \right] \quad (2.8)$$

$$u_y = \frac{K_I}{2\mu} \sqrt{\frac{r}{2\pi}} \sin\left(\frac{\theta}{2}\right) \left[ \kappa + 1 - 2 \cos^2\left(\frac{\theta}{2}\right) \right] \quad (2.9)$$

$$u_z = 0 \quad (2.10)$$

where,

$$\kappa = \begin{cases} \frac{3-\nu}{1+\nu} & \text{(Plane Stress)} \\ 3-4\nu & \text{(Plane Strain)} \end{cases} \quad (2.11)$$

$K_I$  : stress intensity factor in mode I

$u$  : crack tip displacement component

$\mu$  : shear modulus

$r$  : distance from crack tip

$\theta$  : angle from horizontal (x-direction)



## **CHAPTER 3**

### **SOME APPLICATION AREAS OF ROCK FRACTURE MECHANICS**

Rocks are complex materials and they may contain natural fractures or flaws. Under such circumstances, the conventional design criteria, which are based on uniaxial compressive strength, tensile strength, shear strength etc., are not suitable. Instead of conventional methods, fracture mechanics approach could be considered.

Some application areas of rock fracture mechanics can be listed as hydraulic fracturing, rock blasting, rock cutting, underground coal mine dust control, underground opening design, and comminution in mineral processing

#### **3.1 Hydraulic Fracturing**

Hydraulic fracturing is a technique applied to form fractures that extend from a borehole into rock formations. A fluid is pumped into the borehole or well. Afterwards, when the pressure of this fluid exceeds the fracture gradient of the rock formation a hydraulic fracture is created and to keep fractures open proppants (like sand) are used (Figure 3. 1).

This method is used to restore or increase the rate at which fluids like water, oil or gas can be produced from the reservoir formations. Application areas of the hydraulic fracturing in industry are stimulating production from oil and gas wells and ground water wells, and inducing rock to cave in mining. According to Watson (1910), the first industrial use of hydraulic fracturing was in 1903 to separate granite blocks from bedrock.

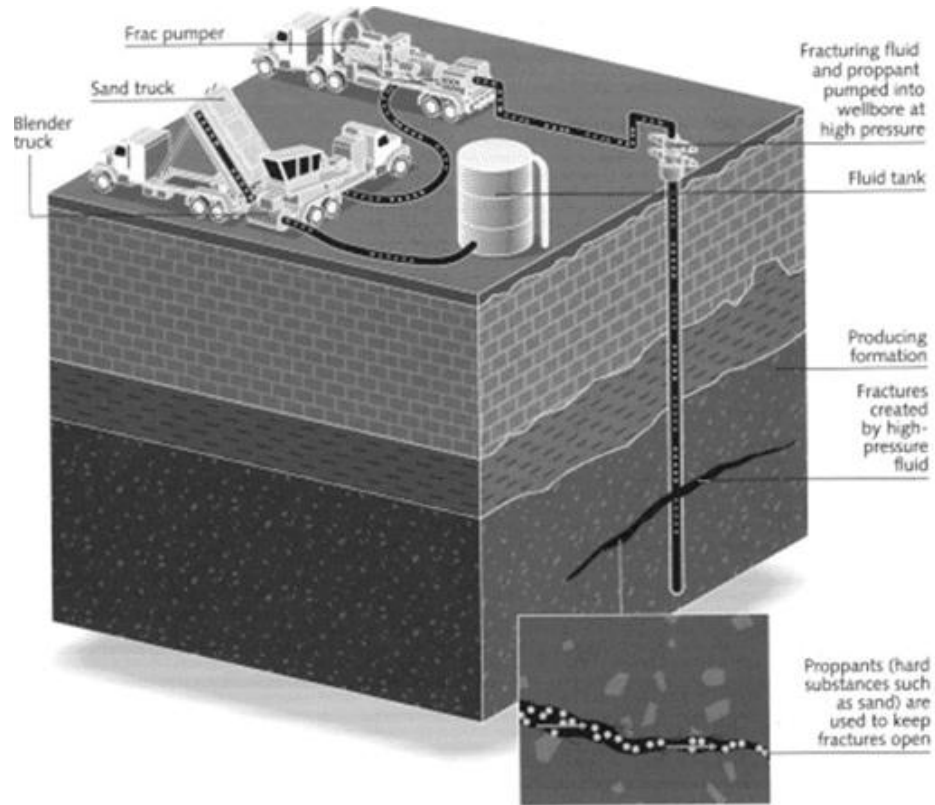


Figure 3. 1 Hydraulic fracturing method (Boss International, 2009)

### 3.2 Rock Blasting

In rock blasting, while fractures propagate through the rock, energy is absorbed near the extending crack tips to form new fracture surfaces. The energy consumed per unit fracture surface is defined as energy release rate and the critical energy release rate manages the fracture propagation. The relation between the energy release rate and the stress intensity factor is given in equations below. This application was firstly realized by Bieniawski (1967).

$$G = \frac{1}{E} K_I^2 \quad \text{for plane stress} \quad (3.1)$$

$$G = \frac{1-\nu^2}{E} K_I^2 \quad \text{for plane strain}$$

where,

$G$  : energy release rate (MPa.m)

$E$  : elastic modulus (MPa)

$\nu$  : Poisson's ratio

$K_I$  : stress intensity factor for mode I (MPa $\sqrt{m}$ )

### 3.3 Rock Cutting

Mechanical breakage can be performed by indenters or drag bits. While indenter applies a force predominantly, perpendicular to the rock surface, drag bit applies a force approximately parallel to the rock surface (Figure 3. 2). In both types, mode I (tensile) fractures are formed near the tool tip and propagate to form chips in front of the tool so fracture mechanics approach can be used in this process. Finite element simulation of rock cutting was conducted early by Saouma and Kleinosky (1984).

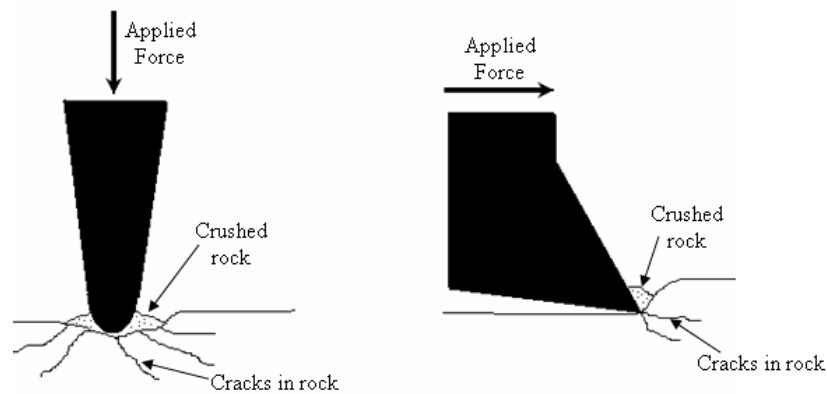


**Figure 3. 2 An indenter and a drag bit, respectively  
(Modified from Hood and Roxborough, 1992)**

### 3.4 Underground Coal Mine Dust Control

In underground coal mines, coal dust formation is not required since it may cause pneumoconiosis and explosions. In order to reduce coal dust, fine fragment formation must be minimized and this is related to fracture mechanics. Therefore, it is significant to study the mechanics of fracture propagation and quantify the fracture process. This approach was adopted by Zipf et al. (1986). They used mixed

mode crack propagation principles to include coal fracture toughness as a parameter controlling unstable crack growth.

### **3.5 Underground Opening Design**

Fracture mechanics may be considered in estimating stability of underground openings if there are fracture zone formations around openings and fracture mechanics approach may help evaluation of the support system requirements. If fracture zone extension can be predicted correctly, by knowing the in-situ properties, support loading can be determined. Pathan (1987) tried to apply fracture mechanics in estimating stability of underground openings in various rock types.

### **3.6 Comminution in Mineral Processing**

Comminution is a process to break rock in to required sizes. In the mineral processing plant, comminution occurs in two stages which are crushing and grinding. To obtain rocks in required sizes, the relationship between the applied energy and the resultant size or surface area is concerned.

Griffith (1921) showed that materials fail by crack propagation when this is energetically feasible, i.e. when the energy released by relaxing the strain energy is greater than the energy of the new surface produced. Brittle materials relieve the strain energy mainly by crack propagation, whereas "tough" materials can relax strain energy without crack propagation by the mechanism of plastic flow, where the atoms or molecules slide over each other and energy is consumed in distorting the shape of the material. Crack propagation can also be inhibited by encounters with other cracks or by meeting crystal boundaries. Fine-grained rocks, such as taconites, are therefore usually tougher than coarse-grained rocks (Wills and Napier-Munn, 2006).

## **CHAPTER 4**

### **MODE I FRACTURE TOUGHNESS TESTS USED IN ROCK CORES**

In rock fracture toughness testing, core specimens are generally preferred because the rock is readily obtainable in the form of core pieces and after coring it needs only little machining. By cutting and grinding rock cores; rods, half and whole discs are prepared for fracture toughness tests.

Rock is a brittle material and since all of the brittle materials are weak in tension, generally mode I (tensile mode) is the most critical loading mode in rock mechanics applications. Several methods have been proposed in order to determine mode I fracture toughness value. These methods could be classified in terms of their loading conditions. In general, load to achieve opening mode crack propagation can be applied to the specimen by direct tension, compression, and bending.

#### **4.1 Tests Applied with Tensile Load**

Due to the practical difficulties, direct tensile load application to the specimens is not a common practice among fracture tests. Short rod (SR) method is one of the suggested methods by ISRM (2007) and tensile load is directly applied perpendicular to the initial notch plane in SR method.

##### **4.1.1 Short Rod Method**

Short rod (SR) method was introduced by Barker (1977), and it became a suggested method by ISRM after the study of Ouchterlony (1987, 1988). This method is used to evaluate just mode I fracture toughness value.

In specimen preparation, a rectangular grip groove is machined in one end of the short rod specimen and two slots, which must form a triangular ligament, are cut at

opposing angles (Figure 4. 1). The specimen geometry is restricted in dimensions listed in Table 4. 1.

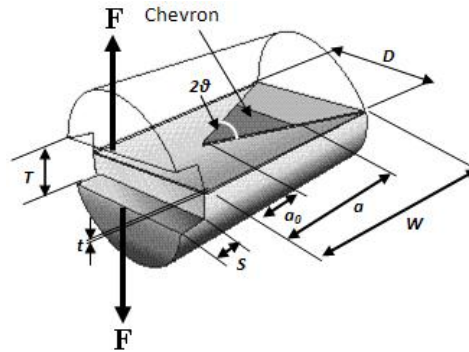


Figure 4. 1 SR Specimen dimensions and loading conditions (Modified from DiJon Inc., 2009)

Table 4. 1 SR Specimen dimensions (Ouchterlony, 1988)

Symbol	Definition	Value	Tolerance
$D$	Specimen diameter	$D$	$>10 \times$ grain size
$W$	Specimen length	$1.45D$	$\pm 0.02$
$\theta$	Subtended chevron angle	$54.6^\circ$	$\pm 1.0^\circ$
$a_0$	Distance to Chevron notch tip	$0.48D$	$\pm 0.02D$
$W-a_0$	Chevron length	$0.97D$	$\pm 0.02D$
$t$	Notch width	$\leq 0.03D$ or $1\text{mm}^*$	

\* whichever is greater

Fracture toughness evaluation by using SR method is performed in two levels. In Level 1 testing, maximum load during bending is recorded and in Level 2 testing, load and displacement measurements are taken into account to correct the fracture toughness value.

Fracture toughness is achieved by considering equation, which was derived by ISRM (2007) for Level 1 testing, is in below:

$$K_{SR} = C_K 24.0 F_{\max} / D^{1.5} \quad (4. 1)$$

where,

$K_{SR}$  : fracture toughness (MPa $\sqrt{\text{m}}$ )

$F_{\max}$  : failure load (MN)

$D$  : specimen diameter (m)

$C_K$  : correction factor to account for the size variation of the specimen;

$$C_K = 1 - \frac{0.6\Delta W}{D} + \frac{1.4\Delta a_0}{D} - 0.01\Delta\theta$$

$\Delta W$  : Variation in specimen height (m)

$\Delta a_0$  : Initial position of chevron notch apex (m)

$\Delta\theta$  : Chevron notch angle (in radians)

After determining fracture toughness value with Level 1 testing, a nonlinearity correction factor is computed to estimate corrected fracture toughness value. Correction factor is calculated by considering Load-CMOD curves (Figure 4. 2) and equation below:

$$K_{SR}^c = \sqrt{\frac{1+p}{1-p}} K_{SR} \quad \text{and} \quad p = \Delta x_0 / \Delta x \quad (\text{Figure 4. 2}) \quad (4. 2)$$

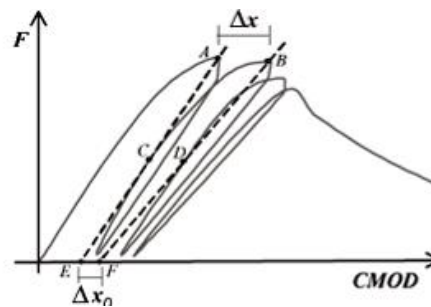


**Figure 4. 2** Correction factor definition based on Load-CMOD plot (Sousa and Bittencourt, 2001)

Fracture toughness values of some rock types determined by using SR method are listed in Table 4. 2.

**Table 4. 2 Fracture toughness values of some rock types determined by using SR method**

<b>Rock</b>	<b>Location or Name</b>	<b><math>K_{Ic}</math> (MPa√m)</b>	<b><math>K_{Ic}(\text{corrected})</math> (MPa√m)</b>	<b>Reference</b>
<b>Tuff</b>	Ogino	1.02±0.05	1.06±0.05	Matsuki et al., 1987
<b>Limestone</b>	Irondequoit	1.36	-	Gunsallus & Kulhawy, 1984
<b>Limestone</b>	Shelly	1.40±0.03	1.44±0.04	Meredith, 1983
<b>Limestone</b>	Klinthagen	1.41±0.19	1.87±0.25	Ouchterlony, 1987
<b>Sandstone</b>	Grimsby	1.47	-	Gunsallus & Kulhawy, 1984
<b>Granite</b>	Merrivale	1.50±0.10	1.80±0.13	Meredith, 1983
<b>Sandstone</b>	Älvdalen	1.54±0.08	1.91±0.14	Ouchterlony, 1987
<b>Granite</b>	Pink	1.58±0.08	1.85±0.06	Meredith, 1983
<b>Granite</b>	Westerly	1.64±0.03	1.82±0.07	Meredith, 1983
<b>Dolostone</b>	Falkirk	1.66	-	Gunsallus & Kulhawy, 1984
<b>Dolostone</b>	Kankakee	1.66	-	Gunsallus & Kulhawy, 1984
<b>Granite</b>	Kråkemåla	1.69±0.17	2.22±0.24	Ouchterlony, 1987
<b>Dolostone</b>	Oatka	1.78	-	Gunsallus & Kulhawy, 1984
<b>Dolostone</b>	Markgraf	1.80	-	Gunsallus & Kulhawy, 1984
<b>Granite</b>	Strath Halladale	1.80±0.10	2.19±0.11	Meredith, 1983
<b>Marble</b>	Ekeberg	1.83±0.35	2.25±0.36	Ouchterlony, 1987
<b>Sandstone</b>	Pennant	1.98±0.06	2.56±0.07	Meredith, 1983
<b>Granite</b>	Stripa	2.01±0.14	2.36±0.13	Sun & Ouchterlony, 1986
<b>Granite</b>	Westerly	2.04±0.05	2.27±0.03	Ouchterlony, 1987
<b>Limestone</b>	Reynales	2.06	-	Gunsallus & Kulhawy, 1984
<b>Granite</b>	Stripa	2.37±0.15	2.70±0.27	Ouchterlony, 1987
<b>Granite</b>	Råsjö	2.37±0.32	2.80±0.33	Ouchterlony, 1987
<b>Dolostone</b>	Romeo	2.47	-	Gunsallus & Kulhawy, 1984
<b>Dolerite</b>	Whin Sill	2.86±0.12	3.26±0.09	Meredith, 1983
<b>Granodiorite</b>	Finnsjön	2.95±0.11	3.35±0.08	Ouchterlony, 1987

The core axes should be adjusted either parallel or perpendicular to any anisotropy planes like bedding planes. Application of this method is complicated since lots of steps must be followed to achieve the test. Since tensile load is directly applied perpendicular to the initial notch plane, this may result in bonding failures at the specimen-loading platen contacts, especially for hard rock types.



## 4.2 Tests Applied with Compressive Load

Disc type specimen (with or without notch or hole) loaded with compression through its diametral plane fails in tension if crack initiates from the center of the disc specimen. When crack propagation starts from the center, mode I failure is seen through the diametral plane. To achieve central crack initiation, various methods were studied. They could be listed chronologically as follows:

- Cracked straight through Brazilian disc (CSTBD) method (Awaji and Sato, 1978)
- Diametral compression (DC) test (Szendi-Horvath, 1980a)
- Cracked chevron notched Brazilian disc (CCNBD) method (Shetty et al., 1985)
- Modified ring (MR) test (Thiercelin and Roegiers, 1986)
- Brazilian disc (BD) test (Guo et al., 1993)
- Flattened Brazilian disc (FBD) method (Wang and Xing, 1999)

### 4.2.1 Cracked Straight Through Brazilian Disc Method

Cracked straight through Brazilian disc (CSTBD) method is also named as straight notched Brazilian disc (SNBD) method. It was initially used by Awaji and Sato (1978). Atkinson et al. (1982) formulated stress intensity factor for this model geometry. This method allows testing under mode I, mode II and mixed mode I-II loading conditions by using the same specimen arrangement and the same experimental setup.

A straight notch is opened to circular disc with drill bit and wire saw in specimen preparation. Notched specimen is loaded through its diametral plane. Notch direction is selected according to required loading mode. If mode I fracture toughness is going to be calculated, the notch must be perpendicular to tangent of loading ends of the specimen (Figure 4. 3, (a)). If mode II or mixed mode I-II fracture toughness is going to be studied, the angle ( $\alpha$ ) must be different from  $90^\circ$  and  $180^\circ$  (Figure 4. 3, (b)).

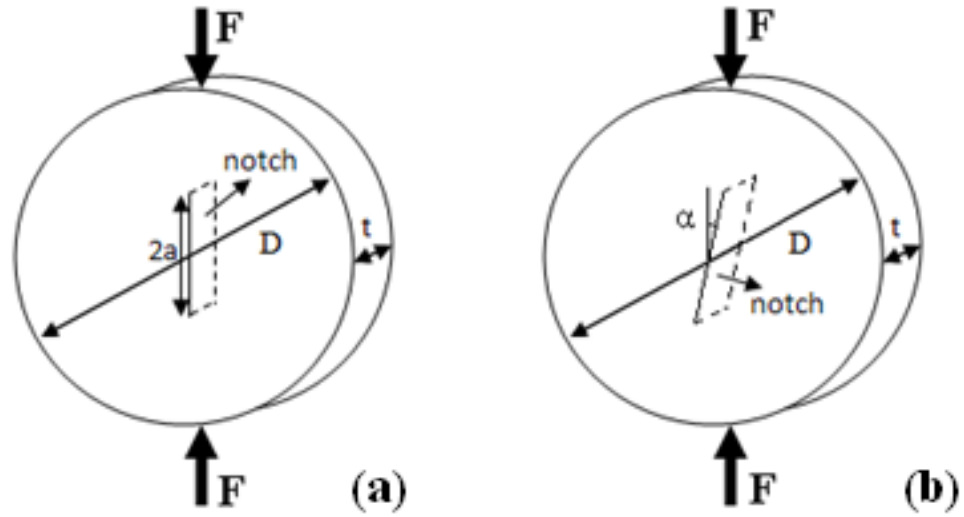


Figure 4. 3 SNBD Specimen dimensions and loading conditions for mode I and mode II or mixed mode I-II, respectively

The expression below is used in fracture toughness computation of SNBD:

$$K_I = \frac{F\sqrt{a}}{\sqrt{\pi R t}} N_I \quad (4.3)$$

where,

- $K_I$  : Stress intensity factor (MPa $\sqrt{m}$ )
- $F$  : Failure load (MN)
- $a$  : Notch length (m)
- $R$  : Specimen radius (m)
- $t$  : Specimen thickness (m)
- $N_I$  : Dimensionless coefficient which depends on  $a/R$  and orientation angle ( $\alpha$ )

$$N_I = 1 - 4 \sin^2 \alpha + 4 \sin^2 \alpha \left( -4 \cos^2 \alpha \left( \frac{a}{R} \right)^2 \right) \quad (4.4)$$

Table 4. 3 shows the fracture toughness values of some rocks calculated by using SNBD method.

**Table 4. 3 Fracture toughness values of some rocks analyzed by using SNBD method**

<b>Rock</b>	<b>Location or Name</b>	<b><math>K_{Ic}</math> (MPa<math>\sqrt{m}</math>)</b>	<b>Reference</b>
<b>Antler Sandstone</b>	Ardmore, Oklahoma	0.0055 $\pm$ 0.0015	Krishnan et al., 1998
<b>Limestone</b>	Central Province of Saudi Arabia	0.35 (for D=84mm)	Khan & Al-Shayea, 2000
<b>Limestone</b>	Central Province of Saudi Arabia	0.42 (for D=98mm)	Khan & Al-Shayea, 2000
<b>Limestone</b>	Central Province of Saudi Arabia	0.42 (for D=98mm)	Khan & Al-Shayea, 2000

In study of Krishnan et al. (1998), they concluded that the SNBD method was the most convenient method when soft sandstone was considered because mode I, mode II and mixed mode I-II loading conditions could be easily achieved with the same setup. In addition, effect of anisotropy like bedding planes could be omitted by adjusting the notch orientation in anisotropic area.

#### **4.2.2 Diametral Compression Test**

Diametral compression (DC) method is also termed as single edge crack Brazilian disk (SECBBD) method (Altındağ, 2000). This method was developed by Szendi-Horvath (1980b). This test is used only to determine mode I fracture toughness value.

To achieve DC test, a straight notch is cut along the diameter on one face of the disc type specimen. After opening the notch, disc is loaded through the diametral plane and the notch remains parallel to the loading line or loading strip (Figure 4. 4). In the experiment, in order to avoid load concentration on specimen's loaded ends, the platens used for loading may be covered with a soft rubber sheath or with felt, or the loading ends of the specimen may be flattened.

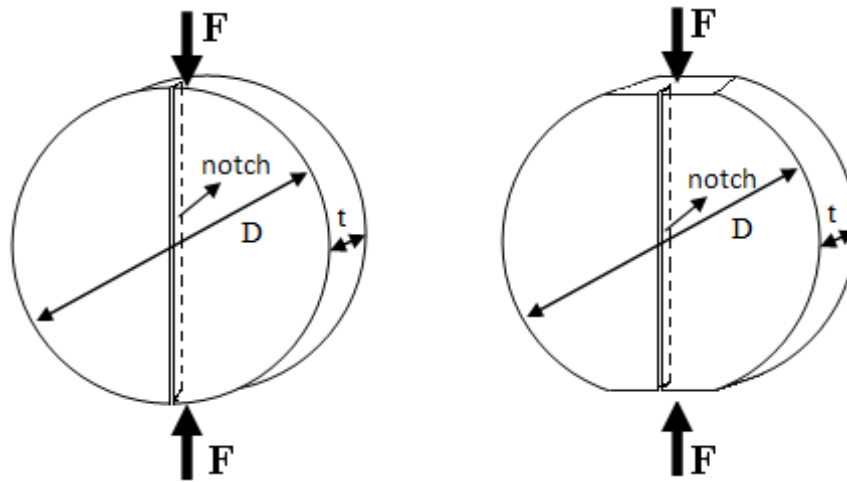


Figure 4. 4 Diametral Compression Test Specimen dimensions and loading conditions for line loading and strip loading, respectively

The fracture toughness can be calculated by using the equations below:

$$\text{For line loading } K_{Ic} = \frac{1.264 \times F \times \sqrt{a}}{B \times D} \quad (4.5)$$

$$\text{For strip loading } K_{Ic} = \frac{1.264 \times \left( \sin 2\alpha - \alpha \right) \times F \times \sqrt{a}}{B \times t} \quad (4.6)$$

where,

- $K_{Ic}$  : fracture toughness (MPa $\sqrt{m}$ )
- $F$  : load at failure (MN)
- $a$  : notch length (m)
- $t$  : length of flat loading surface (m)
- $B$  : disc thickness (m)
- $D$  : disc diameter (m)
- $\alpha$  :  $\sin^{-1} \left( \frac{a}{D} \right)$  (in radians)

Fracture toughness values of some rock types evaluated by using DC test are tabulated in Table 4. 4

**Table 4. 4 Fracture toughness values of some rocks determined by using DC test**

Rock	Location or Name	$K_{Ic}$ (MPa $\sqrt{m}$ )	Reference
Coal	Cadley Hill Coal Mine	0.129 $\pm$ 0.017	Singh & Pathan, 1988
(Black Coking) Coal	New South Wales	0.219 $\pm$ 0.028	Szendi-Horvath, 1982
Siltstone	-	0.800	Singh & Pathan, 1988
Marble	Muğla	0.939	Altındağ, 2000
Sandstone	Ryefield	1.040	Singh & Pathan, 1988
Marble	Muğla	1.187	Altındağ, 2000
Granite	-	1.650	Singh & Pathan, 1988
Marble	Izmir, Torbalı	1.739	Altındağ, 2000
Basalt	-	1.800	Singh & Pathan, 1988
Limestone	Fethiye	2.177	Altındağ, 2000
Limestone	Isparta	2.478	Altındağ, 2000
Sandstone	Isparta	2.850	Altındağ, 2000
Andesite	Isparta	2.920	Altındağ, 2000

According to previous studies on DC test, the fracture toughness determination for coal, rocks and many brittle materials is possible with this method. Fracture toughness value is independent of notch length ( $a$ ) and normalized notch length ( $a/B$ ). To obtain representative results with this test, thickness to diameter ratio ( $B/D$ ) must be greater than 0.8.

#### 4.2.3 Cracked Chevron Notched Brazilian Disc Method

Cracked chevron notched Brazilian disc (CCNBD) method is also expressed as chevron-notched Brazilian disc (CNBD) method. CCNBD specimens were introduced by Shetty et al. (1985) to measure the fracture toughness of ceramics. CCNBD specimen can be used to determine fracture toughness in mode I, mode II and mixed mode (mode I-II).

To prepare a CCNBD specimen, circular cuts are opened to the centers of both sides of the disc shaped specimen. Specimen is loaded in compression along the diametral plane (Figure 4. 5). Fracture toughness value is computed by an equation which is based on the dimensionless stress intensity factor. Dimensionless stress intensity factor is calculated by using numerical methods and an equation can be derived by fitting the numerical results. Mode I fracture toughness value is computed with the equation:

$$K_{Ic} = \frac{F_{max}}{t\sqrt{R}} Y_{min}^* \quad (4.7)$$

where,

$K_{Ic}$  : Fracture toughness (MPa $\sqrt{m}$ )

$F_{max}$  : Failure load (MN)

$R$  : Specimen radius (m)

$t$  : Specimen thickness (m)

$Y_{min}^*$  : Critical dimensionless stress intensity factor ( $Y_{min}^* = ue^{v\alpha_1}$ )

$u$  and  $v$ : constants determined by  $\alpha_0$  ( $a_0/R$ ) and  $\alpha_B$  ( $t/R$ )

$\alpha_1$  : Half of the notch length on disc faces over radius ( $a_1/R$ )

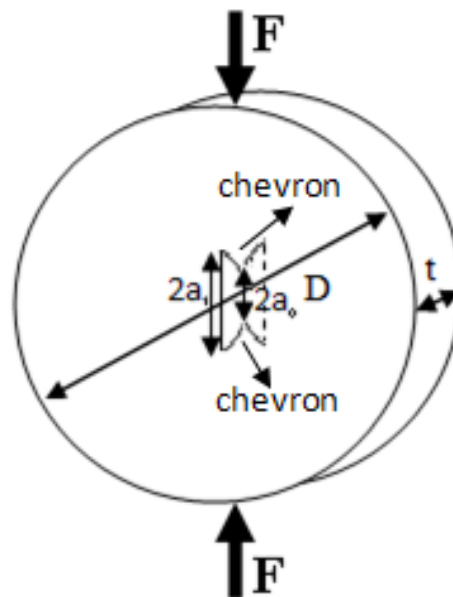


Figure 4. 5 CCNBD Specimen dimensions and loading conditions

Some rock types tested by using CCNBD method to evaluate mode I fracture toughness value were listed in Table 4. 5.

**Table 4. 5 Fracture toughness values of some rocks by using CCNBD Method**

Rock	Location or Name	$K_{Ic}$ (MPa $\sqrt{m}$ )	Reference
Sandstone	Raniganj Coalfield (fine grained)	0.24	Dwivedi et al., 2000
Granite	Utinga (Rift plane)	0.60	Almeida et al., 2006
Granite	Utinga (Grain plane)	0.73	Almeida et al., 2006
Limestone	Arki	0.79	Dwivedi et al., 2000
Granite	Utinga (Hardway plane)	0.82	Almeida et al., 2006
Granite	Favela (Grain plane)	0.90	Almeida et al., 2006
Granite	Favela (Rift plane)	0.97	Almeida et al., 2006
Granite	Favela (Hardway plane)	1.16	Almeida et al., 2006
Dolomite	Rajpur Dariba	1.09	Dwivedi et al., 2000
Granite	Stanstead	1.17	Nasseri & Mohanty, 2008
Granite	Stanstead	1.22	Iqbal & Mohanty, 2006
Limestone	Chongqing	1.26	Wang & Xing, 1999
Agglomerate	Sardar Sarovar Project site	1.32	Dwivedi et al., 2000
Granite	Keochang (D=54mm)	1.34	Chang et al., 2002
Granite	Bigwood	1.35	Nasseri & Mohanty, 2008
Granite	Keochang (D=75mm)	1.35	Chang et al., 2002
Dolerite	Sardar Sarovar Project site	1.43	Dwivedi et al., 2000
Granite	Westerly	1.43	Nasseri et al., 2007
Basalt	Sardar Sarovar Project site	1.51	Dwivedi et al., 2000
Granite	Laurentian	1.52	Nasseri & Mohanty, 2008
Granite	Barre	1.54	Nasseri & Mohanty, 2008
Granite	Barre	1.80	Iqbal & Mohanty, 2006
Granite	Laurentian	1.81	Iqbal & Mohanty, 2006

CCNBD method can be considered to be the most practical method among ISRM suggested methods (ISRM, 2007). Specimen preparation and experimental procedure are much easier than the others. However, there are some limitations in the specimen geometries. Restrictions of the dimensions are listed in the table and the graph given below (Table 4. 6 and Figure 4. 6).

**Table 4. 6 Dimensional restrictions for CCNBD Method**

Line	Equation
0	$\alpha_1 \geq 0.4$
1	$\alpha_1 \geq \alpha_B/2$
2	$\alpha_B \leq 1.04$
3	$\alpha_1 \leq 0.8$
4	$\alpha_B \geq 1.1729 \alpha_1^{1.6666}$
5	$\alpha_B \geq 0.44$

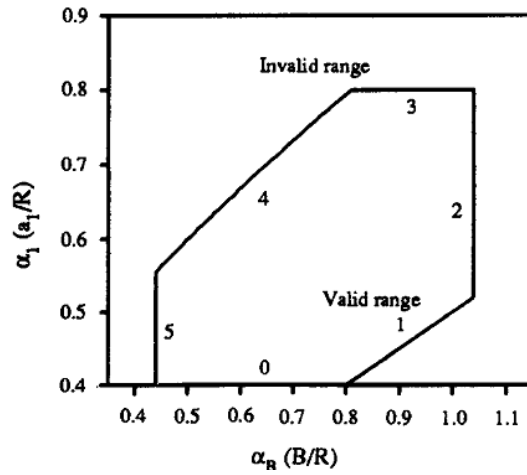


Figure 4. 6 Dimensional restrictions for CCNBD Method (Fowell, 1993)

#### 4.2.4 Modified Ring Test

Modified ring (MR) test was proposed by Thiercelin and Roegiers (1986) to determine fracture toughness of Berea sandstone. This method is for determination of mode I fracture toughness value only.

A cylindrical hole is drilled to the center of Brazilian disc specimen and the loading ends are flattened to avoid compressive load concentration on the loaded ends. Force or displacement can be applied to the specimen on the flattened ends. The specimen geometry is demonstrated in Figure 4. 7.

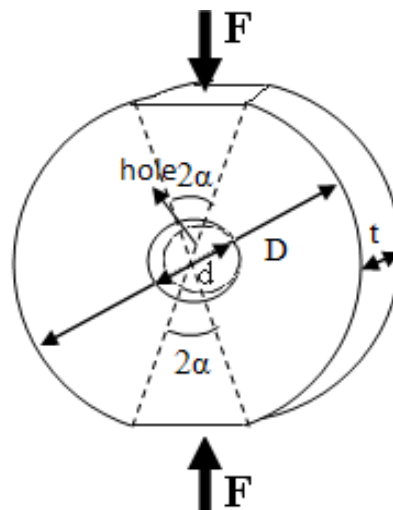


Figure 4. 7 Modified ring test specimen dimensions and loading configuration



The fracture toughness can be determined by using the relationship below:

$$\left( \frac{\sigma_{ac}}{K_{I_{max}}} \right)_{model} = \left( \frac{\sigma_{ac}}{K_{Ic}} \right)_{lab} \quad (4.8)$$

where,

$K_{I_{max}}$  : Stress intensity factor computed from the numerical modeling (MPa√m)

$K_{Ic}$  : Fracture toughness (MPa√m)

$\sigma_{ac} = \frac{F_{min}}{2L \times t}$  (for experimental results) and  $\sigma_{ac} = \frac{1}{2L}$  (for model ratio)

$F_{min}$  : Local minimum load (MN)

$2L$  : Length of flat loading surface (m)

$t$  : Disc thickness (m)

$\sigma_{ac}$  for models is  $\sigma_{ac}=1/2L$ , since load is  $F = 1$  unit (N) and thickness is  $t = 1$  unit (m) thickness in the modeling work.

Fracture toughness values of some rocks determined by using MR test are listed in Table 4. 7.

**Table 4. 7 Fracture toughness values of some rocks determined by using MR test**

Rock	Location or Name	$K_{Ic}$ (MPa√m)	Reference
Limestone	Oak Ridge	0.70 (v=0.45)	Lemiszki & Landes, 1996
Limestone	Oak Ridge	0.80 (v=0.25)	Lemiszki & Landes, 1996
Sandstone	Cardium	0.98±0.14	Thiercelin, 1987
Sandstone	Berea	1.11±0.06	Thiercelin, 1987
Chalk	Sintered	1.15 ± 0.15	Proveti & Michot, 2006
Limestone	Indiana	1.20	Lemiszki & Landes, 1996
Sandstone	Berea	1.33±0.043	Thiercelin & Roegiers, 1986
Sandstone	Berea	1.40	Lemiszki & Landes, 1996
Sandstone	Oak Ridge, Maroon	1.70 (v=0.45)	Lemiszki & Landes, 1996
Sandstone	Oak Ridge, Maroon	1.90 (v=0.25)	Lemiszki & Landes, 1996
Sandstone	Mesa Verde	2.12±0.23	Thiercelin, 1987
Mudstone	Mesa Verde	2.12	Thiercelin, 1987
Sandstone	Oak Ridge, Gray	2.25 (v=0.45)	Lemiszki & Landes, 1996
Sandstone	Oak Ridge, Gray	2.30 (v=0.25)	Lemiszki & Landes, 1996
Granite	Sao Paulo	2.57±0.49	Pehovaz-Alvarez 2004
Basalt	Sao Paulo	2.69±0.34	Pehovaz-Alvarez 2004

Some advantages of the MR test are: specimen models can be analyzed in plane strain condition and there is no need to model the geometry in 3D, in experiments, pre-cracking and crack length measurements are not necessary in tests.

#### 4.2.5 Brazilian Disc Specimen

In order to establish a simple method to determine fracture toughness of rocks, crack propagation behavior of Brazilian test was studied analytically and experimentally by Guo et al. (1993). The conventional Brazilian test is illustrated in Figure 4. 8.

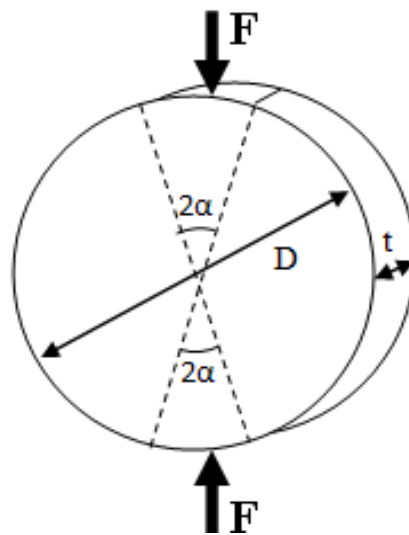


Figure 4. 8 Brazilian disc specimen dimensions and loading condition

The fracture toughness value is determined by using the equation below:

$$K_{Ic} = F_{min} \times B \times \phi(a/R) \quad (4.9)$$

where,

$K_{Ic}$  : Fracture toughness (MPa $\sqrt{m}$ )

$F_{min}$  : Local minimum load in load in load-displacement curves (MN)

$$B = \frac{2}{\pi^{3/2} \times R^{1/2} \times t \times \alpha}$$

$R$  : Disc radius (m)

$t$  : Disc thickness (m)

$\phi(a/R)$ : Dimensionless stress intensity factor determined from numerical modeling

$a$  : Half crack length (m)

$\alpha$  : Half loading arc angle (in radians)

Fracture toughness values of some rocks found by Brazilian test are given in Table 4. 8.

**Table 4. 8 Fracture toughness values of some rocks determined by using Brazilian Test**

Rock	Location or Name	$K_{Ic}$ (MPa $\sqrt{m}$ )	Reference
Sandstone	Australia	0.67 $\pm$ 0.05	Guo et al., 1993
Marble	Yeosan	0.99 $\pm$ 0.16	Chang et al., 2002
Marble	Australia (Fine-grained)	1.00 $\pm$ 0.07	Guo et al., 1993
Marble	Australia (Coarse-grained)	1.12 $\pm$ 0.19	Guo et al., 1993
Granite	Keochang	1.29 $\pm$ 0.15	Chang et al., 2002
Limestone	Australia (White)	1.38 $\pm$ 0.20	Guo et al., 1993
Limestone	Australia (Grey)	1.58 $\pm$ 0.16	Guo et al., 1993
Basalt	Australia	3.01 $\pm$ 0.49	Guo et al., 1993

The Brazilian test method is relatively simple and practical, since no notch is cut in the disc specimen. Some of the fracture toughness values determined by using Brazilian test are close to the some of the results obtained by using chevron bend (CB) method which is a suggested method by ISRM (2007). For instance; by using Brazilian test, fracture toughness of the sandstone, fine-grained marble and coarse-grained marble were found to be equal to 0.67 MPa $\sqrt{m}$ , 1.00 MPa $\sqrt{m}$  and 1.12 MPa $\sqrt{m}$ , respectively, while by using CB method they were equal to 0.68 MPa $\sqrt{m}$ , 0.96 MPa $\sqrt{m}$  and 1.19 MPa $\sqrt{m}$ , respectively (Guo et al., 1993).

#### **4.2.6 Flattened Brazilian Disc Method**

Guo's Brazilian disc method (Guo et al., 1993) has some disadvantages like: crack initiation and propagation could not be guaranteed to be located at the center, stress intensity factor solutions for Guo's method did not match with the solutions for center cracked disc, arc loading was hard to apply and although stress distribution

on the loading arc was not uniform, it was assumed uniform in Guo's method. By considering these drawbacks, Wang and Xing (1999) modified Guo's Brazilian disc method by flattening the loading ends of the disc. The shape of the flattened Brazilian disc is seen in Figure 4. 9.

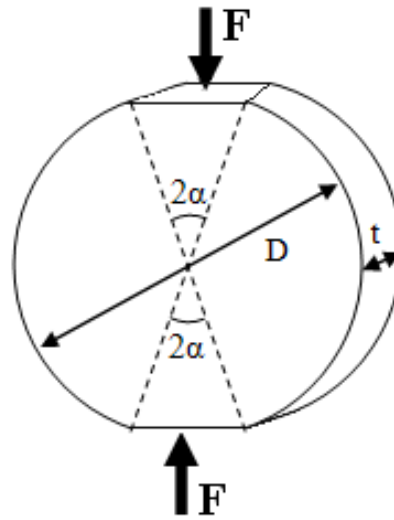


Figure 4. 9 FBD specimen dimensions and loading conditions

The fracture toughness value is computed from the equation below:

$$K_{Ic} = \frac{F_{min}}{\sqrt{R} \times t} \phi_{max} \quad (4. 10)$$

where,

$K_{Ic}$  : Fracture toughness (MPa√m)

$F_{min}$  : Minimum local load (MN)

$R$  : Disc radius (m)

$t$  : Disc thickness (m)

$\phi_{max}$  : Maximum dimensionless stress intensity factor determined from numerical modeling

Table 4. 9 shows fracture toughness values of some rocks evaluated by using FBD method.

**Table 4. 9 Fracture toughness values of some rocks determined by using Flattened Brazilian Disc Method**

<b>Rock</b>	<b>Location or Name</b>	<b><math>K_{Ic}</math> (MPa√m)</b>	<b>Reference</b>
<b>Marble</b>	China	0.97	Wang & Wu, 2004
<b>Limestone</b>	Chongqing	1.25	Wang & Xing, 1999
<b>Marble</b>	China	1.34	Wang & Wu, 2004

For the FBD guarantees crack initiation is at the center of the disc when loading angle is greater than  $20^\circ$  ( $2\alpha \geq 20^\circ$ ). By using this method, elastic modulus (by knowing Poisson's ratio) and tensile strength can be calculated, (Wang et al., 2004).

In the study of Wang and Xing (1999), fracture toughness value of Chongqing limestone determined by this method (1.25 MPa√m) is in good agreement with the value determined by cracked chevron notched Brazilian disc (CCNBD) method (1.26 MPa√m) suggested by ISRM (2007).

### **4.3 Tests Under Bending Load**

Mode I failure can also be induced by applying bending on the specimen. Bending is supplied by at least three rollers. Two rollers, which are located at the same distance from the notch, are set under the specimen. One roller is at the top center of the specimen. To determine mode I fracture toughness value of the materials, methods with bending load are listed as follows:

- Straight notched semi-circular bending (SNSCB) method (Chong and Kuruppu, 1984)
- Chevron notched semi-circular bending (CNSCB) method (Kuruppu, 1997)
- Chevron bend (CB) test (Ouchterlony, 1988)
- Straight edge cracked round bar bending (SECRBB) method (Ouchterlony, 1982)

#### **4.3.1 Straight Notched Semi-circular Bending Method**

Straight notched semi-circular bending (SNSCB) specimen is named shortly as semi-circular bend (SCB) specimen. The SCB method was proposed by Chong and Kuruppu (1984). Mode I, mode II and mixed mode I-II loading conditions can be

produced by changing the notch inclination angle with respect to the loading direction.

In specimen preparation, a whole disc specimen cut into two equal halves and a straight notch at required length is cut initiating from the center of the flat surface of the halves. After that, specimens are loaded as in Figure 4. 10.

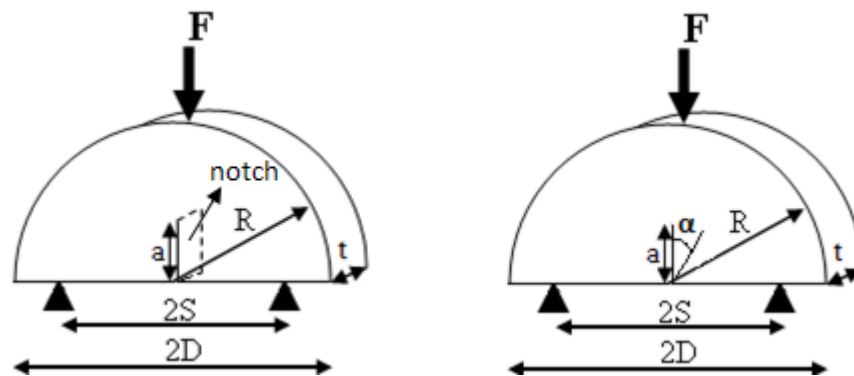


Figure 4. 10 SCB specimen dimensions and loading conditions for mode I and mode II/mixed mode I-II, respectively

Fracture toughness value is computed by using the formula below:

$$K_{Ic} = \frac{F\sqrt{\pi a}}{Dt} Y_I \quad (4. 11)$$

where,

$K_{Ic}$  : Fracture toughness (MPa $\sqrt{m}$ )

$F$  : Failure load (MN)

$a$  : Notch length (m)

$D$  : Specimen diameter (m)

$t$  : Specimen thickness (m)

$Y_I$  : Dimensionless stress intensity factor depends on  $a/R$  and is computed by numerical modeling

Fracture toughness values of some rocks determined by applying SCB method are tabulated in Table 4. 10.

**Table 4. 10 Fracture toughness values of some rocks analyzed by using SCB method**

Rock	Location or Name	$K_{Ic}$ (MPa $\sqrt{m}$ )	Reference
Johnstone	Synthetic rock (water cont.=18%)	0.062	Lim et al., 1994
Sandstone	Coarse grained	0.275	Singh & Sun, 1990 (b)
Sandstone	Coarse grained	0.350	Singh & Sun, 1990 (b)
Limestone	Central Province of Saudi Arabia	0.680	Khan & Al-Shayea, 2000
Granite	Keochang	0.684 $\pm$ 0.187	Chang et al., 2002
Limestone	Welsh	0.850	Singh & Sun, 1990 (a)
Marble	Yeosan	0.871 $\pm$ 0.154	Chang et al., 2002
Granite	Fine-grained	0.884 $\pm$ 0.022	Donovan & Karfakis, 2004
Andesite	Ankara, Gölbaşı	0.930 $\pm$ 0.110	Alkılıçgil, 2006
Oil Shale	Colorado	1.020	Chong et al., 1987
Quartzite	Sioux	1.244 $\pm$ 0.071	Donovan & Karfakis, 2004
Limestone	Dolomitic	1.331 $\pm$ 0.080	Donovan & Karfakis, 2004
Granite	Newhurst	1.720	Whittaker et al., 1992

#### 4.3.2 Chevron Notched Semi-circular Bending Method

Chevron notched semi-circular bending (CNSCB) method was proposed by Kuruppu (1997). He performed a 3D finite element analysis to get stress intensity factors at the crack tip of a CNSCB specimen as a function of the crack length. This method is used to evaluate mode I fracture toughness only.

The notch is cut in both side of the specimen with an angle to provide v-shape notch with required angle as illustrated in Figure 4. 11. The loading configuration is the same as the SCB Method.

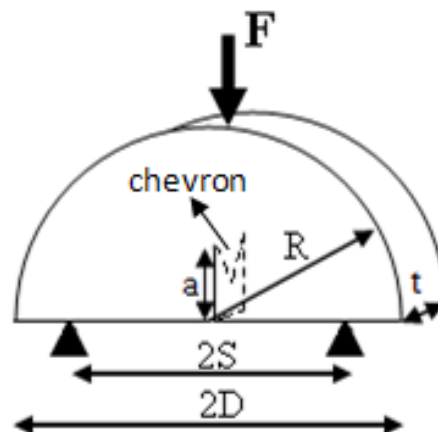


**Figure 4. 11 CNSCB Specimen dimensions and loading conditions**

Fracture toughness value can be computed based on the normalized stress intensity factor as seen in equation below:

$$K_{Ic} = \frac{F}{t\sqrt{R}} K_{ND} \quad (4.12)$$

where,

$K_{Ic}$  : Fracture toughness (MPa√m)

$F$  : Failure load (MN)

$R$  : Specimen radius (m)

$t$  : Specimen thickness (m)

$K_{ND}$  : Normalized stress intensity factor

$$K_{ND} = \frac{K_I}{F} t\sqrt{R}$$

$K_I$  : Stress intensity factor (MPa√m) determined by numerical analyses.

Table 4. 11 illustrates the fracture toughness values of some rocks determined by applying CNSCB method.

**Table 4. 11 Fracture toughness values of some rocks determined by using CNSCB Method**

Rock	Location or Name	$K_{Ic}$ (MPa√m)	Reference
Ultramafic schist	Goldfields	0.680±0.120	Kuruppu, 2002
Marble	Yeosan	1.113±0.037	Chang et al., 2002
Granite	Keochang	1.393±0.027	Chang et al., 2002
Porphyry	Goldfields	1.440±0.080	Kuruppu, 2002
Sandstone	Goldfields	1.550±0.170	Kuruppu, 2002
Basalt	Goldfields	1.610±0.100	Kuruppu, 2002
Dolerite	Goldfields	1.750±0.130	Kuruppu, 2002

#### 4.3.3 Chevron Bend Test

Chevron bend (CB) test was initially conducted by Ouchterlony (1988), and it became another suggested method of ISRM (2007). This technique is performed to determine only mode I fracture toughness value.

In laboratory work, core samples are cut into required lengths and two notches which are chevron shaped ligaments are machined in opposite angles to the



specimen. Then specimen is subjected to three-point bending load (Figure 4. 12). The specimen geometry dimensions are listed in Table 4. 12.

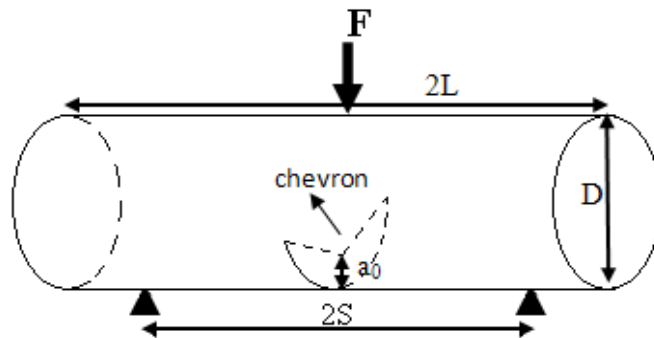


Figure 4. 12 CB Specimen dimensions and loading conditions

Table 4. 12 CB Specimen dimensions (Ouchterlony, 1988)

Symbol	Definition	Value	Tolerance
$D$	Specimen diameter	$D$	$>10 \times$ grain size
$2L$	Specimen length	$4D$	$>3.5D$
$2S$	Support span	$3.33D$	$\pm 0.02D$
$\theta$	Subtended chevron angle	$90.0^\circ$	$\pm 1.0^\circ$
$a_0$	Distance to Chevron notch tip	$0.15D$	$\pm 0.10D$
$t$	Notch width	$\leq 0.03D$ or $1\text{mm}^*$	
* whichever is greater			

Fracture toughness estimation by using CB method is performed in two levels as in SR Method. In Level 1 testing, maximum load during bending is recorded and in Level 2 testing, load and displacement measurements are recorded to correct the fracture toughness value.

Fracture toughness calculation and its correction are done by the same equations used in SR method, which are Equation (4.1) and Equation (4.2).

Fracture toughness values of some rocks estimated by using CB Method are listed in Table 4. 13.

**Table 4. 13 Fracture toughness values of some rocks determined by using CB Method**

Rock	Location or Name	$K_{Ic}$ (MPa√m)	Reference
Sandstone	Ambergate, Derbyshire	0.39±0.05	Brown&Reddish,1997
Chalk	unknown, Italy	0.41±0.09	Brown&Reddish,1997
Siltstone	Ripley, Derbyshire	0.50±0.11	Brown&Reddish,1997
Marble	Carrara, Italy	0.66±0.14	Brown&Reddish,1997
Limestone	Middleton	0.73±0.08	Bearman, 1999
Limestone	Harrycroft	0.82±0.03	Bearman, 1999
Limestone	Ashbourne, Derbyshire	1.07±0.08	Brown&Reddish,1997
Limestone	Rüdersdorf	1.12 ± 0.06*	Backers, 2004
Sandstone	Flechtlinger	1.15 ± 0.05*	Backers, 2004
Sandstone	Montcliffe	1.18±0.15	Bearman, 1999
Granite	Penryn, Cornwall	1.52±0.05	Brown&Reddish,1997
Granite	Aeu	1.60±0.13*	Backers, 2004
Granite	Mountsorrel, Leicestershire	1.64±0.08	Brown&Reddish,1997
Limestone	Wredon	1.70± 0.13	Bearman, 1999
Granite	Penryn	1.83± 0.07	Bearman, 1999
Quartzite	Nuneaton, Warwickshire	1.88±0.14	Brown&Reddish,1997
Basalt	Buxton, Derbyshire	2.01±0.36	Brown&Reddish,1997
Sandstone	Pennant	2.10± 0.16	Bearman, 1999
Andesite	Whitwick	2.17± 0.20	Bearman, 1999
Diorite	Bolton Hill	2.22± 0.18	Bearman, 1999
Greywacke	Ingleton	2.38± 0.20	Bearman, 1999
Granite	Mizunami	2.380 ± 0.12*	Backers, 2004
Marble	Carrara	2.440 ± 0.07*	Backers, 2004
Quartzite	Nuneato	2.44± 0.08	Bearman, 1999
Dolerite	unknown, Africa	2.48±0.16	Brown&Reddish,1997
Diorite	Cliffe Hill	2.77±0.07	Bearman, 1999
Slate	Kirkby in Furness, Cumbria	2.80±0.12	Brown&Reddish,1997
Diorite	Äspö	3.830±0.03*	Backers, 2003
Greywacke	Cornish	3.15±0.21	Bearman, 1999
*Corrected $K_{Ic}$ values			

#### 4.3.4 Straight Edge Cracked Round Bar Bending Method

Straight edge cracked round bar bending (SECRBB) method was introduced by Ouchterlony (1981). Then Haberfield and Johnstone (1990) employed this method for synthetic rock fracture toughness evaluation. This method is also termed as straight edge-notched round bar in bending (SENRBB) method, and it can be used for mode I, mode II and mixed mode (mode I-II) fracture toughness testing.

In experimental work, core samples are cut into required length and a straight notch in required length and angle is sawed through the center of the core as in Figure 4. 13.

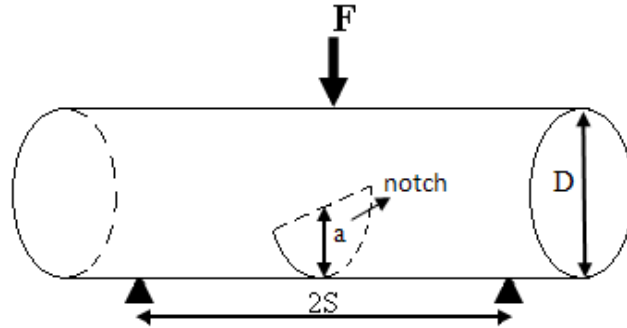


Figure 4. 13 SECRRBB Specimen dimensions and loading conditions

Fracture toughness equation was derived by Ouchterlony (1981). The equation is as follows:

$$K_{Ic} = 0.25 \left( \frac{2S}{D} \right) \left( \frac{F}{D^{1.5}} \right) \times Y_1' \quad (4. 13)$$

where,

$$Y_1' = \frac{2 \left( \frac{D}{2S} \right) \left[ 450.853 \left[ \frac{1}{3.33} \left( \frac{2S}{D} \right) \right]^2 \left( \frac{a}{D} \right)^{1.5} \right]^{0.5}}{\left[ \left( \frac{a}{D} \right) - \left( \frac{a}{D} \right)^2 \right]^{0.25}} \quad (4. 14)$$

$K_{Ic}$  : Fracture toughness (MPa√m)

$F$  : Load at failure (MN)

$a$  : Notch length (m)

$D$  : Disc diameter (m)

$2S$  : Support span (m)

Fracture toughness values of some rocks obtained by using SECRRBB are listed in Table 4. 14.

**Table 4. 14 Fracture toughness values of some rocks obtained by using SECRBB method**

Rock	Location or Name	$K_{Ic}$ (MPa $\sqrt{m}$ )	Reference
Tuff	Tage	0.35	Funatsu et al., 2004
Sandstone	Kimachi	0.43	Funatsu et al., 2004
Limestone	Central Province of Saudi Arabia	0.55	Khan & Al-Shayea, 2000

#### 4.4 Comparison Between Mode I Fracture Toughness Values

Fracture toughness values of some rocks determined by using each method are listed in each method. However, these tables could not be used to estimate fracture toughness values of rocks. Since rock properties used in these tables were not described in details. There was no information about humidity, temperature, material properties of the rock. Exact locations of the drilled rock cores were not known; the cores were taken from the outcrop which may weathered there or from the underground. Listing fracture toughness values with their compressive strength values may give an idea about the rocks. Specimen diameter affects the fracture toughness value with some fracture toughness testing methods.

Some rock types are listed according to fracture toughness, testing method, uniaxial compressive strength, description, and reference in Table 4. 15, Table 4. 16 and Table 4. 17. Description includes name of the rock or location of the quarry, specimen diameter for some methods and grain size for some rock types.

**Table 4. 15 Fracture toughness values of some rocks**

Mat	$K_{Ic}$ (MPa $\sqrt{m}$ )	Method	$\sigma_c$ (MPa)	Description	Reference
JST	0.06	SCB	2	Synthetic rock (water cont.=18%)	Lim et al., 1994 (b)
SST	0.01	SNBD	1	(Antler) Ardmore, Oklahoma ( $D = 72$ mm)	Krishnan et al., 1998
SST	0.24	CCNBD	80	Raniganj Coalfield (fine grained)	Dwivedi et al., 2000
SST	1.15	CB	96	Flechtinger	Backers, 2004
SST	1.18	CB	76	Montcliffe	Bearman, 1999

JST: Johnstone, SST: Sandstone  
 CB: Chevron bend, CCNBD: Cracked chevron notched Brazilian disc, SCB: Semi-circular bending, SNBD: Straight notched Brazilian disc

**Table 4. 16 (continued) Fracture toughness values of some rocks**

Mat.	$K_{Ic}$ (MPa $\sqrt{m}$ )	Method	$\sigma_c$ (MPa)	Description	Reference
SST	1.33	SCB	74	Berea	Thiercelin and Roegiers, 1986 (Park 2006)
SST	1.39	MR	74	Berea	Doolin, 1994 (Park, 2006)
SST	1.47 <sub>8</sub>	SR	114 <sub>7</sub>	Grimsby	Gunsallus & Kulhawy, 1984
SST	1.55	CNSCB	72-200	Goldfields	Kuruppu, 2002
SST	2.10	CB	162	Pennant	Bearman, 1999
SST	2.85	DC	97	Isparta	Altındağ, 2000
LST	0.35	SNBD	105	Central Province of Saudi Arabia ( $D = 84\text{mm}$ )	Khan & Al-Shayea, 2000
LST	0.42	SNBD	105	Central Province of Saudi Arabia ( $D = 98\text{ mm}$ )	Khan & Al-Shayea, 2000
LST	0.55	SECRBB	105	Central Province of Saudi Arabia ( $D = 24\text{ mm}$ )	Khan & Al-Shayea, 2000
LST	0.68	SCB	105	Central Province of Saudi Arabia ( $D = 98\text{ mm}$ )	Khan & Al-Shayea, 2000
LST	0.73	CB	48	Middleton	Bearman, 1999
LST	0.79	CCNBD	110	Arki	Dwivedi et al., 2000
LST	0.82	CB	53	Harrycroft	Bearman, 1999
LST	1.12	CB	40	Rüdersdorf	Backers, 2004
LST	1.36 <sub>3</sub>	SR	113 <sub>11</sub>	Irondequoit	Gunsallus & Kulhawy, 1984
LST	1.70	CB	157	Wredon	Bearman, 1999
LST	2.06 <sub>4</sub>	SR	125 <sub>8</sub>	Reynales	Gunsallus & Kulhawy, 1984
LST	2.18	DC	77	Fethiye	Altındağ, 2000
LST	2.48	DC	81	Isparta	Altındağ, 2000
DST	1.09	CCNBD	125	Rajpur Dariba	Dwivedi et al., 2000
DST	1.66 <sub>21</sub>	SR	172 <sub>19</sub>	Falkirk	Gunsallus & Kulhawy, 1984
DST	1.66 <sub>4</sub>	SR	150 <sub>24</sub>	Kankakee	Gunsallus & Kulhawy, 1984
DST	1.78 <sub>15</sub>	SR	142 <sub>13</sub>	Oatka	Gunsallus & Kulhawy, 1984
DST	1.80 <sub>3</sub>	SR	168 <sub>35</sub>	Markgraf	Gunsallus & Kulhawy, 1984
DST	2.47 <sub>3</sub>	SR	237 <sub>19</sub>	Romeo	Gunsallus & Kulhawy, 1984

DST: Dolostone, LST: Limestone, SST: sandstone  
 CB: Chevron bend, CCNBD: Cracked chevron notched Brazilian disc, CNSCB: Chevron notched semi-circular bending, DC: Diametral compression, MR: Modified ring, SECRBB: straight edge cracked round bar bending, SCB: Semi-circular bending, SNBD: Straight notched Brazilian disc, SR: Short rod

**Table 4. 17 (continued) Fracture toughness values of some rocks**

Mat.	$K_{Ic}$ (MPa $\sqrt{m}$ )	Method	$\sigma_c$ (MPa)	Description	Reference
SCH	0.68	CNSCB	50-160	Goldfields (Ultramafic)	Kuruppu, 2002
SCH	1.23	CCNBD	69	Rajpur Dariba (Quartz-Calclite)	Dwivedi et al., 2000
SCH	1.27	CCNBD	87	Bamnia Kalan (Quartz-Mica)	Dwivedi et al., 2000
MRB	0.87	SCB	-	Yeosan	Chang et al., 2002
MRB	0.94	DC	36.57	Muğla	Altındağ, 2000
MRB	0.99	BD	-	Yeosan	Chang et al., 2002
MRB	1.13	CNSCB	-	Yeosan	Chang et al., 2002
MRB	1.19	DC	54.12	Muğla	Altındağ, 2000
MRB	1.74	DC	72.94	Izmir, Torbalı	Altındağ, 2000
MRB	2.44	CB	101	Carrara	Backers, 2004
DOL	1.43	CCNBD	158	Sardar Sarovar Project site	Dwivedi et al., 2000
DOL	1.75	CNSCB	118-173	Goldfields	Kuruppu, 2002
GRT	0.68	SCB	-	Keochang	Chang et al., 2002
GRT	1.22	CCNBD	173 <sub>3</sub>	Stanstead	Iqbal & Mohanty, 2006
GRT	1.29	BD	-	Keochang	Chang et al., 2002
GRT	1.34	CCNBD	-	Keochang ( $D = 54$ mm)	Chang et al., 2002
GRT	1.35	CCNBD	-	Keochang ( $D = 75$ mm)	Chang et al., 2002
GRT	1.39	CNSCB	-	Keochang	Chang et al., 2002
GRT	1.60	CB	134	Aeu	Backers, 2004
GRT	1.80	CCNBD	212 <sub>3</sub>	Barre	Iqbal & Mohanty, 2006
GRT	1.81	CCNBD	259 <sub>2</sub>	Laurentian	Iqbal & Mohanty, 2006
GRT	1.83	CB	132	Penryn	Bearman, 1999
GRT	2.38	CB	166	Mizunami	Backers, 2004
BAS	1.51	CCNBD	180	Sardar Sarovar Project site	Dwivedi et al., 2000
BAS	1.61	CNSCB	79-200	Goldfields	Kuruppu, 2002
AND	2.17	CB	139	Whitwick	Bearman, 1999
AND	2.92	DC	113	Isparta	Altındağ, 2000
DIO	2.22	CB	129	Bolton Hill	Bearman, 1999
DIO	2.77	CB	275	Cliffe Hill	Bearman, 1999
DIO	3.83	CB	219	Äspö	Backers, 2003
GRW	2.38	CB	226	Ingleton	Bearman, 1999
GRW	3.15	CB	165	Cornish	Bearman, 1999

AND: Andesite, BAS: Basalt, DIO: Diorite, DOL: Dolerite, GRT: Granite, GRW: Greywacke, MRB: Marble, SCH: Schist  
BD: Brazilian disc, CB: Chevron bend, CCNBD: Cracked chevron notched Brazilian disc, CNSCB: Chevron notched semi-circular bending, DC: Diametral compression, SCB: Semi-circular bending

Generally, as the compressive strength increases, fracture toughness value also increase. When rock types are considered, sedimentary rocks (like sandstone and limestone) have smaller fracture values. Metamorphic rocks (like schist and marble) are in the middle range according to fracture toughness values. Igneous rocks (like dolomite, andesite, basalt, granite, and diorite) have the greater fracture toughness values. For example from these tables, with cracked chevron notched Brazilian disc (CCNBD) method, fracture toughness values of sedimentary rock change between 0.24 MPa√m and 1.09 MPa√m, metamorphic rocks range between 1.23 MPa√m and 1.43 MPa√m, and igneous rocks vary between 1.22 MPa√m and 1.51 MPa√m.

Applied method also affects the fracture toughness value. Usually, for the same rock, higher fracture toughness values are determined with methods having chevron notch and lower fracture toughness values are determined with bending methods. For example, in the study of Chang et al. (2000), fracture toughness value of Yeosan marble was determined as 0.87 MPa√m and 1.13 MPa√m with semi-circular bending (SCB) and chevron-notched semi-circular bending (CNSCB) methods, respectively, and fracture toughness of Keochang marble was determined as 0.68 MPa√m and 1.39 MPa√m with semi-circular bending (SCB) and chevron-notched semi-circular bending (CNSCB) methods, respectively,

Some methods depend on specimen size like straight notched Brazilian disc (SNBD) method, and as the size of the specimen is increased, fracture toughness values also increases (Khan & Al-Shayea, 2000). Some methods do not base on specimen size like cracked chevron notched Brazilian disc (CCNBD) method (Chang et al., 2002).

#### **4.5 Comparison of Mode I Fracture Tests on Disc Type Specimens**

Fracture toughness tests are generally applied to rocks in disc or cylinder geometries due to the availability of rocks usually in core pieces. In order to choose the simplest fracture testing method with reasonable fracture toughness results, methods can be compared with each other in terms of specimen preparation, loading method,

experimental set-up and equipment, and applicability of the method to mixed mode fracture toughness estimation.

In specimen preparation, the first step is coring rocks. Coring rocks in long pieces and taking cores in greater diameters can be time consuming as well as the problems associated with core fragility due to its large size. This can be a problem especially for weak rocks. Long cores are needed for CB and SECRBB fracture testing methods.

For a testing method which requires only hole at the center of the disc, a hole is drilled through the disc with a smaller diameter bit. After cutting and flattening specimens in required thicknesses, second step is machining an initial notch in the desired dimensions if a notch is necessary for a particular testing method. Initial notch preparation is a difficult process. When a single straight notch is employed for a particular testing method and if this can be achieved with a regular rotary saw, this is regarded to be the simplest way of introducing a notch to the specimen. On the other hand, if a straight notch intersecting both faces of the specimen is required at the center of the specimen, this can be machined only with a wire saw. This can be a difficult operation, since before wire saw usage; a hole must be drilled through the specimen center to guide the saw. Chevron notch initiation is also a difficult process as two notches with the same size and geometry should be cut through the specimen on both faces and both notches must overlap each other.

When all notch types and preparation of appropriate specimens for a particular testing method are considered, a classification can be conducted in terms of lack of an initial notch, having a hole, having a straight notch machined with a rotary saw, having a chevron notch and having a straight notch cut from a hole guiding a wire saw. Fracture testing methods above can be categorized from the simplest method to the hardest one according to the preparation procedures and notch types as follows: BD method, FBD method, MR test, DC method, SCB method, SECRBB method, CCNBD method, CNSCB method, SR method, CB method, and CSTBD method.



Comparing the loading methods for rock fracture testing, compressive loading method is the easiest method, since it does not require any special loading fixtures and alignment precautions as in the case of bending type loading configurations.

Including the loading configuration and loading method in a classification attempt, all methods above can be classified from the simplest method to the most difficult one as follows: BD method, FBD method, MR test, DC method, CCNBD method, CSTBD method, SCB method, CNSCB method, SECRBB method, CB method and SR method.

Testing procedure is another factor in deciding the ease of a particular fracture testing method. All methods, except CB and SR methods, are simple methods according to the testing procedure. Although CB and SR methods are among the suggested methods by ISRM, they are complex methods because a number of sophisticated steps in the evaluation process must be followed to achieve proper results in these tests. Fracture toughness evaluation by using these methods is performed in two levels. In Level 1 testing, maximum load during bending is recorded, and in Level 2 testing, load and displacement measurements are taken into account to correct the fracture toughness value.

Another factor in selection of a proper method is the availability of mode II and mixed mode fracture toughness determination with that method. CCNBD, SCB, CNSCB, SECRBB and CSTBD methods are appropriate methods for mode II and mixed mode fracture toughness determinations, since they offer special specimen, notch and loading configurations for these purposes.

In fracture toughness tests, chevron notch machining in specimens is a difficult process. Chevron notch is preferred, since, by machining an initial chevron notch, pre-cracking process before testing is not required, and by using a chevron notch stable crack propagation is achieved during the tests. On the other hand, stable crack propagation can be achieved without a chevron notch in compressive loading methods like FBD method and MR test method.

BD method with specimens without flat loading ends is not a reliable method, because, crack initiation which is supposed to be at the center of the loaded disc may start at the loading ends due to the infinite compressive stresses under the line loads here.

Although it is a relatively simple fracture testing method, SCB method with low fracture loads can sometimes be difficult to implement in practical experiments and is error prone, as it will be more difficult to obtain accurate load-displacement recordings (Fowell et al, 2006). Fracture toughness results obtained by conventional SCB method are usually lower than the toughness values determined by the suggested methods (Chang et al., 2002; Kuruppu, 2002; Pehovaz-Alvarez, 2004).

A comparison of some of the rock fracture testing methods is summarized in Table 4. 18.

**Table 4. 18 Comparison between fracture tests**

Method	Notch Type			Loading Method	Set-up of equipment	Pre-crack	Mixed Mode Evaluation
	Straight		Chevron				
	Rotary saw	Wire saw	Rotary Saw				
<b>SR</b>	-	-	Yes	Tensile	Complex	-	No
<b>CSTBD</b>	-	Yes	-	Compressive	Simple	Yes	Yes
<b>DC</b>	Yes	-	-	Compressive	Simple	Yes	No
<b>SECRBB</b>	Yes	-	-	3-point bending	Simple	Yes	Yes
<b>SCB</b>	Yes	-	-	3-point bending	Simple	Yes	Yes
<b>CCNBD</b>	-	-	Yes	Compressive	Simple	-	Yes
<b>MR</b>	-	-	-	Compressive	Simple	-	No
<b>CB</b>	-	-	Yes	3-point bending	Complex	-	No
<b>BD</b>	-	-	-	Compressive	Simple	-	No
<b>CNSCB</b>	-	-	Yes	3-point bending	Simple	-	Yes
<b>FBD</b>	-	-	-	Compressive	Simple	-	No

Considerations and comparisons so far suggest that the simplest mode I fracture toughness testing methods are FBD method and MR test if reliable results for fracture toughness can be produced.

In this thesis study, FBD method and MR test were conducted and their results were compared to the mode I fracture toughness results found by the simplest ISRM method, which is CCNBD method. Specimen geometrical parameters were analyzed to identify under which conditions FBD method and MR test produce close results to the results of the suggested method.

## **CHAPTER 5**

### **NUMERICAL MODELLING WITH ABAQUS PROGRAM**

Before conducting experiments for fracture toughness determination with flattened Brazilian disc (FBD) method and modified ring (MR) test, numerical modeling was used for stress and stress intensity factor analyses. In numerical modeling, ABAQUS package program was preferred. Before using this program, to assess the accuracy of stress intensity factor results of ABAQUS program, two problems having well-known analytical stress intensity factor expressions were modeled.

#### **5.1 ABAQUS Program**

ABAQUS is a commercial finite element program used for stress, heat transfer, and other types of analyses in structural, mechanical, civil, biomedical, and related engineering applications. It was developed by Habbitt, Karlson and Sorensen, Inc. (HKS) in 1978.

In this study, ABAQUS program was preferred because it is a very user friendly and reliable program. For stress analyses, some modules are followed step by step. Firstly, “Part module” is used to create, edit, and manage the parts in the current model. In “Property module”, material properties of the model are defined. Then, “Assembly module” is basically used to create part instances and position them relative to each other in a global coordinate system. “Step module” is used to perform a sequence of one or more analysis steps. The sequence of steps provides a convenient way to capture changes in the loading and boundary conditions of the model. Loads and boundary conditions are defined considering “Step module” in “Load module”. “Mesh module” is used to generate meshes on parts and assemblies of the model. “Job module” is used to submit the analysis for processing. During process, job module can monitor progress of the process. “Visualization module” finally demonstrates the results of the analysis in terms of deformed shapes, contours, symbols, animations, and graphs.

For stress intensity factor analyses, “Interaction module” is used to define a crack in a region. Then a history output request is defined in “Step module” to obtain stress intensity factor data around crack tips. Under the menu options of “Step module” J-Integral and stress intensity factor computation options are available. For stress intensity factor computations, J-integral method is used by ABAQUS program.

J-integral is defined as a path-independent line integral that measures the strength of the singularities for stresses and strains near a crack tip (Figure 5. 1). J-integral is termed as  $J$  and it was introduced by Rice (1968).

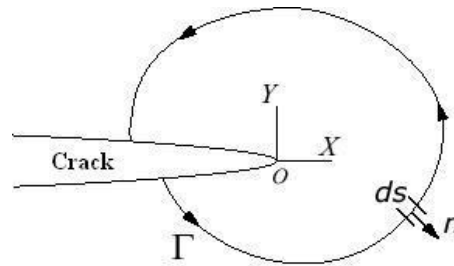


Figure 5. 1 J-integral contour path surrounding a crack-tip

$J$  is derived from the expression below:

$$J = \int_{\Gamma} w dy - T_i \frac{\partial u_i}{\partial x} ds \quad (5. 1)$$

where,

$w$  : strain energy density, ( $w = \int_0^{\varepsilon_{ij}} \sigma_{ij} d\varepsilon_{ij}$ )

$T_i$  : traction vector, ( $T_i = \sigma_{ij} n_j$ )

$\Gamma$  : an arbitrary path around the crack tip

$n$  : unit outer normal vector to path  $\Gamma$

$\sigma$  : stress component

$\varepsilon$ : strain

$u$  : displacement vector  
 $s$  : distance along the path  $\Gamma$

## 5.2 Verification Examples

Verification model examples to assess accuracy of stress intensity evaluation of ABAQUS program were chosen to have similar geometries with FBD and MR. Infinite plate with central crack was modeled for FBD model while infinite plate with a hole was modeled for MR model. Both verification models have analytical solutions for stress intensity factor. Stress intensity factor results determined with ABAQUS were compared with the results computed with analytical expressions.

### 5.2.1 Central Crack in Infinite Plate

Central crack in infinite plate was modeled with ABAQUS finite element program as in Figure 5. 2. In the problem, height ( $H$ ) and width ( $W$ ) of the plate were 100 mm and model was in plane stress condition. Crack length ( $2a$ ) was equal to 2 mm. To provide mode I loading conditions at the crack, 1 Pa tensile stress ( $\sigma$ ) was applied along upper and lower boundaries of the model.

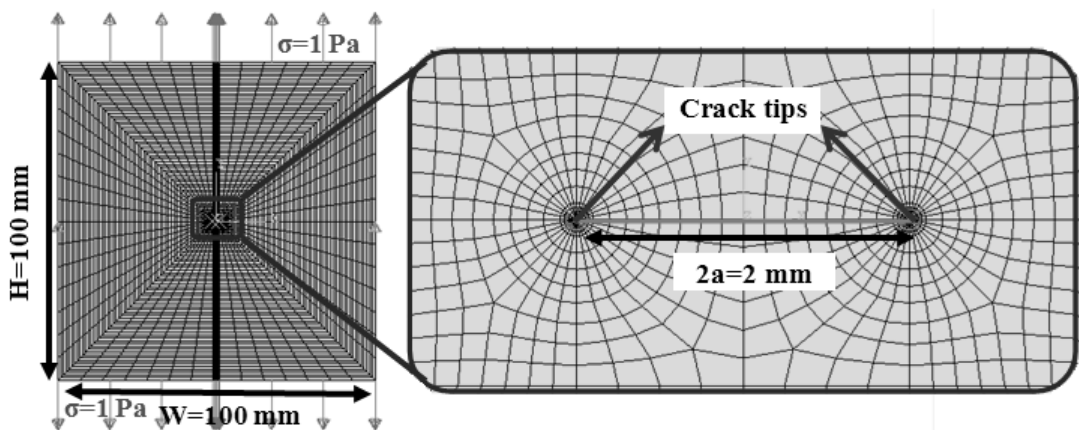


Figure 5. 2 Central crack in infinite plate model

Analytical solution for mode I stress intensity factor value of this model is in equation below:

$$K_I = \sigma\sqrt{\pi a} \quad (5.2)$$

where,

$K_I$ : Stress Intensity Factor (Pa $\sqrt{m}$ )

$\sigma$ : Applied stress = 1 Pa

$a$ : Half crack length = 1 mm

When stress intensity factor was calculated with the equation, it was determined as 0.05605 Pa $\sqrt{m}$ . When stress intensity factor in both crack tips were computed with ABAQUS program, both were found as 0.05619 Pa $\sqrt{m}$ . The error in the computation was equal to 0.252 %, when compared to the analytical solution.

In this verification problem, elastic modulus and Poisson's ratio were defined as 10 GPa and 0.25, respectively. In order to examine how mechanical properties influence the stress intensity factor, with extreme elastic modulus and Poisson's ratio values, model was analyzed again. For elastic modulus values between 5 GPa and 200 GPa, stress intensity factors were found as constant and it was equal to 0.05619 Pa $\sqrt{m}$ . Poisson ratio of materials ranges between 0.0 and 0.5. With these extreme values, which are 0.0 and 0.5, stress intensity factor was equal to 0.05617 Pa $\sqrt{m}$  and 0.05621 Pa $\sqrt{m}$ , respectively. The difference from the analytical solution for these values was found to be less than 0.077 %. It can be concluded that elastic modulus and Poisson's ratio do not significantly affect the stress intensity factor computation in numerical modeling work.

### **5.2.2 Infinite Plate with a Hole and Symmetric Double through Cracks**

Infinite plate with a hole intersected by two cracks was modeled with ABAQUS finite element program as in Figure 5. 3. In the problem, height ( $H$ ) and width ( $W$ ) of the plate were 100 mm and modeled in plane stress condition. Crack lengths ( $a$ ) were equal to 0.4 mm while radius of the hole was equal to 1 mm. To produce a

mode I loading condition at the crack tips, 1 Pa tensile stress ( $\sigma$ ) was applied along both ends of the specimen.

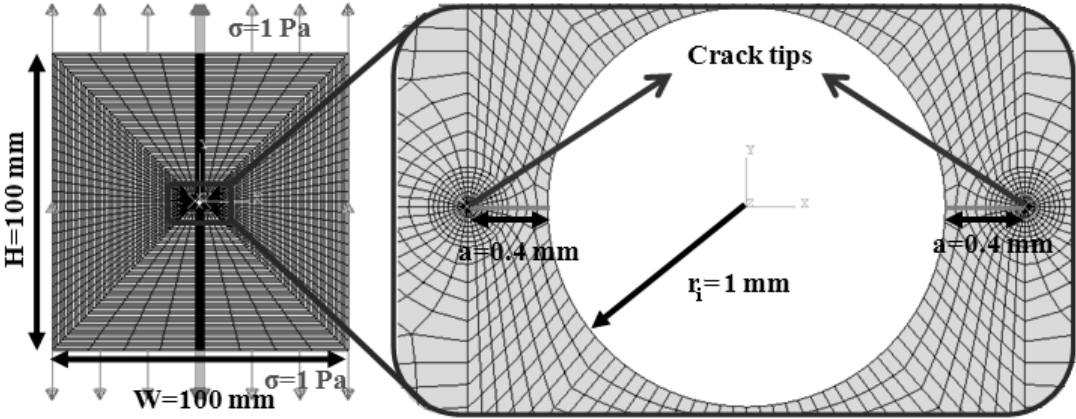


Figure 5. 3 Infinite plate with hole model

Analytical solution for mode I stress intensity factor of this problem is in the equation below:

$$K_I = f \left( \frac{a + r_i}{r_i} \right) \sigma \sqrt{\pi (a + r_i)} \tag{5.3}$$

where,

- $K_I$  : Stress intensity factor (Pa√m)
- $\sigma$  : Applied stress (Pa)
- $a$  : Half crack length (m)
- $r_i$  : Hole radius (m)

$$f = \frac{K_I}{\sigma \sqrt{\pi (a + r_i)}} : \text{Normalized stress intensity factor}$$

$f$  values for various dimensions are tabulated in Table 5. 1.



**Table 5. 1 Normalized stress intensity factor values for different geometries (Wang, 1996)**

$(a+r_i)/r_i$	$f((a+r_i)/r_i)$	$(a+r_i)/r_i$	$f((a+r_i)/r_i)$	$(a+r_i)/r_i$	$f((a+r_i)/r_i)$
1.01	0.3256	1.08	0.7843	1.30	1.0358
1.02	0.4514	1.10	0.8400	1.40	1.0536
1.04	0.6082	1.20	0.9851	1.80	1.0495
1.06	0.7104	1.25	1.0168		

In this verification study,  $((a+r_i)/r_i)$  was equal to 1.40. Therefore, with the corresponding normalized factor  $f = 1.0536$ , mode I stress intensity factor was calculated analytically as  $0.06987 \text{ Pa}\sqrt{\text{m}}$ . Stress intensity factors computed with ABAQUS program, were equal to  $0.06977 \text{ Pa}\sqrt{\text{m}}$ . The error in the computation was equal to 0.143 %.

Elastic modulus and Poisson's ratio effects on stress intensity factor were also studied in this verification problem. Similar to the former verification problem, stress intensity factor did not change with different elastic moduli. Models having Poisson's ratios between 0.0 and 0.5, stress intensity factors were equal to  $0.06974 \text{ Pa}\sqrt{\text{m}}$  and  $0.06978 \text{ Pa}\sqrt{\text{m}}$ , respectively. The difference between results was equal to only 0.051 %. Elastic modulus and Poisson's ratio do not seem to affect the stress intensity factor computation in this verification example either. Stress intensity factors determined by changing elastic modulus and Poisson's ratio in numerical modeling are not affected since the expressions (Equations 5.2 and 5.3) used in analytical calculations of stress intensity factor do not depend on elastic modulus and Poisson's ratio.

For both models, central crack in infinite plate and infinite plate with hole intersected by two cracks, the stress intensity factor results of ABAQUS program are in good agreement with the results of analytical expressions. Therefore, ABAQUS program can be used confidently in determination of stress intensity factors of FBD and MR specimens.

## CHAPTER 6

### NUMERICAL MODELING OF FLATTENED BRAZILIAN DISC

Stresses and stress intensity factors were investigated for flattened Brazilian disc (FBD) specimen model by using ABAQUS finite element package program. FBD geometry is illustrated in Figure 6. 1.

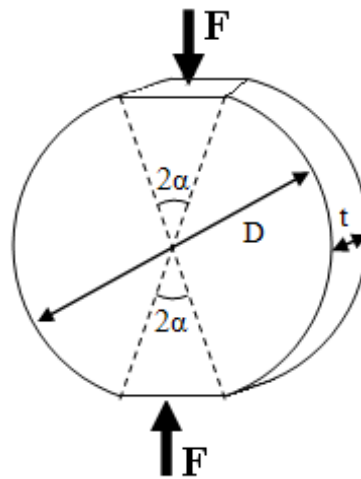


Figure 6. 1 Geometry and boundary conditions of FBD Specimen

#### 6.1 Parameters Affecting Stress Analyses

Before changing loading angle of the specimen model for stress analyses, boundary conditions, thickness, diameter, mesh intensity, and friction coefficient for the loading end-platen contacts on stress distributions were studied for one model geometry. Loading angle  $2\alpha = 20^\circ$  was preferred, since for a valid test it was a proposed loading angle by some researchers (Wang and Xing, 1999; Wang et al., 2004; Kaklis et al., 2005).

### 6.1.1 Boundary Conditions

A number of options for fixity and load application types were tried to find the more realistic boundary conditions with the simpler modeling work. Specimen geometry with 75 mm diameter and 1 m thickness (in 2D plane strain condition) was modeled. Elastic modulus and Poisson's ratio were equal to 12 GPa and 0.15, respectively for the model material.

Option 1: In the first option, the whole specimen geometry was modeled. The top flat end of the specimen was fixed in vertical y-direction and central plane between flat ends fixed in horizontal x-direction. To apply force, a reference point was added almost 3 mm below of the bottom flat end center of the model and this reference point was coupled with the bottom flat end of the specimen model in vertical y-direction (Figure 6. 2). A unit positive vertical load ( $F_y = 1$  N) was applied on the reference point. A unit load was applied since the load is directly proportional to stresses. As the load increases, stresses also increase with the same ratio.

Horizontal (S11) and vertical (S22) stress distributions are as seen in Figure 6. 3. The highest horizontal stress which is tension is at the center of the specimen model. It is equal to 7.90 Pa. The lowest horizontal and vertical stresses, which are compression, equal to -49.65 Pa and -84.19 Pa, respectively, and they are at the flattened ends.

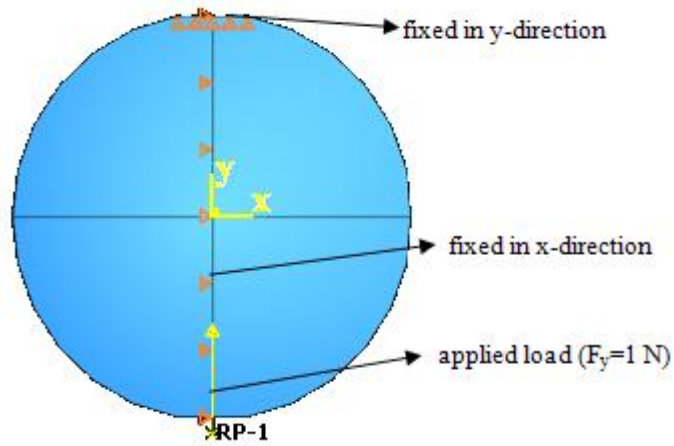


Figure 6. 2 Boundary conditions of Option 1

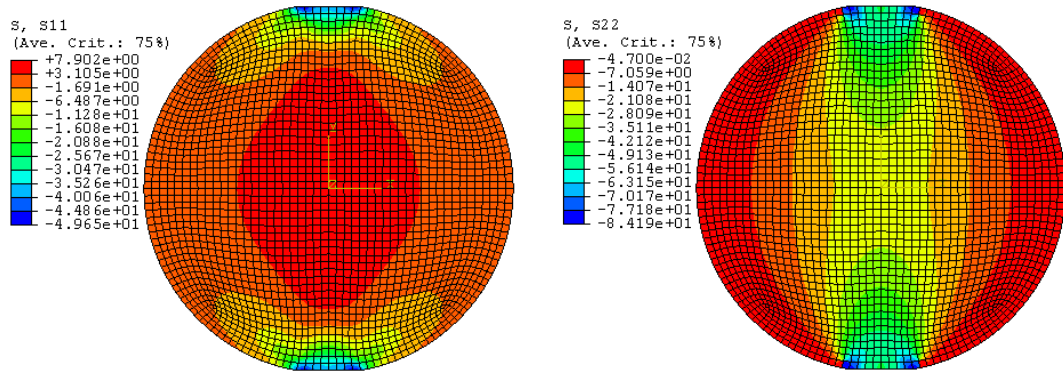


Figure 6. 3 (S11) and vertical (S22) stress distribution for Option 1

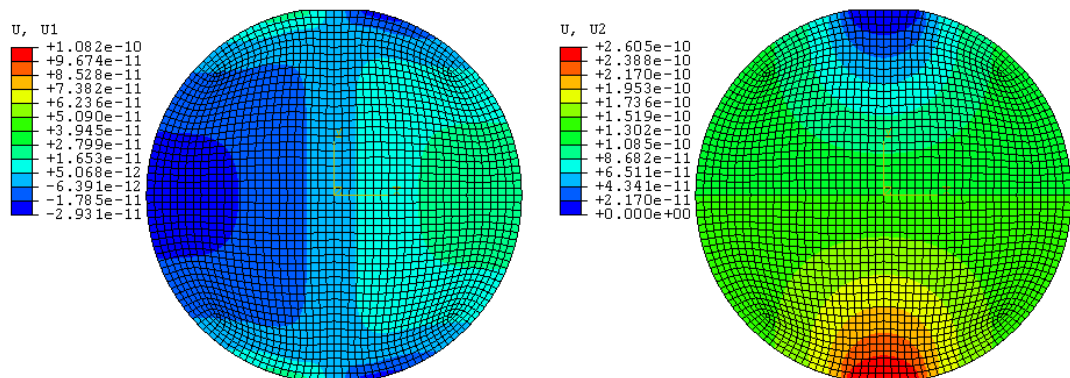


Figure 6. 4 Horizontal (U1) and vertical (U2) displacement contours for Option 1

Horizontal (U1) and vertical (U2) displacement contours are illustrated in Figure 6. 4. Horizontal displacement, at right-hand side of the specimen model has positive values, while at left-hand side of the specimen model it has negative values. Absolute values of the displacements are symmetric at the right and left side of the model. Since the model was fixed at the top flattened end, vertical displacement is nearly zero.

Option 2: In the second option, the whole specimen geometry was modeled as in the Option 1. But as in the experiment, load was not applied to the specimen model directly. Two analytic rigid shells to behave as platens were introduced; boundary conditions were applied to the shells by using reference points. Upper analytic rigid shell was fixed in all directions from its reference point. Lower one was fixed in all directions except vertical y-direction and a unit positive vertical load ( $F_y = 1$  N) in y-direction was applied. To avoid rigid body motion in specimen model, central plane between flat ends was fixed in horizontal x-direction (Figure 6. 5). An interface between specimen and analytic rigid shells was formed, and friction coefficient for this interface was taken as 0.4. This value was adopted from Kaklis et al. (2005).

Horizontal (S11) and vertical (S22) stress distributions of Option 2 are as in Figure 6. 6. The highest horizontal stress which is tension is at the center of the specimen model. It is 7.9 Pa as in Option 1. The lowest horizontal and vertical stresses, which are compression, equal to -49.78 Pa and -84.12 Pa, respectively, and they are at the flattened ends. These results are almost the same as the results of Option 1; the difference is due to the interface in Option 2. Displacement contours are also the same as the contours in Option 1 (Figure 6. 7). Since defining an interface is physically more realistic than applying load directly to the specimen, Option 2 is more preferable than Option 1.

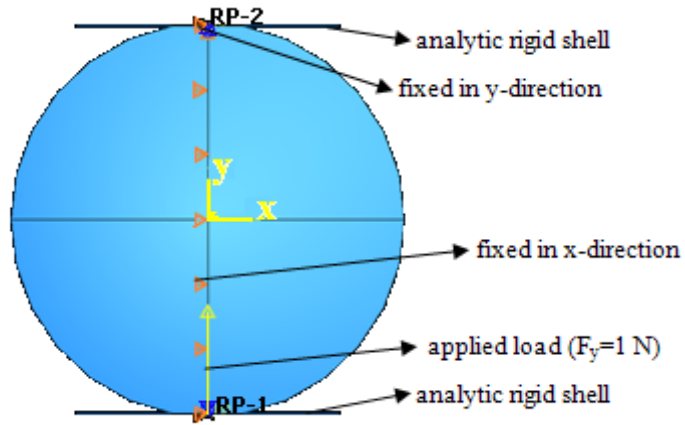


Figure 6. 5 Boundary conditions of Option 2

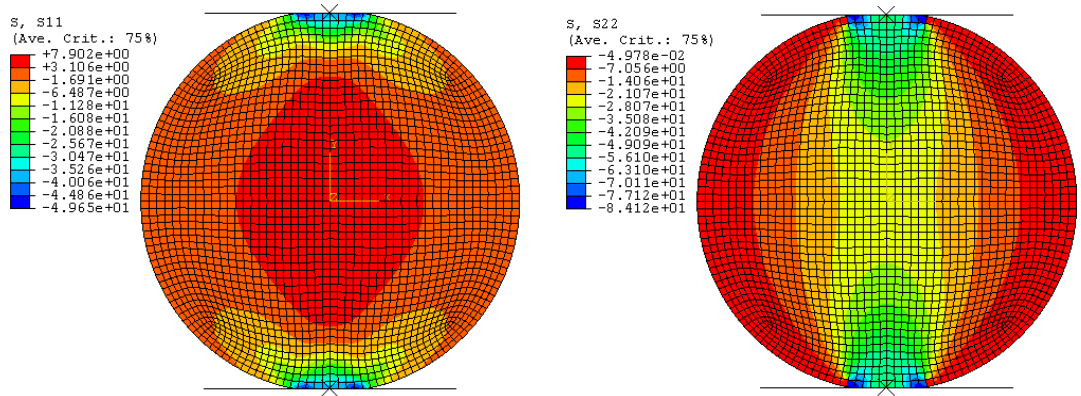


Figure 6. 6 Horizontal (S11) and vertical (S22) stress distribution for Option 2

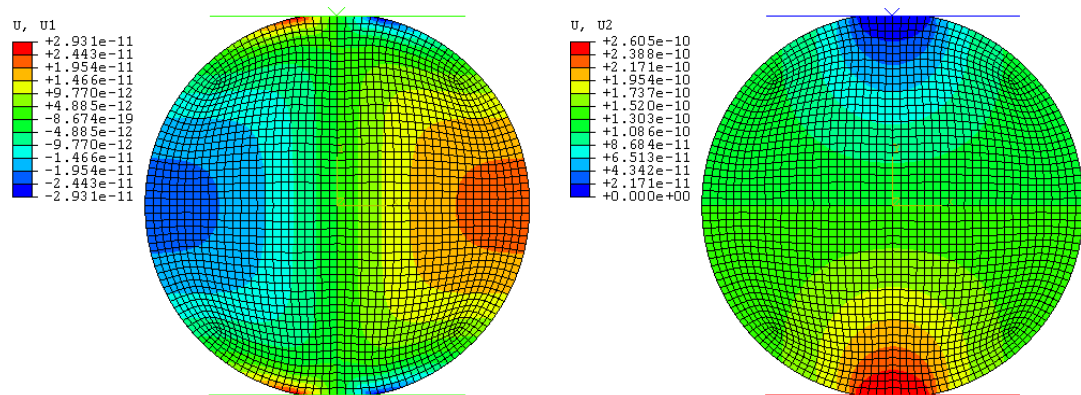
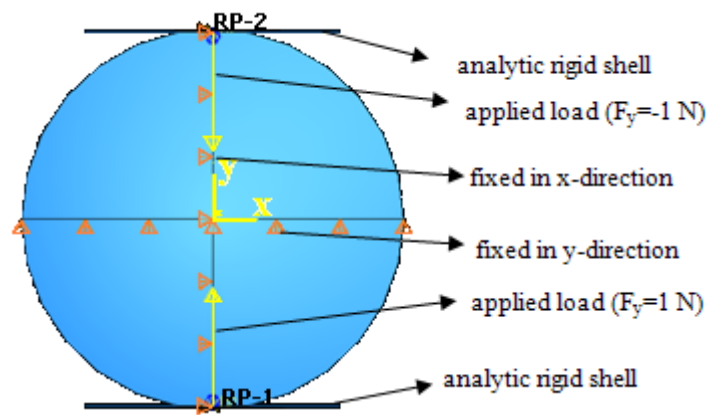


Figure 6. 7 Horizontal (U1) and vertical (U2) displacement contours for Option 2

Option 3: In the third option, the whole specimen geometry was modeled with two analytic rigid shells as in Option 2. The difference with Option 2 was the load. It was applied on both shells: a unit negative vertical load ( $F_y = -1$  N) was applied to the upper rigid shell while a unit positive vertical load ( $F_y = 1$  N) was applied to the lower rigid shell. Reference points for both shells were fixed in all directions except vertical y-direction. To avoid rigid body motion of the specimen model, central plane between flat ends and central plane perpendicular to the loading direction were fixed in horizontal x-direction and in vertical y-direction, respectively (Figure 6. 8). Friction coefficient of the interface was used as in Option 2, i.e.,  $\mu = 0.4$ .



**Figure 6. 8 Boundary conditions of Option 3**

Stress and horizontal displacement (U1) values are the same as Option 2. Vertical displacement is half of the displacement of Option 2 for loaded flattened end ( $2.605e^{-10} / 2 \approx 1.303e^{-10}$ ). These results show that boundary conditions of Option 2 and Option 3 produce the same results.

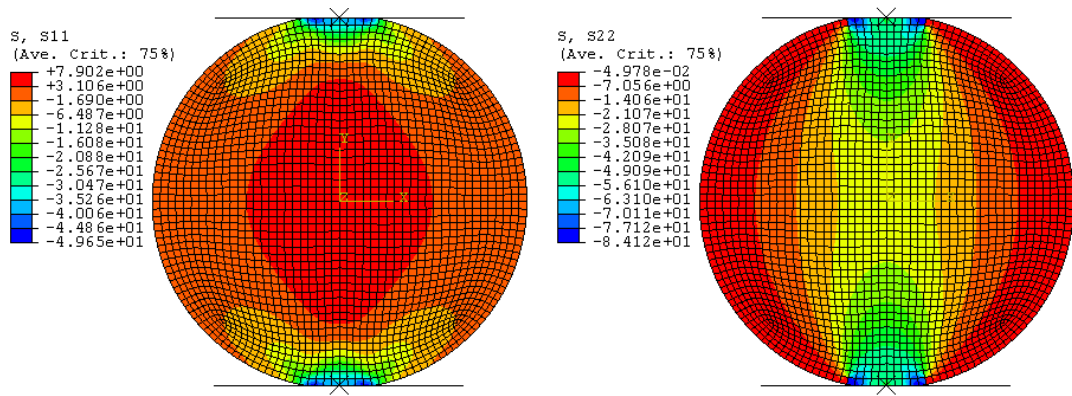


**Figure 6. 9 Horizontal (S11) and vertical (S22) stress distribution for Option 3**

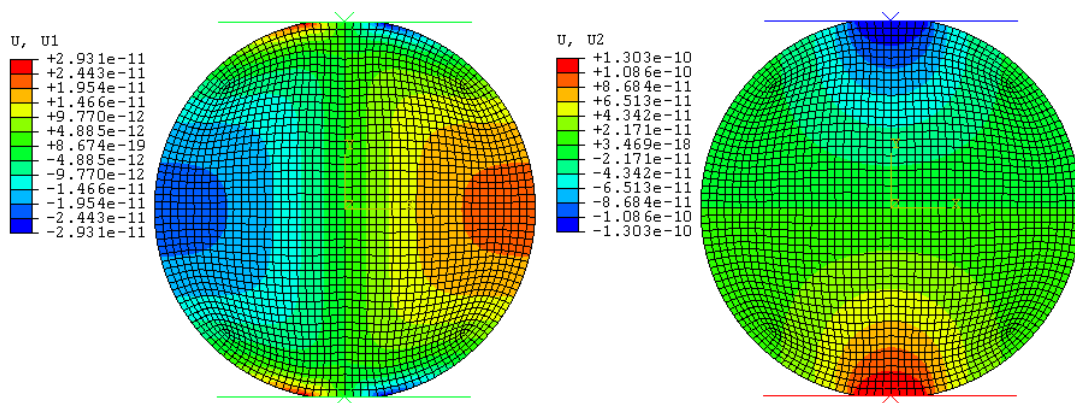


**Figure 6. 10 Horizontal (U1) and vertical (U2) displacement contours for Option 3**

Option 4: In the fourth option, by considering symmetric boundary conditions in Option 3, one quarter of the specimen geometry with one analytic rigid shell on the top of the flattened end was used. Half of one unit negative vertical load ( $F_y = -0.5$  N) was applied to the upper rigid shell's reference point and reference point was fixed in all directions except vertical y-direction. Left end of the quarter part was at the center and it was defined as symmetric in horizontal x-direction. Bottom end of the quarter part was at the center and it was defined as symmetric in vertical y-direction (Figure 6. 11).

As seen from the Figure 6. 12 and Figure 6. 13, all stress and displacement results almost coincide with the results of Option 3. Therefore, there is no need to model whole geometry of the specimen. Meshing the whole model and analyzing it is a



time consuming process and a quarter of the model is enough to simulate the specimen model. As a result, in the further modeling work, boundary conditions and model geometry in Option 4 are used.

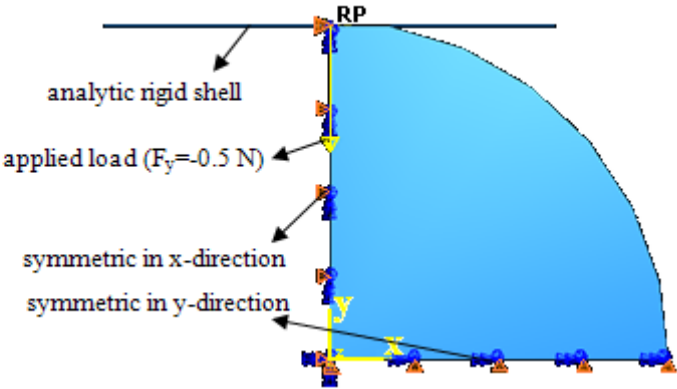


Figure 6. 11 Boundary conditions of Option 4

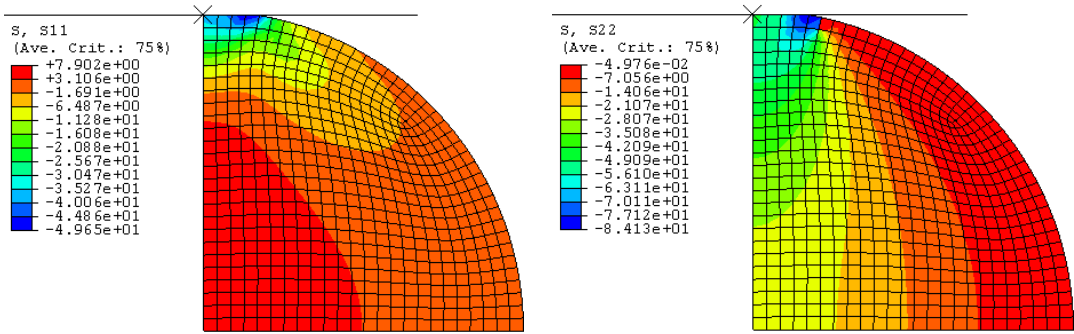


Figure 6. 12 Horizontal (S11) and vertical (S22) stress distribution for Option 4

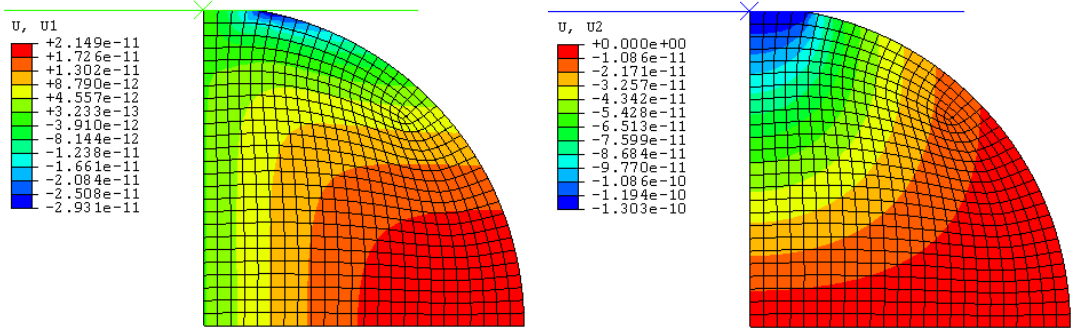


Figure 6. 13 Horizontal (U1) and vertical (U2) displacement contours for Option 4

### 6.1.2 Effect of Specimen Thickness

In 3D models, specimen thicknesses ( $t$ ) were taken as 5 mm, 10 mm, 40 mm, 80 mm, 120 mm, 160 mm and 200 mm and results were compared to decide if plane strain (2D) modeling was accurate enough to save modeling time and effort. A specimen geometry with 75 mm diameter and  $20^\circ$  loading angle was modeled as in the previous section. Material properties were constant, and elastic modulus and Poisson's ratio were taken as 12 GPa and 0.15, respectively. Loading contact friction coefficient was taken as 0.4.

In 3D models, symmetric conditions are also valid for the 3<sup>rd</sup> dimension (z-direction), therefore, half of the specimen thicknesses ( $t/2$ ) were used as 2.5 mm, 5 mm, 20 mm, 40 mm, 60 mm, 80 mm and 100 mm, respectively (Figure 6. 14).

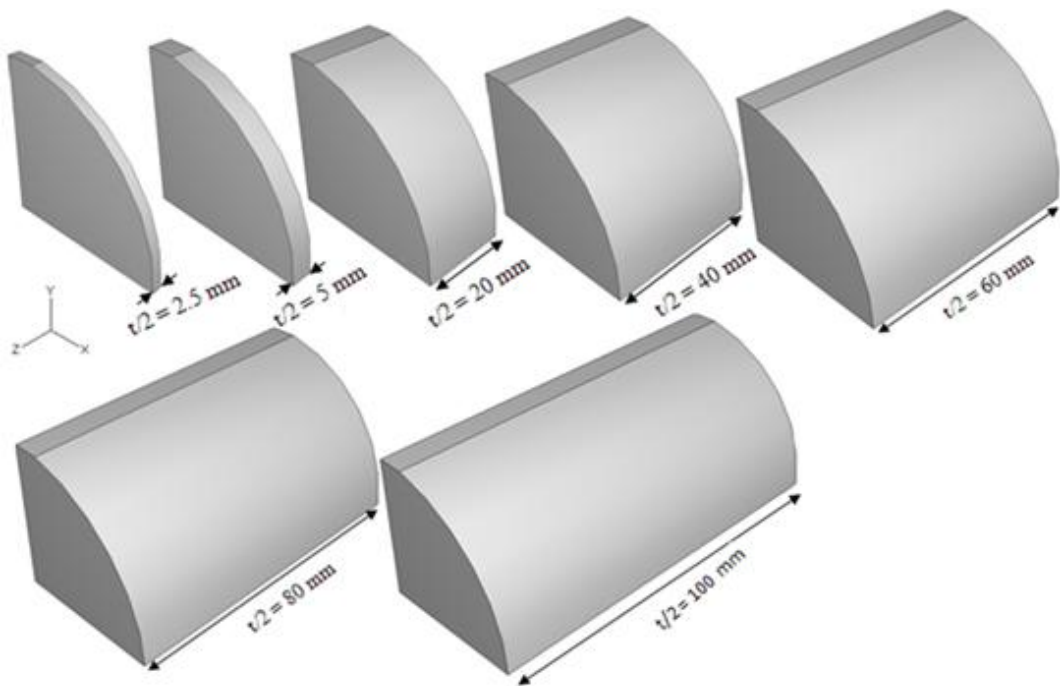
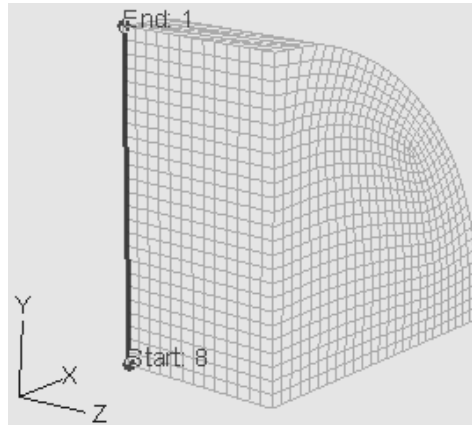


Figure 6. 14 Specimen models in various thicknesses in 3D

Horizontal (S11) and vertical (S22) stresses are more critical at loading ends and at the center. A path through the center line of the model was drawn from center to top of the models, and stresses were examined along the central line of the model to

understand how stress distributions were affected from thickness variations (Figure 6. 15).



**Figure 6. 15 Path used in stress distribution graphs**

In Figure 6. 16, x axis is for horizontal stresses ( $S_{11}$ ) and vertical stresses ( $S_{22}$ ), and y axis shows vertical distance over specimen radius (dimensionless vertical distance,  $y_i/R$ ). As seen from Figure 6. 16, absolute values of the stresses decrease with increasing thickness. When stress values are multiplied with thicknesses, the results are almost constant as illustrated in Figure 6. 17. At the center of the specimen models, the maximum difference for  $S_{11}*t$  between plane strain condition and 3D model was observed for 80 mm thickness. The difference was equal to 6.72%. At the center of the specimen models, the maximum difference for  $S_{22}*t$  between plane strain condition and 3D model was for 40 mm thickness. The difference was equal to 1.26%. These differences are due to the mesh intensity in the 3<sup>rd</sup> dimension. Therefore, geometries can be modeled in 2D plane strain. As a result, the future modeling can be conducted in plane strain conditions with 1 m unit thickness.

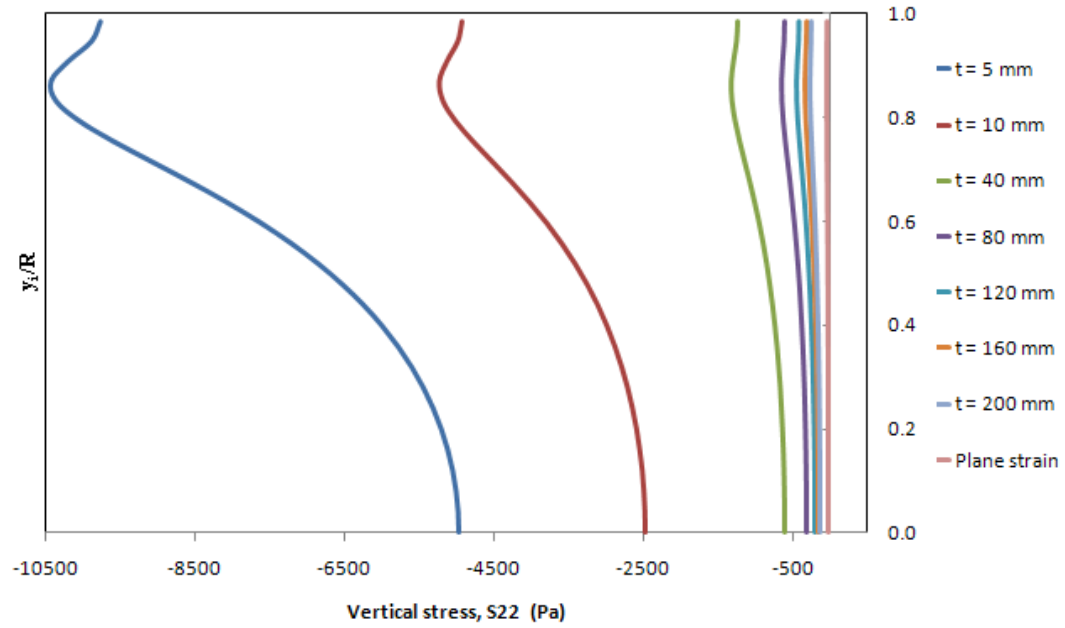
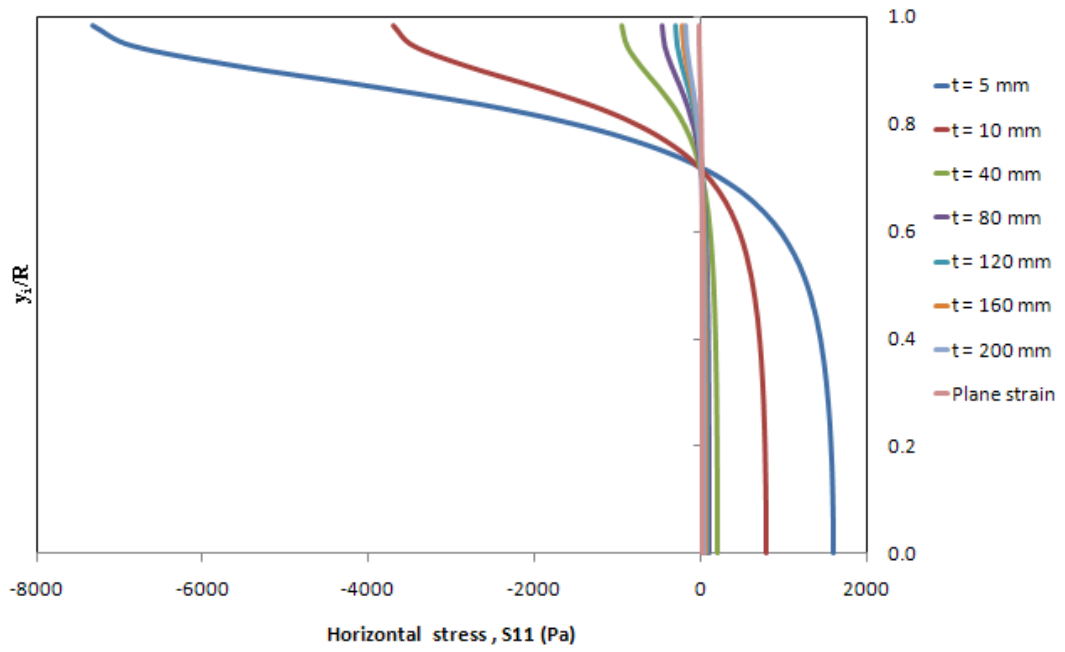


Figure 6. 16 S11 and S22 versus  $y_1/R$  graphs, respectively

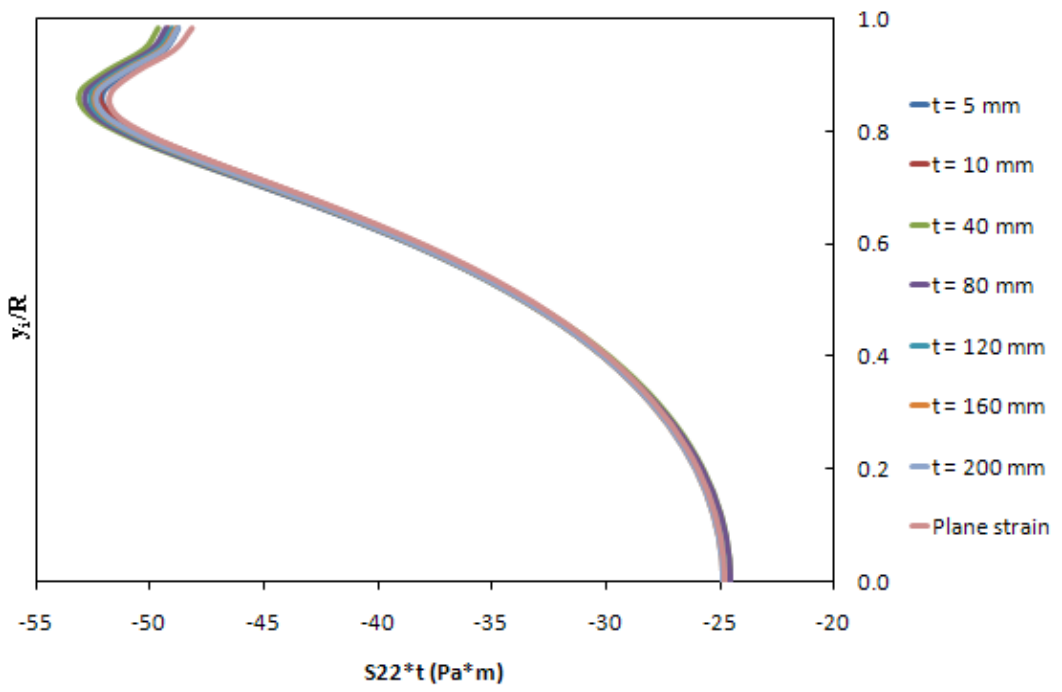
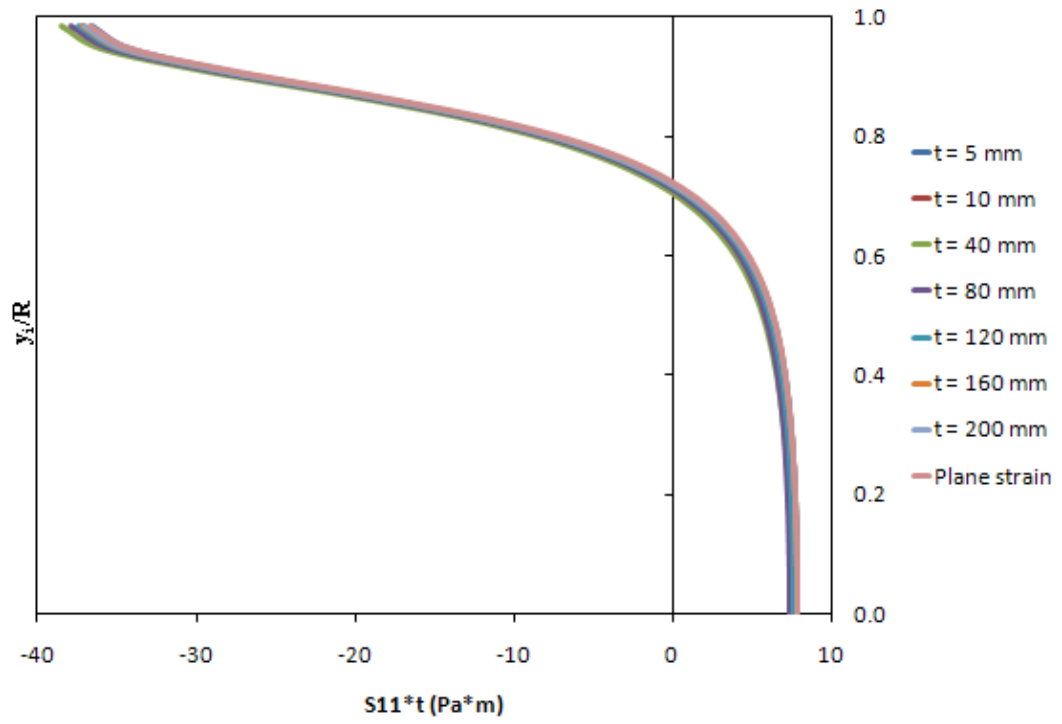


Figure 6. 17  $S_{11} \cdot t$  and  $S_{22} \cdot t$  versus  $y_i/R$  graphs

### 6.1.3 Effect of Specimen Diameter

To see the diameter influence on stresses, various models with diameters between 25 mm and 150 mm (25 mm, 50 mm, 75 mm, 100 mm, 125 mm, 150 mm) were analyzed. Figure 6. 18 illustrates the studied radii.  $2\alpha$  was kept at  $20^\circ$  as in the previous boundary condition and specimen thickness modeling work.

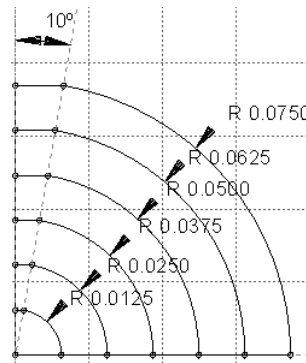


Figure 6. 18 Specimen sketch in different radii

Horizontal (S11) and vertical (S22) stress distributions were plotted through the center line again in Figure 6. 19. As seen from the figure below, absolute values of the stresses decrease with increasing diameter. When stress values are multiplied with diameter, the results almost coincide as illustrated in Figure 6. 20. This means that when stress distribution through central line is computed for one specimen diameter, for the other specimen diameters stress distribution can be predicted without constructing new models. Diameter is going to be taken as 75 mm for future work since it is an intermediate diameter value in the diameter ranges of experimental work.

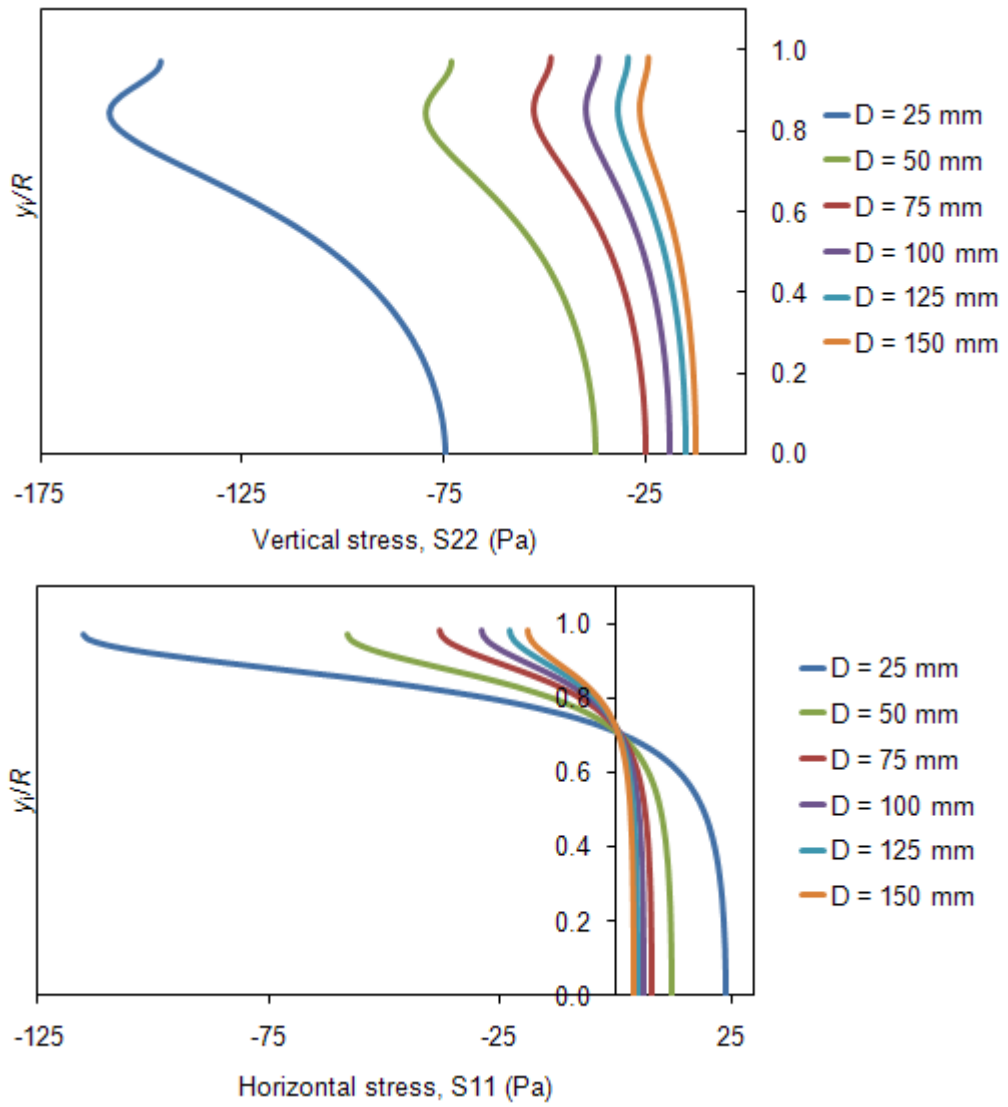


Figure 6. 19 Figure S11 versus  $y_i/R$  and S22 versus  $y_i/R$  graphs, respectively

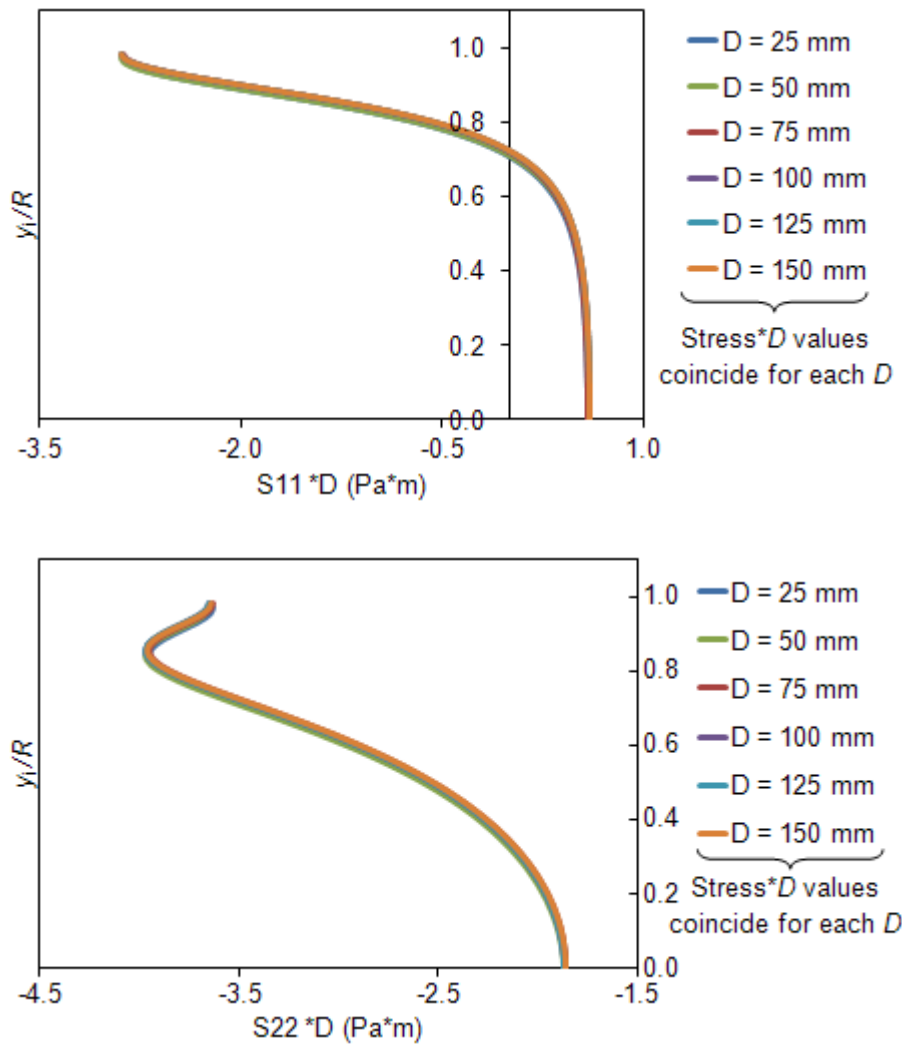


Figure 6. 20  $S_{11} * D$  and  $S_{22} * D$  versus  $y/R$  graphs

#### 6.1.4 Effect of Mesh Intensity

In mesh intensity studies, diameter was 75 mm, thickness was 1 m (in 2D Plane strain condition) and material properties of the model were 12 GPa for elastic modulus and 0.15 for Poisson's ratio and at the interface, friction coefficient was equal to 0.4 at the interface as before.

To make a meaningful judgment about how mesh intensity affects stress values; number of elements on critical parts where crack may initiate should be considered. In this study, vertical central line of the specimen geometry is the most critical since the crack may start from flattened end or center of the specimen according to the geometric parameters of the models. In Figure 6. 21, the numbers on the elements



define the number of elements through the central line. Analyses were done for vertical center line having 10, 20, 30, 40, 50, 60, 70, 100, 150 and 200 elements.

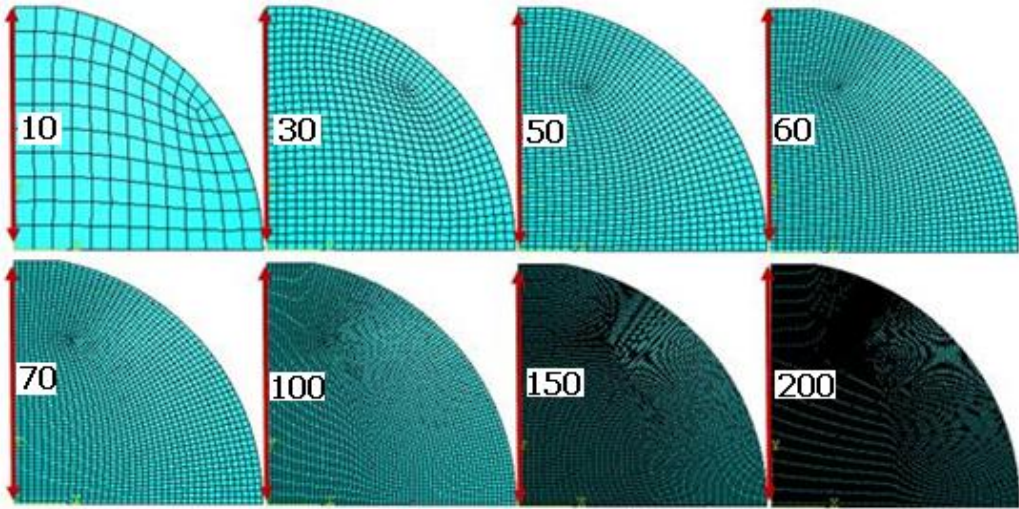


Figure 6. 21 Number of elements along the central line for different mesh intensities

Horizontal (S11) and vertical (S22) stress values on the flattened end and at the center versus number of elements through the vertical center line are plotted in Figure 6. 22. As seen from the figure, the number of elements does not influence the stresses at the center of the model, while stresses on the flattened end are affected significantly by mesh density. The difference between horizontal (S11) stresses of the lowest (10 elements) and the highest (200 elements) number of elements cases for the flattened end is greater than 20%.

$$\left[ \frac{S11_{(10\text{ elements})} - S11_{(200\text{ elements})}}{S11_{(200\text{ elements})}} \times 100 = \frac{39.3663 - 30.8490}{-39.3663} \times 100 = 21.64\% \right]$$

The variation of vertical (S22) stresses for the lowest (10 elements) and the highest (200 elements) number of elements on the flattened end is around 3.5%.

$$\left[ \frac{S22_{(10\text{ elements})} - S22_{(200\text{ elements})}}{S22_{(200\text{ elements})}} \times 100 = \frac{49.1409 - 47.4108}{-49.1409} \times 100 = 3.52\% \right]$$

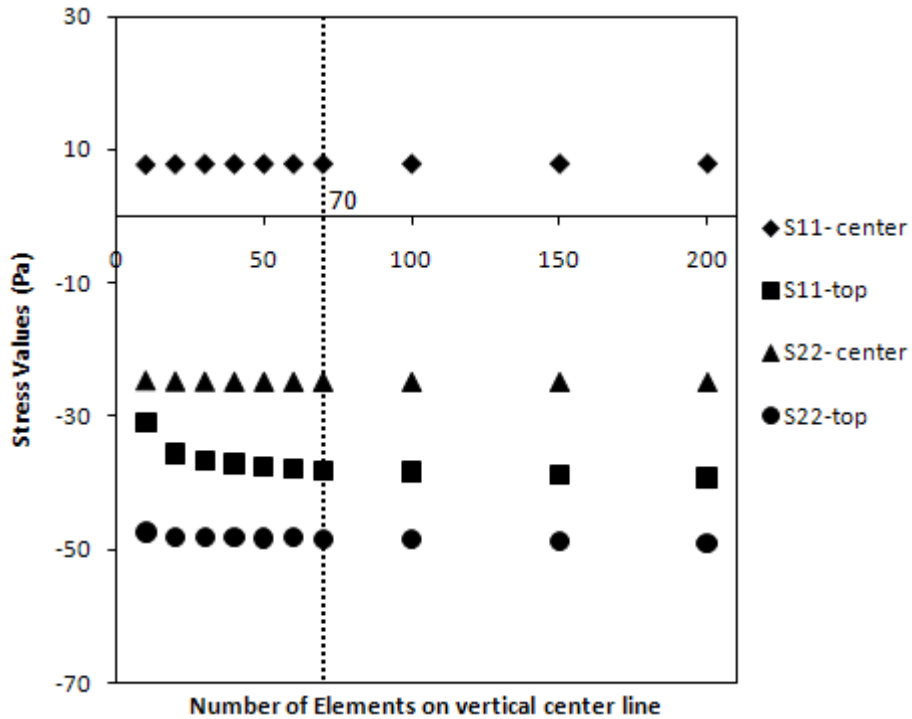


Figure 6. 22 Convergence in stresses with increasing mesh intensity along vertical center line

When number of elements is taken as 70 along the center line, the difference in variation of stress distribution magnitudes stays below 3%.

$$\left[ \frac{S11_{(200\text{ elements})} - S11_{(70\text{ elements})}}{S11_{(200\text{ elements})}} \times 100 = \frac{(-39.3663) - (-38.3621)}{-39.3663} \times 100 = 2.55\% \right]$$

$$\left[ \frac{S22_{(200\text{ elements})} - S22_{(70\text{ elements})}}{S22_{(200\text{ elements})}} \times 100 = \frac{(-49.1409) - (-48.4331)}{-49.1409} \times 100 = 1.44\% \right]$$

When displacement contours were taken into account, similar results were obtained. Displacement distributions were not affected significantly when number of elements was kept above 70 along the central line (Figures 6.23 and 6.24).

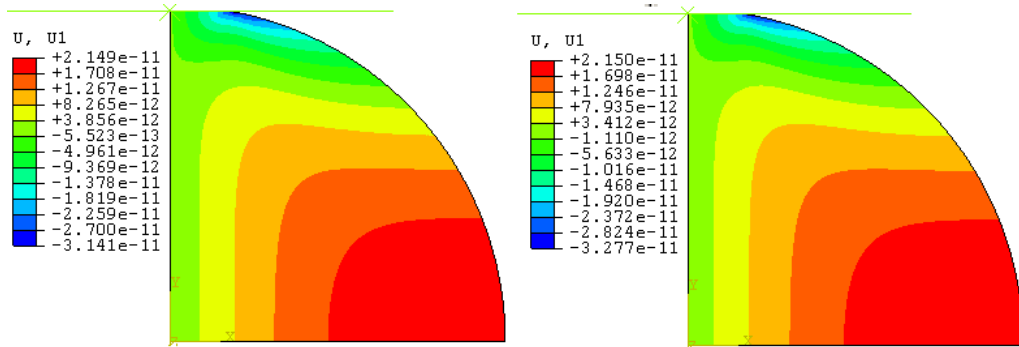


**Figure 6. 23 Horizontal (U1) displacement contours for 70 elements and 200 elements respectively**

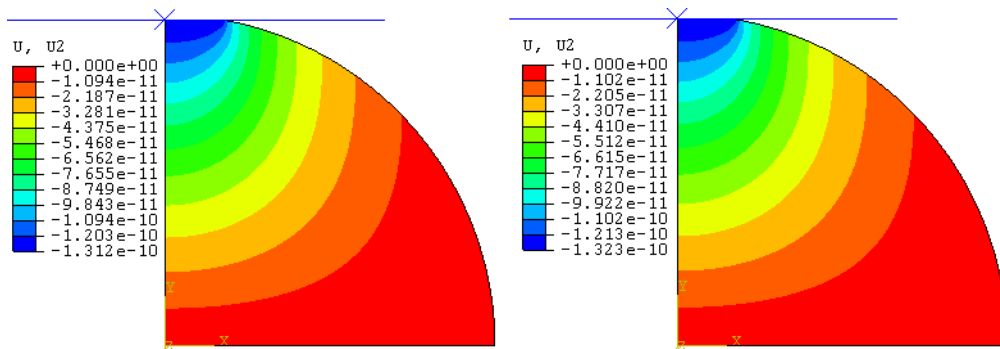


**Figure 6. 24 Vertical (U2) displacement contours for 70 elements and 200 elements respectively**

Further modeling work on stress analyses are going to be conducted with mesh intensity having at least 70 elements on vertical line and almost 2000 elements as total. 70 elements in the modeling runs save time and effort with respect to 200 elements. These limits are for model geometries with 75 mm diameter with loading angle of 20°. When the diameter is increased or decreased, these numbers are going to be the same. But, as the angle increases this value decreases proportional to the length of the reduced center line distance.

### 6.1.5 Effect of Friction Coefficient

To determine effect of the friction coefficient ( $\mu$ ) on the stress distribution, various friction coefficient values were applied to the contact properties for specimen model having 75 mm diameter with 20° loading angle. Values changed from a frictionless contact surface condition to higher friction coefficient contact conditions.

Coefficients applied were 0.0, 0.4, 0.8, 1.2, 1.6, 3.0, 10.0 and 50.0. As seen from Figure 6. 25, the stresses do not change observably while the friction coefficient value is changed from 0 to 50. When stresses at the flattened end which is the contact location were examined in detail, stresses were close to each other for friction coefficients 0 and 50 (Figure 6. 26).

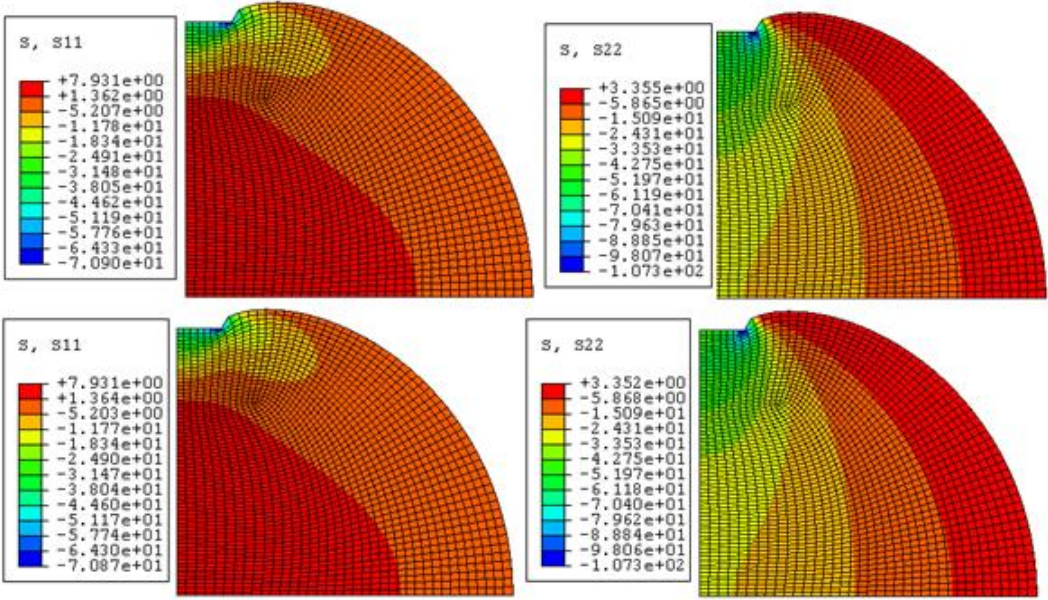


Figure 6. 25 S11 and S22 stresses for models having  $\mu=0.0$  and  $\mu=50$ , respectively

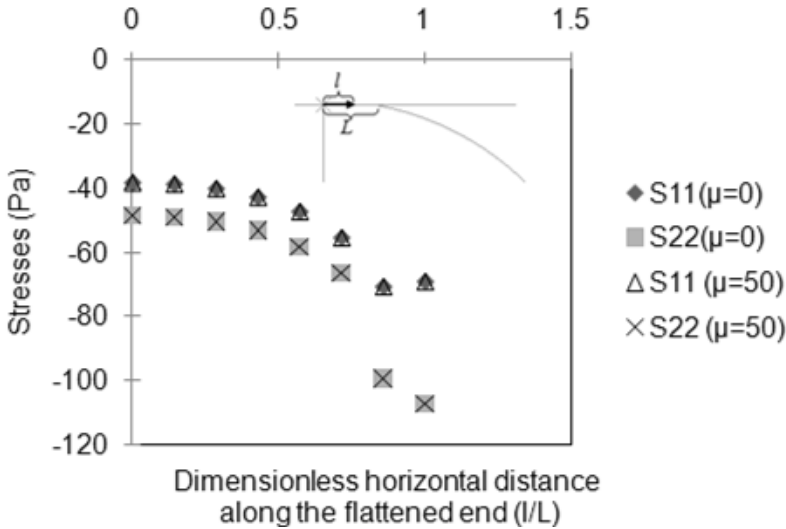
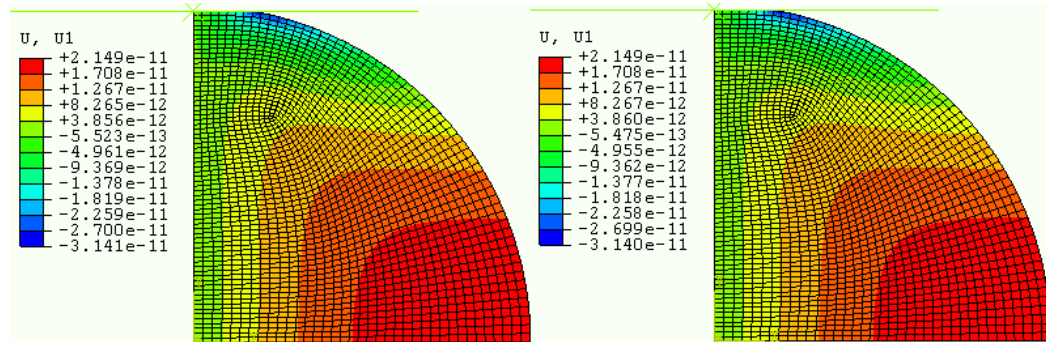
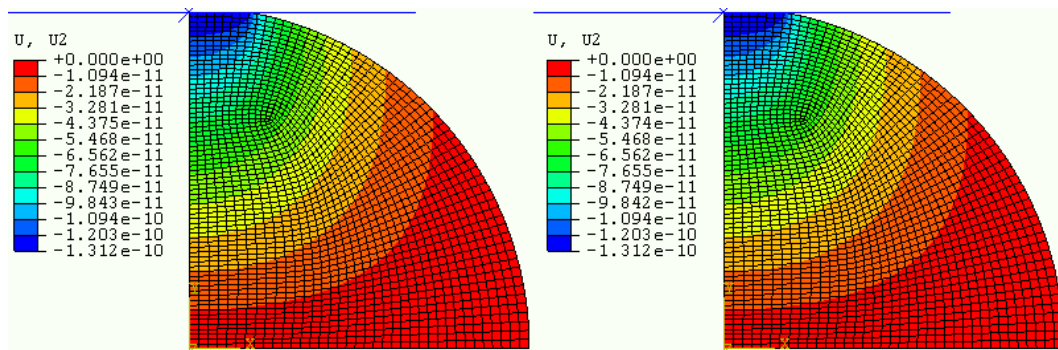


Figure 6. 26 Stresses along the horizontal distance through the flattened end

Displacement contour values also do not depend on the friction coefficient value (Figures 6.27 and 6.28).



**Figure 6. 27 Horizontal (U1) displacement contours for having friction coefficients of 0.0 and 50 respectively**



**Figure 6. 28 Vertical (U2) displacement contours for having friction coefficients of 0.0 and 50 respectively**

Friction coefficient effect on stress intensity factor was also conducted on the specimen model having 75 mm diameter with 20° loading angle. Results showed that stress intensity factor was not affected from the friction coefficient (Figure 6. 29). By using rigid shell and defining friction coefficient to the contact between flattened end of the specimen and loading platen, boundary conditions at the flattened end behave as slip-allowed boundary condition as in the models studied by Fischer et al. (1996). For this type of boundary condition, Fischer et al. (1996) found that variation in Poisson’s ratio did not affect the stress intensity factor.

According to Fischer et al. (1996), if slip is not allowed at the contacts, Poisson's ratio affects stress distributions and stress intensity factor values.

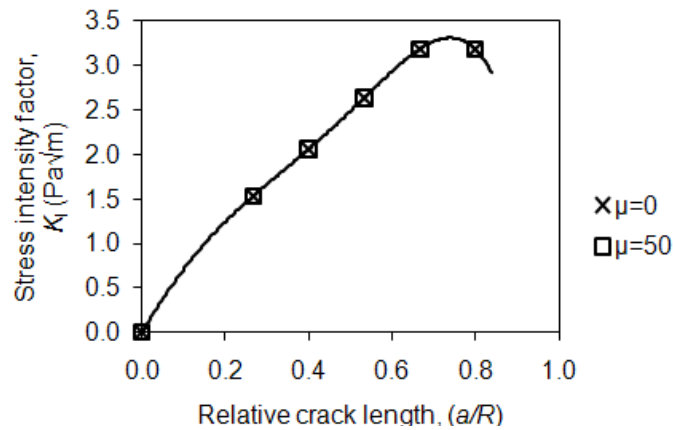


Figure 6. 29 Stress intensity factor versus relative crack length for  $\mu=0$  and  $\mu=50$

In the study of Kaklis et al. (2005) the friction coefficient between platens and rock specimen were taken as 0.4. By considering Kaklis et al. (2005) studies on rocks, in the future studies, analyses are going to be performed with friction coefficient of 0.4.

### 6.1.6 Effect of Loading Angle

In this part, effect of loading angle on stress distribution was studied by taking loading angle ( $2\alpha$ ) as  $10^\circ$ ,  $20^\circ$ ,  $30^\circ$ ,  $40^\circ$ ,  $50^\circ$  and  $60^\circ$ . The sketches of the half of the loading angles ( $\alpha$ ) used in this study are illustrated in Figure 6. 30.

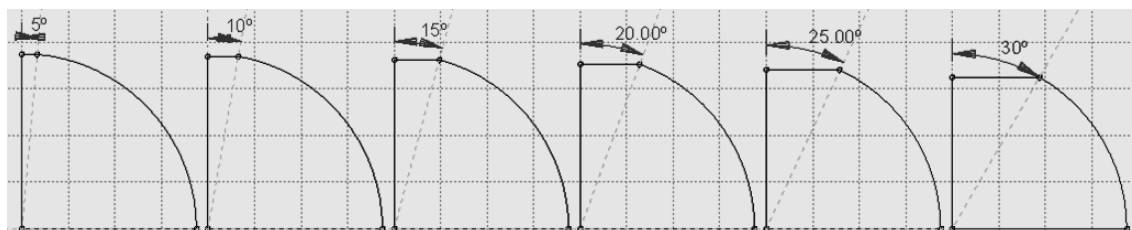


Figure 6. 30 Specimen sketch in different loading angles

Absolute values of the horizontal (S11) and vertical (S22) stresses along the central vertical line decrease with increasing loading angle ( $2\alpha$ ) (Figure 6. 31).

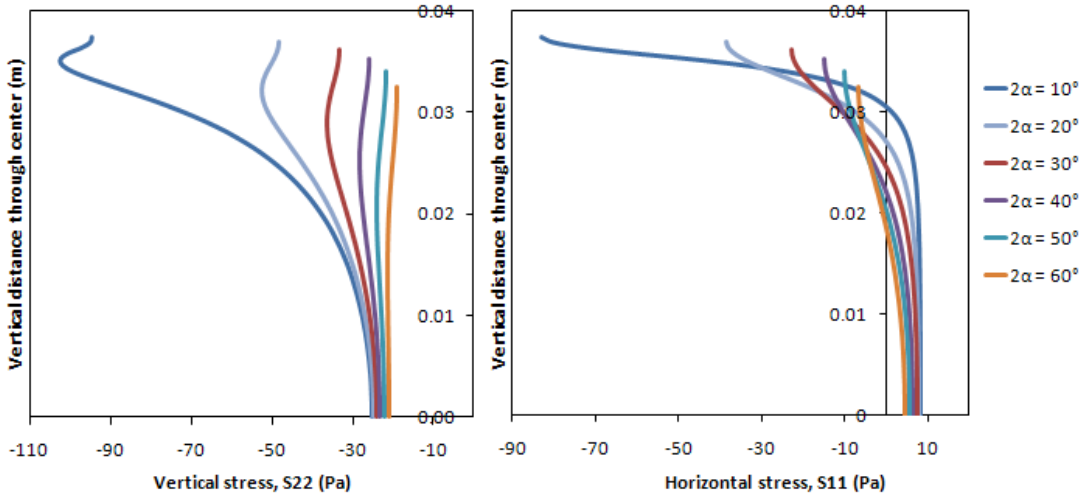


Figure 6. 31 S11 versus y and S22 versus y graphs, respectively

### 6.2 Crack Initiation Location According to Stress Analyses

Before performing stress intensity factor computations, stress distributions were examined to determine crack initiation conditions along the diametral plane of the specimen. To determine crack initiation location along the diametral line, Griffith strength criterion (Griffith, 1921) was applied as in the studies of Wang and Xing (1999), Wang and Wu (2004), Wang et al. (2004), and Kaklis et al. (2005). Analytical expression of the Griffith’s classical fracture theory is as follows (Griffith, 1921; Clausing, 1959, Chang, 1974): (Tensile stress is considered positive in these solutions)

$$\sigma_t - \sigma_t = 0 \quad \text{if} \quad 3\sigma_1 + \sigma_3 \geq 0 \quad (6. 1)$$

$$\sigma_1 - \sigma_3 \geq 0 + 8\sigma_t \sigma_1 + \sigma_3 \geq 0 \quad \text{if} \quad 3\sigma_1 + \sigma_3 < 0 \quad (6. 2)$$

where,

- $\sigma_1$  : maximum principal stress
- $\sigma_3$  : minimum principal stress
- $\sigma_t$  : tensile strength

In Brazilian test, crack initiates at the center when  $3\sigma_1 + \sigma_3 = 0$  and when this condition is satisfied, according to Griffith's theory, tensile strength is,  $\sigma_t = \sigma_I$  for original Brazilian test. However, when the Brazilian disc is flattened, stress conditions at the center change and  $3\sigma_1 + \sigma_3 < 0$  inequality condition governs the tensile crack initiation. Then for tensile strength estimation, governing expression involving both  $\sigma_1$  and  $\sigma_3$  principal stresses, becomes:

$$\sigma_t = \frac{\sigma_1 - \sigma_3}{-8(\sigma_1 + \sigma_3)} \quad (6.3)$$

Left hand side of this equation is also called equivalent stress  $\sigma_G$ , and for Brazilian tensile strength test  $\sigma_G = \sigma_t = 2F/\pi Dt$ .

Distribution of equivalent stress  $\sigma_G = (\sigma_1 - \sigma_3)^2 / [-8(\sigma_1 + \sigma_3)]$  for various loading angles is plotted against the vertical distance from center to the flattened end of the specimen,  $(y_i/R)$  in Figure 6. 32. Horizontal scale of this plot is dimensionless equivalent stress  $\overline{\sigma_G}$ . This was set by normalizing equivalent stress  $\sigma_G$  with the stress perpendicular to the crack plane  $(2F/\pi Dt)$ , which is generally used for tensile strength estimation in Brazilian test for the maximum value of load  $F$  at failure.

Stress distributions to check whether the crack initiation is at the center of the discs were generated for specimen models having 25 mm, 50 mm, 54 mm, 75 mm, 100 mm, and 125 mm diameters. Figure 6. 32 illustrates stress distributions in terms of equivalent stress with different loading angles for specimen models having 75 mm diameter.

Crack initiation occurs at a point where  $\overline{\sigma_G}$  attains its maximum value along the diametral distance  $(y_i/R)$ . As seen in Figure 6. 32, for loading angles around 14 degrees location of maximum stress for crack initiation moves away from the specimen center towards the loading end. This situation can be clearly identified on  $2\alpha=10^\circ$  and  $2\alpha=12^\circ$  stress distribution curves where  $\overline{\sigma_G}$  is around 1.13 for  $2\alpha=10^\circ$  and 1.03 for  $2\alpha=12^\circ$  curves around  $y_i/R=0.77$  and  $y_i/R=0.70$ , respectively. This means that crack initiation is expected to start along the diametral plane, but out of



the center for such loading angles. When loading angles become more than 14 degrees maximum  $\overline{\sigma}_G$  stress location stays right at the center of the disc specimens with values lower than one for increasing loading angles. Therefore, in experimental studies, the minimum loading angle is going to be taken as 15° to be on the safe side.

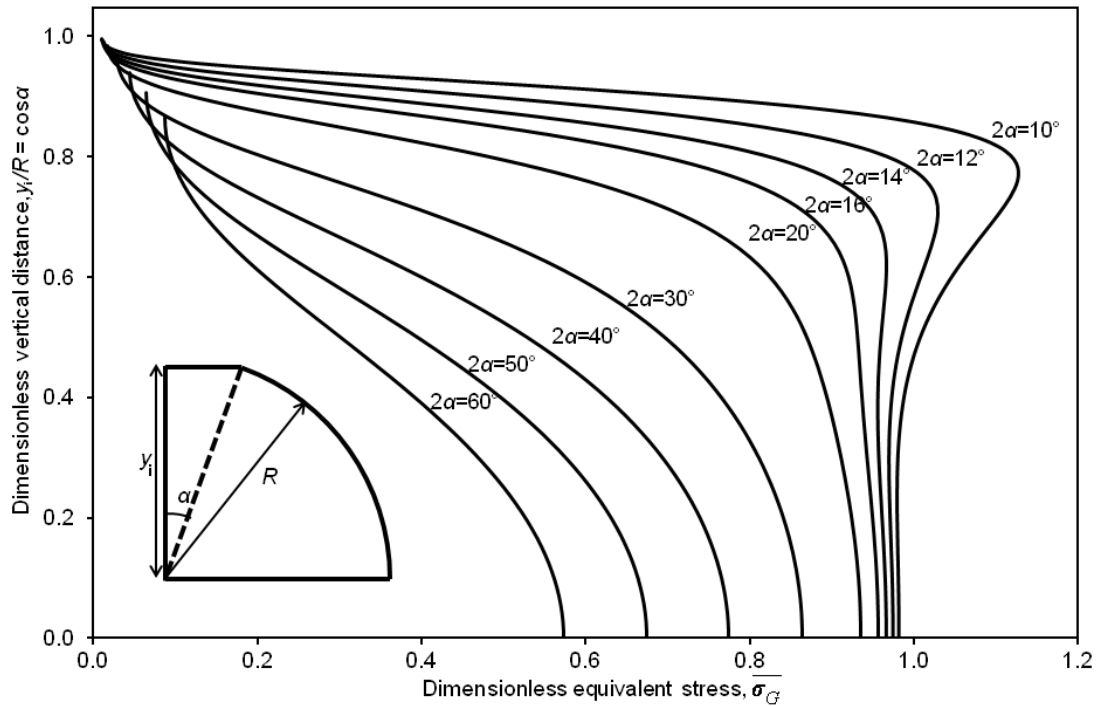


**Figure 6. 32 Normalized stress versus normalized vertical distance graphs (for specimen models having 75 mm diameter)**

Similar works including interpretation of the crack initiation location on Brazilian discs were conducted by Wang and Xing (1999), Wang and Wu (2004), Wang et al. (2004), and Kaklis et al. (2005). By using boundary element method, critical loading angle was found to be greater than 19.5° (Wang and Xing, 1999). This angle was found to be equal to 20° in (Wang and Wu, 2004; Wang et al., 2004) and 15° in (Kaklis et al., 2005) by finite element methods.

In order to generalize the relation between principal stresses at the center of the specimen models and loading angle, loading angle was changed between 15° and

60° which corresponds to dimensionless distance between  $y/R=0.991$  and  $0.866$ , respectively. Dimensionless principal stresses normalized by dividing them to the tensile strength equation  $2F/(\pi Dt)$  of Brazilian test are given in Figure 6. 33. By curve fitting, dimensionless principal stresses in terms of half loading angle  $\alpha$  at the center of the specimens with loading angles between 15° and 60° are:

$$\overline{\sigma}_1 = \frac{\sigma_1}{2F/(\pi Dt)} = 0.94 \cos(\alpha) + 0.04 \quad (6.4)$$

$$\overline{\sigma}_3 = \frac{\sigma_3}{2F/(\pi Dt)} = -1.08 \cos(\alpha) - 1.92 \quad (6.5)$$

Horizontal stress which is used to estimate tensile strength in Brazilian test is equal to the maximum principal stress, while vertical stress is equal to the minimum principal stress.

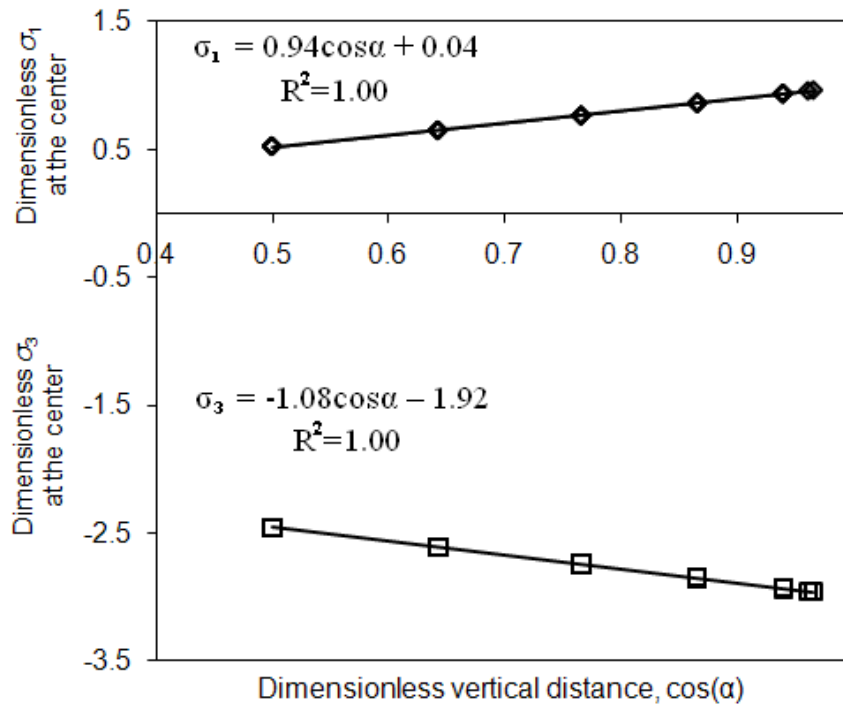


Figure 6. 33 Dimensionless principal stresses versus dimensionless vertical distance plot

By using Equations 6.4 and 6.5, dimensionless equivalent stress can be expressed as a function of half loading angle as (Figure 6. 34):

$$\overline{\sigma_G} = \frac{\sigma_G}{2F/(\pi Dt)} = 0.83 \cos(\alpha) + 0.15 \quad (6. 6)$$

Equation 6.6 can be used as a geometrical factor in tensile strength estimation with FBD specimens. This factor is valid for the loading angle ( $2\alpha$ ) between  $15^\circ$  and  $60^\circ$ .

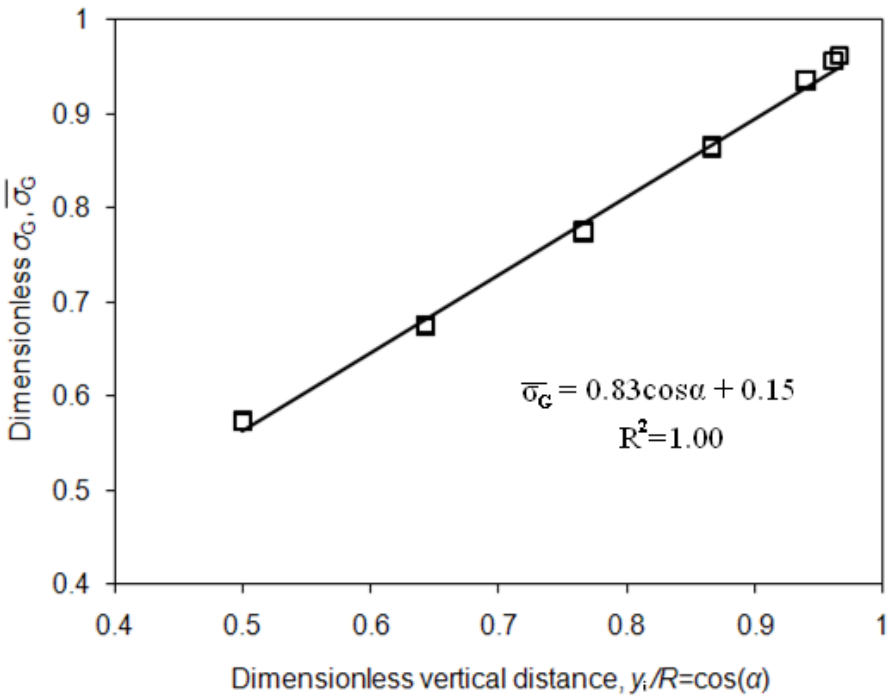


Figure 6. 34 Dimensionless equivalent stress versus dimensionless vertical distance plot

### 6.3 Stress Intensity Factor Analyses

Stress intensity factors are directly proportional to stresses; thus there is no need to analyze how boundary conditions, thickness of the specimen, mesh intensity of the whole model, friction coefficient, elastic modulus and Poisson’s ratio influence the stress intensity factor. Parameters used in stress analyses were used in stress intensity factor analyses. One quarter of the model was modeled with symmetric boundary and 2D plane strain ( $t = 1$  m) conditions, and friction coefficient was

taken as 0.4. Elastic modulus and Poisson's ratio were 12 GPa and 0.15, respectively.

For stress intensity factor evaluation, a contour integral region was considered in rings around the crack tip. At the center of these rings crack tip and crack extension direction were defined as in Figure 6. 35. Large stress concentrations occur at the crack tip. Therefore, a refined mesh must be created around the crack tip to get accurate results for stresses and strains.

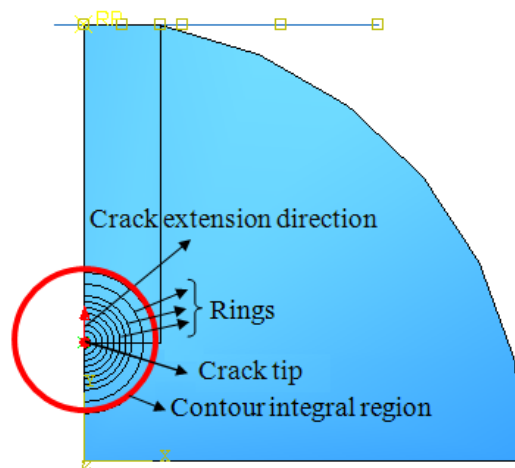


**Figure 6. 35 Contour integral region, crack tip and extension direction**

Since the quarter of the model was studied, in defining the crack, “On symmetry plane (Half-crack model)” option was selected. According to the stress analyses, crack initiated at the center and propagates from center to the flattened end, therefore, crack extension direction was defined with vector having (0,1,0) coordinates. In these analyses, LEFM assumption was applicable, and a  $1/\sqrt{r}$  strain singularity is dominant. To provide this singularity in the models, midside node parameter was taken as 0.25 and “Degenerate Element Control at Crack Tip” was selected as “Collapsed element side, single node” at “Singularity” option of “Edit Crack”.

To provide more accurate results for stress intensity factor, area of the contour integral region and mesh intensity in the contour integral region were optimized before stress intensity factor evaluation according to the loading angle and diameter.

### 6.3.1 Contour Integral Region

Contour integral region is the region where stress intensity factor values are computed. It must be large enough that the average of the stress intensity factor in that region could converge. On the other hand, it must be small enough to provide a sufficient area for smaller and larger cracks to achieve a valid mesh. For instance, for specimens having 37.5 mm radius with 5 mm and 33 mm crack lengths, contour integral region radius cannot exceed 2-3 mm.

To see the contour integral region effect on stress intensity factor, a model having 75 mm diameter with 20° loading angle was conducted. Contour integral region radius was changed from 0.25 mm to 6 mm (Figure 6. 36). The average stress intensity factor was computed as 1.46675 Pa√m for 0.25 mm radius and 1.52819 Pa√m for 6 mm radius. The difference between these values was almost equal to 4%. When radius was taken as 2 mm, stress intensity factor became 1.52181 Pa√m and the difference between 2 mm radius with 6 mm radius decreased to 0.4%. Thus, contour integral ring radius should be taken as 2 mm to get more accurate results with an appropriate mesh.

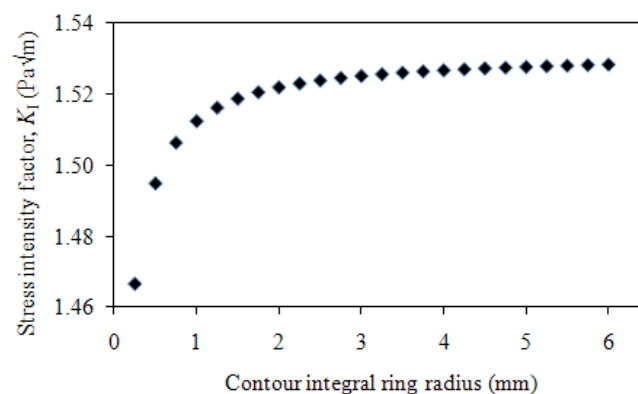


Figure 6. 36 Stress intensity factor variation according to contour integral ring radius

### 6.3.2 Mesh Intensity in the Contour Integral Region

Mesh intensity of the whole specimen used for stress intensity factor analyses was almost the same as mesh intensity of the whole specimen used for the stress analyses (Figure 6. 37). For stress intensity factor analyses mesh intensity in the contour integral region was adjusted to obtain accurate stress intensity factor results.

Mesh refinement around the crack tip is defined in ABAQUS Analysis User's Manual as: The size of the crack-tip elements affects the accuracy of the solutions: the smaller the radial dimension of the elements from the crack tip, the better the stress, strain, etc. results will be and, therefore, the better the contour integral calculations will be. The angular strain dependence is not modeled with the singular elements. Reasonable results are obtained if typical elements around the crack tip subtend angles ( $\beta$ ) in the range of  $10^\circ$  (accurate) to  $22.5^\circ$  (moderately accurate).

In this study, for accurate mesh around the crack tip, contour integral rings for half model) were divided into 16 parts. This means that each crack tip subtend angles ( $\beta$ ) was equal to  $11.25^\circ$  (Figure 6. 38). This value is in the valid range.

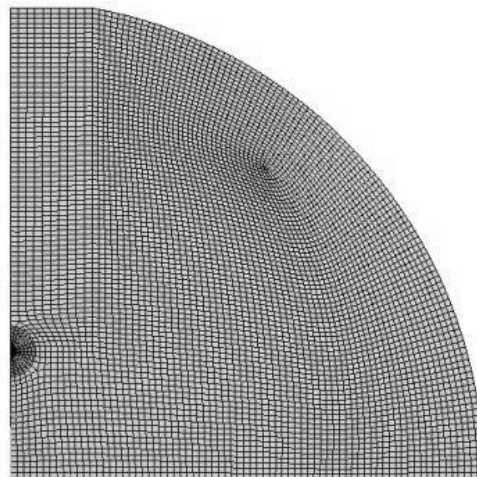
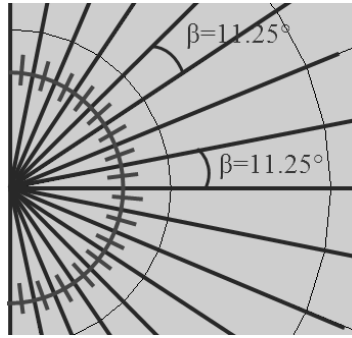
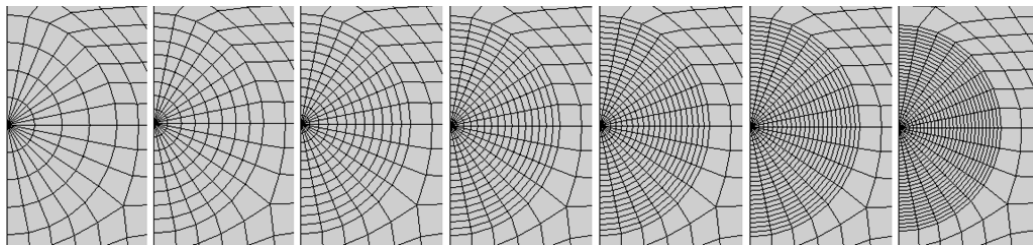


Figure 6. 37 A typical cracked specimen geometry with mesh



**Figure 6. 38 Crack tip elements and crack tip subtend angles**

Besides the crack tip subtend angles, number of contours in the contour integral region is also important in mesh intensity studies. To examine the mesh density influence on stress intensity factor values, number of contours in the contour integral region was changed in between 4 and 28 (4, 8, 12, 16, 20, 24 and 28) as seen in Figure 6. 39.



**Figure 6. 39 Various mesh intensities at the contour integral region  
(No of contours in the contour integral region = 4, 8, 12, 16, 20, 24 and 28, respectively)**

As number of contours increases in contour integral region, stress intensity factor value converges as in Figure 6. 40. The stress intensity factor difference between the coarsest and the finest mesh in this study exceeded 1.5%. The medium mesh used in this study had 16 contours, and the difference between stress intensity factors decreased to 0.34% between medium and the finest mesh intensity. As a conclusion, the medium mesh having 16 contours can be used for stress intensity factor studies.

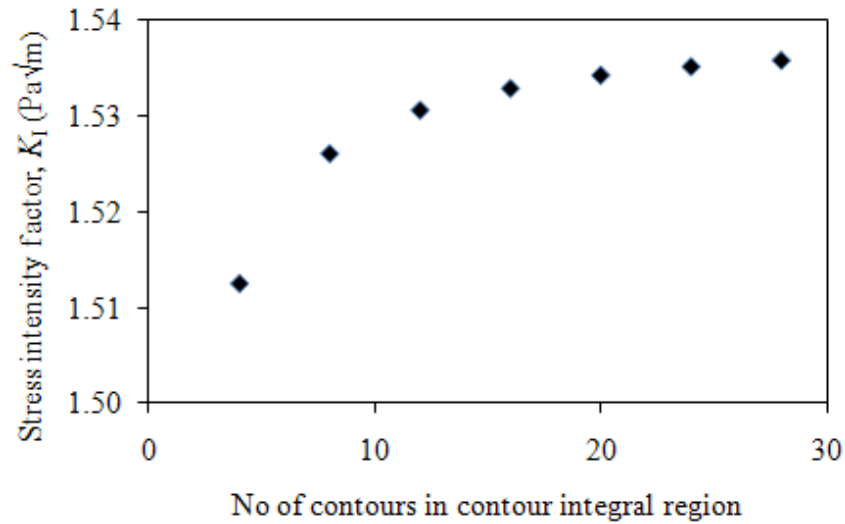


**Figure 6. 40 Stress intensity factor variation according to number of contours in contour integral region**

### 6.3.3 Maximum Stress Intensity Factor Computations

Maximum stress intensity factors at the onset of stable crack propagation or at the local minimum load points were determined for various loading angles, specimen diameters, and specimen thicknesses by numerical modeling.

From the stress analyses, it was determined that crack can be initiated at the center of the specimen and it extends along the diameter when loading angle ( $2\alpha$ ) is equal or greater than  $15^\circ$ . In fracture toughness evaluation, the maximum stress intensity factor is required. This value was found by increasing the crack length which means providing crack propagation in numerical analyses. As in Figure 6. 41, while the crack propagates, i.e. relative crack length increases, dimensionless stress intensity factor increases gradually from zero (I) and it reaches its maximum value (II) then it decreases until final breakage of the disc (III). Region I-II is the part where the unstable crack growth occurs while region II-III is the part where the stable crack growth occurs. In fracture toughness evaluation stable crack growth is considered. Therefore, in stress intensity factor analyses the starting point of the stable crack growth (II) where the stress intensity factor is maximum is concerned.



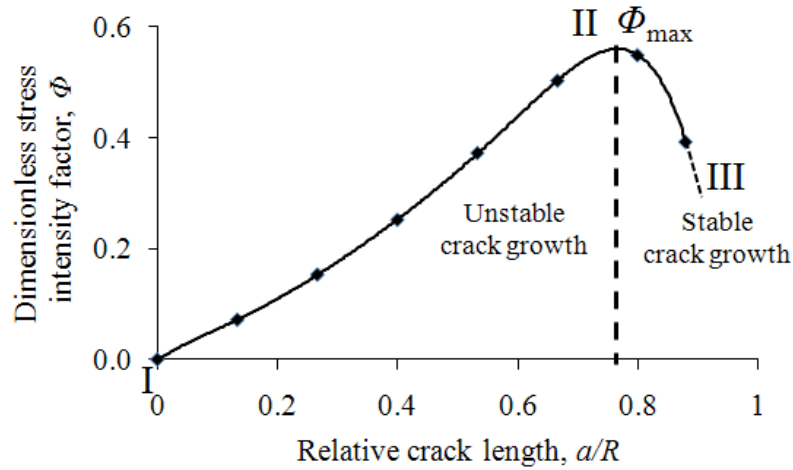


Figure 6. 41 Dimensionless stress intensity factor versus relative crack length

For each model, crack length was increased step by step from zero to larger values. By drawing a sixth order polynomial trend line through stress intensity factor values according to the crack length, an equation was set. Maximum stress intensity factor was found by taking derivative of equation and finding its roots. One of the roots gave the maximum stress intensity factor of the model when it was put in the sixth order polynomial equation. These evaluations were done by using MATLAB Program (MATLAB, 2007). Maximum stress intensity factor computation for a typical model was mentioned in Appendix A, in details.

Modeling results showed that maximum mode I stress intensity factor  $K_{I_{max}}$  is inversely proportional to the disc thickness and the square root of radius, and directly proportional to the applied load, as in (Wang and Xing, 1999). From  $K_{I_{max}}$  computed in the modeling work, maximum dimensionless stress intensity factor can be found by using:

$$\phi_{max} = K_{I_{max}} \frac{\sqrt{Rt}}{F} \quad (6.7)$$

where,

- $\phi_{max}$  : maximum dimensionless stress intensity factor
- $K_{I_{max}}$  : maximum stress intensity factor (MPa $\sqrt{m}$ )
- $F$  : applied load (MN)
- $R$  : disc radius (m)

$t$  : disc thickness (m)

Maximum dimensionless stress intensity factors at the onset of stable crack propagation or at the local minimum load points were determined for various loading angles between 15°-50° for specimens having 54, 75, 100, and 125 mm diameters. This angle range was determined by considering Griffith strength criterion and stress analyses for crack initiation at the centers of discs.

As loading angle changes, dimensionless distance  $y/R$  changes for a disc specimen model. Computed maximum dimensionless stress intensity factors for different loading angles were plotted in Figure 6. 42. A sharper increase in maximum dimensionless stress intensity factor is observed for larger  $y/R$ , which corresponds to smaller width of flattened loading end and smaller loading angles. Using a curve fitting program for the interpretation of the numerical modeling results, following expression for variation of maximum dimensionless stress intensity factor  $\phi_{max}$  with half loading angle  $\alpha$  can be obtained:

$$\phi_{max} = \frac{1}{43.32 - 15.63 \exp(\cos \alpha)} \quad (6.8)$$

where,

$\phi_{max}$  : maximum dimensionless stress intensity factor

$\alpha$  : half of the loading angle

Although Equation 6.11 is valid for maximum stress intensity factor estimation of disc models with loading angles ( $2\alpha$ ) between 6° and 50°, loading angle must be greater than 15° to impose central crack initiation.

During machining of flattened loading ends it is difficult to adjust the loading angle, and thus the width of the flat end precisely. Equation 6.8 gives user a flexibility and chance to determine dimensionless stress intensity factors applicable to particular experimental conditions.

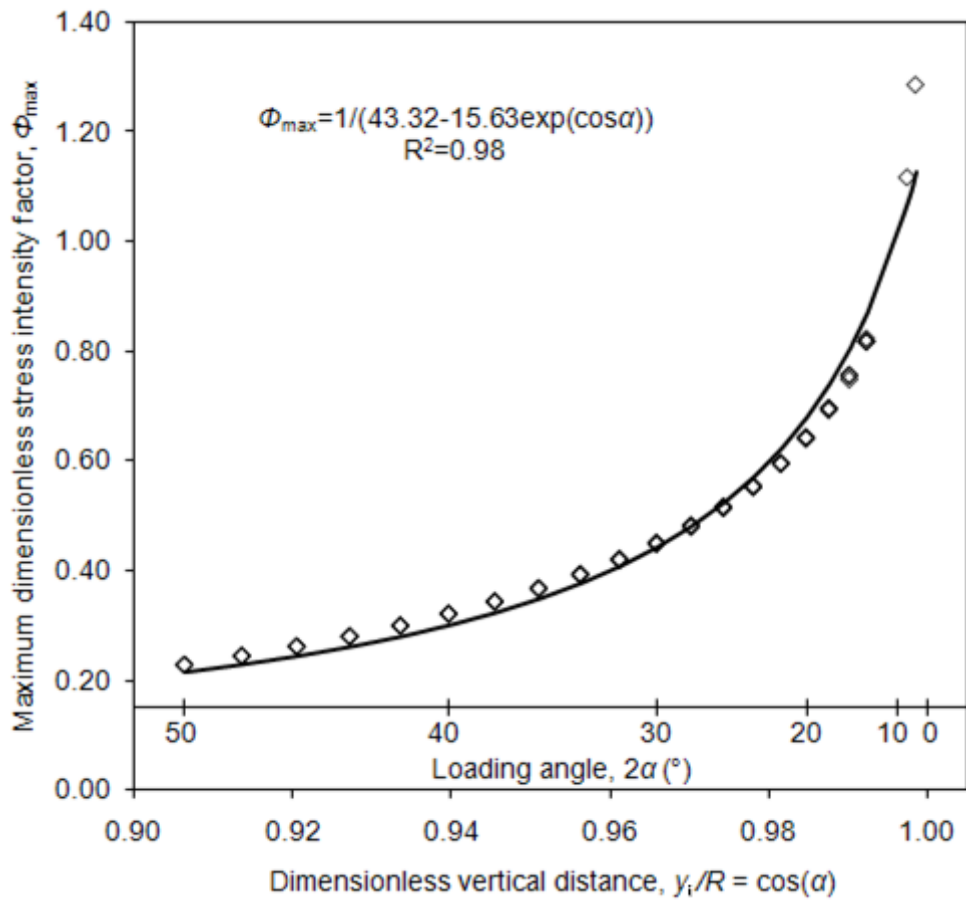


Figure 6. 42 Maximum dimensionless stress intensity factor versus normalized vertical distance

## CHAPTER 7

### NUMERICAL ANALYSES OF MODIFIED RING TEST

Stress distribution and stress intensity factor analyses were carried out on for modified ring (MR) specimen model by using ABAQUS finite element package program. MR specimen geometry is displayed in Figure 7. 1.

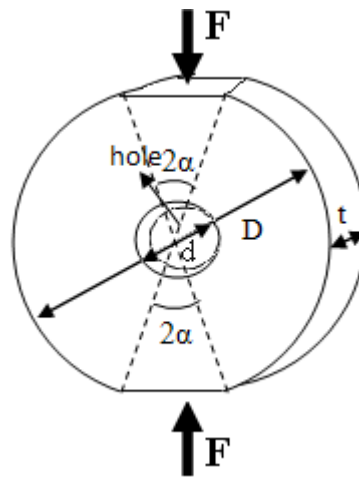


Figure 7. 1 Geometry of MR Specimen

#### 7.1 Parameters Affecting Stress Analyses

For stress and stress intensity factor analyses; a model geometry with loading angle ( $2\alpha$ ) of  $20^\circ$  is considered.  $2\alpha$  was chosen as  $20^\circ$  for consistency with FBD specimen models.

##### 7.1.1 Boundary Conditions

Since load application and specimen model of the MR specimen model is almost the same as the FBD specimen model, a quarter model with symmetric boundary conditions is chosen for numerical modeling of the MR test specimen (Figure 7. 2).

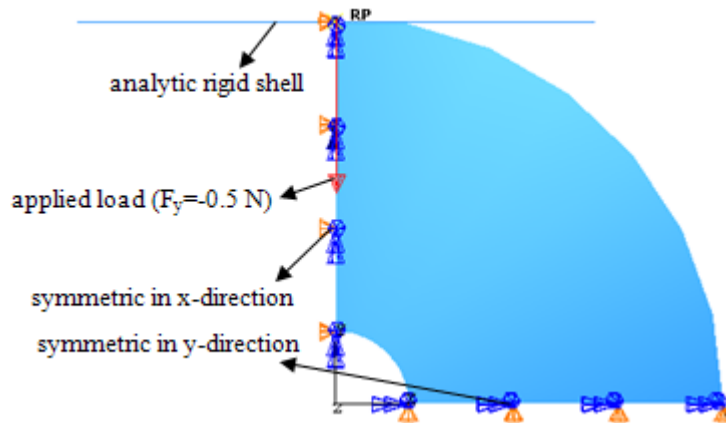
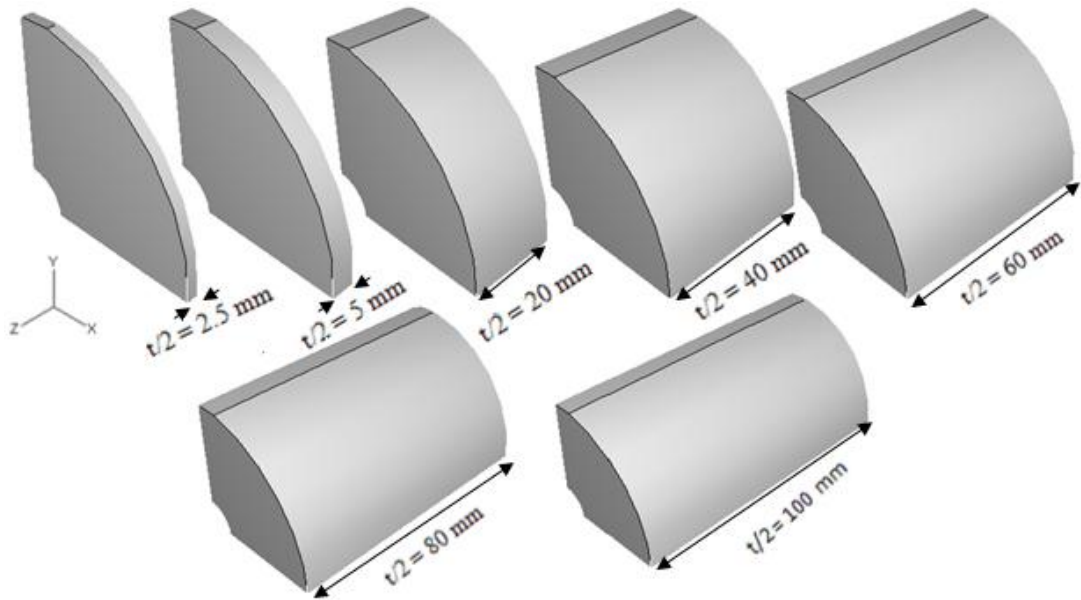


Figure 7. 2 Quarter model geometry considering symmetry along x and y axes

### 7.1.2 Effect of Specimen Thickness

Effect of the variation of thickness in the 3<sup>rd</sup> dimension on stress distribution and stress intensity factor was investigated. Specimen thicknesses were taken as 5 mm, 10 mm, 40 mm, 80 mm, 120 mm, 160 mm and 200 mm for 3D models. Specimen geometry with 75 mm outer and 14 mm inner diameter and 20° loading angle was modeled to investigate thickness effect. Elastic modulus and Poisson's ratio were taken as 12 GPa and 0.15, respectively. Friction coefficient was taken as 0.4.

Symmetric conditions are taken into account for the 3<sup>rd</sup> dimension. Half of the specimen thicknesses were modeled as 2.5 mm, 5 mm, 20 mm, 40 mm, 60 mm, 80 mm and 100 mm, respectively (Figure 7. 3).



**Figure 7. 3 Specimen models with various thicknesses in 3D**

Horizontal ( $S_{11}$ ) and vertical ( $S_{22}$ ) stresses through the center line were examined along the central line of the model to understand how stress distribution was affected from the thickness variation. Central line or vertical distance path  $y_i$  starts from the top of the central hole and ends at the flattened end of the model. In Figure 7. 4, x axis is for horizontal stress ( $S_{11}$ ) and vertical stress ( $S_{22}$ ), and y axis shows vertical distance over the specimen radius (dimensionless vertical distance,  $y_i/R$ ).

As seen from Figure 7. 4, absolute values of the stresses decrease with increasing thickness. When stress values are multiplied with thicknesses, the results are almost constant as illustrated in Figure 7. 5. At the central-hole radius of the specimen models, the maximum difference for  $S_{11}*t$  between plane strain condition and 3D model was observed for 10 mm thickness. The difference was equal to 5.24%. At the center of the specimen models, the maximum difference for  $S_{22}*t$  between plane strain condition and 3D model was for 80 mm thickness. The difference was equal to 6.98%. These differences are due to the mesh intensity in the 3<sup>rd</sup> dimension. Therefore, geometries can be modeled in 2D plane strain. As a result, the future modeling can be conducted in plane strain conditions with 1 m unit thickness.

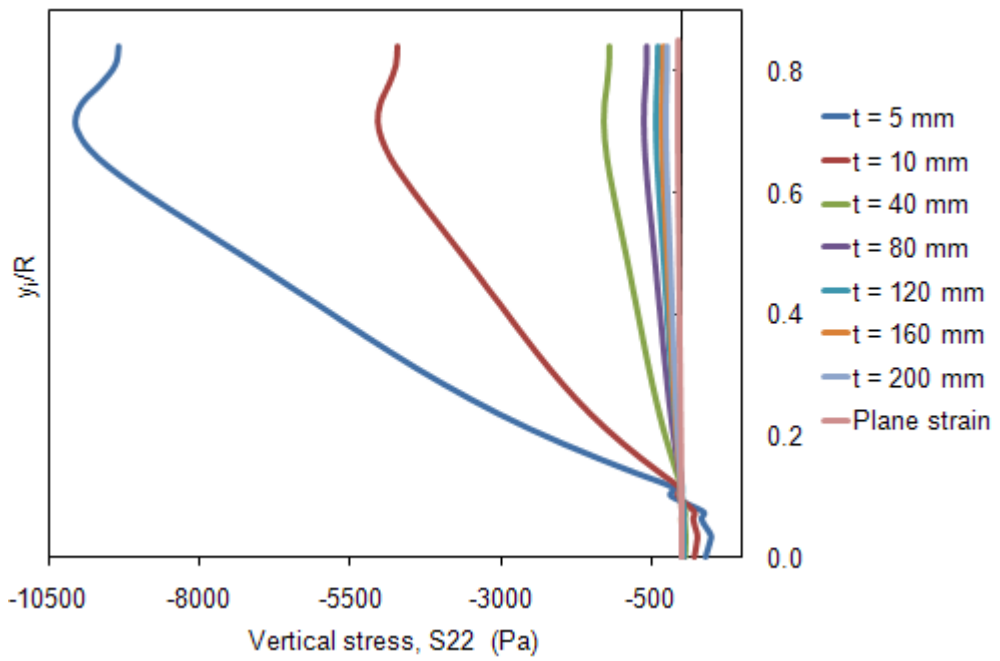
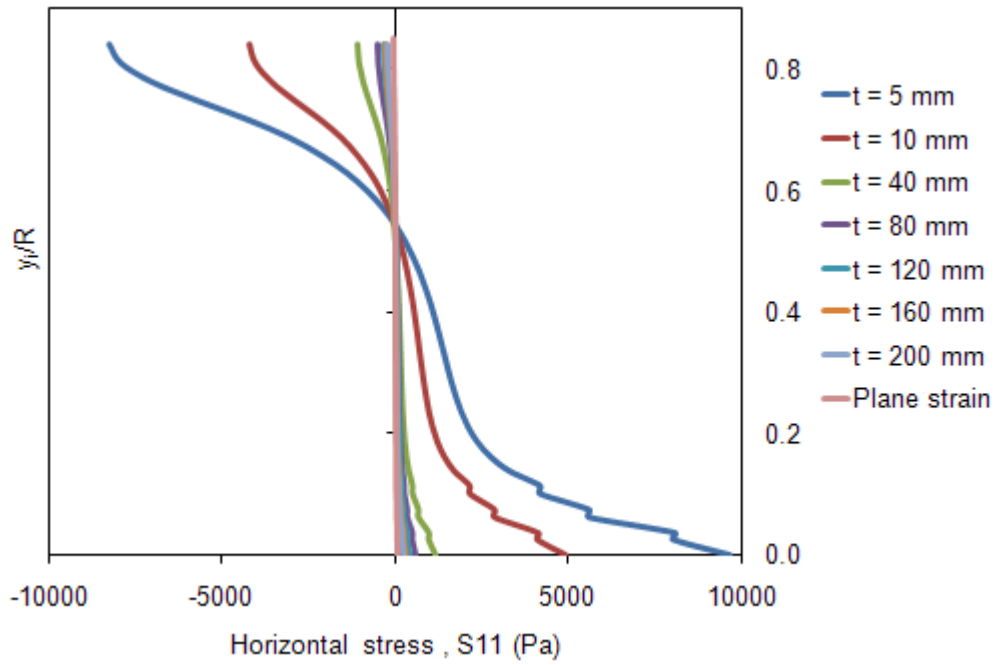


**Figure 7. 4 S11 and S22 versus  $y/R$  graphs, respectively**

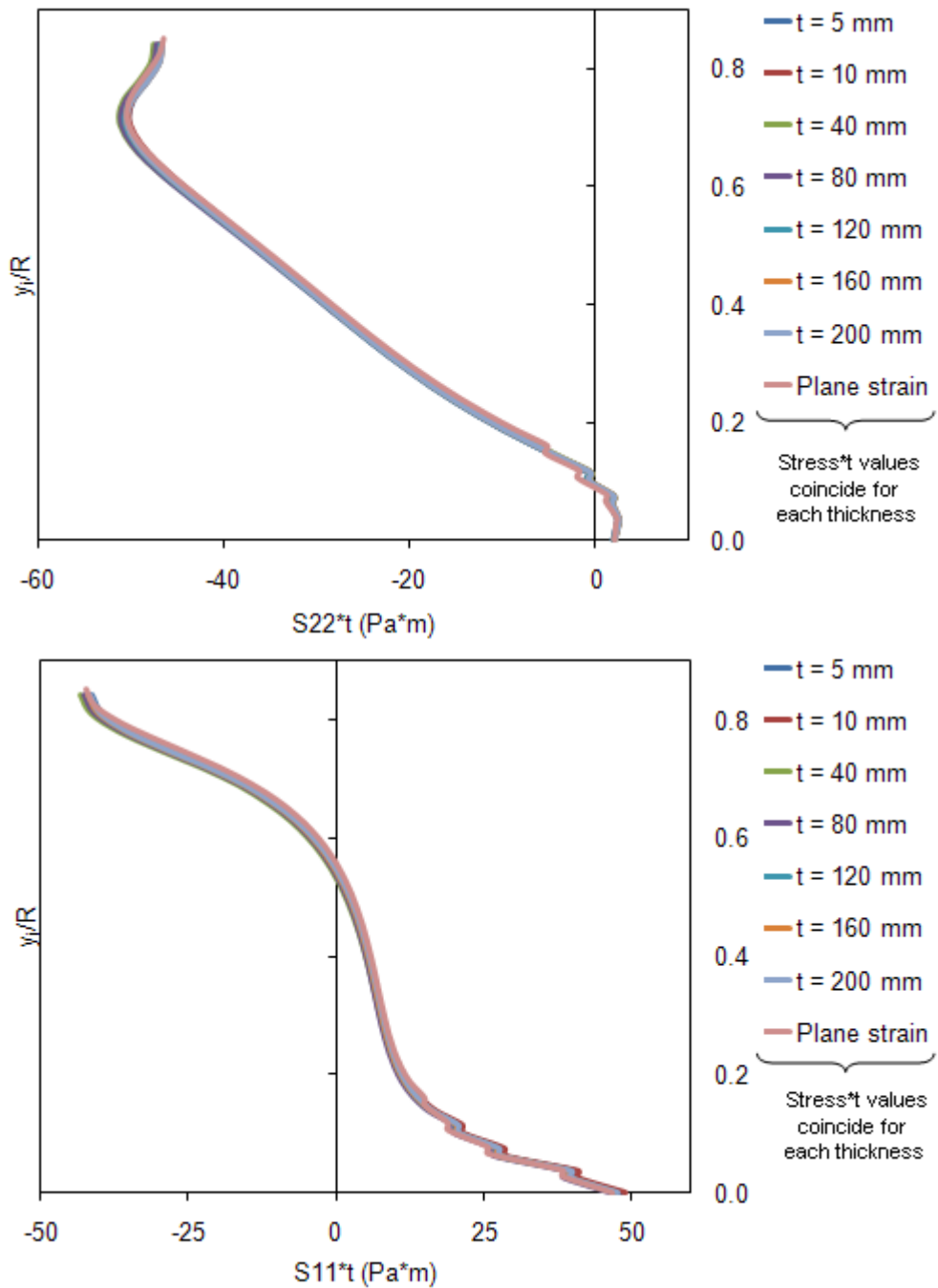


Figure 7. 5  $S11*t$  and  $S22*t$  versus  $y_i/R$  graphs

### 7.1.3 Effect of Mesh Intensity

In mesh intensity studies, specimen diameter was 75 mm, central-hole diameter was 14 mm, thickness was 1 m (in 2D Plane strain condition) and material properties of the model were 12 GPa for elastic modulus and 0.15 for Poisson's ratio and at the interface, friction coefficient was equal to 0.4 at the interface as before.



To make a meaningful judgment about how mesh intensity affects stress values; number of elements on critical parts where crack may initiate should be considered. In this study, vertical central line of the specimen geometry is the most critical since the crack may start from flattened end or central-hole end of the specimen according to the geometric parameters of the models. In Figure 7. 6, the numbers on the elements define the number of elements through the central line. Analyses were done for vertical center line having 10, 20, 30, 40, 50, 60, 70, 100, 150 and 200 elements.

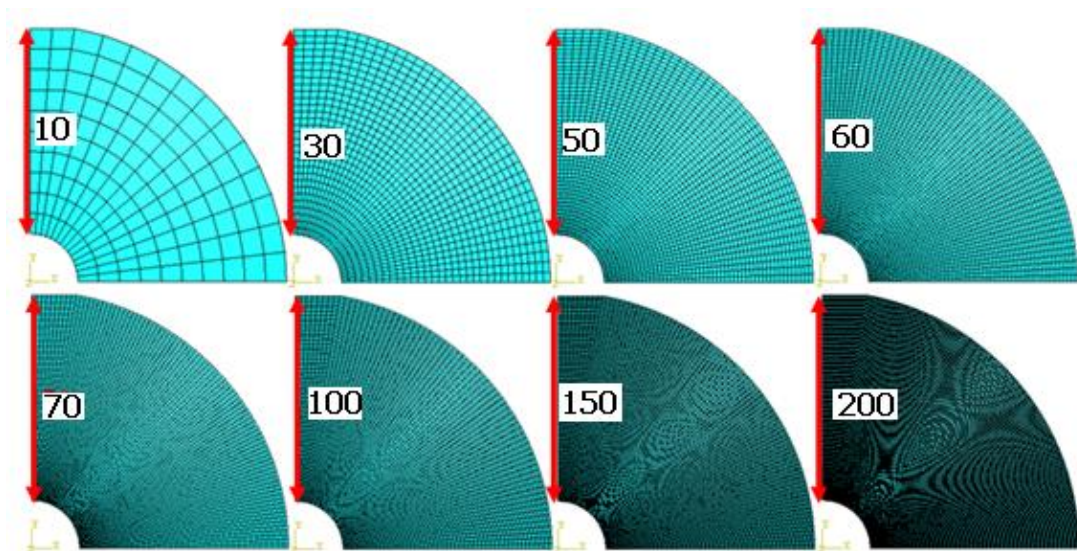


**Figure 7. 6 Number of elements along the central line for different mesh intensities**

Horizontal (S11) and vertical (S22) stress values on the flattened end and at the central-hole face versus number of elements through the vertical center line are plotted as in Figure 7. 7. As seen from the figure, the number of elements does not influence the stresses at the central-hole face of the model, while stresses on the flattened end are affected significantly by mesh density. The difference between horizontal (S11) stresses of the lowest (10 elements) and the highest (200 elements) number of elements on flattened end is greater than 17%.

$$\left[ \frac{S11_{(200\text{ elements})} - S11_{(10\text{ elements})}}{S11_{(10\text{ elements})}} \times 100 = \frac{44.3494 - 36.4154}{-44.349} \times 100 = 17.89\% \right]$$

The variation of vertical (S22) stresses of the lowest (10 elements) and the highest (200 elements) number of elements on the flattened end is around 5.7%.

$$\left[ \frac{S22_{(200\text{elements})} - S22_{(10\text{elements})}}{S22_{(200\text{elements})}} \times 100 = \frac{-47.5070 - (-44.8020)}{-47.5070} \times 100 = 5.69\% \right]$$

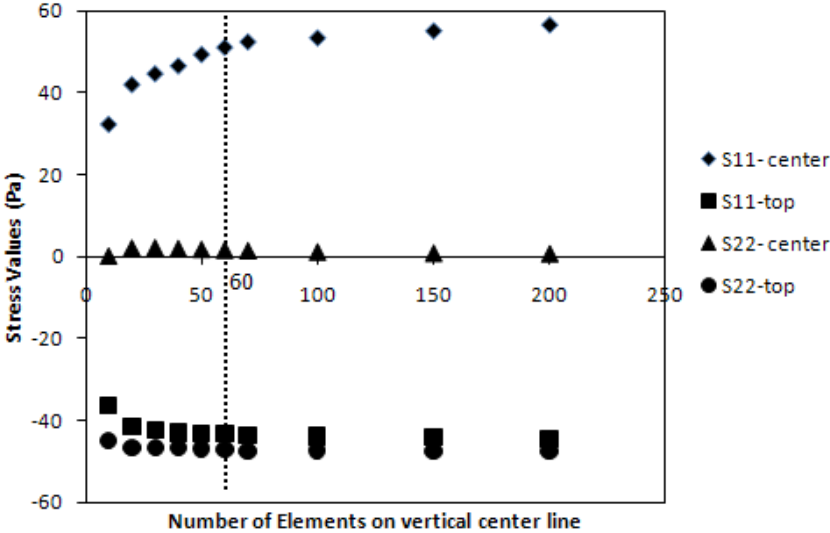


Figure 7.7 Convergence in stresses with increasing mesh intensity on vertical center line

When number of elements is taken as 60 along the center line, the difference in variation of stress distribution magnitudes stays below 3%.

$$\left[ \frac{S11_{(60\text{elements})} - S11_{(10\text{elements})}}{S11_{(60\text{elements})}} \times 100 = \frac{-44.3494 - (-43.1783)}{-44.3494} \times 100 = 2.64\% \right]$$

$$\left[ \frac{S22_{(60\text{elements})} - S22_{(10\text{elements})}}{S22_{(60\text{elements})}} \times 100 = \frac{-47.5070 - (-47.1095)}{-47.5070} \times 100 = 0.84\% \right]$$

When displacement contours were taken into account, similar results were obtained. Displacement distributions were not affected significantly when number of elements was kept above 60 along the central line (Figures 7.8 and 7.9).

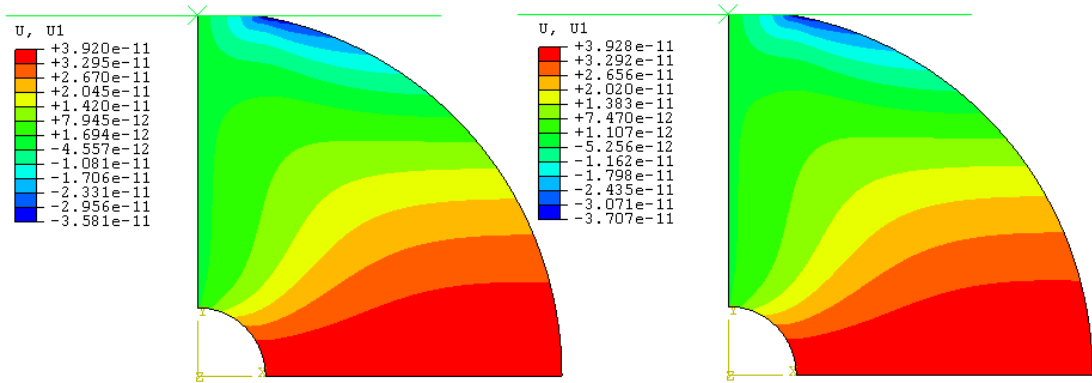


**Figure 7.8 Horizontal (U1) displacement contours for 60 elements and 200 elements, respectively**

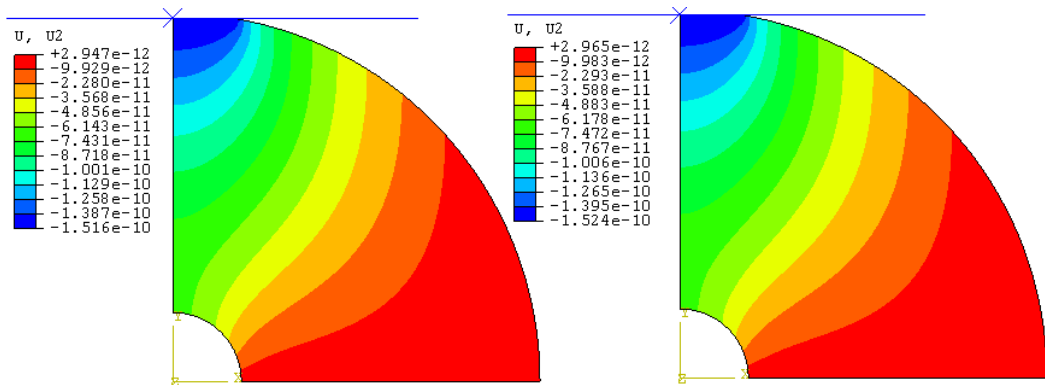


**Figure 7.9 Vertical (U2) displacement contours for 60 elements and 200 elements, respectively**

Further modeling work on stress analyses are going to be conducted with mesh intensity having at least 60 elements on vertical line and almost 3500 elements as total. 60 elements in the modeling runs save time and effort with respect to 200 elements. These limits are for model geometries with 75 mm diameter with 14 mm central-hole diameter and 20° loading angle. When the inner or outer diameter is increased or decreased, the value is going to be changed. But, as the ratio of central-hole diameter over specimen diameter is constant the value is not changed. While the loading angle increases, this value decreases proportional to the length of the reduced line distance.

#### 7.1.4 Effect of Friction Coefficient

Since the boundary conditions were the same for both FBD and MR specimen models, friction coefficient studies on FBD specimen models are also valid for MR specimen models. Stress distribution and stress intensity factor were not affected from the friction coefficient. Friction coefficient is going to be taken as 0.4 for further numerical modeling work.

#### 7.1.5 Effect of Specimen Diameter

To see the specimen diameter effect on stresses, various specimen diameters between 50 mm and 100 mm (50 mm, 60 mm, 70 mm, 75 mm, 80 mm, 90 mm, 100 mm) were analyzed. Figure 7. 10 illustrates the studied radii.  $2\alpha$  and central-hole diameter were kept at  $20^\circ$  and 14 mm, respectively as in the previous specimen thickness and mesh intensity modeling work.

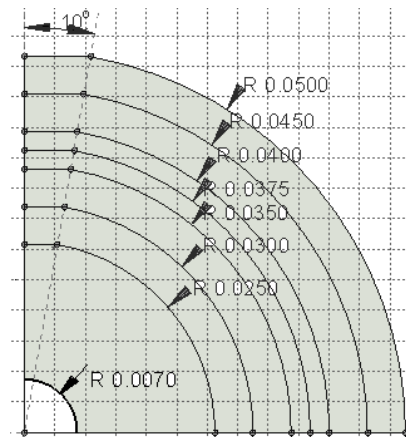


Figure 7. 10 Specimen sketch in different specimen radii

Horizontal (S11) and vertical (S22) stress distributions are plotted through the center line (Figure 7. 11). Dimensionless vertical distance is the vertical central distance starts from the central-hole face and ends at the flattened end over the specimen radius. Dimensionless vertical distance is computed by the equation below:

$$y_i = R \times \cos(\alpha) - r_i \quad (7.1)$$

where,

- $y_i$  : dimensionless vertical distance
- $R$  : specimen radius
- $r_i$  : central-hole radius
- $\alpha$  : half of the loading angle

As seen from Figure 7. 11, absolute values of the stresses decrease with increasing specimen diameter. When stress values are multiplied with diameter, the results do not coincide as in FBD models. Multiplication with diameter merely decreases the difference between stress results (Figure 7. 12). The specimen diameter could not be taken as a constant value as in FBD models.

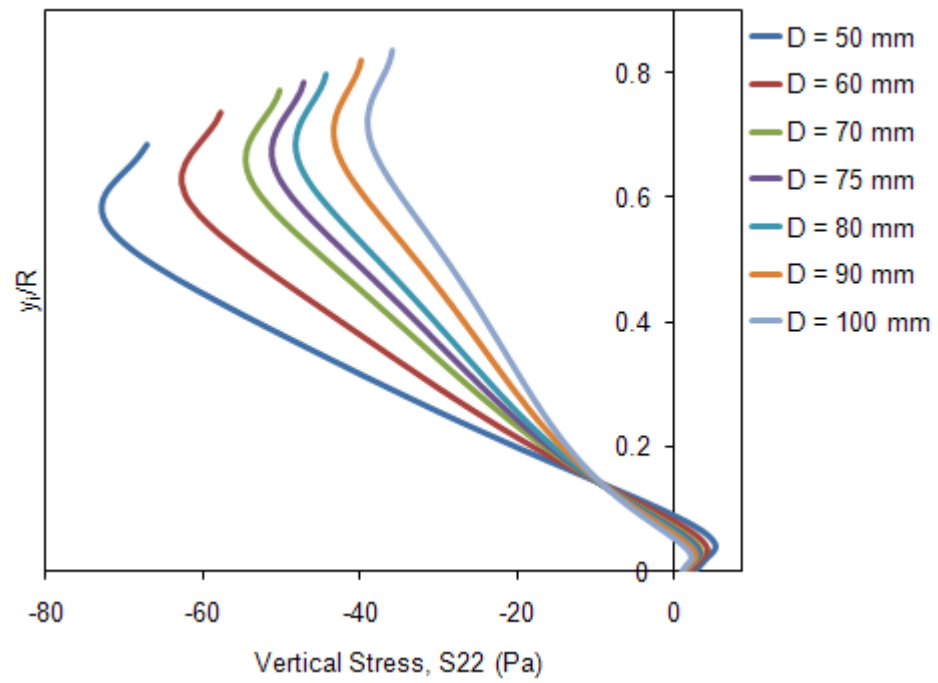
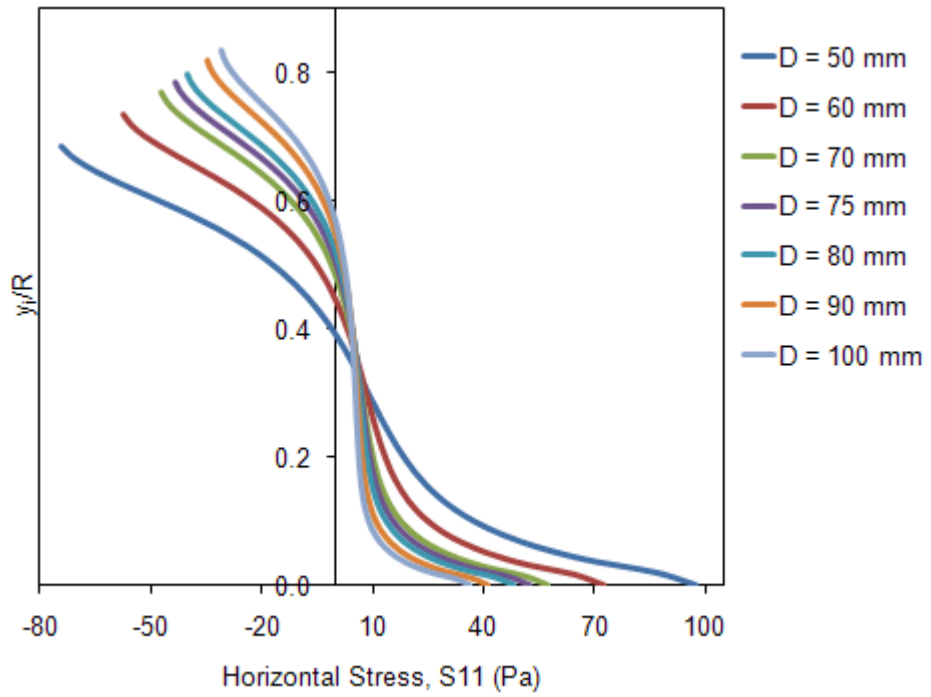


**Figure 7. 11 S11 and S22 versus dimensionless vertical distance graphs, respectively**

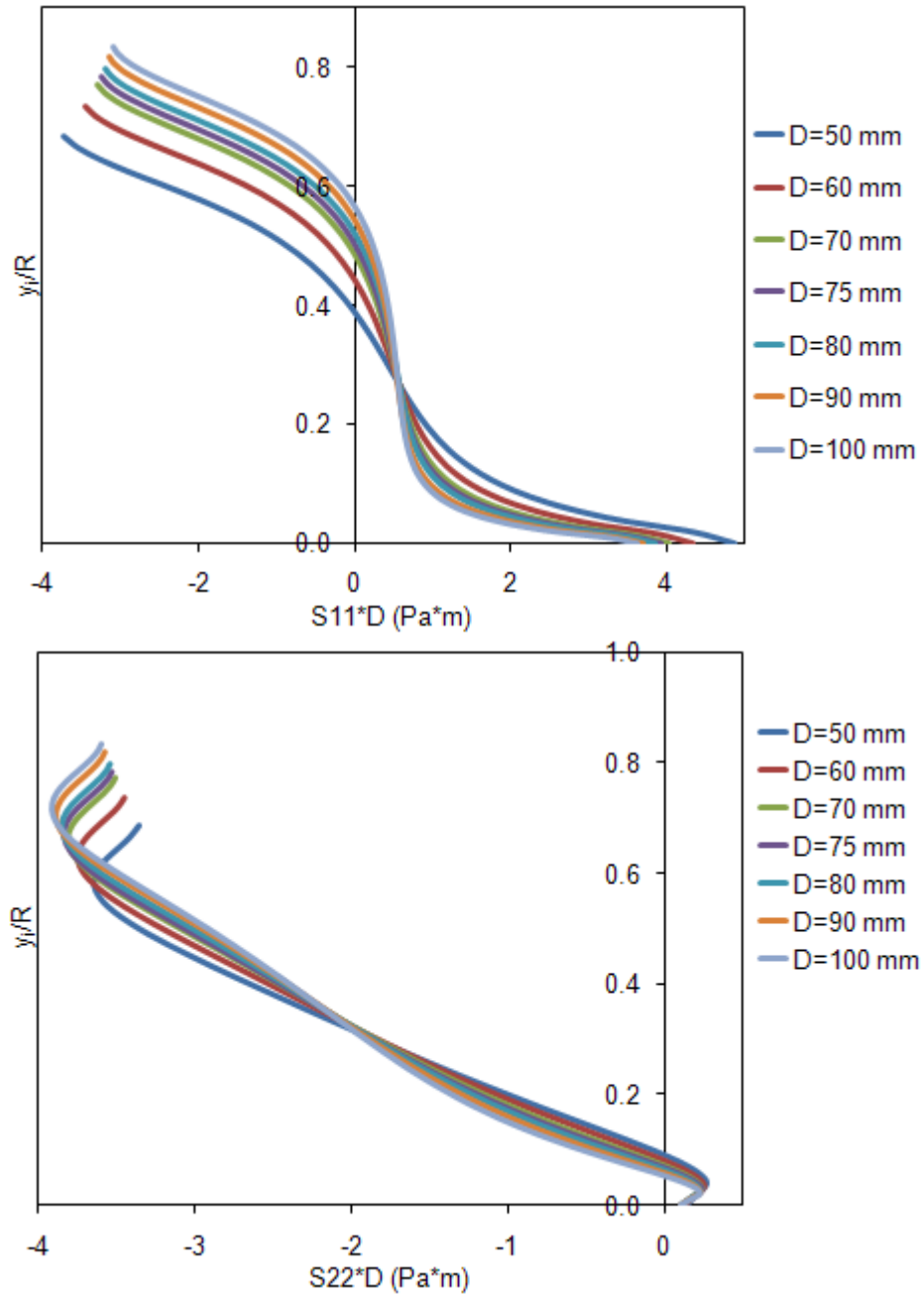
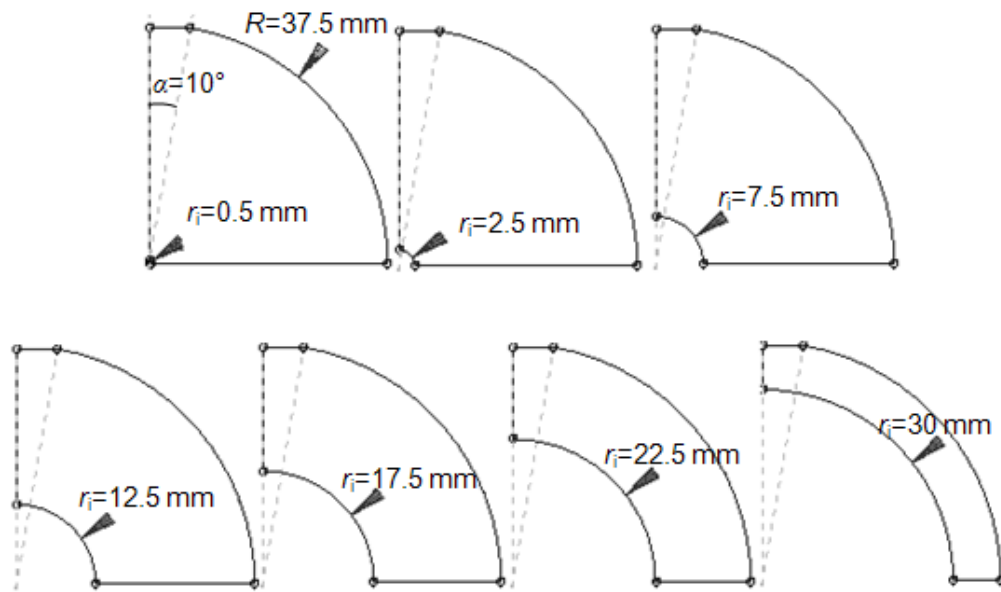


Figure 7. 12  $S_{11}\cdot D$  and  $S_{22}\cdot D$  versus normalized distance graphs

### 7.1.6 Effect of Central-hole Diameter

In order to interpret the hole diameter effect on stresses, different hole diameters between 1 mm and 60 mm (1 mm, 5 mm, 10 mm, 14 mm, 15 mm, 20 mm, 25 mm, 30 mm, 35 mm, 40 mm, 45 mm, 50 mm, 55 mm, 60 mm) with specimen diameter of 75 mm were studied (Figure 7. 13). Material properties of the model were 12

GPa for elastic modulus and 0.15 for Poisson's ratio, and friction coefficient was 0.4, as previously.



**Figure 7.13 Specimen sketch in various central- hole radii**

Horizontal (S11) and vertical (S22) stress distributions are plotted through the center line (Figure 7.14). The figure shows that stress distributions depend on the central-hole diameter.



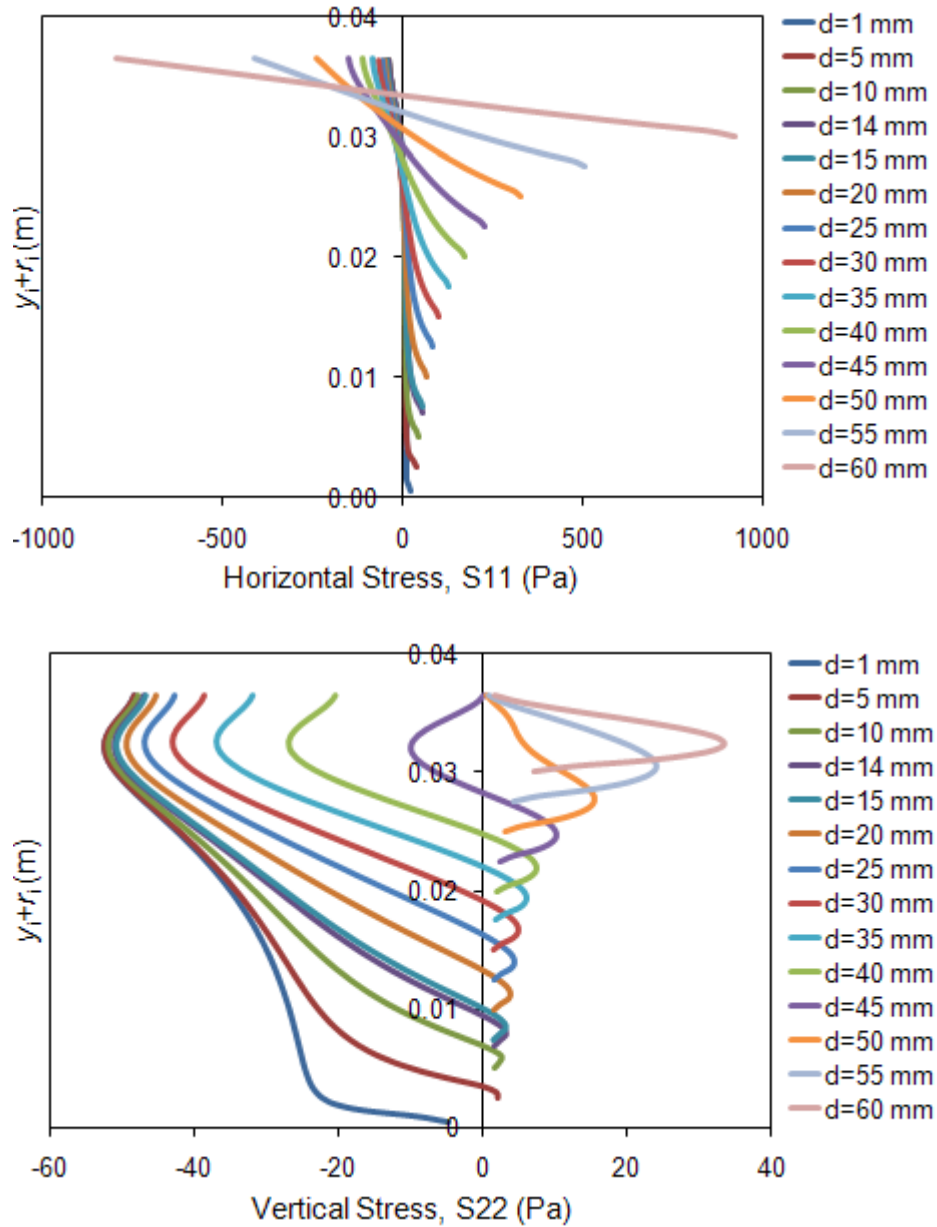


**Figure 7. 14 S11 and S22 versus vertical distance graphs, respectively**

### 7.1.7 Effect of Loading Angle

Effect of loading angle on stress distribution was studied by taking loading angle ( $2\alpha$ ) as  $5^\circ$ ,  $10^\circ$ ,  $20^\circ$ ,  $30^\circ$ ,  $40^\circ$ ,  $50^\circ$ ,  $60^\circ$ ,  $70^\circ$  and  $80^\circ$ . The sketches of the half of the loading angles ( $\alpha$ ) analyzed in this study are illustrated in Figure 7. 15.

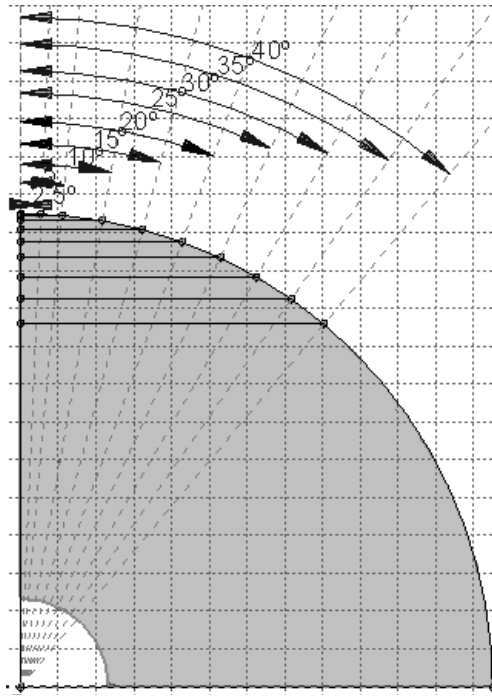


**Figure 7. 15 Various loading angles studied in analyses**

Absolute values of the horizontal (S11) and vertical (S22) stresses along the central vertical line decrease with increasing loading angle ( $2\alpha$ ) (Figure 7. 16).

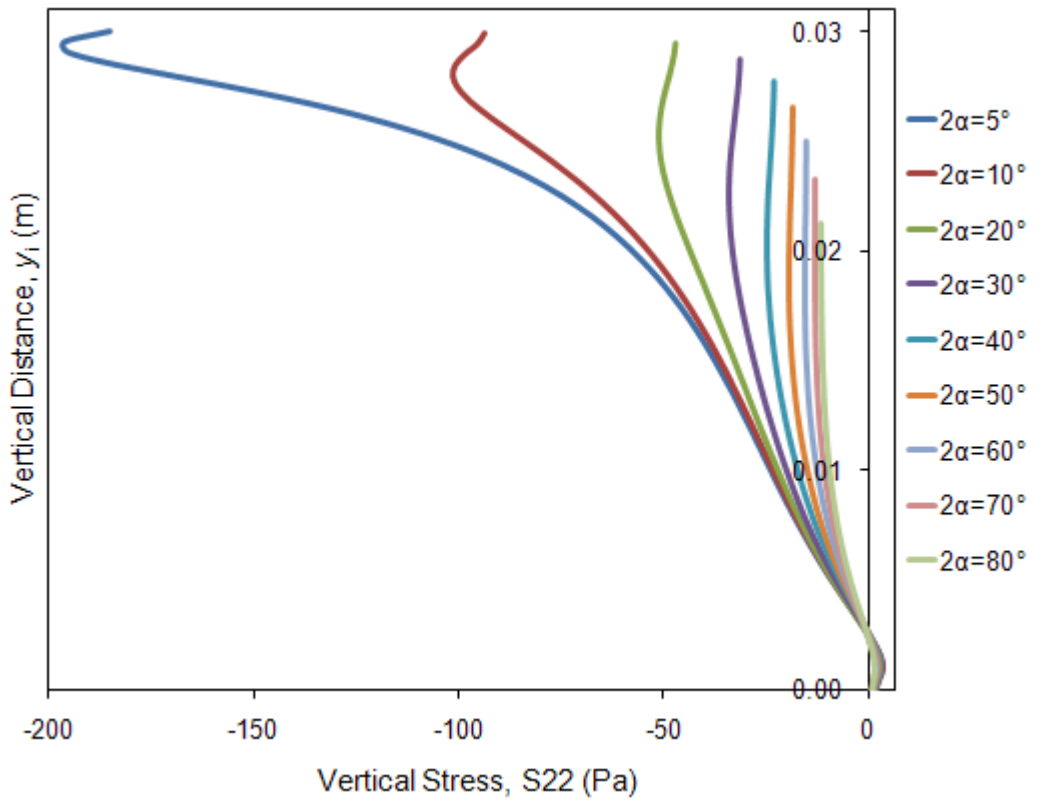
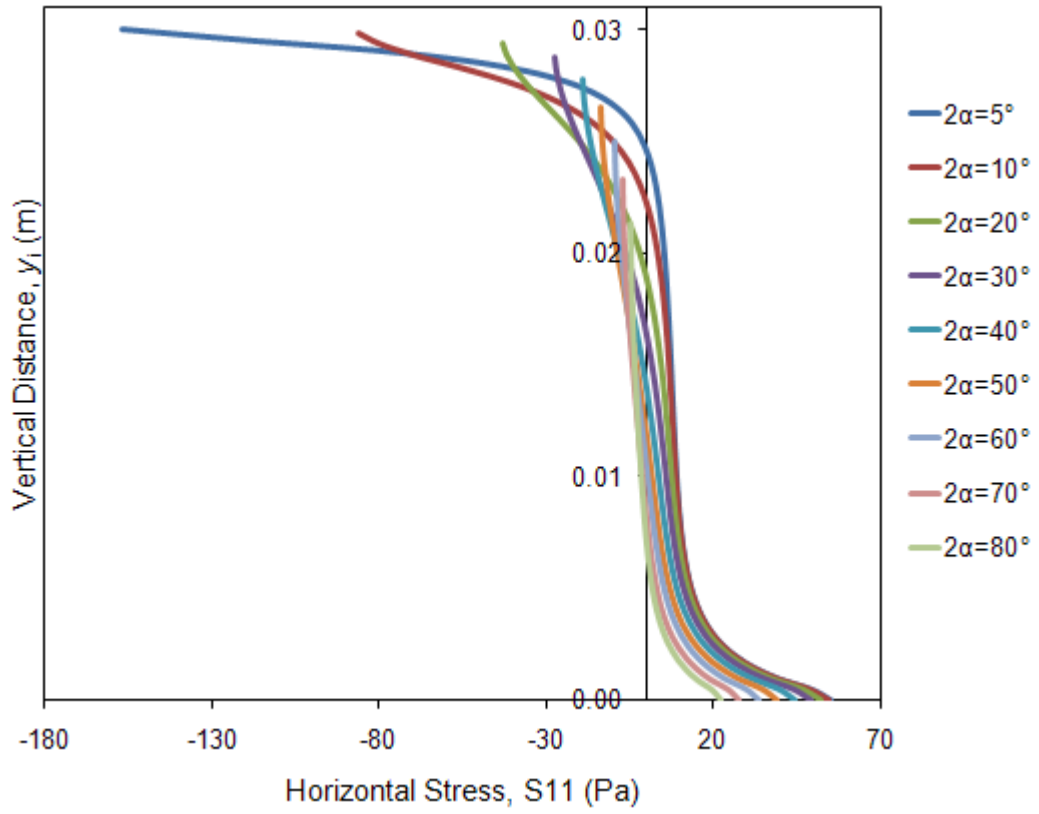


Figure 7. 16  $S_{11}$  and  $S_{22}$  versus vertical distance plots, respectively

Stress analyses show that specimen diameter, central-hole diameter and loading angle influence the stress distribution. In FBD models to determine where crack initiated, Griffith Strength Criterion was used. However, in MR Test, because of the central-hole, crack always initiates from the center with smaller flattened angles. Therefore there is no need to analyze crack initiation location according to stress analyses.

## 7.2 Stress Intensity Factor Analyses

Stress intensity factors are directly proportional to stresses for MR test method as FBD method. There is no need to analyze how boundary conditions, thickness of the specimen, mesh intensity of the whole model and friction coefficient influence the stress intensity factor. Contour integral region and mesh intensity in the contour integral region used in FBD model is also applicable for MR specimen models. Therefore, contour integral ring radius was taken as 2 mm and number of contours in this region was taken as 16 with  $11.25^\circ$  crack tip subtend angles ( $\beta$ ) (Figure 7. 17).

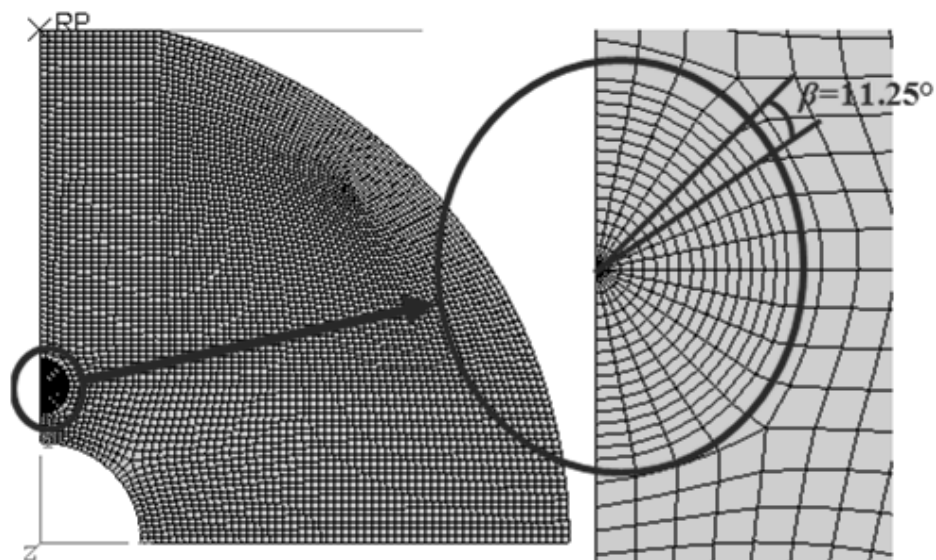


Figure 7. 17 Mesh intensity in whole model and in contour integral region

### 7.2.1 Maximum Stress Intensity Factor Computations

As in FBD method, for fracture toughness estimation, maximum stress intensity factor is required. To obtain this value for MR test, the same steps as in FBD method were followed. MATLAB code written for FBD method was used for MR test models too. Details of this code are in Appendix A.

Maximum stress intensity factors were determined for various specimen diameters ( $D=\{50 \text{ mm}, 54 \text{ mm}, 75 \text{ mm}, 100 \text{ mm}\}$ ), hole diameters ( $d=\{5, 10, 15, 20\}$ ) and loading angles ( $2\alpha=\{14^\circ, 16^\circ, 18^\circ, 20^\circ, 22^\circ, 24^\circ, 26^\circ, 28^\circ, 30^\circ, 32^\circ, 34^\circ, 36^\circ, 38^\circ, 40^\circ\}$ ). All combinations of these values were analyzed. As the loading angle increases linearly, maximum stress intensity factor and relative crack length decrease linearly. For greater loading angles this linear relation is not satisfied.  $K_{I\max}$  results are demonstrated in Figure 7. 18. The results that did not satisfy linear increase were ignored.

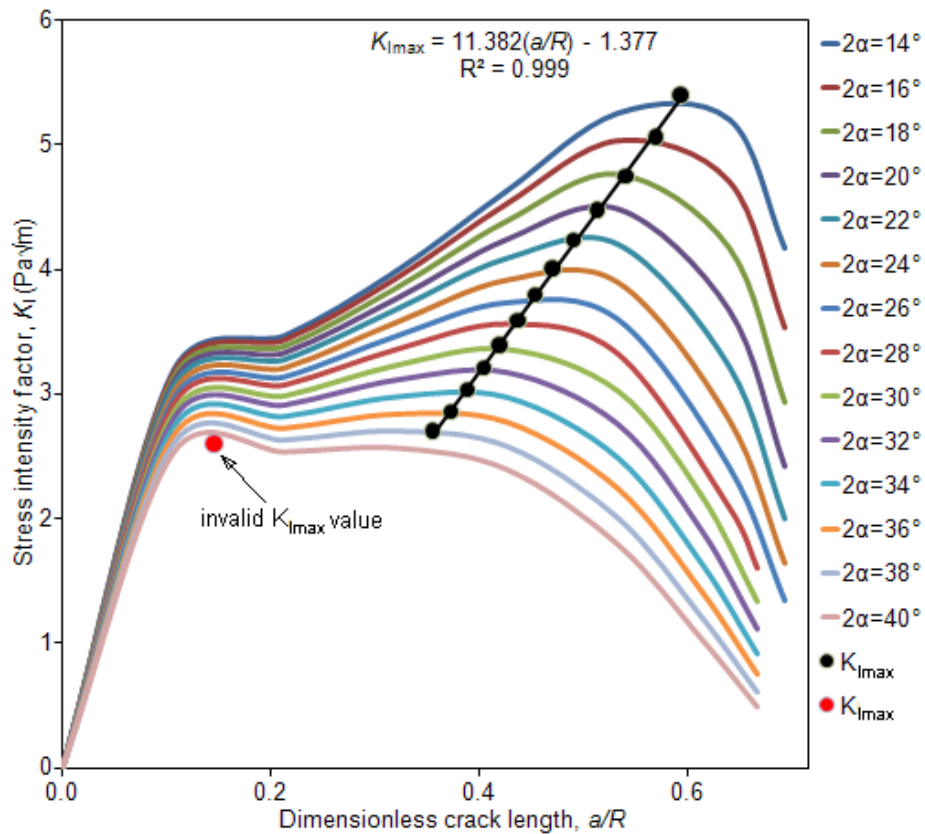


Figure 7. 18 Stress intensity factor versus dimensionless crack length for various loading angles (for  $D = 75 \text{ mm}$  and  $d = 15 \text{ mm}$ )

$K_{I_{max}}$  values and crack lengths corresponding to  $K_{I_{max}}$  were computed from the numerical modeling results.  $K_{I_{max}}$  can be normalized for a tensile crack of length  $(a+r_i)$ . This  $K_{I_{max}}$  is equal to  $\sigma\sqrt{\pi(a+r_i)}$ , where the nominal stress  $\sigma$  is taken as the value of the maximum tensile stress perpendicular to crack plane  $(F/\pi R)$  with Brazilian type loading. Dimensionless maximum stress intensity factor ( $\Phi_{max}$ ) can be expressed by the equation below:

$$\phi_{max} = \frac{K_{I_{max}} R \sqrt{\pi}}{\sqrt{a+r_i}} \quad (7.2)$$

Computing  $\Phi_{max}$  for various dimensionless central-hole diameter ( $d/D$ ) values,  $\Phi_{max}$  using the linear fit equations is given in Figure 7. 19.

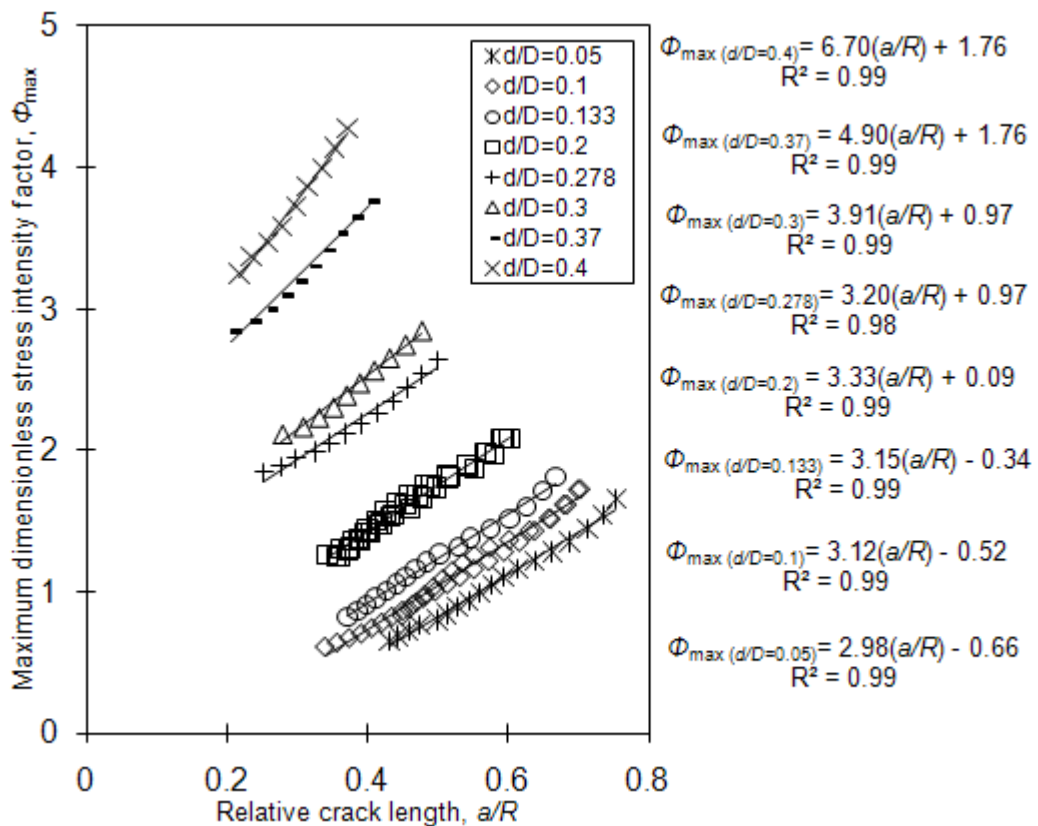


Figure 7. 19  $\Phi_{max}$  versus relative crack length ( $a/R$ ) for various  $d/D$  ratios

In experimental work, crack length corresponding to the point of stable crack propagation cannot be detected clearly. In order to determine  $\Phi_{\max}$ , an expression without the crack length is given in the equation below:

$$\ln \phi_{\max} = -3.470 + 4.498 \left( \frac{d}{D} \right)^{1.5} + 3.866 \cos \alpha \quad (7.3)$$

This equation was obtained by a simple surface fitting to the 3D graph in terms of  $\Phi_{\max}$ ,  $\cos \alpha$ , and  $d/D$  (Figure 7. 20).

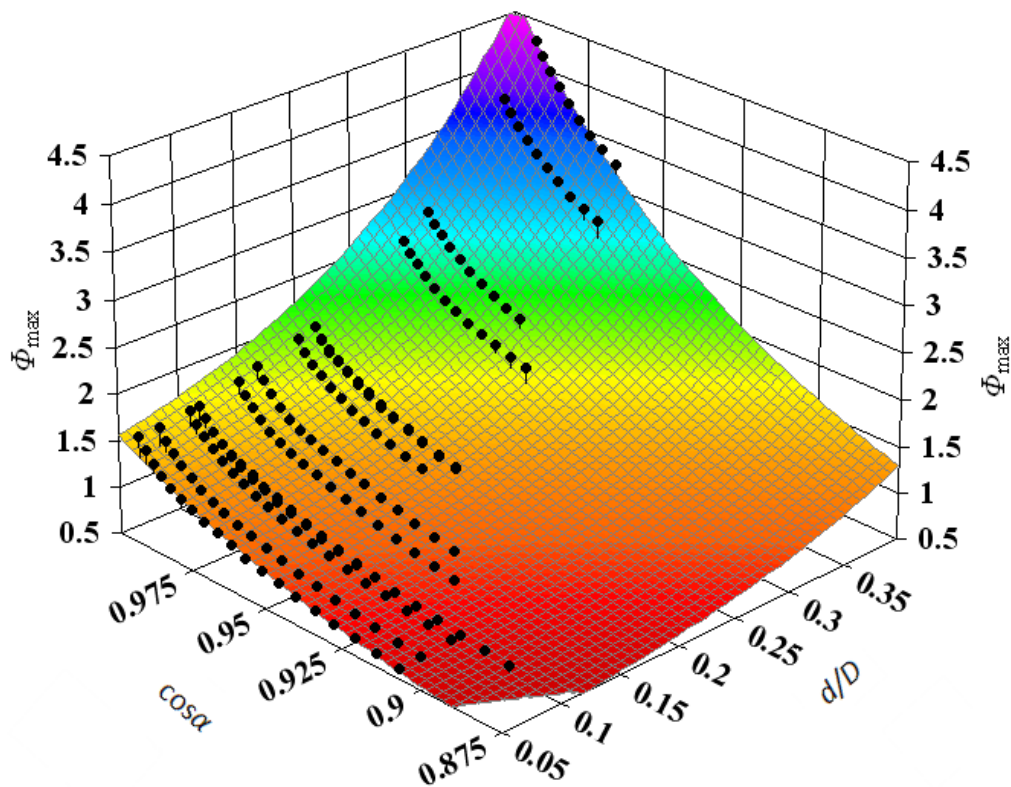


Figure 7. 20 3D graph and surface fitted for  $\Phi_{\max}$  versus  $\cos \alpha$  and  $d/D$

## CHAPTER 8

### FRACTURE TOUGHNESS TESTS

In experimental studies, pink colored Ankara Gölbaşı andesite and white colored Afyon marble blocks were used for specimen preparation. In order to determine mineral content, texture and matrix of rocks, petrographic analyses were done. The details of the petrographic analyses are in Appendix B.

To have an idea about the physical properties of rocks before fracture tests, uniaxial compressive strength tests and Brazilian tests were conducted on andesite and marble core specimens.

#### **8.1 Relevant Mechanical Properties of Andesite and Marble**

Uniaxial compressive strength test was conducted according to ISRM (1979) suggested method. Uniaxial compressive strength, elastic modulus, Poisson's ratio of the andesite and the marble were determined by using MTS 815 servo-controlled loading machine. In the tests, MTS 815 loading frame was used with an external 500 kN load cell with  $\pm 0.25$  kN accuracy and two external displacement transducers (having 10 mm capacity with  $\pm 0.005$  mm accuracy). A circumferential extensometer to measure circumferential strain was attached for the determination of Poisson's ratio (Figure 8. 1).





**Figure 8. 1 UCS test specimen with circumferential extensometer before and after the test**

Uniaxial compressive strength and deformability test data for andesite and marble are given in Table 8. 1 and Table 8. 2, respectively.

**Table 8. 1 UCS data and results of andesite rock**

Name	Diameter mm	Length mm	$\sigma_c$ MPa	$E$ MPa	$\nu$
UCS-A1	54.09	129.10	85.11	12365	0.156
UCS-A2	54.04	126.76	75.96	12126	0.140
UCS-A3	54.11	129.07	86.52	12530	0.158
UCS-A4	54.79	143.81	83.31	12400	0.140
UCS-A5	54.46	134.17	79.97	12280	0.160
UCS-A6	54.46	141.86	86.18	12300	0.170
<b>Avg.:</b>			<b>82.84±4.14</b>	<b>12334±135</b>	<b>0.15±0.01</b>

**Table 8. 2 UCS data and results of marble rock**

Name	Diameter mm	Length mm	$\sigma_c$ MPa	$E$ MPa	$\nu$
UCS-M1	54.5	134.13	52.45	34633	0.119
UCS-M2	54.5	133.90	50.29	34549	0.102
UCS-M3	54.5	127.13	54.10	33625	0.151
UCS-M4	54.5	131.62	52.43	34370	0.111
<b>Avg.:</b>			<b>52.32±1.56</b>	<b>34294±459</b>	<b>0.12±0.02</b>

Indirect tensile strength test, on andesite and marble disc specimens were carried according to the ISRM (1978) suggested method. Brazilian tensile strengths of the andesite and the marble were determined by using MTS 815 servo-controlled

loading machine with an external 500.00±0.25 kN load cell. To avoid infinite compressive stress concentrations at loading ends, jaws were used as in Figure 8. 2.



**Figure 8. 2 Brazilian disc specimen before and after the test**

Brazilian test data for andesite is listed in Table 8. 3 and for marble are tabulated in Table 8. 4.

**Table 8. 3 Brazilian test data and results of the andesite rock**

Name	Diameter mm	Thickness mm	$\sigma_t$ MPa
<b>Braz-A1</b>	53.45	29.35	6.60
<b>Braz-A2</b>	53.43	27.86	5.94
<b>Braz-A3</b>	53.30	27.32	7.15
<b>Braz-A4</b>	53.40	28.06	7.86
<b>Braz-A5</b>	53.47	30.23	7.45
<b>Braz-A6</b>	53.40	32.00	7.03
<b>Avg.:</b>			<b>7.00±0.67</b>

**Table 8. 4 Brazilian test data and results of the marble rock**

Name	Diameter mm	Thickness mm	$\sigma_t$ MPa
<b>Braz-M1</b>	54.43	27.60	5.34
<b>Braz-M2</b>	54.45	27.12	5.10
<b>Braz-M3</b>	54.45	28.75	5.55
<b>Braz-M4</b>	54.44	26.34	4.84
<b>Braz-M5</b>	54.44	25.91	4.81
<b>Avg.:</b>			<b>5.13±0.32</b>

## **8.2 Mode I Fracture Toughness Tests with SCB and the Suggested CCNBD Methods**

Fracture toughness values of andesite and marble were determined firstly by using semi-circular bending (SCB) and cracked chevron notched Brazilian disc (CCNBD) methods. SCB method was preferred due to the simplicity of the specimen preparation and the test procedure. This is a well-known fracture toughness method. CCNBD method was preferred because it is one of the suggested methods by ISRM, and also it is the simplest suggested method among the others in terms of the specimen preparation, laboratory setup, and evaluation of the results.

The main fracture studies were done on flattened Brazilian disc (FBD) method and modified ring (MR) test. The fracture toughness results with these methods were later compared with the results of FBD and MR methods.

### **8.2.1 Tests with SCB Method**

All steps in specimen preparation and testing for SCB method are illustrated in Figure 8. 3 through Figure 8. 6.

Andesite and marble blocks were bored to rock cores. After that, rock cores were cut into discs. To flatten the specimen faces, discs were polished with grinding machine to required thicknesses (Figure 8. 3).

By the help of goniometer, center of the disc was marked and a line passing through the disc diameter was drawn and by considering this line, the disc was cut into halves by following this line with Smartcut 1004 precision diamond saw apparatus. It was so difficult to hold the disc with hand during cutting, therefore, a holding fixture was attached to the cutting machine (Figure 8. 4).

To cut notch properly to the half discs, an apparatus having V-bed and 4 rollers was designed and required notch length was adjusted with a digital caliper fixed to sawing machine. By pushing the apparatus having half disc specimen through the track, a straight notch with desired length was cut through the specimen. After notch was cut, load application points were marked on the sample and placed on three-

point bending apparatus (Figure 8. 5). Each roller supports used in the experiments has 10 mm diameter and 100 mm length.

MTS 815, servo-controlled hydraulic testing machine, was used as loading system. To measure the load, an external 500 kN load cell with  $\pm 0.25$  kN accuracy was added to the system. In order to measure vertical displacement two external linear displacement transducers which have a capacity of 10 mm with  $\pm 0.005$  mm accuracy were used. Specimens were loaded in a displacement-controlled way at a constant rate of 0.005 mm/sec.

When SCB specimen reaches critical load a crack initiates and propagates as in Figure 8. 6.

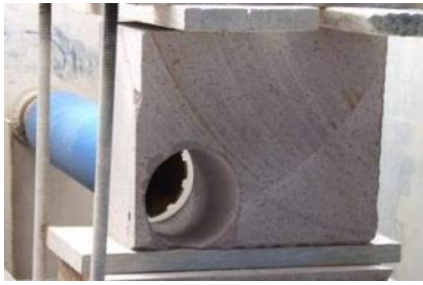


**Figure 8. 3 Boring Machine (on the left) and polishing machine (on the right)**

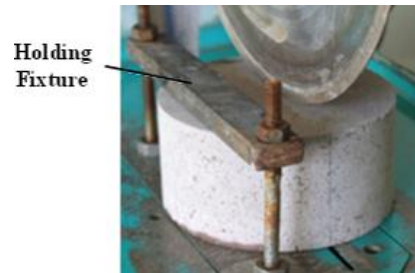


**Figure 8. 4 Diametral line drawing with goniometer (on the left) and fixed disc on cutting machine with holding fixture (on the right)**

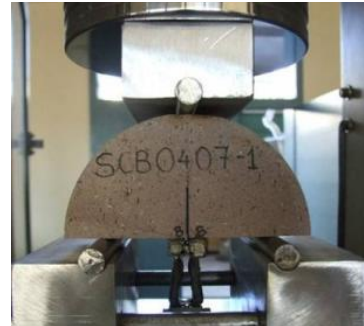


**Figure 8. 5 Cutting platform for half disc specimens (on the left) and loading configuration (on the right)**



**Figure 8. 6 Semi-circular bending specimens after cracking and fracturing**

## 8.2.2 Specimen Geometries for SCB Method Tests

In andesite rock experiments, radii and thicknesses of the specimens were equal to 50 mm and notch lengths were taken between 5 and 10 mm. Specimens were coded before testing, and in specimen coding, SCB denotes semi-circular bending specimen, A (for andesite) or M (for marble) indicates rock type used in an experiment, and number at the end of the code defines the specimen number (Figure 8. 7). Details of the dimensions are tabulated in Table 8. 5. The specimen dimensions of the andesite rock were adopted from Alkılıçgil (2006). Specimens having smaller notch lengths were preferred for SCB tests since variation of stress intensity factor in small notch length ranges is steadier.

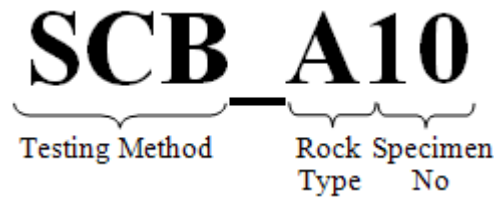


**Figure 8. 7 Specimen coding; SCB: semi circular bending, A: rock type (A for andesite and M for marble), 10: specimen number**

**Table 8. 5 Dimensions of the andesite SCB specimens**

Specimen	<i>D</i> mm	<i>R</i> mm	<i>a</i> mm	<i>t</i> mm	<i>S</i> mm	<i>a/R</i>	<i>S/R</i>
SCB_A1	98.12	49.06	5.75	50.30	30.75	0.12	0.63
SCB_A2	98.26	49.13	4.75	50.22	30.75	0.10	0.63
SCB_A3	100.00	50.00	5.13	50.05	30.56	0.10	0.61
SCB_A4	100.00	50.00	5.00	49.91	35.50	0.10	0.71
SCB_A5	100.00	50.00	5.50	50.58	35.88	0.11	0.72
SCB_A6	99.50	49.75	11.00	51.03	30.88	0.22	0.62
SCB_A7	100.00	50.00	10.25	49.52	30.75	0.21	0.62
SCB_A8	100.00	50.00	10.50	50.55	35.75	0.21	0.72
SCB_A9	100.00	50.00	10.00	50.11	35.88	0.20	0.72
SCB_A10	99.00	49.50	10.25	50.75	35.75	0.21	0.72

In marble rock experiments, radii and thicknesses were around 37 and 50 mm. Notch lengths for both radii were taken around 10 mm. Results for the specimens having 37 mm radii and thicknesses were adopted from the study of Tez (2008). The details of the dimensions are listed in Table 8. 6.

**Table 8. 6 Dimensions of the marble SCB specimens**

Specimen	<i>D</i> mm	<i>R</i> mm	<i>a</i> mm	<i>t</i> mm	<i>S</i> mm	<i>a/R</i>	<i>S/R</i>
SCB_M1	99.00	49.15	7.50	51.50	29.15	0.15	0.60
SCB_M2	99.25	48.80	10.00	51.25	28.80	0.20	0.60
SCB_M3	74.55	37.28	10.00	36.56	22.37	0.27	0.61
SCB_M4	74.60	37.30	10.00	36.96	22.38	0.27	0.61
SCB_M5	74.61	37.31	9.00	37.08	22.38	0.24	0.60
SCB_M6	74.57	37.29	9.00	36.63	22.37	0.24	0.61
SCB_M7	74.60	37.30	10.00	37.02	22.38	0.27	0.60

### 8.2.3 Fracture Toughness Evaluation for SCB Method Tests

Fracture toughness value of materials for SCB specimen can be evaluated by using Equation 4.11. Since the expressions in Equation 4.11 are important for mode I fracture toughness evaluation, they are presented again in this section.

$$K_{Ic} = \frac{F\sqrt{\pi a}}{Dt} Y_I \quad (8. 1)$$

where,

- $K_{Ic}$  : Fracture toughness (MPa√m)
- $F$  : Failure load (MN)
- $a$  : Notch length (m)
- $D$  : Specimen diameter (m)
- $t$  : Specimen thickness (m)
- $Y_I$  : Dimensionless stress intensity factor

$Y_I$  in this equation could be calculated by using the following equation. This equation was derived in the study of Alkılıçgil (2006).

$$Y_I = \frac{0.615 - 9.676\left(\frac{a}{R}\right) + 18.904\left(\frac{a}{R}\right)^2 - 9.987\left(\frac{a}{R}\right)^3 + 5.235\left(\frac{S}{R}\right)}{1 - 1.136\left(\frac{a}{R}\right) + 0.876\left(\frac{a}{R}\right)^2 - 0.866\left(\frac{a}{R}\right)^3 - 0.019\left(\frac{S}{R}\right)} \quad (8.2)$$

where,

$a/R$ : Dimensionless notch length

$S/R$ : Dimensionless span length

By using the expressions above and experimental failure loads, fracture toughness of andesite was determined as  $0.94 \pm 0.09 \text{ MPa}\sqrt{\text{m}}$  with ten specimens, while fracture toughness of marble was calculated as  $0.56 \pm 0.06 \text{ MPa}\sqrt{\text{m}}$  with seven specimens. The dimensionless stress intensity factors, failure loads and fracture toughness values of each specimen are tabulated in Table 8. 7 for andesite and in Table 8. 8 for marble.

**Table 8. 7 Dimensionless stress intensity factors, failure loads and fracture toughness values of andesite specimens**

Specimen	$Y_I$	$F_{\max}$ kN	$K_{Ic}$ MPa $\sqrt{\text{m}}$
SCB_A1	3.328	12.10	1.10
SCB_A2	3.328	12.47	1.03
SCB_A3	3.328	10.08	0.85
SCB_A4	3.970	8.34	0.83
SCB_A5	3.970	8.11	0.84
SCB_A6	3.153	9.04	1.04
SCB_A7	3.153	7.54	0.86
SCB_A8	3.831	6.65	0.92
SCB_A9	3.831	6.95	0.94
SCB_A10	3.831	6.95	0.95
<b>Avg. <math>\pm</math> Stdev.</b>			<b>0.94 <math>\pm</math> 0.09</b>



**Table 8. 8 Dimensionless stress intensity factors, failure loads and fracture toughness values of andesite specimens**

Specimen	$Y_I$	$F_{max}$ kN	$K_{IC}$ MPa $\sqrt{m}$
SCB_M1	3.114	6.76	0.64
SCB_M2	3.051	5.49	0.59
SCB_M3	3.173	2.66	0.55
SCB_M4	3.129	2.98	0.60
SCB_M5	3.092	2.78	0.52
SCB_M6	3.140	2.41	0.47
SCB_M7	3.123	2.81	0.56
<b>Avg.±Stdev</b>			<b>0.56±0.06</b>

#### 8.2.4 Tests with CCNBD Method

CCNBD specimens having around 125 mm diameters were cored with boring machine and core samples were cut and flattened into thicknesses around 55 - 60 mm. All steps in specimen preparation and testing are illustrated in Figure 8. 8 through Figure 8. 15.

Center of the disc was marked and a line passing through the disc diameter was drawn on both sides by considering inhomogeneities. This line was drawn to assure that part that will include chevron notch do not intersect any heterogeneity or major defect. Load was applied to the end points of this line. Afterward, another line was drawn perpendicular to this line to both sides (Figure 8. 8).

Before specimen was mounted to the sawing machine, a flat rock block was mounted to the cutting machine platform and a notch was opened to the rock block with the diametral saw used for chevron notch opening to the disc specimens. Then, a knife piece having an equal thickness with notch thickness was placed to the notch. Then two flat pieces having same thicknesses were used at both sides of the knife piece. Afterward, disc specimen was placed on these pieces and perpendicularity and parallelism of the specimen with horizontal and saw were controlled by a level (Figure 8. 9).

Subsequently, saw was mounted to the machine and digital caliper was set to zero at this level. Then, specimen was fixed and saw was lowered to the required notch depth read from the digital caliper, and at this level to the center of the saw, a plum-line was tied to determine the center of the notch-end. This point was marked and fixed with a flat iron stick (Figure 8. 10). These adjustments were done because sawing machine follows a circular path when it is moved.

After these adjustments, specimen was placed to platform again; this time line perpendicular to saw was aligned with the fixed flat iron stick which shows the notch center location. Then chevron notch was machined to one face (Figure 8. 11).

Next, two adjustments below the specimen were taken and plumber-line was adjusted again for second face and notched face of the specimen was mounted on the knife piece in order to ensure that the notches cut in both sides aligned properly with each other. Second chevron notch was machined to the specimen, and the specimen was ready to fracture test (Figure 8. 12).

The CCNBD specimen was mounted to the loading frame for testing (Figure 8. 13). CCNBD specimens were also tested with MTS 815, and the same load and displacement recording system were used for CCNBD tests. Fractured CCNBD specimens are illustrated in Figure 8. 14.

A constant displacement controlled load, which was equal to 0.002 mm/sec, was applied to each CCNBD specimen.



**Figure 8. 8 Diametral line drawing with goniometer (on the left) and line perpendicular to diametral line drawing with goniometer and set-square (on the right)**



**Figure 8. 9 A flat block with knife piece (on the left), horizontal plane measurement perpendicular to notch (on the center) and horizontal plane measurement parallel to notch (on the right)**



**Figure 8. 10 Digital caliper adjustment (on the left) and plum-line and flat iron stick adjustment (on the right)**



**Figure 8. 11 Specimen placed exact location before cutting (on the left) and after cutting (on the right)**



**Figure 8. 12 Plum-line and flat iron stick adjustment for the second notch (on the left), specimen placement (at the center) and prepared specimen (on the right)**

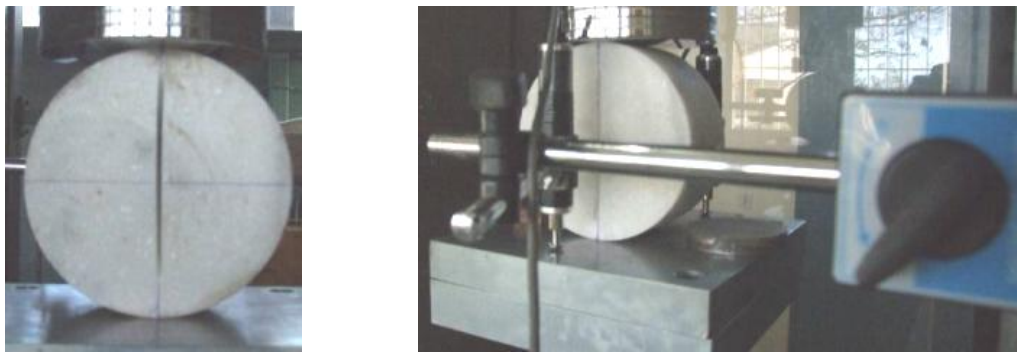


**Figure 8. 13 Loaded specimen through diametral plane (on the left) and loading setup of CCNBD specimen with transducers (on the right)**



**Figure 8. 14 CCNBD specimens after fracturing**

### 8.2.5 Specimen Geometries for CCNBD Method Tests

In Rock Mechanics Lab of Mining Department of Middle East Technical University, the rotary sawing machine has flexibility to operate with saws having minimum 110 mm diameter. Therefore, geometry and dimensions of the CCNBD specimens were decided by considering the saw diameters that can be used on the machine.

For proper specimen preparation in CCNBD method all parameters of the geometry should be converted in to dimensionless forms with respect to the radius and the diameter of the specimen. The parameters used in the geometrical descriptions are as follows: (Figure 8. 15)

$$\begin{cases} \alpha_0 = a_0/R \\ \alpha_1 = a_1/R \\ \alpha_B = B/R \\ \alpha_s = D_s/R \end{cases} \quad (8.3)$$

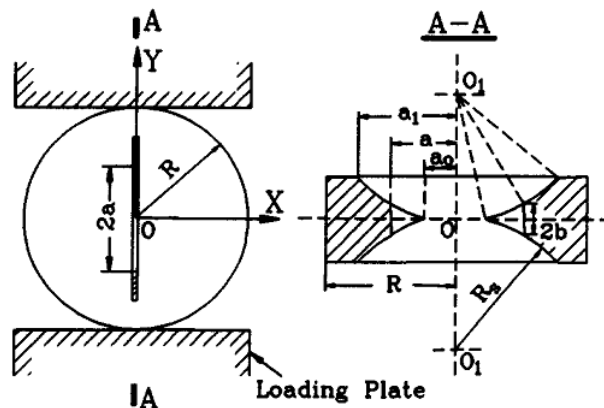


Figure 8. 15 The CNBD specimen geometry with recommended test fixture (Fowell, 1995)

Following suggestions for geometrical factors, for a 110 mm saw diameter, specimen must have at least 112 mm diameter. However, when oscillation of the saw is considered, the diameter must be greater than this value. In the laboratory, 125 mm and 150 mm diameter coring bits are available. Therefore, to be on the safe side with the minimum sample size requirement, 125 mm diameter specimens were

proposed. According to the suggestions, for 125 mm diameter, specimen thickness should be between 40 mm and 62 mm.

Suggested specimen dimensions and limitations for this test are plotted as in Fowell's graph (1995) and seen in the Figure 8. 16, all specimen geometries used for the suggested test method were in the valid ranges. Specimens were coded before testing, and in specimen coding, CCNBD denotes chevron-notched Brazilian disc specimen, A (for andesite) or M (for marble) indicates rock type used in a particular experiment and number at the end of the code defines the specimen number (Figure 8. 17). The details of the specimen dimensions for andesite and marble are listed in Table 8. 9, and in Table 8. 10, respectively.

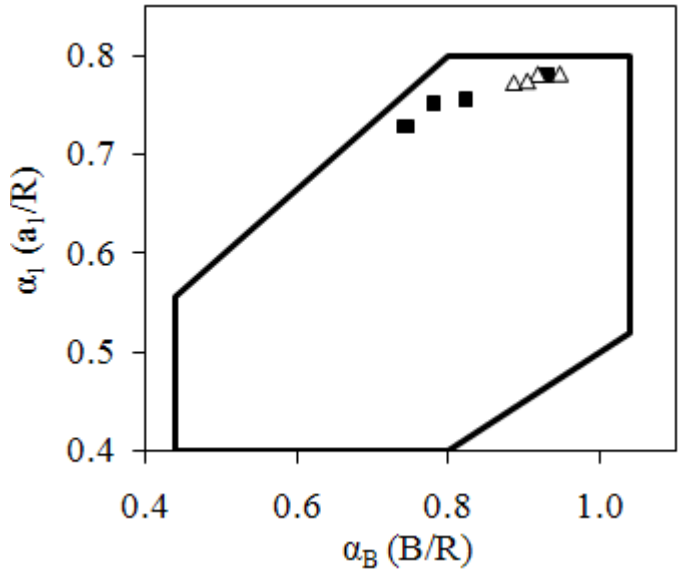


Figure 8. 16 CCNBD specimen geometries in Fowell's graph



Figure 8. 17 Specimen coding; CCNBD: cracked chevron notched Brazilian disc, A: rock type (A for andesite and M for marble), 4: specimen number

**Table 8. 9 Dimensions of the andesite CCNBD specimens**

Specimen	<i>B</i>	<i>R</i>	$\alpha_0$	$\alpha_B$	$\alpha_1$
CCNBD_A1	58.1450	62.5250	0.111955	0.929948	0.779556
CCNBD_A2	48.6125	62.2875	0.224764	0.780454	0.751455
CCNBD_A3	46.1250	61.8500	0.105093	0.745756	0.728369
CCNBD_A4	50.7775	61.6650	0.105408	0.823441	0.755573
CCNBD_A5	45.9350	61.9475	0.129142	0.741515	0.728401

**Table 8. 10 Dimensions of the marble CCNBD specimens**

Specimen	<i>B</i>	<i>R</i>	$\alpha_0$	$\alpha_B$	$\alpha_1$
CCNBD_M1	57.4900	62.5400	0.167893	0.919252	0.781337
CCNBD_M2	55.5075	62.5175	0.159955	0.887871	0.772396
CCNBD_M3	56.6050	62.5275	0.127944	0.905282	0.774154
CCNBD_M4	59.2525	62.4975	0.056002	0.948078	0.781712

### 8.2.6 Fracture Toughness Evaluation for CCNBD Method Tests

Fracture toughness value of rock types tested by the suggested CCNBD method can be estimated with the Equation 4.7. Since the expressions in Equation 4.7 are important for mode I fracture toughness evaluation, they are presented again in this section.

$$K_{Ic} = \frac{F_{max}}{t\sqrt{R}} Y_{min}^* \quad (8.4)$$

where,

$K_{Ic}$  : Fracture toughness (MPa $\sqrt{m}$ )

$F_{max}$  : Failure load (MN)

$R$  : Specimen radius (m)

$t$  : Specimen thickness (m)

$Y_{min}^*$  : Critical dimensionless stress intensity factor ( $Y_{min}^* = ue^{v\alpha_1}$ )

$u$  and  $v$ : constants determined by  $\alpha_0$  ( $a_0/R$ ) and  $\alpha_B$  ( $t/R$ )

$\alpha_1$  : Half of the notch length on disc faces over radius ( $a_1/R$ )

$u$  and  $v$  values in the expression were determined from Table 8. 11.  $u$ ,  $v$ ,  $Y_{\min}^*$  and fracture toughness values of rocks are tabulated in Table 8. 12 and Table 8. 13. Table 8. 12 shows the andesite results while Table 8. 13 demonstrates marble results. Average fracture toughness values of andesite and marble were determined as  $1.45 \pm 0.06 \text{ MPa}\sqrt{\text{m}}$  and  $1.08 \pm 0.07 \text{ MPa}\sqrt{\text{m}}$ , respectively.

**Table 8. 11 Values of  $u$  and  $v$  (Fowell, 1995)**

$a_0$	<b>0.100</b>	<b>0.150</b>	<b>0.175</b>	<b>0.200</b>	<b>0.225</b>	<b>0.250</b>	<b>0.275</b>	<b>0.300</b>
<b><math>u</math></b>								
$a_B$								
<b>0.720</b>	0.2611	0.2628	0.2637	0.2650	0.2667	0.2683	0.2705	0.2727
<b>0.760</b>	0.2598	0.2612	0.2625	0.2637	0.2650	0.2668	0.2693	0.2719
<b>0.800</b>	0.2582	0.2602	0.2611	0.2625	0.2641	0.2657	0.2680	0.2706
<b>0.840</b>	0.2572	0.2586	0.2599	0.2612	0.2628	0.2649	0.2672	0.2699
<b>0.880</b>	0.2562	0.2578	0.2593	0.2602	0.2621	0.2642	0.2668	0.2691
<b>0.920</b>	0.2553	0.2572	0.2582	0.2598	0.2613	0.2634	0.2658	0.2684
<b>0.960</b>	0.2549	0.2566	0.2578	0.2593	0.2612	0.2633	0.2655	0.2685
<b>1.000</b>	0.2547	0.2564	0.2576	0.2591	0.2610	0.2630	0.2653	0.2679
<b><math>v</math></b>								
<b>0.720</b>	1.7536	1.7580	1.7616	1.7647	1.7661	1.7698	1.7708	1.7722
<b>0.760</b>	1.7497	1.7553	1.7568	1.7600	1.7635	1.7656	1.7649	1.7652
<b>0.800</b>	1.7474	1.7506	1.7538	1.7557	1.7581	1.7611	1.7613	1.7603
<b>0.840</b>	1.7430	1.7487	1.7500	1.7522	1.7545	1.7547	1.7551	1.7548
<b>0.880</b>	1.7392	1.7438	1.7446	1.7487	1.7490	1.7492	1.7478	1.7487
<b>0.920</b>	1.7357	1.7390	1.7413	1.7423	1.7440	1.7446	1.7443	1.7432
<b>0.960</b>	1.7299	1.7337	1.7358	1.7370	1.7372	1.7373	1.7372	1.7346
<b>1.000</b>	1.7243	1.7279	1.7300	1.7308	1.7310	1.7307	1.7306	1.7297

**Table 8. 12  $u$ ,  $v$ ,  $Y_{\min}^*$ ,  $F_{\max}$  and  $K_{Ic}$  values of andesite specimens**

Specimen	$u$	$v$	$Y_{\min}^*$	$F_{\max}$ kN	$K_{Ic}$ MPa $\sqrt{\text{m}}$
<b>CCNBD_A1</b>	0.2556429	1.7350763	0.9887	21.3	1.45
<b>CCNBD_A2</b>	0.2645398	1.7607388	0.9934	17.6	1.44
<b>CCNBD_A3</b>	0.2604164	1.7516157	0.9327	16.6	1.35
<b>CCNBD_A4</b>	0.2577923	1.7453261	0.9638	19.5	1.49
<b>CCNBD_A5</b>	0.2612975	1.7544429	0.9379	18.3	1.50
<b>Avg.±Stdev.</b>					<b>1.45±0.06</b>



**Table 8. 13**  $u$ ,  $\nu$ ,  $Y_{\min}^*$ ,  $F_{\max}$  and  $K_{Ic}$  values of marble specimens

Specimen	$u$	$\nu$	$Y_{\min}^*$	$F_{\max}$ kN	$K_{Ic}$ MPa $\sqrt{m}$
CCNBD_M1	0.2579336	1.7407158	1.0050	14.0	0.98
CCNBD_M2	0.2582401	1.7432915	0.9927	14.2	1.02
CCNBD_M3	0.2566313	1.7390995	0.9863	15.9	1.11
CCNBD_M4	0.2534708	1.728416	0.9788	18.7	1.24
<b>Avg.±Stdev.</b>					<b>1.08±0.07</b>

### **8.3 FBD Method Tests for Mode I Fracture Toughness Determination**

Rock discs were prepared from andesite in various diameters, then polished into required thicknesses. All steps in specimen preparation and testing are illustrated in Figure 8. 18 through Figure 8. 21. According to the desired loading angle, upper and lower end one side of the disc was flattened with grinding machine (Figure 8. 18). The other end of the specimen must be flattened parallel with equal length to the other flattened side. To achieve this, a set square was used as in Figure 8. 19. One side of the set square was positioned at the flattened part and the other side was tangent to the disc face.

As in SCB and CCNBD methods, MTS 815 testing system was used as the loading system. Loading rate was set to 0.001 mm/sec. FBD specimen under loading is seen in Figure 8. 20. Fractured FBD specimens are displayed in Figure 8. 21.



**Figure 8. 18 Flattening loading end with grinding machine**



**Figure 8. 19 Adjustment to get parallel loading ends**



**Figure 8. 20 FBD specimen under loading**



**Figure 8. 21 FBD specimens after fracturing**

### 8.3.1 Specimen Geometries for FBD Method Tests

For andesite rock, discs having 54 mm, 75 mm and 100 mm diameters were prepared and tested. For each diameter group, loading angle values targeted were 16°, 25° and 35° with about 5 to 15% acceptable deviation bands around them. Deviation bands in the individual angle groups were considered, since it is difficult to machine the flattened ends exactly to the desired width and loading angle with a pinpoint accuracy in a rock like material. Specimen thickness was set to the half specimen diameter for each specimen. Loading rate was taken as  $10^{-3}$  mm/sec for all specimen diameter and loading angle studies. Forty specimens were prepared for diameter and loading angle studies; 17 of them were in 54 mm diameter group, 12 of them were in 75 mm diameter group, and the rest were in 100 mm diameter group. Specimens were coded before testing, and in specimen coding, A (for andesite) indicates rock type used in the experiment, 75 (or 54, or 100) is used for specimen diameter, 00 shows hole diameter in flattened Brazilian disc specimens (means no hole), 25 (or 15, or 35) illustrates loading angle, and number at the end of the code defines the specimen number (Figure 8. 22). The andesite specimen geometries in terms of diameter, flattened width, thickness and loading angle are listed in Table 8. 14.

**A750025-2**

└───┬───┬───┬───┬───┘

Rock Specimen Hole Loading Specimen  
Type Diameter Diameter Angle No

**Figure 8. 22 Specimen coding; A: rock type (A for andesite), 75: specimen diameter, 00: central-hole diameter, 25: loading angle, 2: specimen number**

**Table 8. 14 Dimensions of the andesite FBD specimens**

Specimen	<i>D</i> (mm)	<i>2L</i> (mm)	<i>t</i> (mm)	<i>2α</i> (°)	Specimen	<i>D</i> (mm)	<i>2L</i> (mm)	<i>t</i> (mm)	<i>2α</i> (°)
A540015-1	54	9.16	26.05	19	A750025-1	75	16.55	35.87	26
A540015-2	54	7.58	26.34	16	A750025-2	75	16.10	36.22	25
A540015-3	54	8.54	27.61	18	A750025-3	75	16.74	36.58	26
A540015-4	54	8.35	25.97	18	A750025-4	75	18.62	35.00	29
A540015-5	54	7.44	28.00	16	A750025-5	75	15.08	36.75	23
A540015-6	54	7.66	27.89	16	A750025-6	75	15.67	37.63	24
A540025-1	54	9.92	26.73	21	A750035-1	75	21.28	35.05	33
A540025-2	54	10.66	27.50	23	A750035-2	75	22.47	37.85	35
A540025-3	54	10.65	25.90	23	A750035-3	75	23.24	35.12	36
A540025-4	54	11.06	26.45	23	A1000015-1	101	13.35	50.60	15
A540025-5	54	13.81	27.23	29	A1000015-2	100	13.05	48.72	15
A540035-1	54	14.36	25.32	31	A1000015-3	100	12.85	49.39	15
A540035-2	54	17.61	23.23	38	A1000015-4	100	13.07	49.55	15
A540035-3	54	16.38	24.64	35	A1000025-1	101	22.24	48.96	25
A540035-4	54	16.76	25.22	36	A1000025-2	100	22.33	51.53	26
A540035-5	54	16.62	26.45	36	A1000025-3	101	23.44	49.93	27
A540035-6	54	16.98	29.87	36	A1000025-4	100	19.59	50.23	23
A750015-1	75	10.18	37.87	16	A1000035-1	100	28.62	53.16	33
A750015-2	75	9.81	35.77	15	A1000035-2	100	30.06	51.91	35
A750015-3	75	10.05	37.06	15	A1000035-3	101	33.91	54.81	39

### 8.3.2 Fracture Toughness Evaluation for FBD Method Tests

Fracture toughness value for FBD testing method is calculated by using the Equation 4.10. Since the expressions in Equation 4.10 are important for mode I fracture toughness evaluation, they are presented again in this section.

$$K_{Ic} = \frac{F_{min}}{\sqrt{R \times t}} \phi_{max} \quad (8.5)$$

where,

$K_{Ic}$  : Fracture toughness (MPa√m)

$F_{min}$  : Minimum local load (MN)

$R$  : Disc radius (m)

$t$  : Disc thickness (m)

$\phi_{\max}$  : Maximum dimensionless stress intensity factor determined from numerical modeling

In this equation, maximum dimensionless stress intensity factor  $\Phi_{\max}$  is determined from the following equation:

$$\phi_{\max} = \frac{K_{I\max} \sqrt{R} \times t}{F} \quad (8.6)$$

where  $K_{I\max}$  is the maximum stress intensity factor .

In numerical modeling for FBD method,  $F$  and  $t$  were set to unit load 1 N and unit thickness 1 m, respectively. Therefore,  $\phi_{\max}$  can be expressed as  $\phi_{\max} = K_{I\max} \sqrt{R}$  . By curve fitting to the numerical modeling results for the estimation of dimensionless maximum stress intensity factor, an expression ( $\Phi_{\max}=1/(43.32-15.63\exp(\cos\alpha))$ ) was developed in terms of half loading angle as mentioned in numerical modeling work for FBD method in Chapter 6.

By using the equations above, fracture toughness values for andesite specimens were determined as in Table 8. 15.

**Table 8. 15  $\Phi_{max}$ ,  $F_{min}$ , and  $K_{Ic}$  values of FBD andesite specimens**

Specimen	$\Phi_{max}$	$F_{min}$ (kN)	$K_{Ic}$ (MPa $\sqrt{m}$ )	Specimen	$\Phi_{max}$	$F_{min}$ (kN)	$K_{Ic}$ (MPa $\sqrt{m}$ )
A540015-1	0.659	14.21	2.18	A750025-1	0.523	21.01	1.58
A540015-2	0.754	13.90	2.41	A750025-2	0.537	26.41	2.02
A540015-3	0.692	11.54	1.75	A750025-3	0.518	22.40	1.64
A540015-4	0.707	14.98	2.47	A750025-4	0.467	25.71	1.78
A540015-5	0.763	11.06	1.83	A750025-5	0.570	24.84	1.99
A540015-6	0.749	10.53	1.71	A750025-6	0.551	29.85	2.26
A540025-1	0.619	15.14	2.12	A750035-1	0.407	37.32	2.24
A540025-2	0.583	13.09	1.68	A750035-2	0.382	31.92	1.67
A540025-3	0.583	10.47	1.43	A750035-3	0.366	42.88	2.31
A540025-4	0.566	15.55	2.02	A1000015-1	0.784	39.06	2.69
A540025-5	0.458	15.44	1.57	A1000015-2	0.787	35.26	2.55
A540035-1	0.441	14.88	1.57	A1000015-3	0.793	26.76	1.93
A540035-2	0.348	18.54	1.68	A1000015-4	0.786	35.48	2.52
A540035-3	0.380	16.30	1.53	A1000025-1	0.528	30.91	1.48
A540035-4	0.370	15.55	1.38	A1000025-2	0.521	54.93	2.48
A540035-5	0.373	16.20	1.38	A1000025-3	0.503	25.79	1.16
A540035-6	0.363	15.43	1.14	A1000025-4	0.579	62.29	3.22
A750015-1	0.765	20.89	2.18	A1000035-1	0.403	86.63	3.65
A750015-2	0.785	8.26	1.13	A1000035-2	0.381	95.67	4.12
A750015-3	0.772	22.69	2.44	A1000035-3	0.331	109.56	2.94

Fracture toughness results show that fracture toughness value depends on both specimen diameter and loading angle. It is impossible to say a constant fracture toughness value for FBD method.

Fracture toughness values determined with FBD method will be compared later with the results of CCNBD and SCB methods. For proper geometries which produce close fracture toughness ranges with the CCNBD method, loading rate and thickness effects on fracture toughness will be investigated.

#### **8.4 MR Tests for Mode I Fracture Toughness Determination**

Specimen preparation of the MR test specimens was similar to FBD method test specimen preparation. All steps in specimen preparation and testing are illustrated in Figure 8. 23 through Figure 8. 26.

A central-hole in discs was drilled with drill bits by using a lathe as in Figure 8. 23. This equipment assures drilling the hole at the center of the disc (Figure 8. 24). Specimens were polished and loading parts of the discs were prepared by flattening.

Coring bits were used for central-hole diameters greater than 30 mm, not to disturb rock specimen with drilling bits. To drill a hole greater than 30 mm diameter, firstly, rock blocks were cored with a smaller hole. Without changing the block position, coring bit was changed to greater diameter coring bits which were used for coring the specimen to the right inner diameters. This way, holes were positioned at centers of the disc specimens. Cores were later cut, sliced and polished into the required thicknesses. Afterwards, flattened ends were machined by grinding.

After the specimens were ready for the tests (Figure 8. 25), loading rate was set to 0.001 mm/sec and specimens were loaded to initiate and propagate cracks. Fractured MR specimens are seen as in Figure 8. 26.

Fracture toughness values determined with MR tests will be compared with the results of CCNBD and SCB tests. Fracture toughness value of the andesite rock determined with CCNBD method was compared to the results of MR tests. Specimen dimensions with close fracture toughness results were determined by comparisons to the suggested CCNBD method results for andesite rock. Results will be checked for marble rock to investigate the applicability of the MR test to yield results close to the suggested method for another rock type.



**Figure 8. 23 Lathe with drilling bit**



**Figure 8. 24 Drilled specimens**



**Figure 8. 25 MR specimen while loading**

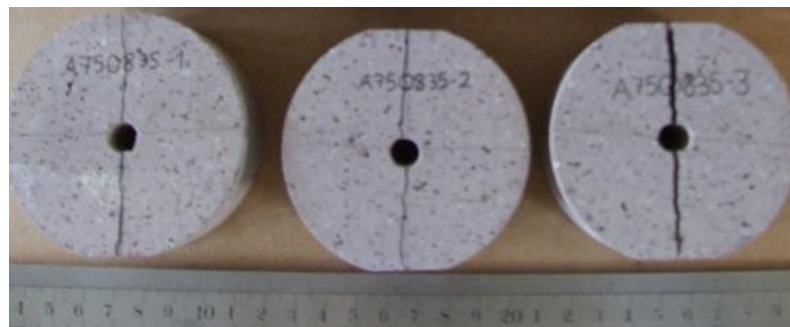


**Figure 8. 26 MR specimens after fracturing**



### 8.4.1 Specimen Geometries for MR Tests

For investigating specimen diameter and loading angle effects on fracture toughness of andesite, specimens with 54 mm, 75 mm and 100 mm diameters were prepared, and for each diameter group, loading angle was varied as  $17\pm 2^\circ$ ,  $25\pm 2^\circ$  and  $35\pm 3^\circ$ . Deviation bands in the individual angle groups were considered, since it is difficult to machine the flattened ends exactly to the desired width and loading angle. To generalize the comparison of diameters, central-hole diameters were normalized with specimen diameters, and dimensionless central-hole diameters ( $d/D$ ) used were 0.1, 0.2 and 0.3. 54 mm discs had 5 mm, 10 mm, and 14 mm diameter central holes, 75 mm discs had 8 mm, 14 mm, and 26 mm diameter central-holes, and 100 mm discs had 10 mm, 21 mm, and 32 mm diameter central-holes. A total of 81 specimens were prepared; 29 of them were in 54 mm diameter group, 27 of them were in 75 mm diameter group, and the rest was in 100 mm diameter group.

The specimen coding is explained Figure 8. 27. In the code; A (for andesite) indicates rock type used in the experiment, 54 (or 75, or 100) is used for specimen diameter, 10 shows inner hole diameter in the modified ring test specimens, 35 (or 15, or 25) is used for loading angle, and the number at the end of the code defines the specimen number. Dimensions of the andesite specimens are tabulated in Table 8. 16.

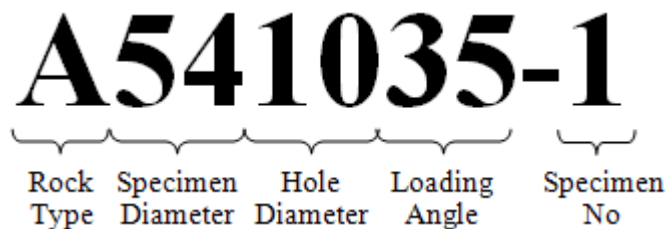


**Figure 8. 27 Specimen coding; A: rock type (A for andesite), 54: specimen diameter, 08: central-hole diameter, 35: Loading Angle, 1: specimen number**

**Table 8. 16 Dimensions of the andesite MR specimens (dimensions in mm, loading angle in °)**

Specimen	<i>D</i>	<i>d</i>	<i>2L</i>	<i>t</i>	<i>2α</i>	Specimen	<i>D</i>	<i>d</i>	<i>2L</i>	<i>t</i>	<i>2α</i>
A540515-1	54	5	9.28	26.05	20	A751425-2	75	14	16.11	37.44	25
A540515-2	54	5	7.91	24.96	17	A751425-3	75	14	15.04	37.65	23
A540515-3	54	5	9.16	24.61	19	A751435-1	75	14	21.54	35.22	33
A540515-4	54	5	9.19	25.90	19	A751435-2	75	14	23.95	33.76	37
A540525-1	54	5	13.81	25.91	29	A752615-1	75	26	9.39	38.10	14
A540525-2	54	5	12.28	24.72	26	A752615-2	75	26	8.59	37.64	13
A540525-3	54	5	13.48	26.27	29	A752615-3	75	26	9.58	38.95	15
A540535-1	54	5	15.21	25.65	32	A752625-1	75	26	16.51	37.55	25
A540535-2	54	5	15.30	25.12	33	A752625-2	75	26	16.14	37.80	25
A540535-3	54	5	15.97	26.09	34	A752625-3	75	26	17.11	37.78	26
A541015-1	54	10	9.46	26.42	20	A752635-1	75	26	25.32	35.71	40
A541015-2	54	10	9.23	27.58	20	A752635-2	75	26	24.79	36.22	39
A541015-3	54	10	9.17	28.16	19	A752635-3	75	26	25.61	37.28	40
A541015-4	54	10	9.01	26.64	19	A752635-4	75	26	21.31	37.50	33
A541025-1	54	10	12.09	27.94	26	A752635-5	75	26	19.84	37.11	31
A541025-2	54	10	12.45	28.64	26	A1001015-1	100	10	13.39	46.56	15
A541025-3	54	10	12.83	28.97	27	A1001015-2	100	10	14.75	43.73	17
A541035-1	54	10	17.87	25.92	38	A1001015-3	99	10	14.86	47.79	17
A541035-2	54	10	17.34	25.87	37	A1001025-1	100	10	21.87	42.76	25
A541035-3	54	10	16.79	29.31	36	A1001025-2	100	10	22.09	44.91	26
A541415-1	54	14	8.25	24.42	17	A1001025-3	99	10	22.87	50.02	27
A541415-2	54	14	8.05	25.31	17	A1001035-1	100	10	29.22	48.33	34
A541415-3	54	14	9.08	24.98	19	A1001035-2	99	10	31.82	50.47	38
A541425-1	54	14	12.67	26.47	27	A1001035-3	100	10	30.15	49.70	35
A541425-2	54	14	10.27	26.58	22	A1002115-1	100	21	14.48	52.17	17
A541425-3	54	14	11.43	25.68	24	A1002115-2	100	21	15.37	50.23	18
A541435-1	54	14	17.45	27.56	37	A1002115-3	100	21	15.60	52.41	18
A541435-2	54	14	14.46	25.92	31	A1002125-1	100	21	21.61	49.91	25
A541435-3	54	14	14.18	26.19	30	A1002125-2	100	21	21.74	52.38	25
A750815-1	75	8	12.19	39.22	19	A1002125-3	100	21	23.99	52.18	28
A750815-2	75	8	11.68	37.01	18	A1002135-1	100	21	28.87	52.79	34
A750825-1	75	8	16.41	34.98	25	A1002135-2	100	21	29.18	53.81	34
A750825-2	75	8	15.82	38.09	24	A1002135-3	100	21	30.37	53.87	35
A750825-3	75	8	17.07	34.09	26	A1003215-1	100	32	14.01	48.60	16
A750835-1	75	8	19.35	37.07	30	A1003215-2	101	32	16.17	49.65	18
A750835-2	75	8	22.50	34.94	35	A1003225-1	101	32	20.16	49.40	23
A750835-3	75	8	25.22	36.33	39	A1003225-2	101	32	20.48	50.68	23
A751415-1	75	14	11.56	36.88	18	A1003225-3	101	32	21.06	51.02	24
A751415-2	75	14	8.77	34.26	13	A1003235-1	101	32	30.21	54.21	35
A751415-3	75	14	10.03	36.29	15	A1003235-2	101	32	29.06	48.10	33
A751425-1	75	14	15.43	36.17	24						

### 8.4.2 Fracture Toughness Evaluation for MR Tests

Fracture toughness values for MR test can be determined with Equation 4.8. Since the expression in Equation 4.10 is important for mode I fracture toughness evaluation, it is presented again in this section.

The fracture toughness values can be determined by using the relationship below:

$$\left( \frac{\sigma_{ac}}{K_{I_{max}}} \right)_{model} = \left( \frac{\sigma_{ac}}{K_{Ic}} \right)_{lab} \quad (8.7)$$

where,

$K_{I_{max}}$  : Stress intensity factor (MPa√m)

$K_{Ic}$  : Fracture toughness (MPa√m)

$\sigma_{ac} = \frac{F_{min}}{2L \times t}$  (for experimental results) and  $\sigma_{ac} = \frac{1}{2L}$  (for model ratio)

$F_{min}$  : Local minimum load (MN)

$2L$  : Length of flat loading surface (m)

$t$  : Disc thickness (m)

$\sigma_{ac}$  for models is  $\sigma_{ac}=1/2L$ , since load is  $F = 1$  unit (N) and thickness is  $t = 1$  unit (m) thickness in the modeling work.

$$K_{Ic} = \frac{F_{min}}{t} K_{I_{max}} \quad (8.8)$$

where  $K_{I_{max}}$  can be determined by using the equation below:

$$K_{I_{max}} = \frac{\phi_{max} \sqrt{a + r_i}}{R\sqrt{\pi}} \quad (8.9)$$

where,

$a$ : crack length (m)

$r_i$ : central-hole radius (m)

$R$ : specimen radius (m)

$\phi_{max}$ : dimensionless maximum stress intensity factor

$$\ln \phi_{\max} = -3.470 + 4.498 \left( \frac{U}{D} \right)^{1.5} + 3.866 \left( \cos \alpha \right)^3$$

A typical load-displacement curve is shown in Figure 4. 14. In this figure,  $F_{\min}$  is marked at the point where initial unstable crack propagation becomes stable corresponding to the  $K_I$  maximum point (Figure 4. 15). In Figure 4. 15, relative crack length ( $a/R$ ) is the crack length-specimen radius ratio.

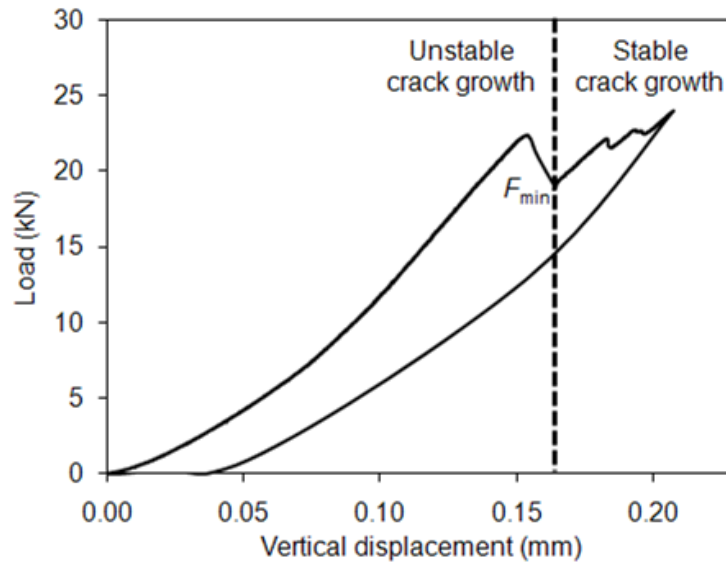


Figure 4. 14 A typical load-displacement curve (for  $D=75\text{mm}$ ,  $d=8\text{ mm}$ ,  $2\alpha=35^\circ$ )

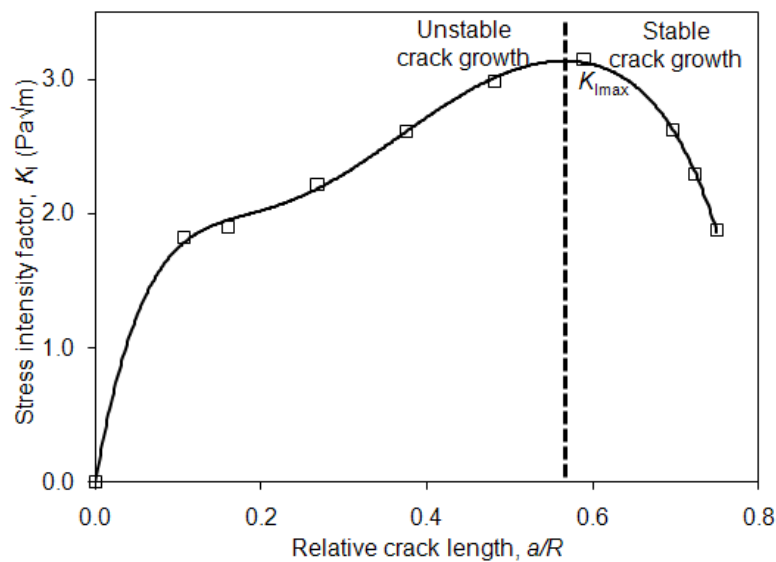


Figure 4. 15  $K_I$  versus relative crack length (for  $D=75\text{ mm}$ ,  $d=8\text{ mm}$ ,  $2\alpha=25^\circ$ )

Fracture toughness values of andesite rock are listed in Table 8. 17. The fracture toughness results showed that fracture toughness value depends on specimen diameter, central-hole diameter, and loading angle.

**Table 8. 17  $\Phi_{\max}$ ,  $F_{\min}$  (kN), and  $K_{Ic}$  (MPa $\sqrt{m}$ ) values of MR andesite specimens**

Specimen	$\Phi_{\max}$	$F_{\min}$ (kN)	$K_{Ic}$ (MPa)	Specimen	$\Phi_{\max}$	$F_{\min}$ (kN)	$K_{Ic}$ (MPa)
A540515-1	1.445	7.87	1.287	A751425-2	1.603	10.76	1.092
A540515-2	1.583	8.70	1.661	A751425-3	1.638	11.43	1.194
A540515-3	1.454	7.23	1.261	A751435-1	1.316	10.50	0.882
A540515-4	1.449	8.15	1.344	A751435-2	1.227	10.86	0.863
A540525-1	1.124	8.70	1.030	A752515-1	3.428	5.40	1.241
A540525-2	1.221	8.85	1.222	A752515-2	3.505	5.48	1.317
A540525-3	1.144	10.03	1.198	A752515-3	3.440	5.28	1.189
A540535-1	1.044	10.04	1.092	A752525-1	2.861	5.95	1.072
A540535-2	1.034	10.57	1.161	A752525-2	2.895	5.42	0.985
A540535-3	1.001	9.52	0.966	A752525-3	2.831	5.23	0.922
A541015-1	1.733	5.05	0.965	A752535-1	2.407	5.54	0.763
A541015-2	1.743	6.74	1.247	A752535-2	2.443	5.08	0.703
A541015-3	1.752	6.30	1.149	A752535-3	2.387	5.40	0.705
A541015-4	1.760	5.57	1.081	A752535-4	2.483	6.00	0.873
A541025-1	1.536	7.14	1.091	A752535-5	2.563	6.09	0.949
A541025-2	1.510	6.85	0.997	A1001015-1	1.652	26.95	2.154
A541025-3	1.490	7.68	1.083	A1001015-2	1.565	28.37	2.259
A541035-1	1.185	6.82	0.788	A1001015-3	1.551	28.90	2.090
A541035-2	1.208	5.80	0.691	A1001025-1	1.289	27.51	1.697
A541035-3	1.244	7.63	0.833	A1001025-2	1.276	32.47	1.888
A541415-1	2.328	3.83	1.073	A1001025-3	1.247	33.37	1.694
A541415-2	2.330	3.88	1.053	A1001035-1	1.038	36.18	1.504
A541415-3	2.244	3.92	1.022	A1001035-2	0.954	37.34	1.346
A541425-1	1.942	4.73	0.954	A1001035-3	1.011	34.42	1.344
A541425-2	2.148	3.97	0.912	A1002015-1	1.990	20.03	1.687
A541425-3	2.040	4.38	0.973	A1002015-2	1.916	20.02	1.670
A541435-1	1.806	5.46	0.817	A1002015-3	1.904	20.52	1.626
A541435-2	1.821	4.41	0.825	A1002025-1	1.685	20.20	1.388
A541435-3	1.828	4.49	0.837	A1002025-2	1.689	21.97	1.440
A750815-1	1.503	18.83	1.828	A1002025-3	1.597	23.35	1.428
A750815-2	1.541	17.49	1.855	A1002035-1	1.416	24.61	1.279

**Table 8. 18 (continued)  $\Phi_{\max}$ ,  $F_{\min}$  (kN), and  $K_{Ic}$  (MPa $\sqrt{m}$ ) values of MR andesite specimens**

<b>Specimen</b>	<b><math>\Phi_{\max}</math></b>	<b><math>F_{\min}</math> (kN)</b>	<b><math>K_{Ic}</math> (MPa)</b>	<b>Specimen</b>	<b><math>\Phi_{\max}</math></b>	<b><math>F_{\min}</math> (kN)</b>	<b><math>K_{Ic}</math> (MPa)</b>
<b>A750825-1</b>	1.272	18.33	1.590	<b>A1002035-2</b>	1.401	26.76	1.347
<b>A750825-2</b>	1.305	17.36	1.429	<b>A1002035-3</b>	1.358	27.04	1.308
<b>A750825-3</b>	1.247	16.04	1.386	<b>A1003015-1</b>	2.989	9.99	1.337
<b>A750835-1</b>	1.150	18.80	1.342	<b>A1003015-2</b>	2.796	10.71	1.281
<b>A750835-2</b>	1.020	18.10	1.177	<b>A1003025-1</b>	2.654	12.45	1.374
<b>A750835-3</b>	0.913	18.23	0.995	<b>A1003025-2</b>	2.570	12.09	1.255
<b>A751415-1</b>	1.826	11.72	1.461	<b>A1003025-3</b>	2.529	12.31	1.244
<b>A751415-2</b>	2.064	10.27	1.620	<b>A1003035-1</b>	2.444	14.98	1.153
<b>A751415-3</b>	1.948	10.24	1.417	<b>A1003035-2</b>	2.206	13.32	1.167
<b>A751425-1</b>	1.618	11.96	1.279				

## CHAPTER 9

### RESULTS AND DISCUSSION

Average fracture toughness value for Ankara andesite with SCB method was computed as  $K_{Ic}=0.94\pm 0.09$  MPa $\sqrt{m}$  with ten specimens having  $99.5\pm 0.8$  mm diameter. Average fracture toughness value of andesite with the suggested CCNBD method was determined as  $K_{Ic}=1.45\pm 0.06$  MPa $\sqrt{m}$  with five specimens having  $124.1\pm 0.7$  mm diameter. The SCB method results were not in a good agreement with the results of the CCNBD method. SCB method results are much lower than the suggested methods' results. Fracture toughness results obtained by conventional SCB method are usually lower than the toughness values determined by the suggested methods (Chang et al, 2002; Kuruppu, 2002; Pehovaz-Alvarez, 2004). This may be due to the bending effect. Bending load decrease the resistance to fracture with the presence of the moments.

Since the CCNBD method is one of the suggested methods by ISRM, the CCNBD method was chosen for  $K_{Ic}$  comparisons between the FBD and MR test results and the suggested method results. Results found were used for comparison purposes in investigating the effects of different factors on  $K_{Ic}$  determination with FBD and MR methods.

#### 9.1 FBD Method Results

Mode I fracture toughness results of the FBD method are presented in this section. FBD method specimen diameters used in the tests were 54 mm, 75 mm and 100 mm. Loading angle ranges were between  $2\alpha=15^\circ-39^\circ$  which corresponds to dimensionless vertical distance ( $y_i/R=\cos\alpha$ ) between 0.99-0.94.

### 9.1.1 Effects of Specimen Diameter and Loading Angle on Mode I Fracture Toughness for FBD Tests

Table 9. 1 for FBD method tests on andesite rock shows average mode I fracture toughness values for different loading angle ranges and specimen diameters. Number of tests evaluated in each loading angle and diameter groups are indicated in the table. For loading angles between 15°-19°, average fracture toughness values were found as 2.06±0.34 MPa√m for 54 mm diameter group, 1.85±0.81 MPa√m for 75 mm group, and 2.42±0.34 MPa√m for 100 mm group. For loading angle range of 21°-29°, average fracture toughness values were 1.76±0.29 MPa√m for 54 mm diameter group, 1.88±0.26 MPa√m for 75 mm group, and 2.08±0.94 MPa√m for 100 mm diameter group. For loading angles between 31°-39°, average fracture toughness values were 1.45±0.19 MPa√m for 54 mm diameter group, 2.07±0.35 MPa√m for 75 mm diameter group, and 3.57±0.59 MPa√m for 100 mm diameter group.

**Table 9. 1 Average fracture toughness values of FBD andesite specimens for various diameters and loading angle ranges**

<i>D</i> (mm)	$2a_{Avg} \pm stdev$ (°)	No of specimens	$K_{Icavg} \pm stdev$ (MPa√m)
54	17±1	6	2.06±0.34
	24±3	5	1.76±0.29
	35±2	6	1.45±0.19
75	15±0	3	1.85±0.81
	25±2	6	1.88±0.26
	35±2	3	2.07±0.35
100	15±0	4	2.42±0.34
	25±2	4	2.08±0.94
	36±3	3	3.57±0.59

For 100 mm specimen diameter group, which is the largest diameter group, standard deviations are larger among all average results. Considering all test results, the closest average value of  $K_{Ic}$  to the result found by the suggested CCNBD method is 1.45±0.19 MPa√m for the andesite rock. This result is for loading angles between 32.5°-38.0° in 54 mm diameter group. The other average  $K_{Ic}$  results fall outside of



the deviation band around the result obtained by the suggested method (Figure 9. 1). Average fracture toughness values of FBD specimens were normalized with the average fracture toughness values of CCNBD specimens in Figure 9. 1.

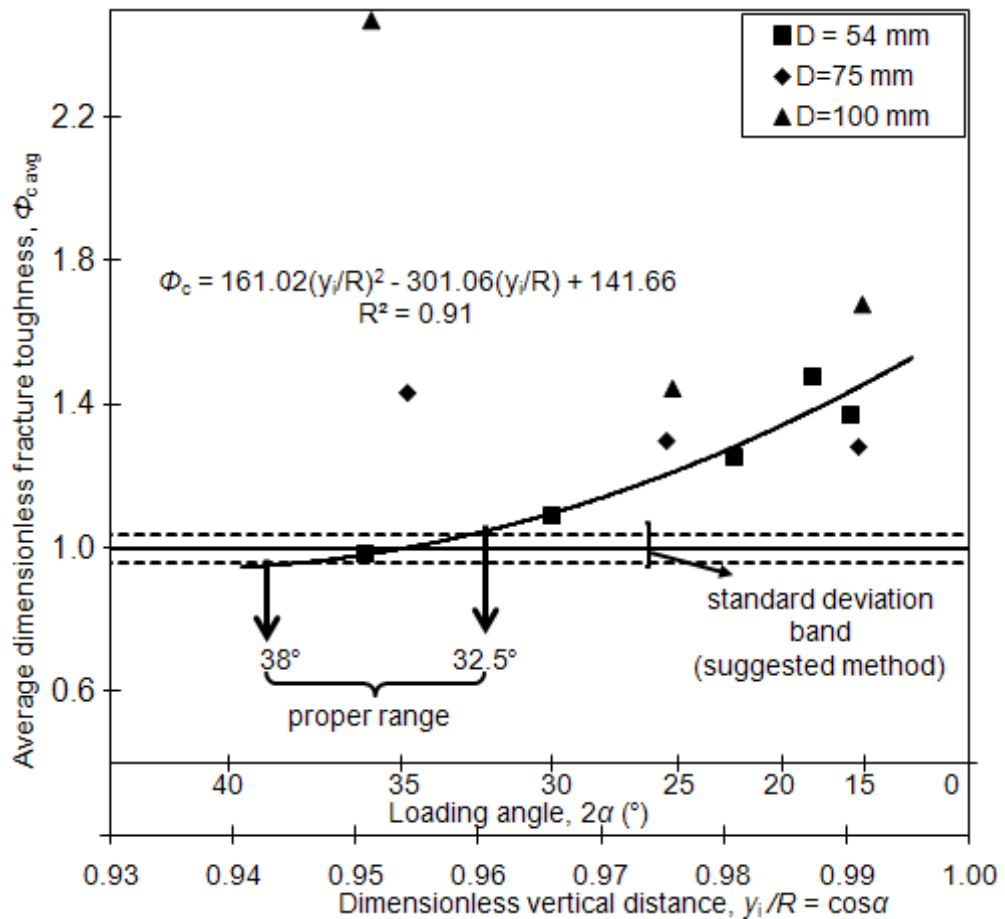


**Figure 9. 1 Average fracture toughness values of andesite for dimensionless vertical distance and various specimen diameters**

Observations on load-displacement plots of size and loading angle effect studies indicated that number of valid tests is much higher for 54 mm specimen diameter group. Therefore, specimens with 54 mm diameter were prepared with loading angle of  $35^\circ \pm 1^\circ$ , and tested for studying the effects of the other factors on mode I fracture toughness.

In Figure 9. 2, dimensionless fracture toughness of andesite was plotted against  $y_i/R$  or cosine of half loading angle for 54 mm diameter specimens. Dimensionless

fracture toughness ( $\Phi_c$ ) of andesite was evaluated by normalizing fracture toughness values of andesite determined by FBD method with the average fracture toughness value found by the suggested CCNBD method. Dashed lines demonstrate the deviation band around the average  $\Phi_c$  result of the suggested method in the figure.

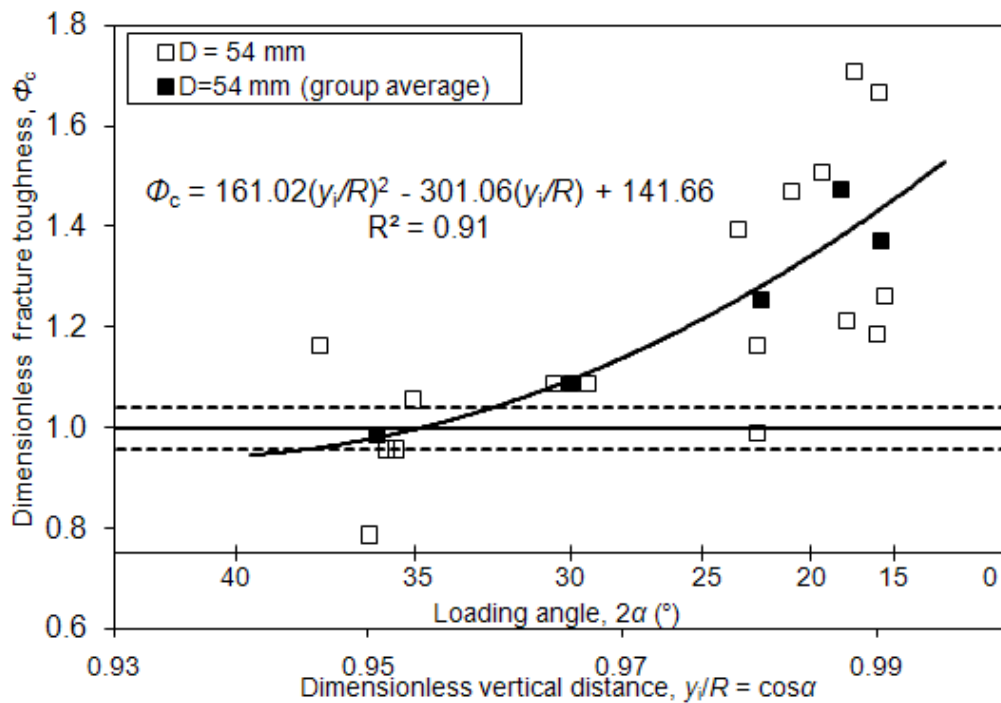


Figure 9. 2 Variations of dimensionless mode I fracture toughness with dimensionless vertical distance for various diameters of FBD andesite rock cores

With curve fitting, when loading angles were in between 32.5 and 38.0 degrees ( $y_i/R=0.960$  and  $0.946$ , respectively), overall results showed that fracture toughness values converged to the result obtained by the suggested CCNBD method. In Figure 9. 2, white squares are for the dimensionless fracture toughness values  $\Phi_c$  of all andesite specimens having 54 mm diameter with loading angles from  $16^\circ$  to  $38^\circ$ . Machining of flattened ends exactly to a desired width and loading angle target is difficult, and there is usually an error band of a few degrees. Considering this error band results were grouped and averaged with respect to the loading angle. Dark squares show the average values of dimensionless fracture toughness values for five different angle ranges, which are  $16 \pm 0^\circ$  (3 specimens),  $19 \pm 2^\circ$  (4 specimens),

23±1° (3 specimens), 30±1° (2 specimens), and 36±1° (5 specimens). With a reasonable correlation, curve fitting shows that mode I fracture toughness of andesite approaches to the result of the suggested method, as indicated by  $\Phi_c$  approaching one in Figure 9. 2.

### **9.1.2 Effect of Thickness on Mode I Fracture Toughness for FBD Tests**

After determining proper specimen geometry for mode I fracture toughness testing with FBD method, effect of the specimen thickness on  $K_{Ic}$  was studied. Effect of specimen thickness on  $K_{Ic}$  was studied with 20 specimens having 54 mm diameter and 35±1° loading angle range. Loading rate was set to 10<sup>-3</sup> mm/sec again for this work. Thicknesses of Brazilian discs were set to 19.7±0.8, 25.9±2.5, 40.9±1.0, and 48.6±1.3 mm, and 5 specimens were prepared for each thickness category.

Average fracture toughness for each thickness group was evaluated. Changing the specimen thickness seemed to have an effect on the mode I fracture toughness. According to the results, average fracture toughness values were equal to 1.37±0.07 MPa√m, 1.42±0.20 MPa√m, 1.25±0.15 MPa√m, and 0.98±0.20 MPa√m for specimens having 19.7±0.8 mm, 25.9±2.5 mm, 40.9±1.0 mm, and 48.6±1.3 mm thicknesses, respectively. The results showed that with a curve fitting to the average values if thickness was kept between 19 mm ( $t/R=0.7$ ) and 34 mm ( $t/R=1.25$ ) for 54.4 mm specimens, fracture toughness value converged to the suggested method's results. Average fracture toughness value for ten FBD specimens in this thickness range was equal to 1.40±0.14 MPa√m. Average of the dimensionless fracture toughness values of andesite for various dimensionless specimen thicknesses are given in Figure 9. 3.

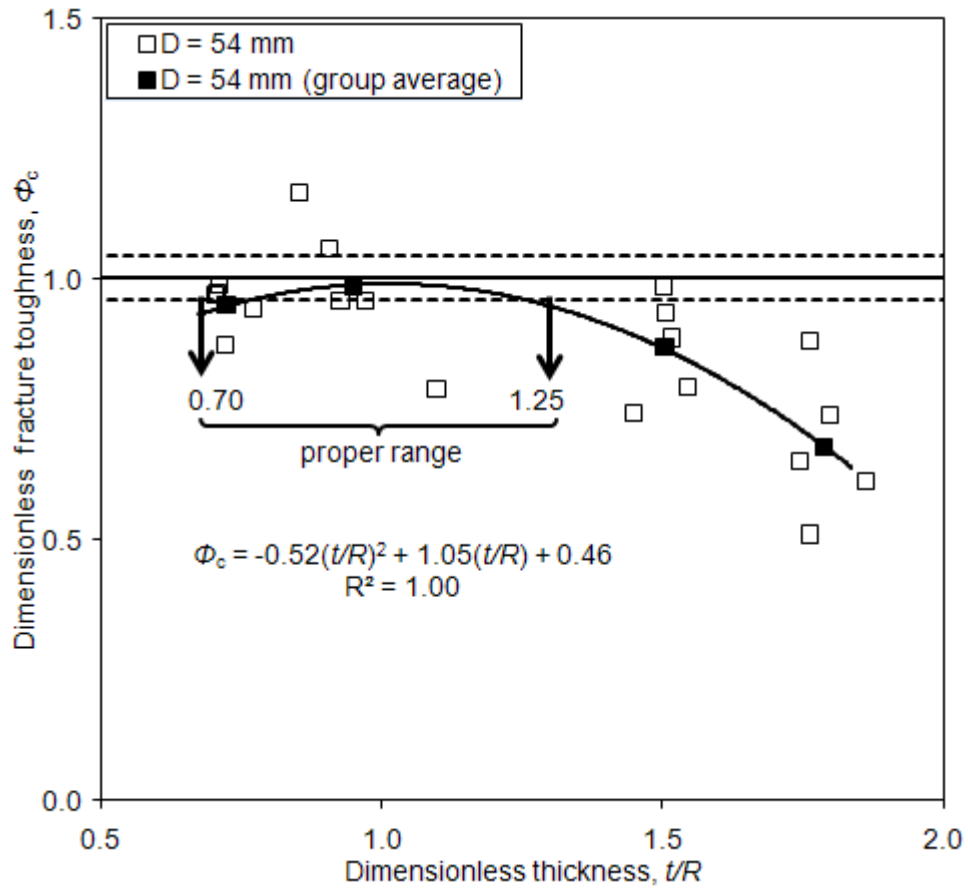
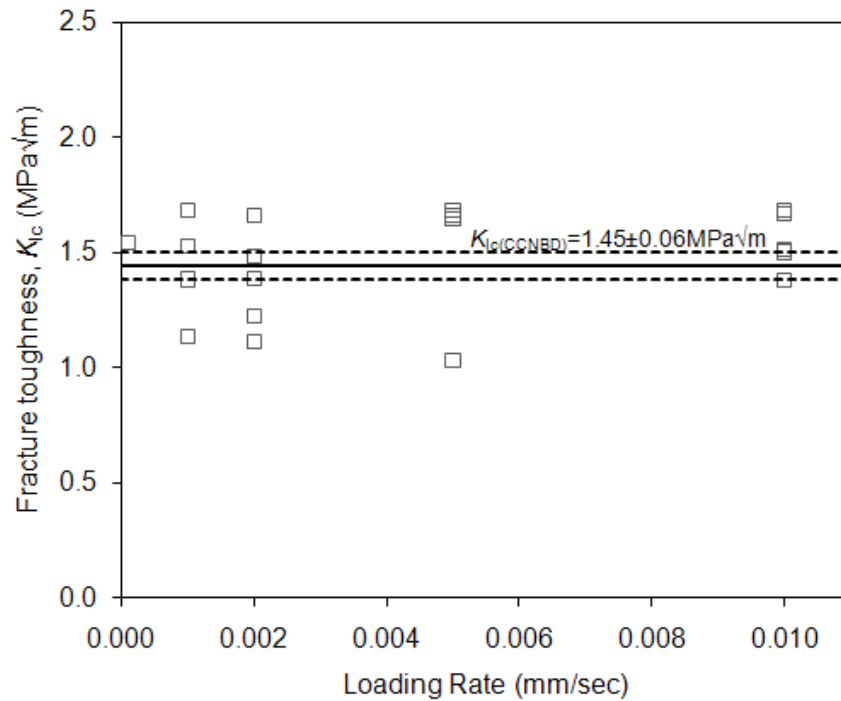


Figure 9.3 Variations of dimensionless fracture toughness value with dimensionless thickness for the FBD andesite specimen

### 9.1.3 Effect of Loading Rate on Mode I Fracture Toughness for FBD Tests

Loading rate investigation was conducted with 20 specimens. Specimens having 54 mm diameter,  $27.0 \pm 1.5$  mm thickness and  $35.5 \pm 1.0^\circ$  loading angle were used in this set of experiments. Loading rate was varied as  $0.1 \cdot 10^{-3}$  mm/sec,  $1 \cdot 10^{-3}$  mm/sec,  $2 \cdot 10^{-3}$  mm/sec,  $5 \cdot 10^{-3}$  mm/sec, and  $10 \cdot 10^{-3}$  mm/sec. This means that loading rate was varied 100 times in a static loading rate range.

Loading rate studies in the static range between  $0.1 \cdot 10^{-3}$  mm/sec and  $10 \cdot 10^{-3}$  mm/sec showed no significant effect of loading rate on fracture toughness;  $K_{Ic}$  was not affected by a loading rate increase of a hundred times (Figure 9.4). Mode I fracture toughness was determined as  $1.46 \pm 0.21$  MPa $\sqrt{m}$  in this category with 20 specimens.



**Figure 9. 4 Mode I fracture toughness versus loading rate for andesite FBD tests**

Results for andesite show that a flattened Brazilian disc specimen is proposed to have a 54 mm diameter (NX size), a thickness between 19 mm and 34 mm, and a loading angle between 32.5° and 38°, in order to produce a compatible mode I fracture toughness result with the suggested method. When all experiments on andesite rock are considered, 25 specimens fall in the geometrical ranges suggested above. Average mode I fracture toughness of andesite rock for the 25 specimens in this category was found as  $1.45 \pm 0.19 \text{ MPa}\sqrt{\text{m}}$ .

#### **9.1.4 Fracture Toughness Results for Andesite and Marble with Proposed Geometrical Parameters for FBD Tests**

To investigate if the proposed specimen geometry on andesite specimen is applicable for another rock type, marble specimens having diameters around 54 mm were prepared with four different loading angle ranges which were  $16 \pm 1^\circ$  (5 specimens),  $26 \pm 1^\circ$  (5 specimens),  $34 \pm 0^\circ$  (2 specimens), and  $37 \pm 0^\circ$  (3 specimens). Average fracture toughness values were calculated as  $1.35 \pm 0.31 \text{ MPa}\sqrt{\text{m}}$  for  $16^\circ$  group,  $1.23 \pm 0.52 \text{ MPa}\sqrt{\text{m}}$  for  $26^\circ$  group,  $1.21 \pm 0.0 \text{ MPa}\sqrt{\text{m}}$  for  $34^\circ$  group and  $1.06 \pm 0.30 \text{ MPa}\sqrt{\text{m}}$  for  $37^\circ$  group.

Dimensionless fracture toughness results of both andesite and marble rock materials having 54 mm diameter are illustrated in Figure 9. 5. In the figure, white squares and triangles illustrate the dimensionless fracture toughness  $\Phi_c$  results of andesite and marble specimens, respectively. Dark squares denote average fracture toughness values of andesite specimens whereas dark triangles symbolize average fracture toughness values of marble specimens for various loading angle ranges. Results show that as the loading angle increases, mode I fracture toughness values of andesite and marble with FBD method converge to the result of the suggested CCNBD method. Fracture toughness values of andesite and marble with the suggested CCNBD method were equal to  $1.45 \pm 0.06 \text{ MPa}\sqrt{\text{m}}$  (with five specimens) and  $1.08 \pm 0.07 \text{ MPa}\sqrt{\text{m}}$  (with four specimens), respectively. Average fracture toughness values of FBD andesite and FBD marble specimens having 54 mm diameter and  $36 \pm 2^\circ$  loading angle were equal to  $1.42 \pm 0.20 \text{ MPa}\sqrt{\text{m}}$  (with five specimens), and  $1.12 \pm 0.23 \text{ MPa}\sqrt{\text{m}}$  (with five specimens), respectively.

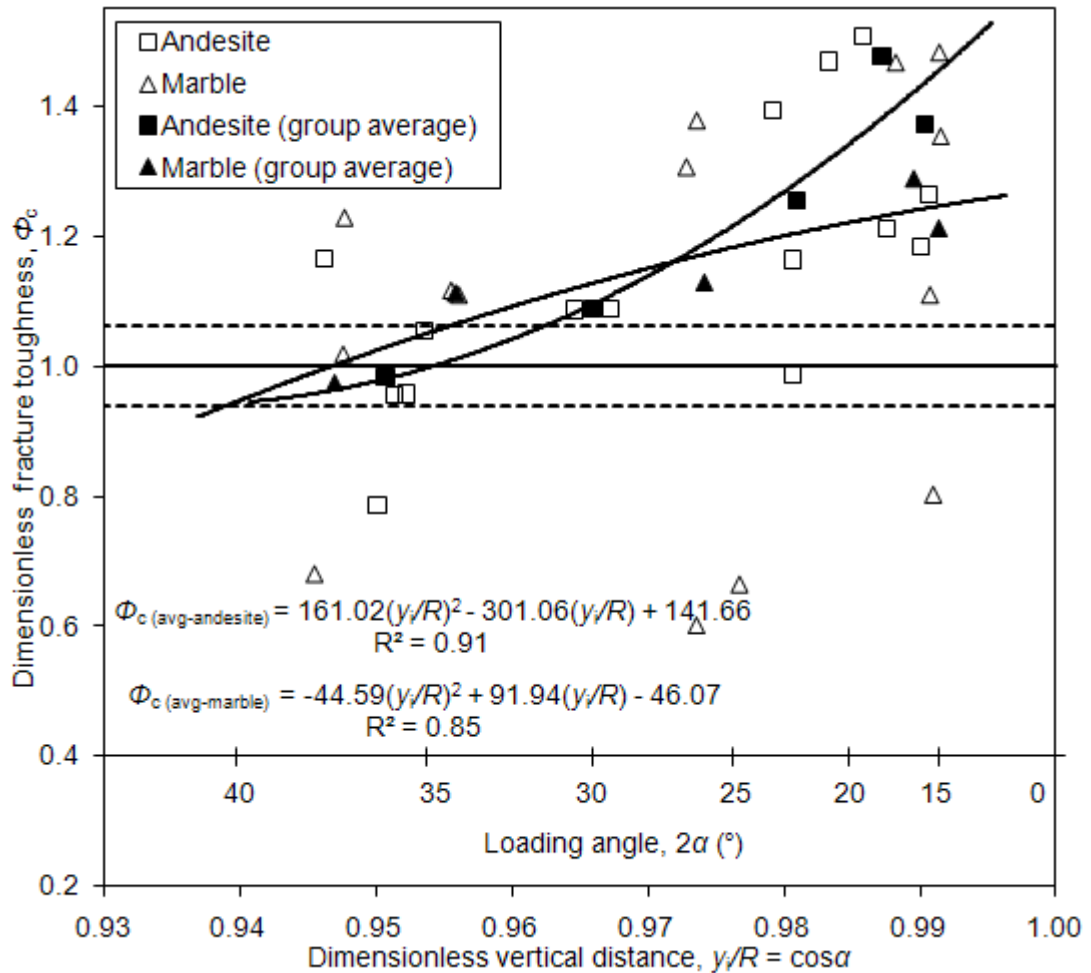


**Figure 9. 5 Variations of dimensionless fracture toughness value with loading angle in the andesite and marble FBD specimens**

It is concluded that for FBD method tests, specimens with 54 mm diameter and  $36 \pm 2^\circ$  loading angle are suggested to be used for mode I fracture toughness determination. Suggested geometrical parameters for FBD method test specimens are given in Appendix C.

## 9.2 MR Test Results

Mode I fracture toughness results of the MR testing method are presented in this section. MR testing method specimen diameters used in the tests were 54 mm, 75 mm and 100 mm. Central-hole diameters used were between 5 mm and 30 mm. Loading angle ranges were between  $2\alpha = 13^\circ - 40^\circ$  which corresponds to dimensionless vertical distance  $((y_i + r_i)/R = \cos\alpha)$  between 0.99-0.94.

### 9.2.1 Effects of Specimen Diameter, Central-Hole Diameter and Loading Angle on Mode I Fracture Toughness for MR Tests

Fracture toughness results of all tests for different specimen diameters, loading angles, and dimensionless central-hole sizes  $d/D=0.1, 0.2, 0.3$  are illustrated in Figure 9. 6. In the figure,  $K_{Ic}$  values of andesite rock determined with MR tests were normalized with the average  $K_{Ic}$  value of andesite obtained from the suggested CCNBD method tests. Dimensionless vertical distance ( $y_i+r_i/R$ ) on x-axis of the figures equals to specimen radius plus the vertical distance between the top of the hole and the loading flat.

In the figure, different specimen diameters are indicated with different colors. Black, white, and grey dots denote specimens having 100 mm, 75 mm, and 54 mm diameters, respectively. For various  $d/D$  ratios, different marker types are used. Circle type, square type, and diamond type are used to define  $d/D$  ratios of 0.1, 0.2, and 0.3, respectively.

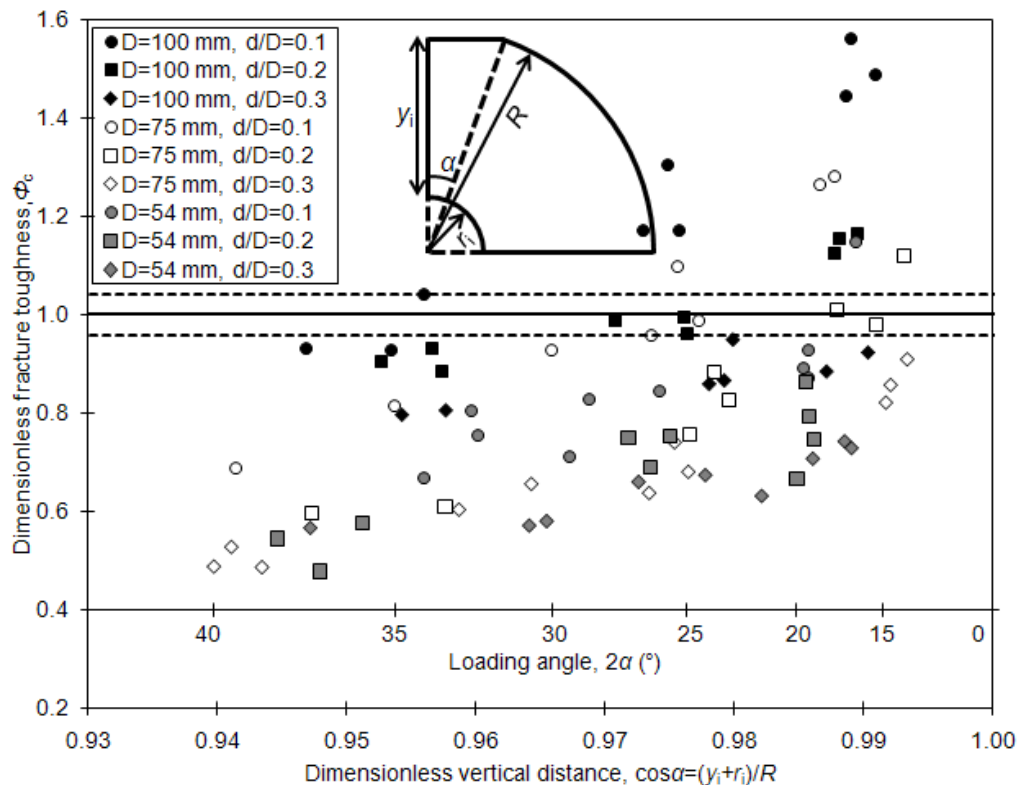
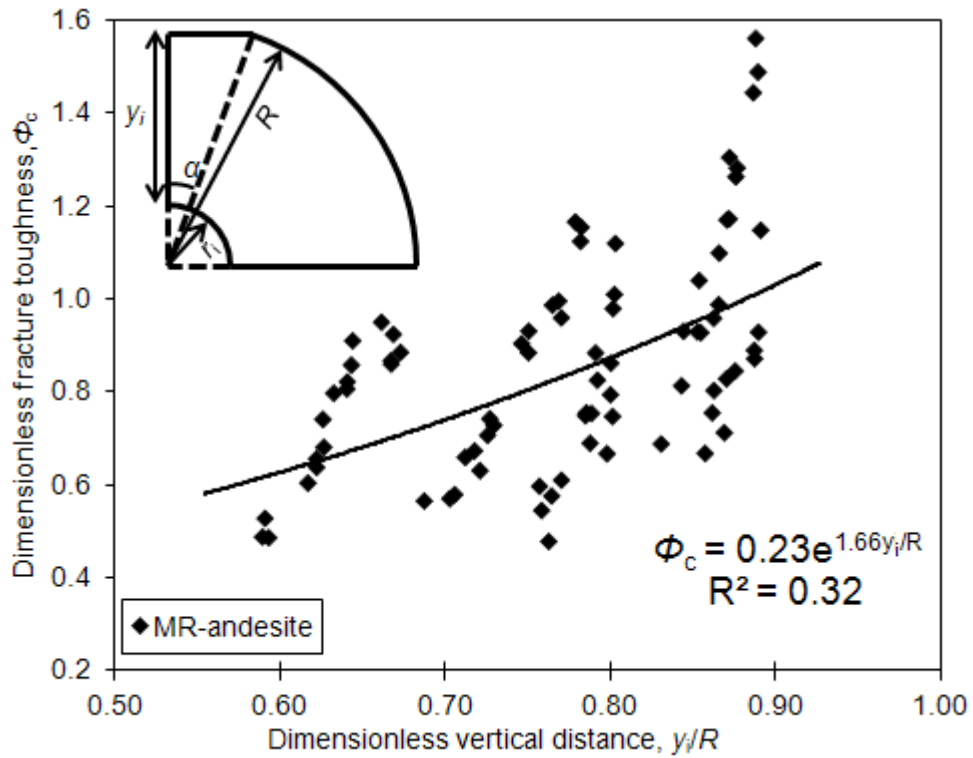


Figure 9. 6 Dimensionless fracture toughness value of andesite rock versus dimensionless vertical distance plot for various specimen diameter and central-hole diameter



In the experimental work of this section, 81 MR tests were conducted. To see the general behavior of the fracture toughness with respect to the vertical distance between the central-hole radius and flattened end of the specimen, a curve fit was applied to the fracture toughness data of all andesite MR tests (Figure 9. 7). Quality indicator  $R^2$  of the fitting processes is not very high. However, it can be concluded that as dimensionless vertical distance ( $y_i/R$ ) increases, dimensionless fracture toughness ( $\Phi_c$ ) also increases. As specimen diameter increases, dimensionless fracture toughness increases.  $R^2$  of this fit is too small to generalize this behaviour and conclusion for all specimen diameters. Therefore, instead of using all test data, exponential fits were applied separately for each specimen diameter group (Figure 9.8, 9.9 and 9.10). In general, fitted curves can be expressed by  $\Phi_c = Ae^{B\cos\alpha}$ . x-axis on these plots were again  $(y_i+r_i)/R$  or loading angle. Plots were subdivided for different central-hole groups. Then, curve fitting was applied separately for different  $d/D$  ratios of 0.1, 0.2, and 0.3.

Curves fitted in Figures 9.8, 9.9 and 9.10 illustrate the relation between dimensionless fracture toughness and the loading angle more accurately. As the loading angle increases, dimensionless fracture toughness decreases. Dimensionless mode I fracture toughness decreases with increasing central-hole diameter for all specimen diameter groups.



**Figure 9. 7 Dimensionless fracture toughness value of andesite rock versus dimensionless vertical distance plot with fitting equation**

With the exponential curve fitted for tests with specimens having 54 mm diameter with 5 mm central-hole and 15.4° loading angle fracture toughness results of andesite approach to the results of the suggested method (Figure 9. 8).

For 54 mm specimen diameter group in Figure 9. 8,  $\Phi_c$  versus  $\cos\alpha$  curves fitted were in exponential forms in terms of  $(y_i+r_i)/R$  or  $\cos\alpha$ . Results of MR mode I fracture toughness tests on 54 mm diameter discs are plotted in Figure 9. 8. Curve fitting for different central-hole diameters of  $d/D=0.1, 0.2$  and  $0.3$  results in exponential trends represented by  $\Phi_c=Ae^{B\cos\alpha}$  with power  $B\cos\alpha$  where B values range from 6.83 to 10.15.

Quality of the fits increased as illustrated by  $R^2$  rising over 0.7, for the smallest  $d/D$  ratio with  $d=5$  mm, fitted curve intersects  $\Phi_c=1$  value and deviation bands around it. Dimensionless  $\Phi_c=1$  value corresponds to the average result of the suggested CCNBD method tests. Deviation bands around this value are computed from the deviations of the results around the average of 5 CCNBD method tests. As seen

from the curve fitted for  $d/D=0.1$  in the figure intersection points of the curve with the  $\Phi_c=1$  and its deviation ranges corresponds to flat end widths of 5.4 mm-8.7 mm, loading angle ranges of  $2\alpha=11.5^\circ-18.5^\circ$  and dimensionless vertical distance  $(y_i+r_i)/R=0.995-0.987$ .

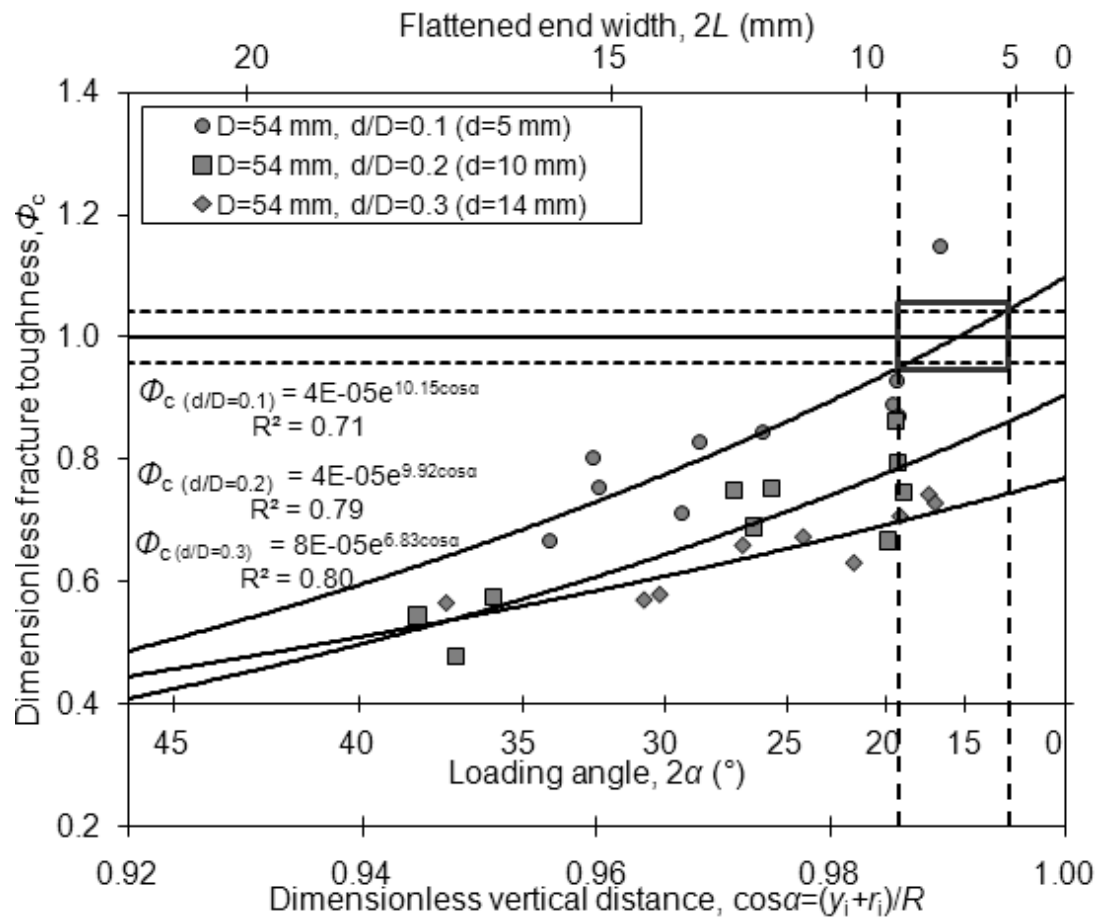


Figure 9. 8  $\Phi_c$  versus dimensionless vertical distance ( $D = 54$  mm)

For tests on discs with diameters of 75 mm, the closest mode I fracture toughness to the average results of the suggested method were obtained by specimens with 8 mm diameter and  $27.4^\circ$  loading angle and with 14 mm diameter central-hole and  $16.2^\circ$  loading angle. These points and suggested geometric range limits around the points are marked in Figure 9. 9, which is again a plot of  $\Phi_c$  versus  $(y_i+r_i)/R$ . Results of MR mode I fracture toughness tests on 75 mm diameter discs are plotted in Figure 9. 9. Curve fitting for different central-hole diameters of  $d/D=0.1, 0.2$  and  $0.3$

results in exponential trends with power  $B\cos\alpha$  where B values range from 10.43 to 13.72.

Quality of curve fitting for 75 mm diameter test results is better indicated by  $R^2$  values over 0.93. Dimensionless  $\Phi_c=1$  value corresponds to the average result of the suggested CCNBD method tests. Deviation bands around this value are computed from the deviations of the results around the average of 5 CCNBD method tests. As seen from the curve fitted for  $d/D=0.1$  in the figure intersection points of the curve with the  $\Phi_c=1$  and its deviation ranges corresponds to flat end widths of 16.7 mm-18.8 mm, loading angle ranges of  $2\alpha=25.7^\circ$ - $29.1^\circ$  and dimensionless vertical distance  $(y_i+r_i)/R=0.975$ - $0.968$ . For  $d/D=0.2$  in the figure intersection points of the curve with the  $\Phi_c=1$  and its deviation ranges corresponds to flat end widths of 8.9 mm-12.1 mm, loading angle ranges of  $2\alpha=13.6^\circ$ - $18.5^\circ$  and dimensionless vertical distance  $(y_i+r_i)/R=0.993$ - $0.987$ .

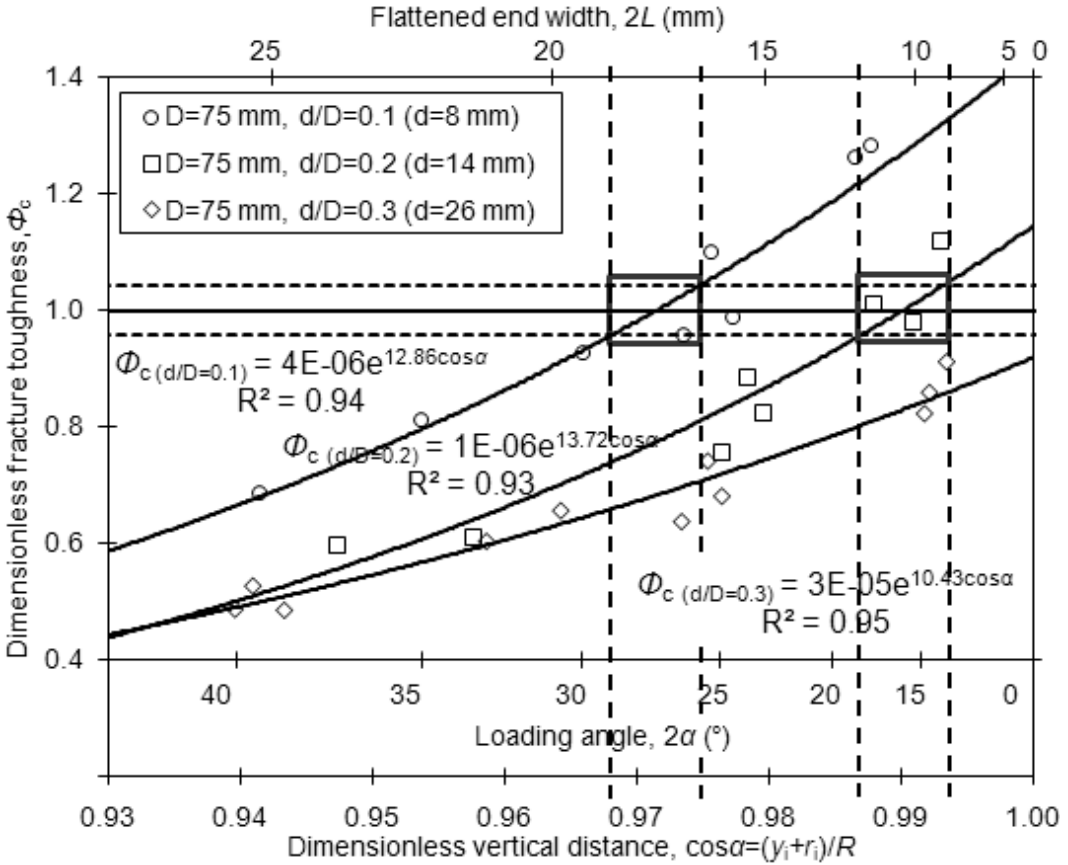


Figure 9.9  $\Phi_c$  versus dimensionless vertical distance ( $D = 75$  mm)

For tests on discs with diameters of 100 mm, the closest mode I fracture toughness to the average results of the suggested method were obtained by specimens with 10 mm diameter and 34.1° loading angle and with 21 mm diameter central-hole and 27.2° loading angle. These points and suggested geometric range limits around the points are marked in Figure 9. 10. Curve fitting for different central-hole diameters of  $d/D=0.1$ , 0.2 and 0.3 results in exponential trends with power  $B\cos\alpha$  where B values range from 4.00 to 11.56.

Quality of curve fitting for 100 mm diameter test results is better indicated by  $R^2$  values over 0.74. Dimensionless  $\Phi_c=1$  value corresponds to the average result of the suggested CCNBD method tests. Deviation bands around this value are computed from the deviations of the results around the average of 5 CCNBD method tests. As seen from the curve fitted for  $d/D=0.1$  in the figure intersection points of the curve with the  $\Phi_c=1$  and its deviation ranges corresponds to flat end widths of 28.3 mm-30.6 mm, loading angle ranges of  $2\alpha=32.9^\circ$ - $35.7^\circ$  and dimensionless vertical distance  $(y_i+r_i)/R=0.959$ - $0.952$ . For  $d/D=0.2$  in the figure intersection points of the curve with the  $\Phi_c=1$  and its deviation ranges corresponds to flat end widths of 21.3 mm-25.9 mm, loading angle ranges of  $2\alpha=24.6^\circ$ - $30.0^\circ$  and dimensionless vertical distance  $(y_i+r_i)/R=0.977$ - $0.966$ .

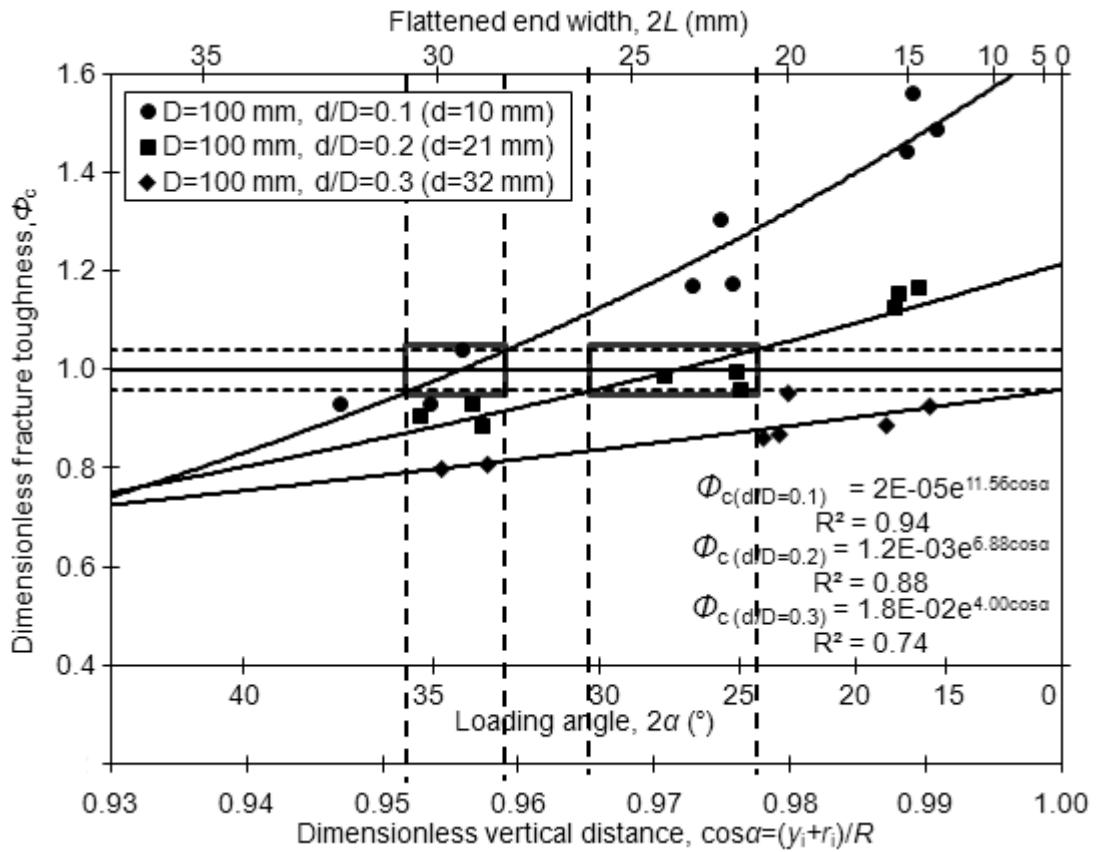


Figure 9. 10  $\Phi_c$  versus dimensionless vertical distance ( $D = 100$  mm)

Fracture toughness results for andesite were averaged and tabulated with respect to the loading angle ranges, in Table 9. 2. Specimen geometries producing fracture toughness results close to the result of the suggested CCNBD method are marked with superscript asterisk in the table. It can be concluded that 54 mm diameter specimens with 0.1, 0.2, or 0.3  $d/D$  ratios, do not yield results close to the suggested method. For 54 mm diameter, tests on specimens with a central-hole diameter of 5 mm ( $d/D=0.1$ ) and loading angle of  $19^\circ \pm 1^\circ$  resulted in a fracture toughness value close to the result of suggested method. The other close results to the suggested method were obtained by 75 mm diameter specimens with 8 mm central-hole diameter and  $25^\circ \pm 1^\circ$  loading angle, and with 14 mm central-hole diameter and  $16^\circ \pm 2^\circ$  loading angle. By 100 mm diameter specimens with 10 mm central-hole diameter and  $36^\circ \pm 2^\circ$  loading angle, and with 21 mm central-hole diameter and  $26^\circ \pm 2^\circ$  loading angle.

**Table 9. 2  $K_{Icavg}$  of andesite rock according to  $2\alpha$ 's for various specimen dimensions**

$D$ (mm)	$d$ (mm)	$2\alpha_{Avg}\pm stdev$ ( $^{\circ}$ )	No of specimens	$K_{Icavg}\pm stdev$ ( $MPa\sqrt{m}$ )	$\Phi_{cavg}\pm stdev$
54	5	19±1	4	1.39±0.19	0.96±0.13*
		28±2	3	1.15±0.10	0.80±0.07
		33±1	3	1.07±0.10	0.74±0.07
	10	19±0	4	1.11±0.12	0.77±0.08
		26±1	3	1.06±0.05	0.73±0.04
		37±1	3	0.77±0.07	0.53±0.05
	14	18±1	3	1.05±0.03	0.73±0.02
		24±3	3	0.95±0.03	0.65±0.02
		33±4	3	0.83±0.01	0.57±0.01
75	8	18±1	2	1.84±0.02	1.27±0.01
		25±1	3	1.47±0.11	1.02±0.07*
		35±5	3	1.17±0.17	0.81±0.12
	14	16±2	3	1.50±0.11	1.04±0.07*
		24±1	3	1.19±0.09	0.82±0.06
		35±3	2	0.87±0.01	0.60±0.01
	26	14±1	3	1.25±0.06	0.86±0.04
		26±1	2	0.99±0.07	0.69±0.05
		32±1	2	0.91±0.05	0.63±0.04
39±1		3	0.72±0.03	0.50±0.02	
100	10	17±1	3	2.17±0.09	1.50±0.06
		26±1	3	1.76±0.11	1.22±0.08
		36±2	3	1.40±0.09	0.97±0.06*
	21	17±1	3	1.66±0.03	1.15±0.02
		26±2	3	1.42±0.03	0.98±0.02*
		34±1	3	1.31±0.03	0.91±0.02
	32	17±2	2	1.31±0.04	0.90±0.03
		23±1	3	1.29±0.07	0.89±0.05
		34±1	2	1.16±0.01	0.80±0.01
* Dimensionless fracture toughness values converged to 1±0.04					

Preparing specimens in large diameters is difficult and needs large rock blocks. 54 mm specimen diameter is suggested only with a central-hole diameter equal to 5 mm and specimens with 19±1° loading angle. 75 mm in the middle size group can be the most proper specimen geometry producing more results close to the result of the suggested method with relatively good fits. For 75 mm diameter, two central-

hole diameter and loading angle groups have results close to the result of the suggested method.

### **9.2.2 Fracture Toughness Results for Andesite and Marble with Proposed Geometrical Parameters for MR Tests**

Marble specimens having 75 mm diameters in the proposed geometric ranges were tested in order to check the proposed specimen dimensions for the other rock types. Afyon marble was used in the experiments.

To normalize the fracture toughness value of the marble as the andesite, mode I fracture toughness value was determined with the suggested CCNBD method. Average fracture toughness value of marble was found as  $1.08 \pm 0.07$  MPa $\sqrt{m}$  with four specimens having 125 mm diameter. With MR method tests, average fracture toughness value of three marble specimens having 75 mm diameter, 8 mm central-hole diameter and 25° loading angle was equal to  $1.07 \pm 0.10$  MPa $\sqrt{m}$ . Average fracture toughness value of three specimens having 75 mm diameter, 14 mm central-hole diameter and  $15 \pm 1^\circ$  loading angle was  $1.05 \pm 0.10$  MPa $\sqrt{m}$ . Fracture toughness values of tests on specimen with 75 mm diameter for andesite and marble were normalized and plotted in Figure 9. 11 with respect to the dimensionless vertical distance. Dark marks in the figure denote dimensionless fracture toughness values of andesite while white marks show dimensionless fracture toughness values of marble. Results showed that the proposed specimen dimensions, which are 75 mm specimen diameter with 8 mm central-hole diameter and 25° loading angle, and 75 mm specimen diameter with 14 mm central-hole and 15° loading angle are proper specimen geometries for mode I fracture toughness testing on disc type rock specimens. Proper specimen geometries for MR test method are given in Appendix C.



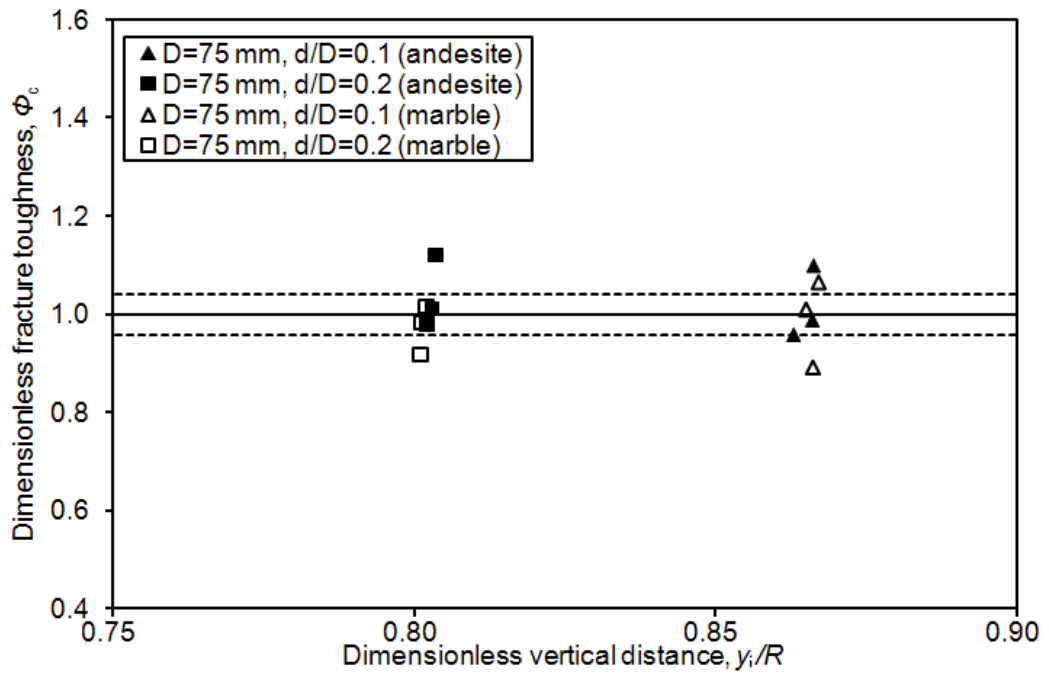


**Figure 9. 11 Dimensionless fracture toughness value of andesite and marble rock types versus dimensionless vertical distance plot for proper specimen geometries in 75 mm diameter group**

## CHAPTER 10

### CONCLUSIONS AND RECOMMENDATIONS

Numerical modeling was conducted for finding mode I stress intensity factor of FBD with different diameters and loading angles. For FBD method, by curve fitting to the numerical modeling results for the estimation of dimensionless maximum stress intensity factor, an expression ( $\Phi_{\max}=1/(43.32-15.63\exp(\cos\alpha))$ ) was developed in terms of half loading angle. Dimensionless maximum stress intensity factor values of FBD specimens increased sharply for loading angle values lower than  $30^\circ$ .

Three diameter groups were 54 mm, 75 mm, and 100 mm in the experimental work of the FBD method. Average fracture toughness results for 75 and 100 mm diameter groups were outside of the deviation band around the results obtained from the suggested CCNBD method.

For FBD method tests, changing the thickness had an effect on fracture toughness. For large thickness values with  $t/R$  ratio greater than 1.25, fracture toughness decreased. This decrease was more than 30% for  $t/R$  greater than 1.75.

Analyses showed that for andesite rock, a FBD specimen should have a 54 mm diameter (NX size), a thickness between 19 mm and 34 mm ( $t/R=0.70$  and  $t/R=1.25$ ), and a loading angle value  $35^\circ\pm 2^\circ$  in order to produce a compatible fracture toughness result with the suggested method.

In static range, changing the loading rate a hundred times between  $0.1*10^{-3}$  mm/sec and  $10*10^{-3}$  mm/sec had no effect on fracture toughness determination with the FBD method.

The FBD method tests were conducted on marble specimens to check the applicability of the proposed specimen geometry to a different rock type. As the

loading angle increased, fracture toughness values of both andesite and marble converged to the results of the suggested method. Compressive strength of Ankara andesite and Afyon marble were determined as 82.84 MPa and 52.32 MPa, respectively. Fracture toughness values of andesite and marble with the suggested CCNBD method were equal to  $1.45 \pm 0.06$  MPa $\sqrt{m}$  (with five specimens) and  $1.08 \pm 0.07$  MPa $\sqrt{m}$  (with four specimens), respectively. Average fracture toughness values of 54 mm diameter FBD andesite and FBD marble specimens in  $32.5^\circ$  and  $38.0^\circ$  loading angle range were equal to  $1.45 \pm 0.19$  MPa $\sqrt{m}$  (with twenty five specimens), and  $1.12 \pm 0.23$  MPa $\sqrt{m}$  (with five specimens), respectively.

Numerical modeling was conducted for finding mode I stress intensity factor of MR specimens with different diameters, central-hole diameters and loading angles. For MR method, by surface fitting to the numerical modeling result for the estimation of dimensionless maximum stress intensity factor, an expression  $\ln \phi_{\max} = -3.470 + 4.498(d/D)^{2.5} + 3.866(\cos \alpha)^3$  was developed in terms of dimensionless central-hole diameter and half loading angle.

Experimental work showed that for andesite rock, 54 mm diameter MR specimens ranging between 5 mm and 15 mm central-hole diameters did not produce reasonable fracture toughness values with loading angles were between  $25^\circ$  and  $35^\circ$ . Tests on specimens with 54 mm to 100 mm diameters with  $15^\circ$  to  $35^\circ$  loading angles, and with central hole diameters of 14 mm (for  $D=54$  mm,  $d/D=0.3$ ), 26 mm (for  $D=75$  mm,  $d/D=0.3$ ), and 32 mm (for  $D=100$  mm,  $d/D=0.3$ ) did not produce fracture toughness values close to the results by the suggested CCNBD method.

Fracture toughness values of MR andesite specimens with 75 mm diameter, with central-hole diameter of 8 mm ( $d/D=0.1$ ), and with  $25^\circ$  loading angle were close to the results of the suggested method. Similarly, mode I fracture toughness results with 75 mm specimen diameter, with central-hole diameter of 14 mm ( $d/D=0.2$ ), and with  $16^\circ$  loading angle were close to the results of the suggested method. Similarly, fracture toughness results of MR andesite specimens having 100 mm diameter with  $d/D=0.1$  dimensionless central-hole diameter and  $35^\circ$  loading angle,

and  $d/D=0.2$  dimensionless central-hole diameter and  $25^\circ$  loading angle produced compatible fracture toughness results with the suggested method.

Smaller diameters can be preferred to simplify specimen preparation, however, tests on 54 mm diameter MR specimens produced higher deviations for  $K_{Ic}$  than the other sizes.

For andesite rock, MR specimens having 75 mm diameter with 8 mm central-hole diameter and  $25^\circ$  loading angle, and 14 mm central-hole diameter and  $16^\circ$  loading angle were proper specimen dimensions for fracture toughness testing compared to the suggested method. Average fracture toughness value of three andesite specimens having 75 mm diameter, 8 mm central-hole diameter and  $25^\circ$  loading was equal to  $1.47 \pm 0.11$  MPa $\sqrt{m}$  compared to  $1.45 \pm 0.06$  MPa $\sqrt{m}$  by CCNBD method. Average fracture toughness value of three andesite specimens having 75 mm diameter, 14 mm central-hole diameter and  $16^\circ$  loading angle was determined as  $1.50 \pm 0.11$  MPa $\sqrt{m}$ . These toughness values were close to the fracture toughness values determined with the suggested CCNBD method, which was equal to  $1.45 \pm 0.06$  MPa $\sqrt{m}$ .

MR tests were conducted on marble specimens to check the applicability of the proposed specimen geometry to different rock types. Average fracture toughness value of three marble specimens having 75 mm diameter, 8 mm central-hole diameter and  $25^\circ$  loading angle was equal to  $1.07 \pm 0.10$  MPa $\sqrt{m}$ . Average fracture toughness value of three specimens having 75 mm diameter, 14 mm central-hole diameter and  $15^\circ$  loading angle was determined as  $1.05 \pm 0.10$  MPa $\sqrt{m}$ . These fracture toughness values determined for marble were again close to the fracture toughness values determined with the suggested CCNBD method, which was equal to  $1.08 \pm 0.07$  MPa $\sqrt{m}$ .

With the FBD method, specimen preparation and testing is much simpler than the other methods. Although specimen preparation MR test is a little more difficult and more time consuming than FBD method, it could be preferred since it produces less deviations in the results for  $K_{Ic}$  than FBD method.

Results showed that if central-holes were drilled in smaller diameters, greater loading angles should be preferred, and vice versa for  $K_{Ic}$  testing.

In order to generalize the conclusions for both testing methods here related to the effects of specimen diameter, central-hole diameter (for MR test) and loading angle on fracture toughness, it is recommended to conduct this study on other rock types, especially on sedimentary rock types.

## REFERENCES

ABAQUS Analysis User's Manual, Version 6.5 Documentation.

ABAQUS/CAE User's Manual, Version 6.5 Documentation.

ABAQUS, Inc., "Modeling Fracture and Failure with ABAQUS", 2006.

ABAQUS Technology Brief, "Fracture Mechanics Study of a Compact Tension Specimen Using ABAQUS/CAE", 2004.

Alkılıçgil, Ç., "Development of a New Method for Mode I Fracture Toughness Test on Disc Type Rock Specimens", M.S. Thesis, METU, Ankara, 145 p., 2006.

Almeida, L.C.R., Vargas Jr, E.do A. and Figueiredo, R.P. de, "Mechanical characterization of rock splitting planes in granitic rocks", Int. J. of Rock Mech. Min. Sci., Technical Note, Vol. 42, Issue 7, pp. 1139-1145, 2006.

Altındağ, R., "The Relationships between Fracture Toughness and other Mechanical Properties of Rocks", Journal of Science and Engineering, Dokuz Eylul University Faculty of Engineering, Turkish, Vol. 2, No. 2, pp. 39-47, 2000.

Atkinson, C., Smelser, R.E. and Sanchez, J., "Combined Mode Fracture via Cracked Brazilian Disk Test", Int. J. Fracture, Vol. 18, No. 4, pp. 279-291, 1982.

Awaji, H. and Sato, S., "Combined Mode Fracture Toughness Measurements by the Disk Test", J. Eng. Mater. Tech. Trans. ASME, Vol. 100, No. 4, pp. 175-182, 1978.

Backers, T., "Äspö Hard Rock Laboratory: Determination of Mode I and Mode II fracture toughness and fracture normal stiffness of Äspödiorite", Laboratory Test Report, pp. 151-161, 2003.

Backers, T., "Fracture Toughness Determination and Micromechanics of Rock Under Mode I and Mode II Loading", Ph.D. Thesis, University of Potsdam, Germany, 138 p., 2004.

Barker, L.M., " $K_{IC}$  Measurements using short rod specimens - the elastic plastic case", Terra Tek Report, Salt Lake City, UT, pp. 77-91R, 1977.

Bearman, R.A., "The use of the point load test for the rapid estimation of Mode I fracture toughness", Int. J. Rock Mech. Min. Sci., Technical Note, Vol. 36, pp. 257-263, 1999.

Bieniawski, Z.T., “Mechanism of Brittle Rock Fracture: Part 1- Theory of the Fracture Process”, International Journal of Rock Mechanics and Mining Sciences & Geomechanical Abstracts, Vol. 4, No: 4, pp. 395-406, 1967.

Bieniawski, Z.T. and Hoek, E., “Brittle Fracture Propagation in Rock Under Compression”, Int. J. of F.M., 1, 1965.

Boss International, [www.bossintl.com](http://www.bossintl.com), last visited on 15<sup>th</sup> August 2009.

Brown, G.J. and Reddish, D.J., “Experimental Relations Between Rock Fracture Toughness and Density”, Int. J. Rock Mech. Min. Sci., Technical Note, Vol. 34, No. 1, pp. 153-155, 1997.

Ceriolo, L. and Tommaso, A.D., “Fracture Mechanics of Brittle Materials: A Historical Point of View”, 2nd Int. PhD Symposium in Civil Engineering, Budapest, 1998.

Chang, C.I., “Brittle fracture and failure criteria of particulate composites”, AIAA/ASME/SAE 15th Structures, Structural Dynamics and Materials Conference; 1974 17-19 April; Las Vegas, Nevada: AIAA; 1974.

Chang, S. H., Chung-In Lee, Jeon, S., “Measurement of rock fracture toughness under modes I and II and mixed-mode conditions by using disc-type specimens”, Engineering Geology, Vol. 66, pp. 79–97, 2002.

Chong, K.P. and Kuruppu, M.D., “New specimen for fracture toughness determination of rock and other materials”, Int. J. Fracture Vol. 26, pp. R59-R62, 1984.

Chong, K.P, Kuruppu, M.D. and Kuszmaul, J.S., “Fracture toughness determination of layered materials”, Engng. Fract. Mech., Vol. 28, pp. 55-65, 1987.

Clausing, D.P., “Comparison of Griffith's Theory with Mohr's Failure Criteria”, The 3rd U.S. Symposium on Rock Mechanics (USRMS); Golden, CO: USRMS, pp. 20-22, 1959.

DiJon Inc., [www.dijoninc.com](http://www.dijoninc.com), last visited on 15<sup>th</sup> August 2009.

Donovan, J.G. and Karfakis, M.G., “Adaptation of a Simple Wedge Test for the Rapid Determination of Mode I Fracture Toughness and the Assessment of Relative Fracture Resistance”, Int. J. Rock Mech. Min. Sci., Technical Note, Vol. 41, pp. 695-701, 2004.

Dwivedi, R.D., Soni, A.K., Goel, R.K. and Dube A.K., “Fracture Toughness of Rocks Under Sub-Zero Temperature Conditions”, Int. J. Rock Mech. Min. Sci., Technical Note, Vol. 37, pp. 1267-1275, 2000.

Fowell, R.J., “ISRM Commission on Testing Methods: Suggested Method for Determining Mode I Fracture Toughness Using Cracked Chevron Notched

Brazilian Disc (CCNBD) Specimens”, *Int. J. Rock Mech. Min. Sci. and Geomech. Abstr.*, Vol. 32, No. 1, pp. 57-64, 1995.

Fowell, R.J. and Xu, C., “The cracked Chevron Notched Brazilian Disk Test-Geometrical Considerations for Practical Rock Fracture Toughness Measurement”, *Preprint Proc. 34<sup>th</sup> U.S. Rock Mech. Symp.*, pp. 657-660, 1993.

Fowell, R.J., Xu, C. and Dowd, P.A., “An Update on the Fracture Toughness Testing Methods Related to the Cracked Chevron-Notched Brazilian Disk (CCNBD) Specimen”, *Pure and Applied Geophysics*, Vol. 163, pp. 1047-1057, 2006.

Funatsu, T., Seto, M., Shimada, H., Matsui, K. and Kuruppu, M., “Combined Effects of Increasing Temperature and Confining Pressure on the Fracture Toughness of Clay Bearing Rocks”, *Int. J. Rock Mech. Min. Sci.*, Vol. 41, pp. 927-938, 2004.

Griffith, A.A., “The Phenomena of Rupture and Flow of Solids”, *Phil. Trans. Roy. Soc.*, London, 1920.

Griffith, A.A., “The phenomenon of rupture and flow in solids”, *Phil. Trans. R. Soc.*, Vol. 221, pp. 163-198, 1921.

Gunsallus, K.L. and Kulhawy, F.H., “A Comparative Evaluation of Rock Strength Measures”, *Int. J. Rock Mech. Min. Sci. and Geomech. Abstr.*, Technical Note, Vol. 21, No. 5, pp. 233-248, 1984.

Guo, H., Aziz, N.I. and Schmidt, L.C., “Rock Fracture-Toughness Determination by the Brazilian Test”, *Engineering Geology*, Vol. 33, pp. 177-188, 1993.

Haberfield, C.M. and Johnston, I.W., “Determination of the Fracture Toughness of a Saturated Soft Rock”, *Canadian Geotechnical Journal*, Vol. 27, No. 6, pp. 276-284, 1990.

Hood, M.C. and Roxborough, F.F., “Rock Breakage: Mechanical”, *SME Mining Engineering Handbook*, Second Edition, SME, H.L. Hartman (senior editor), Vol. 1, pp. 680-721, 1992.

Iqbal, M.J. and Mohanty, B., “Experimental Calibration of Stress Intensity Factors of the ISRM Suggested Cracked Chevron-Notched Brazilian Disc Specimen Used for Determination of Mode-I Fracture Toughness”, *Int. J. Rock Mech. Min. Sci.*, Technical Note, Vol. 43, pp. 1270–1276, 2006.

Irwin, G.R., “Analysis of Stress and Strains Near the End of a Crack Traversing a Plate”, *J. of Applied Mechanics*, A.S.M.E., New York, 1957.

ISRM, “Suggested Methods for Determining Tensile Strength of Rock Materials”, *Int. J. Rock Mech. Min. Sci. & Geomech. Abstr.*, Vol. 15, pp. 99-103, 1978.



ISRM, “Suggested Methods for Determining the Uniaxial Compressive Strength and Deformability of Rock Materials”, Int. J. Rock Mech. Min. Sci. & Geomech. Abstr., Vol. 16, pp. 135-140, 1979.

ISRM, (2007). Suggested Methods for Determining the Fracture Toughness of Rock. Ulusay, R., Hudson, J.A. (Ed.). *The Complete ISRM Suggested Methods for Rock Characterization, Testing and Monitoring: 1974-2006*. (231-258). Ankara, Turkey: Kozan Ofset.

Kaklis, K.N., Agioutantis, Z., Sarris, E. and Pateli, A., “A Theoretical and Numerical Study of Discs with Flat Edges under Diametral Compression (Flat Brazilian Test)”, 5<sup>th</sup> GRACM International Congress on Computational Mechanics, Limassol, 2005.

Kaplan, M.F., “Crack Propagation and the Fracture of Concrete”, J. ACI, No: 60, 1961.

Key to Metals Database, <http://steel.keytometals.com>, last visited on 24th March 2010.

Khan, K. and Al-Shayea, N. A., “Effect of Specimen Geometry and Testing Method on Mixed Mode I-II Fracture Toughness of a Limestone Rock from Saudi Arabia”, Rock Mech. Rock Engng., Vol. 33, pp. 179-206, 2000.

Krishnan, G.R., Zhao, X.L., Zaman, M. and Roegiers, J.C., “Fracture Toughness of a Soft Sandstone”, Int. J. of Rock Mech. Min. Sci., Vol. 35, pp. 695-710, 1998.

Kuruppu, M.D., “Fracture Toughness Measurement of Rocks Using Chevron-Notched Semi Circular Specimen”, Mine Planning and Equipment Selection, Ostrava, pp. 355-360, 2002.

Kuruppu, M.D., “Fracture Toughness Measurement Using Chevron Notched Semi-Circular Bend Specimen”, Int. J. Fract., Vol. 86, pp. L33-L38, 1997.

Lemiszki, P.J. and Landes, J.D., “Fracture Toughness Testing of Core from the Cambro-Ordovician Section on Oak Ridge Reservation”, Proc. of the 2<sup>nd</sup> North American Rock Mech. Symp., Montréal, Québec, Canada, pp. 1627-1634, 1996.

Lim, I.L., Johnston, I.W., Choi, S.K. and Boland, J.N., “Fracture Testing of a Soft Rock with Semi-circular Specimens Under Three-point Bending. Part I-Mode I”, Int. J. Rock Mech. Min. Sci. & Geomech. Abstr., Vol. 31, No. 3, pp. 185-197, 1994.

MATLAB User Guides, Version 7.5.0 Documentation, 2007.

Matsuki, K., Nozuyama, Y. and Takahashi, H., “Size effect in the fracture toughness testing of rocks using a boring core”, Proc. Spring Meeting Min. Metall. Inst, Japan, pp. 193-194, 1987.

Mc Clintock, F.A. and Walsh, P.F., "Friction on Griffith Cracks in Rocks Under Pressure", Proc. 4th National Congress Appl. Mech., Berkeley, 1962.

Meredith, P.G.A., "Fracture mechanics study of experimentally deformed crustal rocks", Unpublished Ph. D. Thesis, University of London, 1983.

Nasseri, M.H.B. and Mohanty, B., "Fracture toughness anisotropy in granitic rocks", Int. J. of Rock Mech. Min. Sci., Vol. 45, pp. 167-193, 2008.

Nasseri, M.H.B., Schubnel, A. and Young, R.P., "Coupled Evolutions of Fracture Toughness and Elastic Wave Velocities at High Crack Density in Thermally Treated Westerly Granite", Int. J. of Rock Mech. Min. Sci., Vol. 44, pp. 601-616, 2007.

Ouchterlony, F., "A presentation of the ISRM Suggested Methods for determining fracture toughness of rock material", Proc. 6th Int. Congr. Rock Mechanics, Balkema, Rotterdam, Vol. 2, pp. 1181-1186, 1987.

Ouchterlony, F., "Extension of the compliance and stress intensity formulas for the single edge crack round bar in bending", ASTM STP, Vol. 745, pp. 237-256, 1981

Ouchterlony, F., "ISRM Commission on Testing methods; Suggested Methods for determining fracture toughness of rock", Int. J. Rock Mech. Min. Sci. & Geomech. Abstr., Vol. 25, pp. 71-96, 1988.

Pathan, A.C., "A Study of Fracture Toughness in Relation to Mine Design", PhD Thesis, Dep. of Mining Eng., University of Nottingham, England, 1987.

Pehovaz-Alvarez H.I., "Non-conventional tests for determining the fracture toughness in rocks: analysis and comparison", PhD Thesis, School of Eng., University of São Paulo, 2004.

Proveti, J.R.C. and Michot, G., "The Brazilian Test: A Tool for Measuring the Toughness of a Material and Its Brittle to Ductile Transition", Int. J. Fract., Vol. 139, pp. 455-460, 2006.

Rice, J.R., "A path independent integral and the approximate analysis of strain concentration by notches and cracks", J. App. Mech., Vol. 35, pp. 379-386, 1968.

Saouma, V.E. and Kleinosky, M.J., "Finite Element Simulation of Rock Cutting: A fracture Mechanics Approach", Proceedings of the 25<sup>th</sup> U.S. Symposium on Rock Mechanics, Northwestern University, Evanston IL, pp. 792-799, 1984.

Shetty, D.K., Rosenfield, A.R. and Duckworth, W.H., "Fracture Toughness of Ceramics Measured by a Chevron-Notched Diametral-Compression Test", J. Am. Ceram. Soc., Vol. 68, pp. c325-c443, 1985.

Shlyapobersky, J. and Chudnovsky, A., "Fracture Mechanics in Hydraulic Fracturing", Rock Mechanics, Tillerson and Wawersik (eds), Balkema, Rotterdam, pp. 827-836, 1992.

Singh, R.N. and Pathan, A.G., "Fracture Toughness of Some British Rocks by Diametral Loading of Discs", Mining Science and Technology, Vol. 6, pp. 179-190, 1988.

Singh R.N. and Sun G.X., "A Numerical and Experimental Investigation for Determining Fracture Toughness of Welsh Limestone", Min. Sci. Tech., Vol. 10, pp. 61-70, 1990 (a).

Singh R.N. and Sun G.X., "An investigation into factors affecting fracture toughness of coal measures sandstone", J. Mines, Metals & Fuels, pp. 111-118, 1990 (b).

Sousa, J.L.A.O. and Bittencourt, T.N., "Experimental Analysis of Fracture Processes in Concrete", Journal of the Brazilian Society of Mechanical Sciences, Vol. 23, No. 4, 2001.

Stead, D., Coggan, J.S., Eberhardt, E., "Realistic Simulation of Rock Slope Failure Mechanisms: The Need to Incorporate Principles of Fracture Mechanics", Int. J. of Rock Mech. Min. Sci., Vol. 41, No. 3, pp. 1-6, 2004.

Sun, Z. and Ouchterlony, F., "Fracture toughness of Stripa granite cores", Int. J. Rock Mech. Min. Sci. & Geomech. Abstr., Vol. 23, pp. 399-409, 1986.

Szendi-Horvath, G., "Fracture Toughness Determination of Brittle Materials Using Small to Extremely Small Specimens", Eng. Fract. Mech., Vol. 13, pp. 955-961, 1980 (a).

Szendi-Horvath, G., "Fracture Toughness of Black Coal", Technical Report 80/2-DA, Commonwealth Scientific and Industrial Research Organization, Australia, 1980 (b).

Szendi-Horvath, G., "On Fracture Toughness of Coal", Australian J. Coal Mining Technol. Res., Vol. 2, pp. 51-57, 1982.

Thiercelin, M. and Roegiers, J.C., "Fracture Toughness Determination with the Modified Ring Test", International Symposium on Engineering in Complex Rock Formations, Beijing, China, pp. 1-8, 1986.

Thiercelin, M., "Fracture Toughness under Confining Pressure Using the Modified Ring Test", In Rock Mechanics: 28<sup>th</sup> US Symposium on Rock Mechanics, Balkema, Rotterdam, pp. 149-156, 1987.

Wang, C.H., "Introduction to Fracture Mechanics", DSTO Aeronautical and Maritime Research Laboratory, Australia, 1996.

Wang, Q.Z., Jia, X.M., Kou, S.Q., Zhang, Z.X. and Lindqvist, P.A., “The Flattened Brazilian Disc Specimen Used for Testing Elastic Modulus, Tensile Strength and Fracture Toughness of Brittle Rocks: Analytical and Numerical Results”, Int. J. of Rock Mech. Min. Sci., Vol. 41, pp. 245-253, 2004.

Wang, Q.Z. and Wu, L.Z., “The Flattened Brazilian Disc Specimen Used For Determining Elastic Modulus, Tensile Strength and Fracture Toughness of Brittle Rocks: Experimental Results”, Int. J. Rock Mech. Min. Sci., Vol. 41, No. 3, pp. 1-5, 2004.

Wang, Q.Z. and Xing, L., “Determination of Fracture Toughness  $K_{IC}$  by Using the Flattened Brazilian Disk Specimen for Rocks”, Eng. Fract. Mech., Vol. 64, pp. 193-201, 1999.

Watson, T.L., Granites of the Southeastern Atlantic States, U.S. Geological Survey Bulletin 426, 1910.

Whittaker, B.N., Singh, R.N. and Sun, G., “Rock Fracture Mechanics-Principles, Design and Applications”, Elsevier, Amsterdam, 1992.

Wills, B.A. and Napier-Munn, J.A., “Wills’ Mineral Processing Technology”, Seventh Edition: An Introduction to the Practical Aspects of Ore Treatment and Mineral Recovery, pp. 108-117, 2006.

Zipf, R, Karl, Jr. and Bieniawski, Z.T., “Mixed Mode Testing for Fracture Toughness of Coal Based on Critical - Energy Density”, Rock Mechanics: Key to Energy Production 27<sup>th</sup> U.S. Symposium on Rock Mechanics, 6 p. 1986.

## APPENDIX A

### CALCULATION OF MAXIMUM STRESS INTENSITY FACTOR

In order to compute maximum stress intensity factor of a specimen model, crack length was increased step by step from zero to larger values. By drawing a 6th order polynomial trend line through stress intensity factor values according to crack length, a 6th order equation was determined. To show these computations, a specimen having 75 mm diameter with 20° loading angle ( $2\alpha$ ) was modeled. Elastic modulus, Poisson's ratio and friction coefficient were taken as 10 GPa, 0.15 and 0.4, respectively. Crack length was changed from 0 to 33 mm (0, 5 mm, 10 mm, 15 mm, 20 mm, 25 mm, 30 mm and 33 mm). For each crack length Mode I stress intensity factor values were determined by using ABAQUS program. The computed values are listed in **Error! Reference source not found.**.

**Table A. 1 Stress intensity factor values according to crack lengths**

x [a (mm)]							
0	5	10	15	20	25	30	33
y [ $K_I$ (Pa $\sqrt{m}$ )]							
0.00000	1.01576	1.53165	2.05775	2.63402	3.18104	3.16939	2.16067

By using MATLAB, a code was written to determine maximum stress intensity factor. To find the maximum stress intensity factor, firstly, the crack length given the maximum stress intensity factor was evaluated. For this specimen model, by using the data in **Error! Reference source not found.**, a 6<sup>th</sup> order polynomial equation as determined. The 1<sup>st</sup> order derivative of this equation was achieved. The real root of this derivative gave the crack length of the maximum stress intensity factor. By substituting this crack length value to the 6<sup>th</sup> order polynomial equation, maximum

stress intensity factor was determined. If more than one real root were determined, by drawing stress intensity factor versus crack length graph, the crack length giving the maximum stress intensity factor could be estimated. Steps of the calculations in MATLAB are as follows:

**Table A. 2 MATLAB code to determine Mode I maximum stress intensity factor value**

<b>MATLAB Code</b>	<b>Explanations</b>
x=[0 5 10 15 20 25 30 33];	: entered [x (=a) values ]
y=[0 1.01576 1.53165 2.05775 2.63402 3.18104 3.16939 2.16067];	: entered [y (=K <sub>I</sub> ) values]
p=polyfit(x,y,6) <b>p=-0 0 -0.0002 0.0042 -0.0455 0.3485 -0</b>	: entered : by using (x,y) (=a, K <sub>I</sub> ), 6 <sup>th</sup> order polynomial equation was achieved
x2 = 0:0.01:33;	: entered
y2 = polyval(p,x2);	: entered
plot(x,y,'o',x2,y2);	: entered
grid on	: x (=a) versus y (=K <sub>I</sub> ) graph was plotted (Figure A. 1)
d=polyder(p) <b>d=-0 0 -0.0008 0.0126 -0.0910 0.3485</b>	:entered : derivative of 6 <sup>th</sup> order polynomial equation was computed
r=roots(d) <b>r= 27.7763 18.7311 +12.3263i 18.7311 -12.3263i 5.0475 + 6.4461i 5.0475 - 6.4461i</b>	:entered : roots of the derivative was found
polyval(p,27.7763) <b>ans = 3.3216</b>	: entered : real root substitute into 6 <sup>th</sup> order polynomial equation : K <sub>I<sub>max</sub></sub> was found

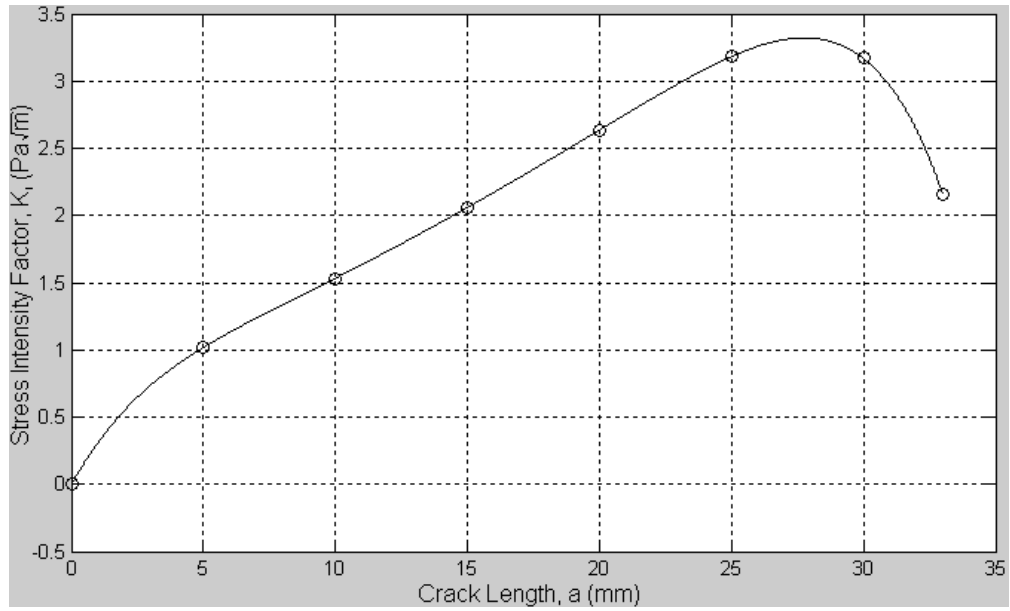


**Figure A. 1 Stress Intensity Factor versus Crack Length plot**

The formulations above were valid for both FBD and MR models. These steps were followed for all specimen geometries.

## APPENDIX B

### PETROGRAPHIC ANALYSES OF ROCKS

Petrographic analyses of andesite and marble were performed in Geological Engineering Department of Middle East Technical University. Petrographic studies showed that marble material only contains calcite whereas andesite is a complex material.

Andesite material is in purple-pinkish color. Phenocrysts are visible in the material and vesicles are coarse enough to recognize. In thin sections of the andesite material (Figure B. 1), biotite, biotite pseudomorphs, plagioclase phenocrysts, plagioclase microlites, opaque minerals, quartz (very few) minerals are seen. Moreover, porphyritic texture, glomeroporphyritic texture, vesicular texture, flow texture are identified. In addition, plagioclase phenocrysts show compositional zoning and polysynthetic twinning. Furthermore, grain supported-plagioclase microlites form the matrix of the andesite mineral. These studies show the andesite can be petrographically classified as “vesicular andesite”.

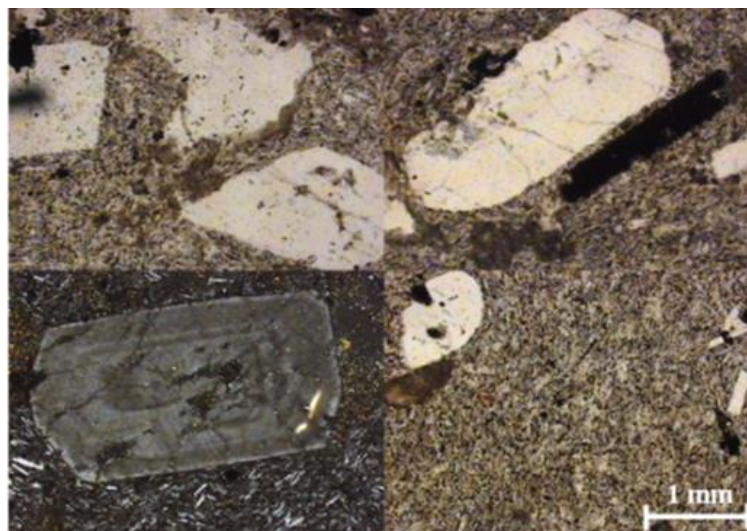


Figure B. 1 Thin sections of andesite



## APPENDIX C

### PROPER SPECIMEN GEOMETRIES FOR FRACTURE TOUGHNESS TESTING

Fracture toughness values conducted with both FBD and MR methods depended on specimen dimensions. Fracture toughness increased with increasing diameter and decreased with increasing loading angle or central-hole diameter.

With flattened Brazilian disc method, the closest result to the suggested method was obtained by 54 mm diameter discs with 35° loading angle. With modified ring test, the closest result to the suggested method was obtained by 75 mm diameter discs with 8 mm central-hole diameter and 25° loading angle, and with 14 mm central-hole diameter and 15° loading angle. Proper specimen geometries are summarized in Table C. 1.

**Table C. 1 Proper specimen geometries for fracture toughness testing with FBD and MR methods**

<b><i>D</i> (mm)</b>	<b><i>d</i> (mm)</b>	<b><math>2\alpha</math> (°)</b>	<b><i>t</i> (mm)</b>
54	0	35	27
75	8	25	37.5
75	14	15	37.5

## VITA

### PERSONAL INFORMATION

Surname, Name: Alkılıçgil, Çiğdem  
Nationality: Turkish (TC)  
Date and Place Birth: 16 June 1980, Eskişehir  
Marital Status: Single  
Phone: +90 312 210 26 70  
Fax: +90 312 210 58 22  
Email: [cheethem@hotmail.com](mailto:cheethem@hotmail.com)

### EDUCATION

Degree	Institution	Year of Graduation
MS	METU Mining Engineering	2006
BS	METU Mining Engineering	2003
High School	Prof.Dr. Orhan Oğuz High School, Eskişehir	1998

### WORK EXPERIENCE

Year	Place	Enrollment
2004 December	METU Department of Mining Engineering	Research and Teaching Assistant
2002 July	Eti Copper Plant, Küre, Kastamonu	Intern Engineering Student
2001 August	Eti Bor Kırka Borax Mine, Eskişehir	Intern Engineering Student

### FOREIGN LANGUAGES

Fluent English

### PUBLICATIONS

Ozdemir, E.B., Alkilicgil, C., Duzgun, H.S. “Numerical Methods in Earthquake-Triggered Landslides: A Case Study from Amasya-Turkey”, European Geological Union, Vienna, Australia, (2009) (Poster Presentation)

Alkilicgil, C., Tutluoglu, L. “Computation of Stress Intensity Factor on Disc Type Rock Specimens with Finite Element Method”, 4. Turkey SIMULIA Abaqus Users Conference, Istanbul, Turkey (Oral Presentation, In Turkish), (2006).

### PARTICIPATED PROJECTS

Investigation of the Effects of Surface Water Drainage System on Waste Dump Area at Turkish Coal Enterprises Soma-Eynez Open Pit Mine, Teknokent Project, (2009)

Slope Design for Turkish Coal Enterprises at Can Open Pit Mine, Project Code No: 06-03-05-2-00-15, (2007)

Slope Design for Turkish Coal Enterprises at Orhaneli Open Pit Mine, Dikmentepe,  
Project Code No: 06-03-05-2-00-10, (2007)

Investigation of Slope Design and Dragline Operation System at Surface Mine  
Panels of Orhaneli Coal Mine, Project Code No: 05-03-05-2-00-13, (2005)

#### **HONORS**

Course Performance Award – 2008 (Middle East Technical University)

Taylan Bozdog Success Award – 2003 (Mining Engineering Department, Middle East Technical  
University)

#### **HOBBIES**

Crossword puzzles, Sudoku, Turkish Classical Music, Badminton (METU Badminton team member,  
1999-2003)